Doctoral Dissertation
Doctoral Program in Material Science and Technology (35th Cycle)

Multifunctional bioinspired surfaces for different host responses

Francesca Gamna

* * * * * *

Supervisors
Prof. S. Spriano
Dr. Sara Ferraris, Co-Supervisor

Politecnico di Torino , 2023

I hereby declare that, the contents and organization of this dissertation constitute my own original work and does not compromise in any way the rights of third parties, including those relating to the security of personal data.

Francesca Gamna
Torino, 2023

Acknowledgment

Those three years were years of change.
When I think of the me of three years ago, I don't recognize myself. I was scared and afraid of the future, not knowing what it meant to do research. And I thought, "But how can I think about scientific research if I've to do research on myself first?" Because I see this path a bit like this: a phase of research through and through. A continuous work to find a right way to solve the problem, accompanied by a dosage work to find out how much I can do myself and how much I can ask for help.
I can't say I've had an easy few years, many things have happened and some have set me back negatively in my work.
Despite everything, I finished this exhausting, beautiful and unforgettable journey and nothing would have been possible if it wasn't for the people who allowed me to work, learn and grow.

First and foremost, I'd like to thank my tutors Silvia Spriano and Dr Sara Ferraris, who not only enabled me to have this experience, but were also an important support throughout my PhD. With patience and enthusiasm, they have shared their knowledge and experience with me, but not only that. They have and will continue to teach me how to weight the work properly, with dedication but without going crazy, always conveying their passion for research.

I'd also like to thank all the people I've met and worked with over the years

who have given me new experiences and knowledge that I value incredibly.. With sincere gratitude, I'd like to thank Prof. Seiji Yamaguchi from the Department of Biomedical Sciences, from the University of Life and Health Sciences, Chubu University; Prof. Biljana Mojsoska from Roskilde University, Prof. Andrea Cochis and Porf. Lia Rimondini from UPO in Novara, Prof. Alessandra Vitale, Prof. Renato Gonnelli and Dr. Erik Piatti,
Thanks also to all my colleagues, Jacopo and Cami; Fabi, Zeta Ale, Ange, Fra, Andre, Dani, Ste, Carla, Mari, Sofi, Eli, Virgi, with whom I drank many, many coffees. My thanks also go to the whole Glance group for the help, knowledge and opportunity to work with them.

And finally, of course, I must thank all the friends who have been with me over the years, who have slapped me and comforted me when I needed it.

And to my mum, because mum is always mum.

Thank you all.

Summary

In short, the topic of this thesis is the functionalization of biomaterials for bone contact applications with different biomolecules to confer multifunctional surface properties. Biomolecules are chemical compounds that play an important role in living being. The here used biomolecules are both natural such as polyphenols and vitamin E (α-tocopherol (αT)) and its derived compound α-tocopherol phosphate (αTP) or artificially synthesized, such as peptoids. The use of natural biomolecules for the functionalization of biomaterials brings advantages, such as lower immune response, different functionalities, natural native ligands, natural degradation process, wide availability, and cost-effectiveness but may have some issues such as the high variability of properties and composition, difficult industrial processes and standardization, control of degradation profiles, sterilization. This is also why it is interesting to compare different biomolecules that have completely different origins. The chosen biomolecules differ in properties and chemical structures; they have antibacterial, anti-inflammatory, antioxidant, and osteoinductive properties, and the challenge of this work is to exploit their ability to give effective functionalities and new capabilities to biomaterial surfaces. Indeed, nowadays the main medical need of biomedical devices is a multifunctional activity able to induce rapid and physiological osseointegration, counteract bacterial biofilm formation, and prevent in situ chronic inflammation at the same time. The substrates used for functionalization were chemically treated titanium surfaces to become bioactive: they have nano-textured surfaces and, in one case, a

calcium titanate layer doped with iodine ions to confer antibacterial properties to the surface. Different functionalization protocols were investigated and improved, from a thick, homogeneous coating to a single molecular layer. The method of functionalization was selected case by case, depending on the molecule used, varying the pH, solvent medium, and temperature, with the aim of optimizing the adhesion and amount of the molecule on the substrate. A protocol of a physical/chemical and biological characterization was also investigated, using different techniques such as ζ-potential titration curve, UV-VIS spectroscopy, Fourier-transform infrared spectroscopy (FTIR), Kelvin probe force microscopy (KPFM), contact angle, photospectroscopy measurements with the Folin&Ciocalteu redox activity test, release tests, and so on. For biological characterization, samples were tested *in vitro* with bacterial and cellular assays. Of course, the same characterization techniques were not used for all molecules, but for each molecule, the right suitable protocol was explored.

The different physicochemical characterizations revealed a continuous homogeneous coating for α-tocopherol and molecular functionalization for peptoids and polyphenols. The grafting of α-tocopherol phosphate, on the other hand, was explored in both ways, either as a homogeneous coating or through molecular functionalization.

Biological tests revealed different properties for each molecule: α-tocopherol has an antifouling effect, through which it provides an antiadhesive coating for both cells and bacteria. α-tocopheryl phosphate and peptoids have an effective antibacterial activity and polyphenols have shown a successful antioxidant ability in a chemically-induced pro-inflammatory environment, thus showing a scavenger activity towards toxic active species responsible for inflammation.

According to the results, surface functionalization of biomaterials is a promising strategy to achieve multifunctional surfaces that combine the properties of the substrate with those of the grafted biomolecule.

Contents:

List of Tables

List of Figures

1. Chapter: Bone implant interaction

1.1 Osseointegration and osseoimmunomodulation

Osseointegration refers to the direct structural and functional contact between the living bone and the surface of a non-natural implant [1]. This means that effective osseointegration is characterized by a firm anchorage between the bone and implant, with no growth of other tissues at the interface. The first material discovered to be capable of being osseointegrated was titanium, when in the 1950s, Professor Per-Ingvar Branemarg, demonstrated that metallic titanium could be permanently incorporated into the bone of a rabbit model [2].

The osseointegration process involves several linked events such as protein adsorption, and coagulation of blood followed by the recognition of the surface

by mesenchymal stem cells and finally, if the surface is suitable, bone formation through their differentiation into bone cells. Osteogenic and immune cells are intimately related, and implant osseointegration is the result of a proper inflammatory response. When bone trauma occurs, there is a strict connection between the cells deputed to host defense and bone remodeling (osteoblasts and osteoclasts): it is called "osteoimmunology"[3].In the case of an implant, cells involved in the foreign body reaction, such as macrophages, lymphocyte T or B, must achieve a balance in polarization and factors expression to modulate the activity of osteoblasts and osteoclasts. The proper immunological response for correct osseointegration is called "osteoimmunomodulation" [4], [5].

Osseointegration can be seen as a limited foreign body reaction, which does not involve chronic inflammation and permanent fibrotic capsule but instead, it results in a new functional bone tissue at the interface with the implant. The first interaction concerns the adhesion of proteins of blood on the surface followed by the interaction with macrophages and blood cells, including red cells and platelets responsible for the clot and the fibrin matrix formation which is fundamental for the migration of osteogenic cells.

After about 2-3 weeks, the interface transforms into a thin temporary fibrous

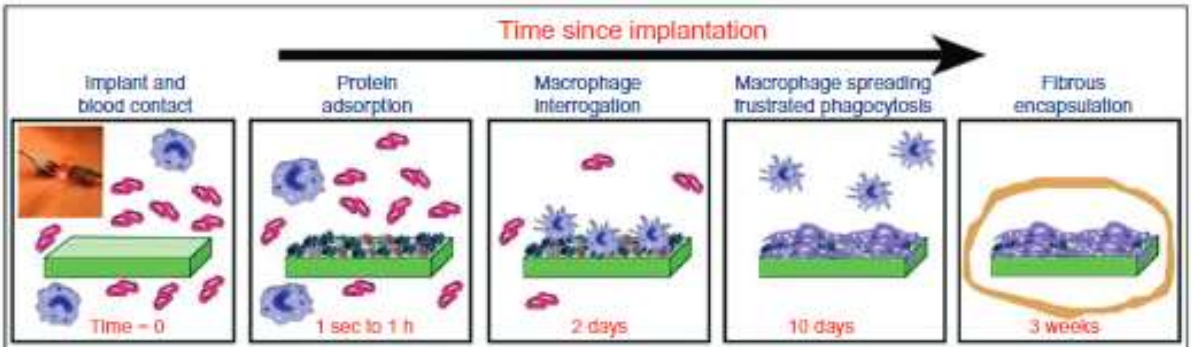

Figure 1.1 Stages of the first 2-3 weeks of implant life [7]

capsule surrounding the implant, with macrophages and giant cells persisting on the surface of the implant throughout the life of the implant (Figure 1.1) [6], [7].

After this period, osseointegration follows 2 common and biological steps:

1. Bone formation
2. Adaptation of bone mass and structure to the loading condition (bone remodeling) [8].

Bone formation is characterized in general by osteocyte formation from

osteoblasts, so from undifferentiated mesenchymal cells. It involves a cascade of cellular events and consisting of 3 distinct events that depend on the implant and the type of stimulus it provides: osteoconduction, osteogenesis, and/or osteoinduction. Osteoconduction relates to the stimulation of bone growth on the surfaces or into pores, channels, or pipes. Osteogenesis relates to the stimulation of osteoprogenitor cell proliferation and biosynthetic activity of osteoblasts. Osteoinduction relates to the recruitment and stimulation of undifferentiated mesenchymal cells to develop into preosteoblasts [9], [10].

Another important process that takes part in the osseointegration process is bone remodeling which is established around the osseointegrated implant. In fact, bone remodeling allows the bone to adapt itself around the implant by filling osteolytic lacunes that may form during the osseointegration [11], [12]. Bone remodeling is performed mainly via the coordinated activities between bone formation and resorption. The protagonists of these two processes are osteoclasts and osteoblasts, respectively. In brief, through bone resorption, osteoclasts destroy old bone and, through bone formation, osteoblasts create new bone that will subsequently mineralize. In particular, bone remodeling is composed of 5 overlapping steps: activation, resorption, reversal, formation, and termination [13]. Upon activation of the remodeling process, osteoclast progenitor cells are recruited, which grow from mononucleated to multinucleated osteoclasts, which are cells activated to start bone resorption. During the resorption phase, osteoclasts resorb the old or damaged bone. Subsequently, the formation phase begins, during which the surface of the bone

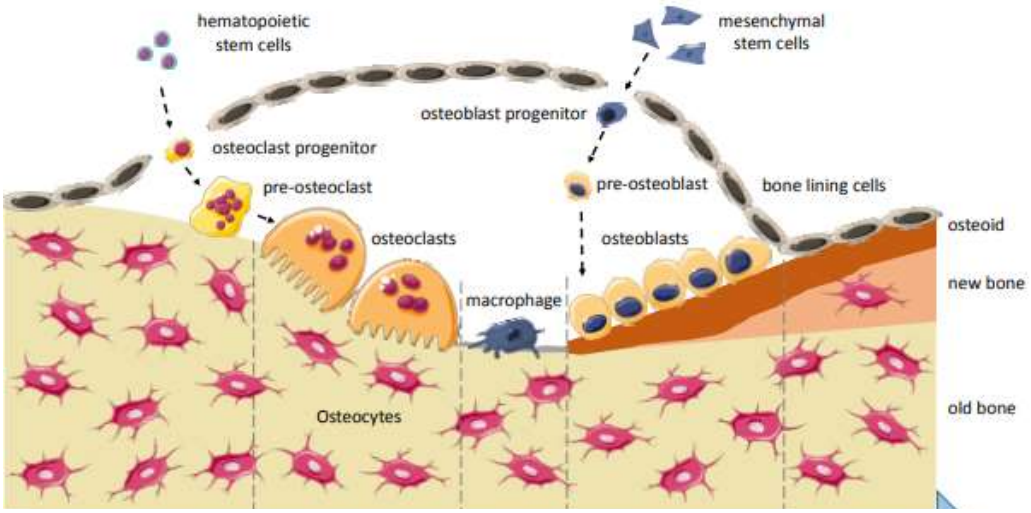

Figure 1.2 Schematic representation of bone remodeling [14]

is prepared for matrix deposition by macrophage cells. Obviously, osteoblasts are the main players in this phase, secreting osteoid, and many of them undergo apoptosis or become trapped in the matrix and differentiate into osteocytes. The remaining osteoblasts transform into osteocytes while the osteoid mineralizes into new bone (Figure 1.2) [14].

Because osteoclasts determine the development of bone resorption, they are responsible for a group of disorders characterized by bone loss, such as osteoporosis [15]. In addition, their activity plays a very important role at the bone-biomaterial interface throughout the implantation period, as it prepares the surface at the interface for the osteoblast activity and enables the remodeling of bone by strengthening its internal structure along mechanical load lines [13]. Going more specifically, osteoclasts differentiation requires stimulation by RANKL which is a cytokine secreted by osteoblasts if stimulated by hormones growth factor (PTH). Osteoblasts, in addition to producing cytokines that favour osteoclastogenesis, secrete OPG, another cytokine also known as osteoclastogenesis inhibitory factor which binds with RANKL decreasing the number of ligands that activate the osteoclasts [16], [17].

The process of this regulation is explained in Figure 1.3 and shows how complex the mechanism of bone remodeling is depending on many different factors: the presence of an external implant can lead to even greater complexity within this process.

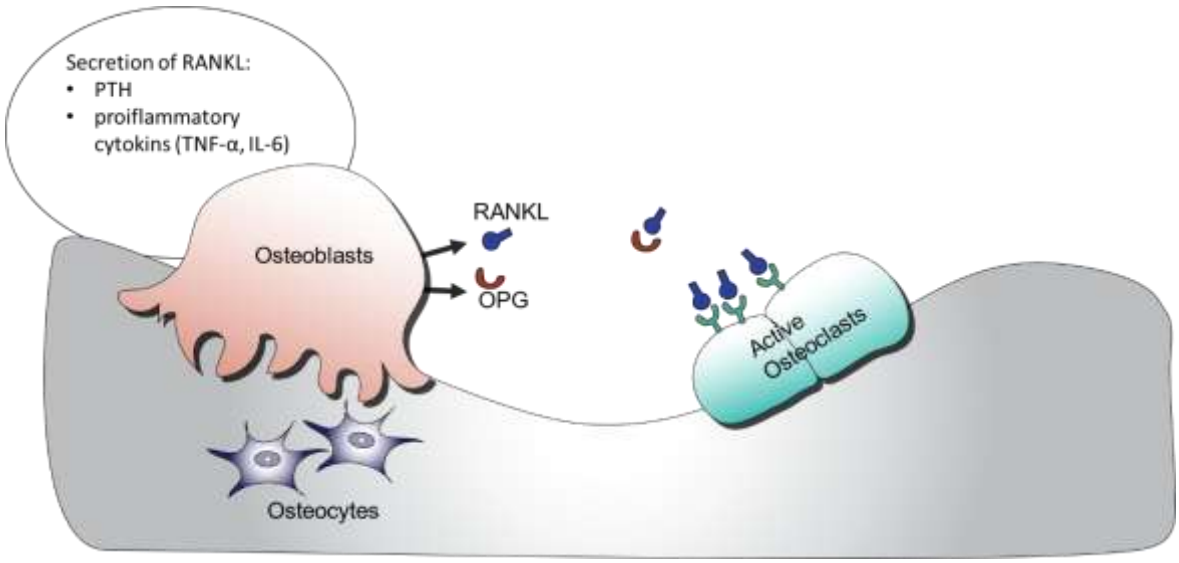

Figure 1.3 Role of osteoblasts, OPG, RANKL, and PTH in the activation of osteoclasts [16]

1.1.1 Surface modification on titanium for permanent devices

Many different surface features influence the process of the osseointegration of an implant including [18], [19]:

1 Implant material and its biocompatibility
2. Implant surface and its design characteristics,
3. State of the host bone
4. Surgical consideration
5. Loading conditions.

As can be seen, the last three points concern factors that do not depend on the implant, while the first two are totally dependent on the type of implant. Several attempts have been made at surface design, in terms of surface modification, topography, and chemistry, to improve implant osseointegration. Among the various materials for implants, titanium and its alloys are frequently used, mostly in dental and orthopaedic implants, for their good mechanical properties, biocompatibility and osteointegration ability. Because titanium is an example of bioinert material, scientific research has focused on topographic and surface modification as a means of making the implant bioactive, stimulating and accelerating the osseointegration process. The topographical texture of implant surfaces has an important role in tissue response. In fact, surface topography is fundamental for the adhesion and differentiation of osteoblasts in the initial stage of osseointegration: micro- and nano-scale rough surfaces have greater surface area for tissue integration than smooth surfaces, and porosity also allows good bone attachment. Nanoscale roughness with size in the magnitude of protein and cell membrane receptors dimensions could also act in cell adhesion, proliferation, and spreading [20].

The ideal submicro- and micro-roughness size that ensures better osseointegration is about 0.4-2 μm as it represents a good balance between high cell adhesion and proliferation, avoiding side effects such as increased ion release and implant weakening [21]. The ideal topography of a bone implant overlaps nano-, micro-, and macro-scale surface features to maximize the number and strength of focal contacts of the osteoblasts.

Several approaches, both mechanical and chemical, such as sandblasting and

acid etching or heat treatments have been developed to modify the topography of the surface, introducing the appropriate micro- and nano-roughness on titanium implants.

Among the different treatments, acid etching is the most widely used. Acid etching can be used as a single treatment or coupled with a blasting treatment. It is used to remove the native oxide layer of titanium, through a controlled corrosion process, and consequently to create a rough and porous surface [22], [23]. The acids used for this type of surface treatment are mixtures of HCl, HF (essential for solubilizing the native titanium oxide layer), HNO_3, or H_2SO_4, the last of which is the most effective in terms of the surface roughness obtained. This treatment is very effective in roughness results, as it creates a homogeneous roughness throughout the substrate, and by acting on the surface topography, it is used for the stimulation of osseointegration [24]

In general, various strategies of topography modification can be also combined, to enhance the cells' response and osseointegration ability. Sandblasting and acid etching are often combined to achieve a synergistic effect between the macro-topography (due to the sandblasting technique) and micro-texture (due to acid etching) of the implant to promote bone formation [20].

Other topographical surface modifications focused, not only on increasing roughness but also on making the implanted surface more resistant to corrosion. Among these, of paramount importance are oxidative treatments.

Oxidation treatments include anodic oxidation, thermal oxidation, plasma immersion ion implantation, plasma electrolytic oxidation, and plasma oxidation [25], [26]. These techniques aim to create a stable oxide layer, much thicker than the native one that allows good protection of the metal surface under aggressive environmental conditions, such as those inside the body. Anodizing is a traditional technique in which the thickness of the oxide layer formed on the surface of titanium is directly related to the anodizing voltage (or current). Thermal oxidation, on the other hand, is an effective method that creates an oxide layer thick enough for anti-corrosion objectives. Among the crystallographic structures of titanium dioxide (TiO_2), anatase is the most biocompatible while rutile has higher mechanical and thermodynamic properties.

To further improve corrosion resistance, heat treatments can be combined with oxidative treatments, leading to the formation of the rutile phase, and increasing the hardness of the oxide layer [25].

In recent years, an interesting combination of acid etching and thermochemical oxidation has been developed to create multiscale topography and high

hydroxylation on titanium surfaces for dental implant applications. The surface topography was found to consist of a microporous layer with an overlapping nano-texture and was achieved by etching in HF and thermal oxidation in hydrogen peroxide. The hydroxyl groups on the surface are important for apatite precipitation and can be used for biomolecule grafting. The resulting modified surfaces showed bioactive behavior as well as improved protein adsorption, and antibacterial activity [27]–[29]. Depending on the concentration of H_2O_2, different oxides can be formed: Ti_2O_3 forms at low concentrations, while TiO_2 forms at higher concentrations.

Another interesting work is based on the combination of chemical and thermal treatment. In this case, a NaOH treatment followed by heat treatment is performed on titanium substrates. The NaOH treatment forms a porous iridescent sodium titanate, while the subsequent heat treatment induces the formation of rutile (TiO_2), increasing the strength of the oxide layer.

These surfaces result to have not only bone-bonding activity but also various other helpful features, such as bone growth promotion, antibacterial activity, osteoconductive and osteoinductive behaviour [30]. Along with the above, there are many other works in the literature dealing with the combination of chemical and heat treatments.

Another type of surface modification of titanium alloys regards coating. Coatings with TiO_2, silica, or hydroxyapatite were studied with the aim to introduce an improved osseointegration ability. The most commonly used coating is hydroxyapatite. The preparation methods employed to fabricate these coatings are plasma spraying, sputtering, electrochemical deposition, dip-coating, sol-gel, sintering, and many more. Hydroxyapatite (HA) is present in the human body and constitutes the inorganic phase of hard tissues which makes it a highly biocompatible material [31]. Apatite formation on the surface of an implant is a key factor in determining whether an implant is osteoconductive and can be integrated with the surrounding bone tissue. It is important because it creates a surface similar to the mineral structure of natural bone. This allows for better osseointegration, which is essential for the long-term stability and success of the implant [32], [33].

Some critical aspects of hydroxyapatite, as a material used as a coating, are low fracture strength and toughness, and resorption of the hydroxyapatite layer resulting in possible loosening of the implant [34]. To increase the coating strength, typically alumina and zirconia are inserted along with hydroxyapatite. The use of fluorapatite to increase coating stability and induce hard tissue

formation and growth has also been explored. These coatings, besides being bioactive, inhibit the release of metal ions from the implant to the surrounding tissues [35]. In addition to inorganic coatings, biochemical methods to create an organic coating have received great interest in recent years. Biomolecules are immobilized on the titanium surface to induce a specific response from the cells and the surrounding tissues: extracellular matrix (ECM) proteins, peptides, growth factors, enzymes, and DNA sequences can be immobilized on the surface to promote bone cell adhesion; to trigger new bone formation, and to enhance the process of bone mineralization.

For immobilization, different techniques based on either physical adsorption or chemical bonding are used. Adsorption is a very simple immobilization method, used to have a release of the biomolecule, which has a linkage with the surface dependent on parameters such as pH, temperature, and solvent. Instead, covalent binding, such as silanization, is more complicated than the adsorption method but it provides the highest surface loading and great biomolecule retention, which is an advantage for a long-lasting effect if an action of the released biomolecule in the surrounding fluids is not required [36].

Different biomolecules have been used to create the coating. Growth factors such as platelet-derived growth factor (PDGF), bone morphogenetic proteins (BMPs), insulin-like growth factor (IGF), or transforming growth factor (TGF)-β were used in order to facilitate osseointegration [37]. Other proteins such as fibronectin, vitronectin, type I collagen, and other ECM proteins present specific amino acid sequences that bind the cell membrane integrins to promote cell adhesion. RGD is a peptide commonly used in titanium surface modification. Peptide sequences are not meant to be released, therefore they are typically covalently attached to the surface [36].

Finally, an organic-inorganic combination is also of interest in inducing the osteogenic behavior of titanium coatings. For example, a coating composed of apatite and amelogenin protein revealed better osteogenic gene expression than than pure titanium or apatite coating surfaces [38].

Titanium as a candidate for temporary devices

The term fracture refers to the disruption of the structural integrity of a bone due to traumatic or spontaneous reasons. In most cases, it is treated with a conservative approach involving immobilization by plaster casts. However, in some circumstances it is necessary to stabilize the bone segments through mechanical devices: in such a case we speak of osteosynthesis. It is a method that involves surgery and implant devices, usually metallic, to aid in the stabilization of the fractured bone segments. In most cases, devices of this type are not permanent, and they are called temporary devices.

Temporary devices are considered as dismissible tools supporting bone self-healing, that are planned to be removed by a second surgery after the tissue has recovered its functionality. Particularly, fracture-fixation implants are used in osteosynthesis to maintain the alignment of the fracture fragments; they include orthopaedic trauma devices such as plates, screws, intramedullary nails, or bone pins. Fixators can be distinguished into internal or external; in the former case, the components, usually made of steel or titanium, are only placed inside the body, while the second type involves also trans-cutaneous elements connected to the bones by screws or tensioned wires [39]–[42]

Titanium alloy and stainless steel are good candidates for applications where mechanical properties are desired to be maintained throughout the entire restorative phase, as they are able to support self-healing, hold the two bone flaps firmly stable, biocompatible, and avoid any risk of compromising the healing of bone fragments [43], [44].

A major limitation present in these types of implants is their subsequent surgical removal, once healing is achieved; a different case is that of bioresorbable implants such as those based on magnesium alloy [45]

Indeed, the surgical procedures can be very complicated if excessive tissue growth had occurred on the device, i.e. an excessive bone on-growth at the interface between the native tissue and the implant, especially in the head of a screw or between the threads of a screw and a plate [46]. Complications during the second surgery can occur in this case such as refracturing of the newly healed bone. To overcome the issues derived from the second surgery, recently, bioresorbable magnesium alloys have been introduced as an appropriate alternative to titanium alloy due to their special properties [47] In fact,

magnesium alloys have emerged as potential candidates for the construction of biodegradable temporary implant devices with good mechanical properties, like low elasticity, similar to human bone [48].

Despite the advantages of magnesium alloys as a biomaterial for temporary implants, their use is still limited in some applications. In fact, the poor corrosion resistance of magnesium means that the implant may lose its mechanical properties before the healing process is complete [49], [50], [51].
That is why, nowadays, most devices used for osteosynthesis are still traditional metallic implants (stainless steel or titanium).

1.2 Infections

In general, orthopedic and dental bacterial infections are still common and they require a high level of attention from scientific research. The estimated annual incidence of infection is around 2% and 1% for hip, knee, and shoulder replacements in both young and old patients and one of the major causes of replacement is the infection of the implantation site. In the case of titanium implants, S. epidermidis and S. Aureus are the bacteria that mainly adhere to the implant surface [52], [53].

Antibiotics are the most widely used drugs in antimicrobial therapies to the present day. As everyone knows, the excessive use of antibiotics has become the main factor for the birth and spread of strains resistant to different groups of drugs, thus developing the phenomenon called antibiotic resistance. Antibiotic resistance occurs when bacteria and/or fungi develop the ability to overcome drugs that are designed to destroy them. This means that germs are not killed and continue to grow, which is why infections caused by antibiotic-resistant bacteria are difficult, and sometimes impossible, to treat.
The figure below broadly explains how antibiotic resistance works (Figure 1.4).

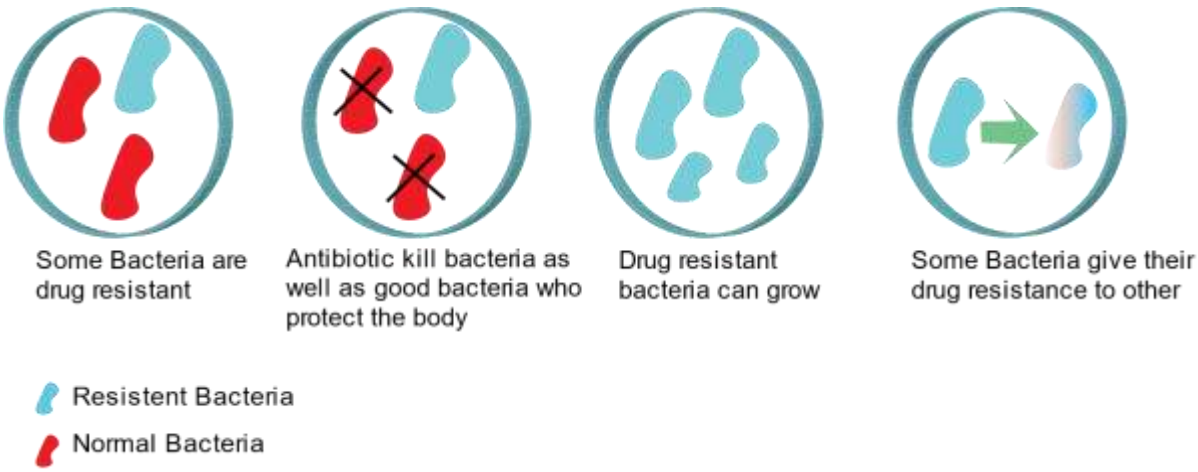

Figure 1.4 Antibiotic Resistance

Bacteria can generally be found in two forms:

- Planktonic, which are found in a free state in solution. They are the most vulnerable to antimicrobials and can therefore be eradicated through the host's natural defense or simple antibiotic therapy.
- Sessile, which are found attached to a surface and are those that begin to secrete EPS, the extracellular matrix of biofilm. The biofilm has a 3D structure that permits it to evade both antibiotic therapy as well as natural defenses. They are commonly associated with a foreign body such as when a prosthesis is implanted into the host because the surfaces in contact with water, could offer a favorable habitat for the growth and reproduction of bacteria and eventually the formation of biofilm [54].

Biofilm is a finite matrix that adheres to a surface, formed as the result of a system of cooperation and coordination of gene expression among bacterial cells. It has a "tower structure" and it is composed of 10% of microorganisms and 90% of self-produced matrix material that usually involves host components including fibrin, immunoglobulins, and platelets [55]. This complex encapsulating structure provides protection to bacterial cells from the immune system, ensuring a flow of nutrients and a site for the adhesion of other bacterial cells. The biofilm matrix is negatively charged so that it is able to break down the antimicrobials which, by binding with the matrix, cannot reach the interior where the bacteria are located. The bacteria are arranged in the matrix, both in central and external positions. The central ones grow very slowly because they are exposed to lower concentrations of oxygen and nutrients, and the outer ones grow faster and are also more susceptible to antimicrobial agents [54]. The signal molecules that are exchanged between the various cells are important because they allow the bacterial community to communicate and cooperate according to a process called quorum sensing. (Figure 1.5).

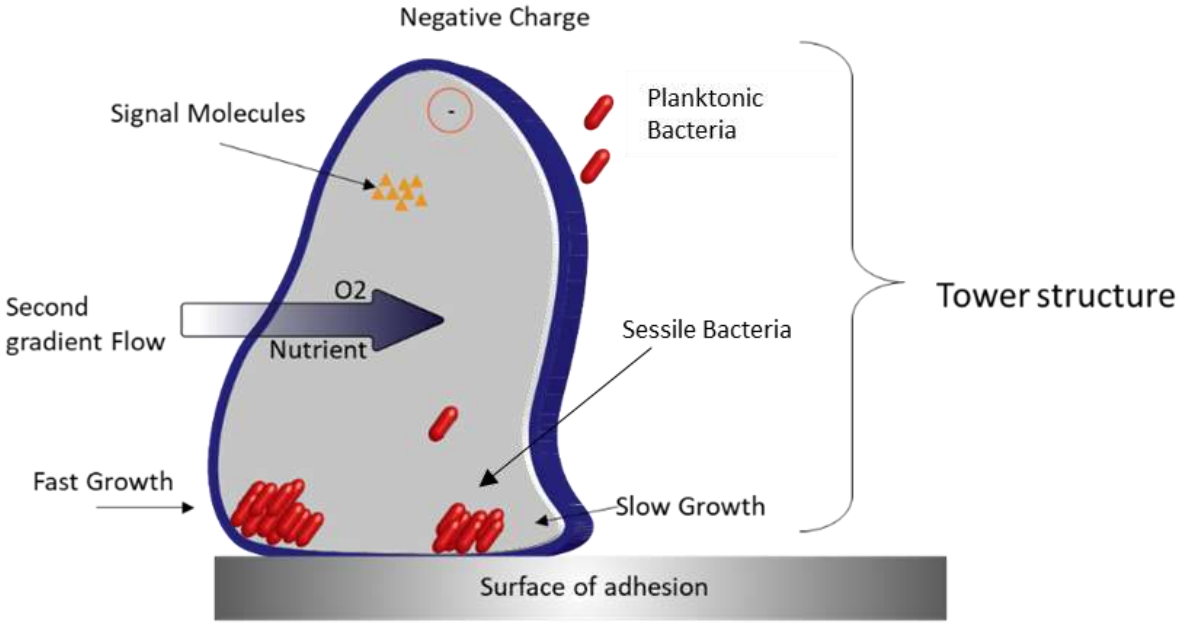

Figure 1.5 Schematic representation of biofilm

Biofilm formation is one of the major problems inducing antibiotic resistance [56]. The mechanism is not yet fully known but it is clear that biofilm should have some intrinsic properties which allow high resistance to conventional antibiotics such as:

(a) biofilm's structure, which interferes with drug diffusion,

(b) the slow growth of biofilm, which causes antibiotics to be taken slowly and this gives time for the infection to spread.

(c) biofilm's phenotype which is considered as a group of bacterial cells that is not affected by antibiotics [57].

Many factors that influence the initial attachment of bacteria to the foreign surface and the subsequent development of the biofilm. The creation of the biofilm occurs more frequently on surfaces that are rougher and more hydrophobic and where there is a high concentration of adsorbed proteins [58].

1.2.1 Surface modifications in order to avoid bacterial infections

There are several ways to achieve an antibacterial surface; biofilm adhesion depends on several factors, such as surface chemistry, charge, wettability, texture, and roughness [58]. In particular, roughness is the main factor that influences bacterial adhesion, and when it exceeds 0.21 μm the adhesion area increases allowing for greater adhesion of bacterial cells [59]. Through surface modification, which can be chemical, physical, or through the formation of a coating, these factors can be modified in order to make the surface less adhesive for bacterial cells. Surfaces can be antiadhesive, with a surface antibacterial action, or capable of releasing antibacterial molecules that can kill bacteria in the surrounding tissue.

Specifically, surface modifications can be passive or active. Passive surface modification mainly involves work on the topography, structure, and chemistry of the implant, where surfaces that reduce bacterial adhesion can be achieved. Active surface modification by which, on the other hand, mainly coatings or grafts, organic or inorganic, with antimicrobial activities are obtained [60]. Surface modification methods can also be either physical or chemical. Chemical surface modification methods are promising approaches to modifying and inducing an antibacterial effect on titanium surfaces. The difficulties, however, relate to the stability of the immobilized biomolecules. As mentioned in the chapter 1.1.1., covalent grafting is the preferred strategy to immobilize a molecule on the surface. The most common is silanization. Alkoxysilane molecules react with the titanium surface exposure group and function as anchor molecules that allow coactive binding to peptides, antibiotics, proteins, and polymers or that have an antimicrobial effect [61].

In contrast, physical adsorption of molecules, although easier, may not be effective for long-term implantation because of possible desorption. Physical modifications mainly involve coatings, which are divided into bacteriostatic (passive) and bactericidal (active). Coatings formed of bacteriostatic materials, such as PEG, repel bacteria without killing them. Superhydrophobic coatings, typically polymeric, can have the same antiadhesive effect. Passive coating methods might turn out to be a good way to achieve antibacterial surfaces, as they can prevent biofilm formation, but their effectiveness is generally limited, may decrease over time as the coating

degrades, and varies greatly depending on the bacterial species.

Active antibacterial coatings, on the other hand, release agents that act as bactericides. [61].

In recent years, inorganic antibacterial agents have been investigated and special attention has grown to metal ions and nanoparticles such as silver nanoparticles and silver ions (Ag^{+}), zinc (Zn^{2+}), copper (Cu^{2+}), iodine (I^{-}) or selenium (Se^{4+}) ions [62]–[65].

In addition to inorganic agents, research has focused on the investigation of natural and organic agents compatible with both the human physiology and constitutive materials of medical devices, that can discourage the use of antibiotics and even potentially interfere with biofilm formation [66]. Figure 1.6 shows a scheme of possible antibacterial surfaces.

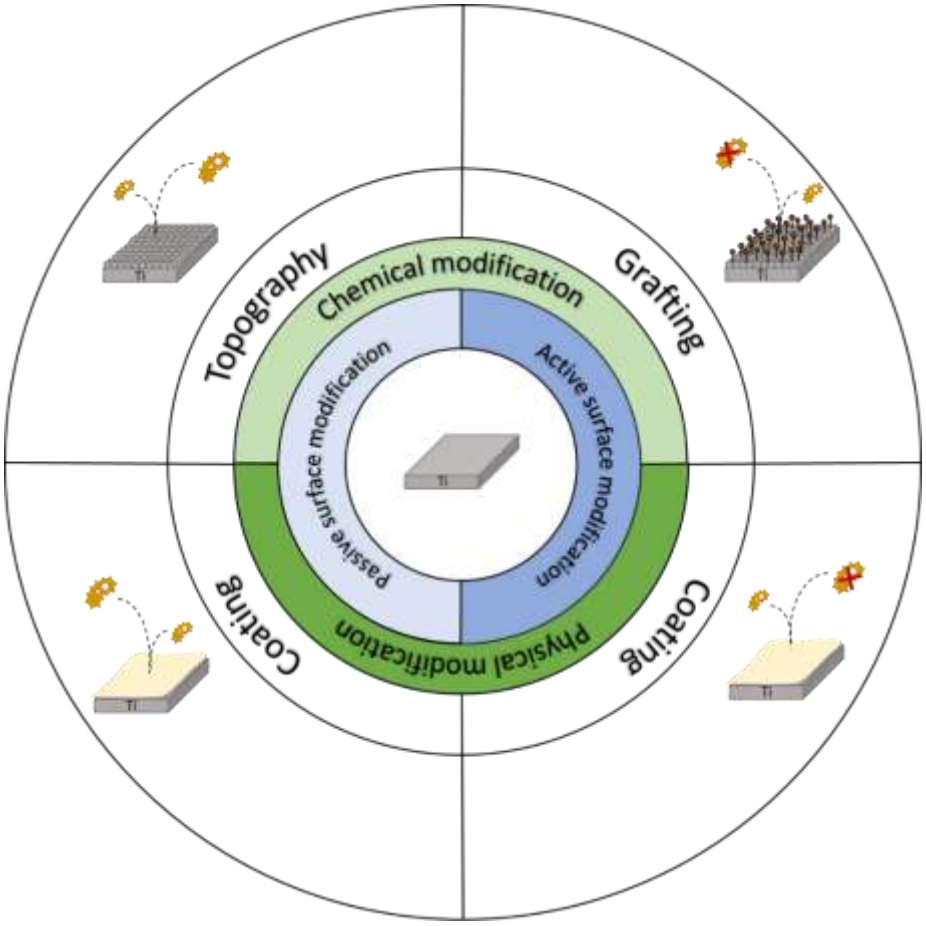

Figure 1.6 Antibacterial surfaces

1.3 Inflammations

The implantation of any biomaterial into the body brings to a local and/or systemic response from the host tissue. The first reaction of the organism is the protein adsorption on the foreign surface derived from a first blood-material interaction. After, the activation of the non-specific immune system causes an acute inflammation, realising a large number of proinflammatory cytokines into the blood that participate in the transduction of the intercellular signal. This type of inflammation is of short duration and often resolves spontaneously without leaving important consequences.

Acute inflammation can be followed by chronic inflammation at the implant site. In this stage, the macrophages release mediators of inflammation such as oxygen free radicals (ROS) and reactive oxygen intermediates, degradative enzymes, and acids on the surface of biomaterials. Chronic inflammation brings also the development of granulation tissue [67].

At this stage, ROS play a key role in the process of inflammation and healing. In fact, excessive production of them in cells and tissues leads to what is called oxidative stress. This imbalance can damage cellular molecules, such as DNA, and interfere with and damage the phospholipid membrane (Figure 1.7). In fact, oxidative stress is implicated in a number of pathological conditions such as cardiovascular and neurodegenerative diseases, cancer, and aging, and plays critical roles in inflammation, fibrosis, and healing, the main events that occur during biomaterial implantation [68], [69]. In particular, after the surgery and implant placement, ROS participates in four different steps from the initial inflammation to the final healing. First, the tissue damaged by surgery causes increased levels of oxidative stress (Figure 1.7 A), immediately after implantation, protein adsorption follows, creating a matrix that leads to a series of molecular bonding events, triggering the formation of oxidants at the implant site (Figure 1.7B).

Finally, acute, and eventually chronic, inflammation and healing process follow, orchestrated by macrophages, which are also regulated by ROS. (Figure 1.7C, D).

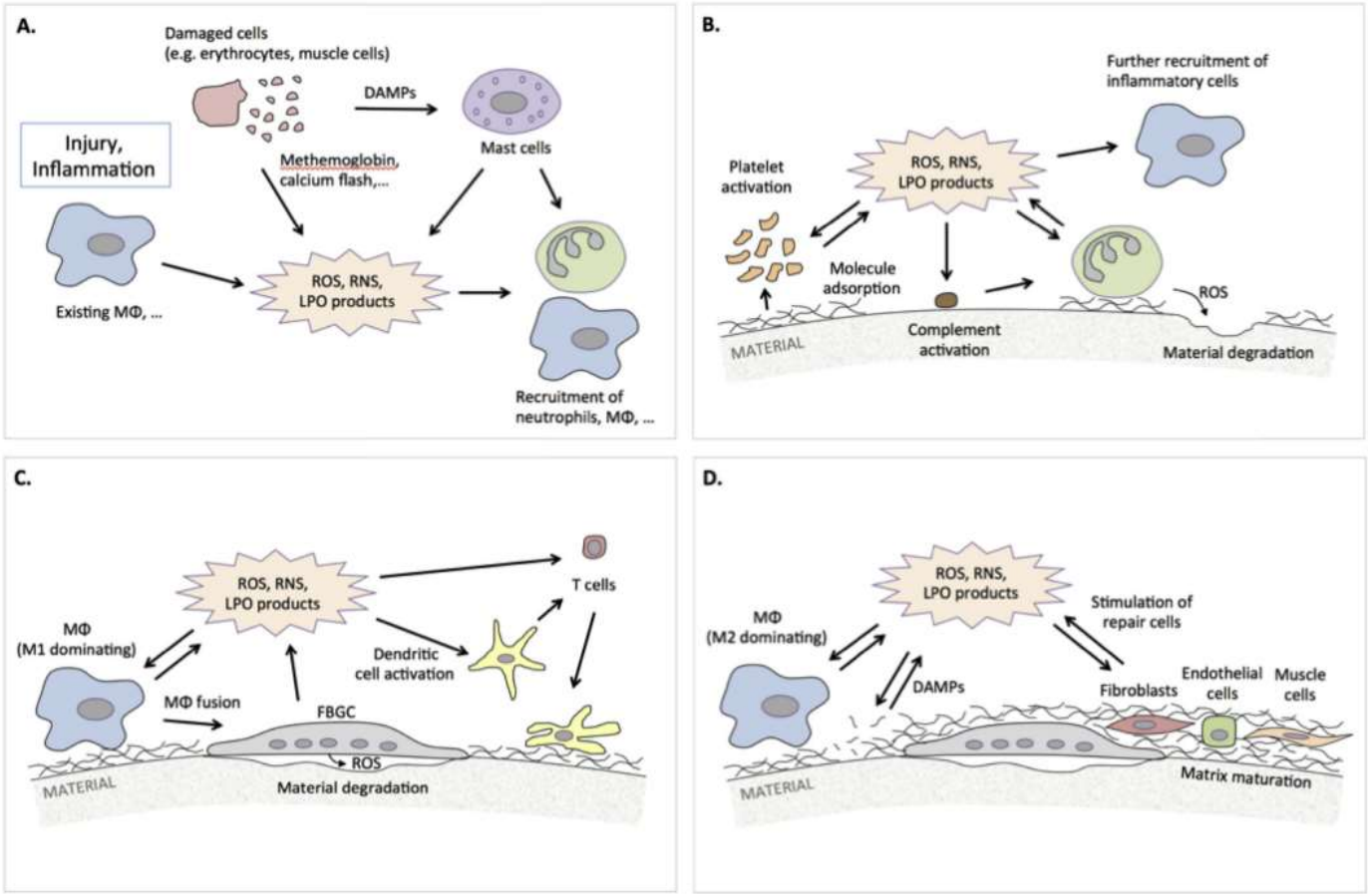

Figure 1.7 Oxidative stress involved after implantation [67]

That said, a successful biomaterial implant requires the balanced expression of both oxidant production and elimination. Inhibiting the production of reactive oxygen species (ROS) after implant placement is an important measure to reduce the release of inflammatory factors, thus, reducing body damage.

1.4 Multifunctional surfaces

Many strategies are still being studied to combine the surface modifications stated before to obtain surfaces with not only antibacterial or osseointegration abilities but also anti-inflammatory, antioxidant, and anticancer activities.
In this way, multifunctional surfaces are obtained that combine different activities to improve the implanted biomaterials. These surfaces should be able to simultaneously perform multiple biological tasks. They are considered smart surfaces, designed to have multiple tasks simultaneously in a bone-contact application perspective (Figure 1.8) [70].

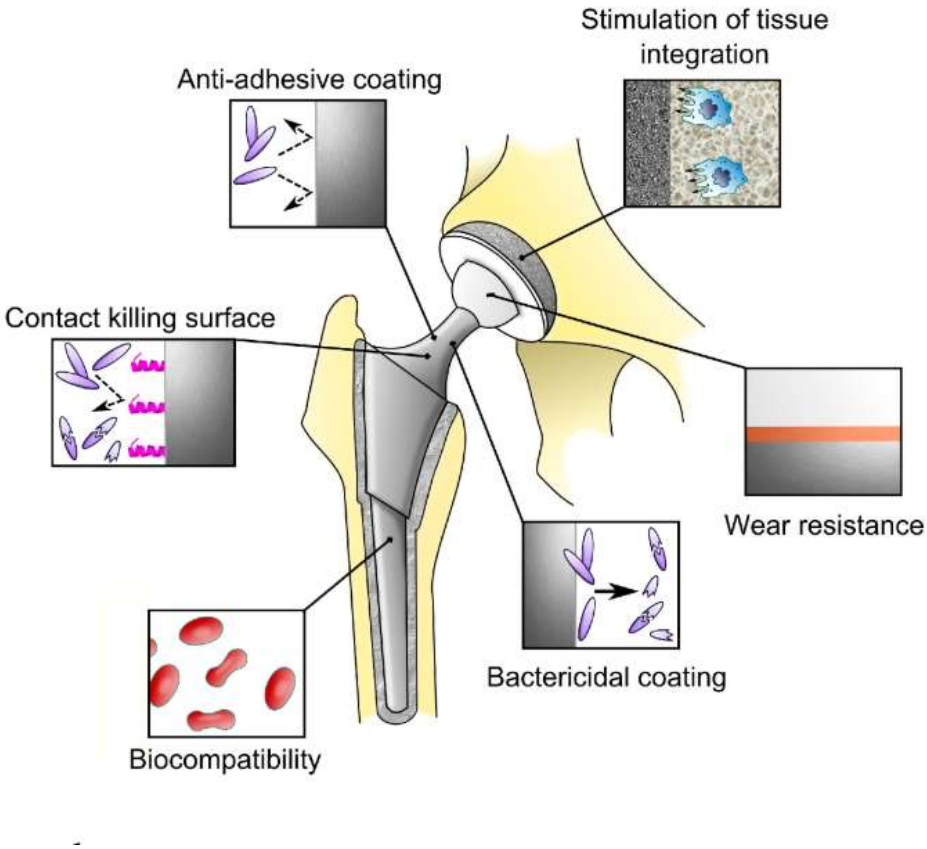

Figure 1.8 Multifunctional surfaces [69]

2. Chapter: Vitamin E

2.1 Introduction

Vitamin E is a commonly used term for tocopherols and tocotrienols (α, β, γ, δ), components of many natural products of both plant and animal origin. Thanks to its powerful antioxidant capacity, vitamin E has been very successful in hip and knee arthroplasty, used to confer resistance to oxidation to irradiated ultra-high-molecular-weight polyethylene (UHMWPE). The positive results of these studies have made vitamin E an important object of research in the biomedical field, highlighting other important properties, such as anti-bacterial, -inflammatory, and -cancer activities. In fact, there is extensive literature dealing with vitamin E in different kinds of material processing, drug delivery, and development of surface coatings. Vitamin E is widely discussed in the literature, and it is possible to find many reviews that discuss the biological role of vitamin E and its applications in food packaging and cosmetics (see next paragraph).The first (bibliographic) part of this chapter is composed by the first 6 paragraphs and aims to give an insight into what α-tocopherol (αT) and its derivatives are, studying their chemical structure, biological role, applications in biomedicine, and ways of detecting or quantifying these molecules. Finally, the second (experimental) part of this chapter concerns the functionalization of

titanium alloy with this molecule in different forms, either as a coating or grafting of a molecular layer. Part of this chapter is included in three published manuscripts (F. Gamna et Al. “Vitamin E: A Review of Its Application and Methods of Detection When Combined with Implant Biomaterials”, 2021, Materials,),
(F. Gamna et Al. “The use of vitamin E as an anti-adhesive coating for cells and bacteria for temporary bone implants”, 2022, Surface and Coatings Technology,) and
(F. Gamna et Al., “Grafting of alpha-tocopheryl phosphate on chemically treated Ti-6Al-4V for antibacterial bone implants”, 2023 Applied Surface Science)

2.2 Chemical Structure of Vitamin E

Vitamin E was discovered by Evans and Bishop in 1922. It includes eight compounds (α, β, γ, δ tocopherols and tocotrienols) naturally present in many fat-containing products of both plant and animal origin, such as vegetable oils, wheat germ, oily seeds, dark-red vegetables, nuts, whole grains, kiwi, mango, egg yolk, and liver. Tocopherols and tocotrienols have the same basic chemical structure characterized by a 16-carbon sidechain attached to the 2-position of a chromane ring (a pyran ring having a benzene ring ortho-fused across positions 2 and 3). The difference between tocopherols and tocotrienol consists of the saturation of the long chain: tocopherols have a fully saturated chain, while tocotrienols have an unsaturated chain. The tocopherols and tocotrienols homologues are named with respect to the position and number of the methyl groups on the phenol ring (Figure 2.1) [71], [72], [73].

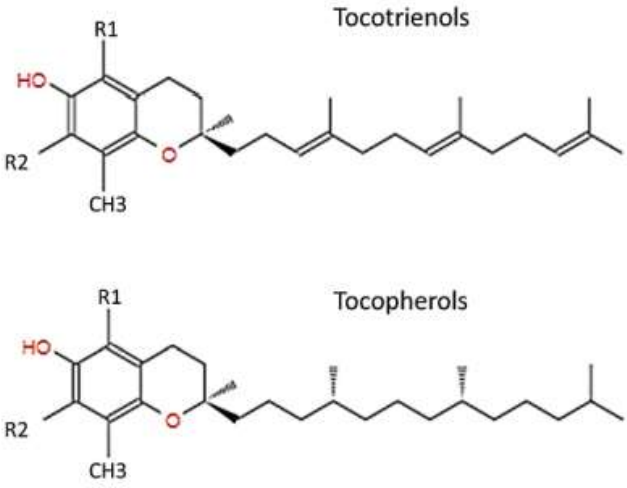

R1	R2	
CH3	CH3	α
CH3	H	β
H	CH3	γ
H	H	δ

Figure 2.1 Structure of tocotrienols and tocopherols

Among all the isoforms of vitamin E, α-tocopherol (αT) is the most abundant in the blood [33], because it is the only one that is absorbed within the body, while the other isoforms are excreted through the intestine. The liver, which takes up nutrients after they are absorbed by the small intestine, absorbs vitamin E thanks to the plasmatic lipoproteins that function as carriers. α-tocopherol is

the only form of vitamin E that is re-secreted through the liver protein of α-tocopherol transfer (αTTP) and distributed to circulating lipoproteins such as low density lipoprotein (LDL).

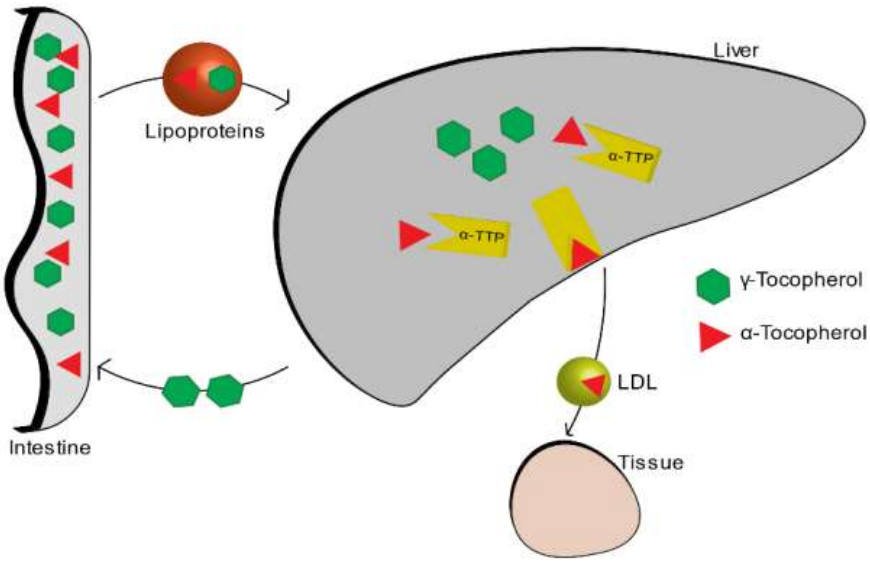

Figure 2.2 Vitamin E metabolism

The other forms are metabolized and then expelled through the intestine (Figure 2.2) [74]. α-tocopherol is liposoluble and since it has a hydroxyl group attached to the ring structure, it is weakly amphiphilic. Thanks to its chemical structure, this compound functions as an effective lipid-soluble antioxidant, protecting cell membranes from peroxidation by scavenging peroxyl, oxygen, and superoxide anion radicals and helping to slow down processes that damage cells. For these reason, α-tocopherol is found at the sites where the free radical production is greatest (the membranes of the mitochondria and endoplasmic reticulum in the heart and lungs for example) [71]. In general, α-tocopherol chemically acts principally as an antioxidant molecule and protects the body from free radicals. Alternative roles of vitamin E, such as modulation of cellular signaling, enzyme activity, and gene expression have recently been proposed. These effects are unrelated to the antioxidant activity of vitamin E and are mostly given by specific interactions with enzymes, structural proteins, lipids, and transcription factors. Among these derived compounds, it is important to devote time to α-tocopherol phosphate, a water soluble form of vitamin E which has gained interest especially after it was found in the plasma and the tissues of animals and humans in a similar amount as α-tocopherol [75].

In the next two paragraphs, we concentrate to explore the biological roles of these two molecules: α-tocopherol and α-tocopheryl phosphate.

2.3 Biological role of α-tocopherol (αT)

α-tocopherol is an example of a phenolic antioxidant. The mechanism of scavenging these molecules consists of the donation of hydrogen from the hydroxyl (-OH) group on the ring structure to free radicals (ROS), which becomes unreactive. After this reaction, also the phenolic compound itself becomes relatively unreactive with a higher stability thanks to the unpaired electron on the oxygen atom which is delocalized into the aromatic ring structure. α-tocopherol is located within the phospholipid membrane of the cell and it occurs with the radical chain embedded in the hydrophobic core of the double layer. Despite its low concentration compared to other membrane lipids, it plays an important role in preserving the integrity of the membrane by preventing lipid peroxidation which causes damage to cellular membranes, lipoproteins, and other molecules that contain lipids, in conditions of oxidative stress [71], [76], [77].

As it is well-known, oxidative stress is a pathological condition caused by the unbalance between the generation and elimination of chemical oxidant species (ROS) and it is involved in several neurodegenerative diseases such as Alzheimer's and Parkinson's disease that are implicated in free radical processes and oxidative damage [78]. Thanks to its important qualities as an antioxidant, α-tocopherol may have an important role in the integrity of the brain. To confirm this, a high level of αTTP was found in the brain [79].

In addition to its chemical anti-ROS action, α-tocopherol is also well known as an important biological anti-inflammatory molecule since it acts on many different factors that affect, directly or indirectly, the immune system. α-tocopherol is able to modulate inflammation in different ways: it affects proinflammatory enzymes such as cyclooxygenase (COX), responsible for prostaglandins (PG)E_2 production [80], [81]. (PG)E_2 is a proinflammatory mediator that has been linked to a variety of age-associated diseases such as cancer, arthritis, and cardiovascular disease [7], [82], [74]. αT modulates the proliferation and activation of certain cells of the immune system such as T cells, lymphocytes, and Natural killer (NK) cells [83]. Finally, αT acts on the secretion of proinflammatory cytokines such as IL-6 and TNF-α. Thanks to these factors, α-tocopherol plays an important role in helping to prevent chronic inflammation [81], [83]. Chronic inflammation is strictly linked to oxidative stress [84] and,

together with it, it is the main cause of age-related diseases and cancer [81].

α-tocopherol has also an important role in the inhibition of platelet aggregation, inhibiting various enzymes such as protein kinase PKC, which is a key signal transduction pathway in several cell types [71], [85]. α-tocopherol has benefits also in dermatology thanks to its free-radical scavenging and anti-inflammatory properties: it protects the skin from various deleterious effects due to UV radiation and accelerates the wound healing process after an injury such as ulcers or burns [86]. Inflammation could be associated also with a large number of different phenomena related to bone health (see Chapter 1): it is thought that thanks to its anti-inflammatory action and regulation of cytokine secretion, α-tocopherol can influence bone remodeling, going to protect the bone against osteoclastic activity, increasing osteoblasts differentiation, and protecting cartilage health [87], [88], [89]. Together with all these considerations, α-tocopherol, due to its antioxidant function, role in anti-inflammatory processes, inhibition of platelet aggregation, and immune system-enhancing activity [1], [9], brings a wide range of benefits from anti-cancer effect [90] to the prevention of disease progression and in improving quality of life in the elderly [91]. The figure below (Figure 2.3) shows a schematic representation of the biological role of α-tocopherol.

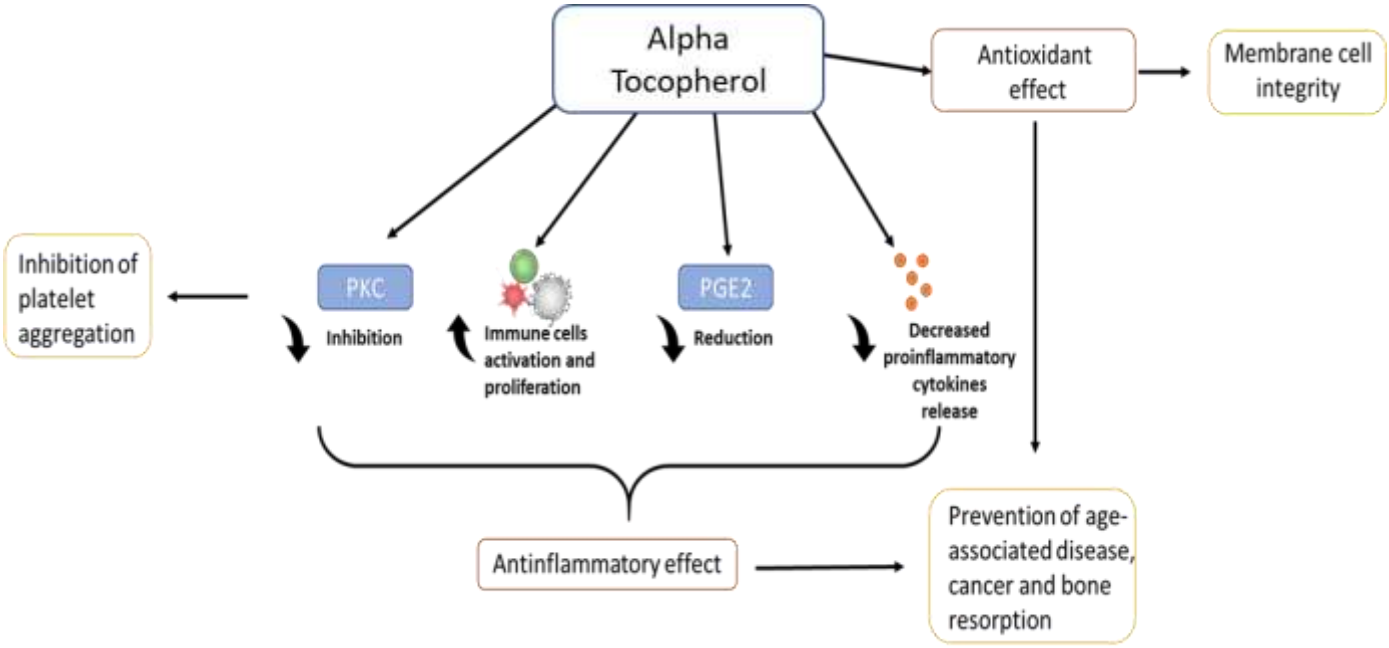

Figure 2.3- Biological role of α-tocopherol

More controversial and still under study, is the anti-bacterial role of α-tocopherol. In the literature, α-tocopherol is used as a natural compound to treat infections caused by specific gram-positive or negative bacteria [92], [93] or as

an antibiotic adjuvant for the treatment of infections [94], [95]. Moreover, the addition of α-tocopherol to materials may have the ability to reduce biofilm formation on the surface. As the literature suggests, it is possible to believe that αT is able to reduce the biofilm formation capacity of a big range of strains (S. aereus and S. epidermidis, etc), without any correlation to the Gram negative or positive group [96]. This, however, comes into opposition with other studies that show instead that α-tocopherol, in combination with other materials, did not reduce biofilm formation [97].

2.3.1 Biological role of α-tocopheryl phosphate (αTP)

As already seen in 2.2, the structures of the αT and αTP differ in the presence of a phosphate group instead of a hydroxyl group on the phenolic ring [98]. αTP was first synthesized and studied in the 1940s, but has only now been re-examined after it was found to be naturally present in food, animals, and human tissues [99], Curiously, the isolation and purification methods used for α-tocopherol, which were used extensively even then, are not the same for the phosphorylated molecule, so that it remained "hidden" for a long time and was only recently discovered [98]. To support this hypothesis, the enzymes αT kinase and αTP phosphatase, which are capable to phosphorylate αT to αTP as well as the reverse reaction (hydroxylation), have been discovered in cells and tissues (Figure 2.4.).

The balance between the two enzymes aims to maintain cellular homeostasis or its inter-conversion may have some cellular signaling functions [100]. Thanks to the presence of these enzymes, α-tocopheryl phosphate can be considered to be a pro-vitamin as it is hydrolysed and distributed in the body as the natural αT [101]. αT is present in the human tissues and, even if still under studies, several functions and activities have been suggested for this molecule, such as modulating signal transduction and gene expression, [100] reducing cell proliferation, the anti-inflammatory effect [102] and even stimulus for angiogenesis and vasculogenesis [101]. In contrast to α-tocopherol, αTP does not have a chemical antioxidant activity per se because the OH group, which is essential for the scavenging of free radicals by α-tocopherol, is phosphorylated [103].

Despite this, however, αTP acts as an antioxidant indirectly because of its chemical structure. In fact, having a negatively charged polar head it is able to bind to the cell membrane with its apolar tail in the middle of the lipid membrane, thus preventing the propagation of free radicals either directly or by interfering in their generation at the enzymatic level [104]. In addition, the antioxidant capacity of α-tocopheryl phosphate may be related to the fact that the molecule converts to α-tocopherol within the tissue, thus providing antioxidant protection [105].

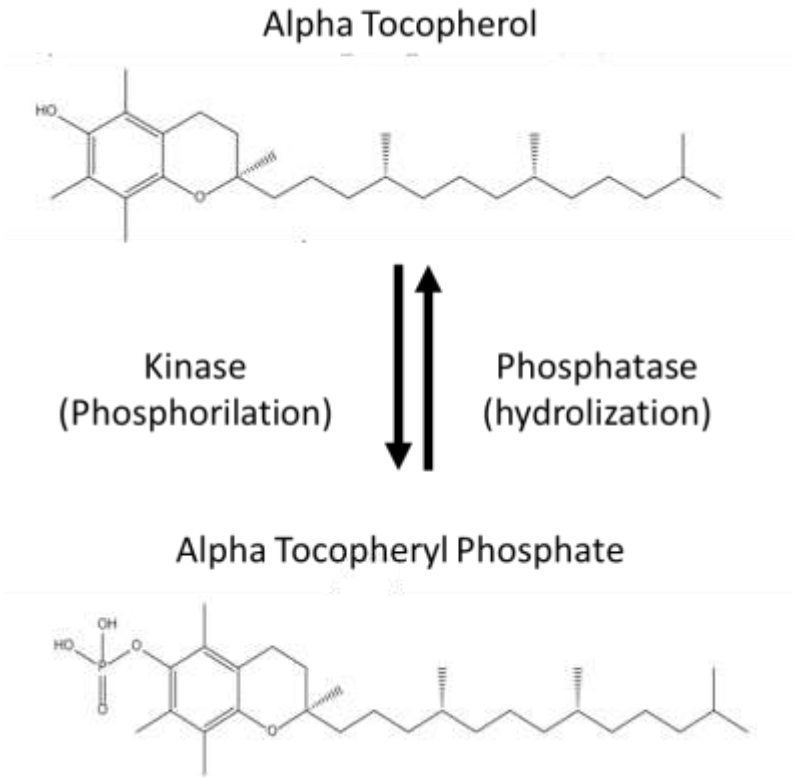

Figure 2.4 Scheme of α-tocopherol phosphorylation

Regarding the antibacterial properties of α-tocopheryl phosphate, further research is needed for a better understanding, as there are not as many papers in the literature analyzing the antibacterial ability of this molecule, compared to α-tocopherol. Few studies are found that claim α-tocopheryl phosphate to have good antibacterial activity against Streptococcus oralis, Streptococcus mutans [106], S.Aureus, and S.Epidermidis [107]

Once the biological role of Vitamin E is understood, it is certainly interesting to analyse its application and detection methods when combined with a biomaterial.

2.4 Biomedical applications of Vitamin E

Vitamin E is being researched as a molecule incorporated or used as a coating on prosthetic materials with the aim of creating implants with additional properties.

2.4.1 Vitamin E in prosthetic implants

Vitamin E in blend form of through bulk diffusion

So far, the use as an antioxidant to stabilize UHWMPE has been the most successful application of α-tocopherol, which has made vitamin E very well known as a useful compound in the biomedical field. Until the late 1990s, before implantation, UHWMPE inserts were sterilized with gamma rays. Unfortunately, this type of sterilization carried out a major oxidative problem for the polymer, since the radiation increases the possibility of oxidative degradation, making it more unstable and fragile, leading to severe implant loosening phenomena [25, 27]. The incorporation into the polymer of antioxidants such as tocopherols was useful to overcome this problem. This idea was born from the use of vitamin E in food packaging industries as an antioxidant of polyolefins [109]. For the incorporation phase, α-tocopherol is typically inserted into the material before sterilization in two ways, before (creating the VE-UHMWPE blend) or after crosslinking irradiation (through bulk diffusion) [110][111][112]. The success of this type of incorporation is guaranteed by the very good biocompatibility of vitamin E which has been proven not to have cytotoxic effects [25] After the well-known success of the use of α-tocopherol combined with UHWMPE, new combinations with other biomaterials have been pursued and are still under study.

Vitamin E as a coating

One of the most common concerns of biomedical implants is the problem of joint replacement because of loosening. Causes of failure include infections and wear, which could cause chronic inflammation by the presence of debris originating in the articular part of the prosthesis. A coating able to have an anti-inflammatory and antibacterial action can certainly help to reduce these events, consequently reducing the phenomena of septic or aseptic loosening of the prostheses. For this reason, although still in the research phase, some works suggest the use of vitamin E for coating metal surfaces with the aim of providing anti-bacterial and anti-inflammatory properties or of helping osseointegration [107], [113]–[115]. These studies employed pure titanium as a substrate, which is a biomaterial commonly used in dental, cranial, and joint implants. As later shown in Table 2.1, the coatings are created by the adsorption of vitamin E on the metal surfaces by leaving the surfaces in the vitamin solution. Given the high hydrophobicity of vitamin E, in all cases the solvent used during the coating formation is ethanol. Then, the biological response (*in vitro* and *in vivo*) of the titanium implants coated with vitamin E has been evaluated. Bidossi et al. made interesting studies on the antimicrobial activity of two different forms of vitamin E: α-tocopherol acetate and α-tocopherol phosphate, derived from the esterification of α-tocopherol with the acetate group and the phosphate group, respectively. It was found that especially tocopherol phosphate is anti-microbial against both gram positive and gram negative and it also has the ability to stimulate osteoblasts, finding many applications in the implant field [31], [34]. Maria Satuè et al. used vitamin E as a chemical antioxidant that protects the 7-DHC molecule; this molecule is activated during UV irradiation becoming a precursor of vitamin D and it is employed as a coating on titanium [33], [34].

Table 2.1 Vitamin E in Prosthetic devices and biomaterials

Material	Molecule	Combination	Method of combination	Results	Application	Ref.
UHWMPE	αT	Blending	1: Blending of vitamin E with UHMWPE resin powder and following irradiation for crosslinking	Vitamin E is able to prevent oxidation during gamma sterilization of UHWMPE.	Material stabilizer	[110],[111],[112]
			2: Vitamin E is diffused into an already crosslinked UHWMPE			
Pure Titanium	αT+ 7-DHC	Coating	Preparation of a solution of 7-DHC+Tocopherol (1:1) in ethanol 10 µl of the prepared solution left on the surface and further UV-irradiated and incubate for 48h at 23°C	Vitamin E is able to protect 7-DHC from oxidation during UV-irradiation vitamin E helps osseointegration of the coated samples both in vivo and in vitro.	Molecule stabilizer	[113], [114]
	αT Acetate	Coating	Spreading of the solution of αT Acetate in ethanol (500mg/ml) on a sandblasted disk of titanium.	Low anti-microbial activity shown in vitro apart against S. aureus and S. epidermidis.	Coating for implants in order to prevent implant-associated infections	[107]
	αTP	Coating	Spreading of a solution of αT Acetate in ethanol (500mg/ml) on a sandblasted disk of titanium.	Good anti-microbial activity shown in vitro against every strain (S. aureus, S. epidermidis, P. aeruginosa, and P.acnes). Good bone stimulation shown in vivo.	Coatings for dental implants in order to prevent implant-associated infections and help osseointegration	[107], [115]

2.4.2 Vitamin E in tissue engineering

Thanks to its antioxidant and anti-inflammatory ability, α-tocopherol has become an interesting object of research in the world of wound healing and tissue regeneration. In the literature, vitamin E is found combined, encapsulated or blended, with different types of polymeric materials treated either as scaffolds, hydrogels, or films.

Vitamin E in wound healing

Wound healing is an important physiological process to maintain the integrity of the skin after trauma. Wound healing involves several phases: hemostasis, inflammation, proliferation, and maturation [116], [117]. Vitamin E is harnessed to aid the healing process by creating a wound dressing with other polymers that provide the physical structure, and with which it can have a synergistic effect to enhance skin regeneration.

For complete skin regeneration, the preferred dressing structures are hydrogels and scaffolds, as they are three-dimensional and facilitate cell attachment and growth. In the biomedical field, from tissue engineering to drug delivery, biopolymers commonly used are biodegradable polyesters, especially poly-e-caprolactone (PCL), poly(lactide) (PLA), and poly(lactide-co-glicolide) aci(PLGA). These materials ensure biocompatibility, biodegradability, and good mechanical performance. Polysaccharides, including chitosan, hyaluronic acid, and cellulose, in addition to having good biocompatibility and many hydrolysable groups, also have a structure that mimics the extracellular matrix (ECM). Chitosan hydrogel is an example of a perfect biomaterial for wound dressing, in fact, Arian Ehterami et al. prepared and tested chitosan/alginate hydrogel loaded with vitamin E- for dorsal skin wound healing in a rat model that ensured epidermal cell proliferation with even a new generation of hair follicles, promising successful wound healing [118]. As mentioned, scaffolds are widely used for this purpose. However, the use of polyesters, typically with better mechanical performance than polysaccharides, may not provide a favourable surface for cell attachment.Chinnasamy Gandhimathi et al. produced PLA-PCL nanofiber scaffolds, through electrospinning, and incorporated silk fibroin to enhance cell adhesion and vitamin E to provide a low-stress environment for cells. The created scaffolds were able to induce fibroblast

proliferation and collagen secretion [119].

Saba Zahid et al. instead thought of using the two biomaterials (PLA and PCL), but for obtaining two layers, one of porous PCL and the other one of PLA film incorporating vitamin E, in this way, they were able to obtain a bi-layer of electrospun nanofibers that supports cell proliferation and also angiogenesis [120]. Instead, polysaccharide scaffolds do not present the above problem: electrospun cellulose acetate mats loaded with vitamin E prove effective for dermal therapy due to greater flexibility, and good vitamin E release kinetics [121].

In addition to three-dimensional structures, polymeric films can be more easily obtained to aid wound healing. Gabriela Garrastazu Pereira et al. selected two polysaccharides, hyaluronic acid, and sodium alginate to create a polymeric film loaded with vitamin E acetate and Aloe Vera, characterizing it both mechanically and chemically [122]. Similarly, Sonia Trombino et Al. prepared a collagen film esterified with α-tocopherol (collagen α-tocopherulate) for wound healing applications, exploiting the antioxidant capacity of the molecule [123].

Vitamin E in tissue repair

Tissue repair refers to the compensatory regeneration of tissue, resulting in the restoration of the tissue structure and function. Tissues can be repaired by implanting structures, preferably three-dimensional such as scaffolds, that are able to stimulate cell proliferation and adhesion for complete tissue regeneration [124]. In this context, the same materials already described are used, which can support the new tissue both mechanically and at the cellular level.

Generally, polymers with high mechanical properties are used for hard tissues, while a high mechanical performance is not required for soft tissues such as the cardiac one.

For example, Poly(3-hydroxybutyrate) (P(3HB)) and bioactive glasses show to have favourable properties for hard tissue regeneration. Superb K. Misra et al. created a Poly(3-hydroxybutyrate) (P(3HB))/bioactive glass scaffold, adding vitamin E as an antioxidant capable to enhance protein adsorption [125]. Instead, contrary to what they expected, Filippo Renò et al. prepared a PLA films blended with vitamin E which induce a reduction in osteoblast cell attachment and spreading [126]. This research team has published many works on these films. Their studies reveal that vitamin E confers important characteristics to the PLA surface: anti-adhesion for bacteria, increased hydrophilicity and therefore higher protein adsorption, and anti-adhesion for osteoblasts obtaining a new type of polymer that can be used in tissue engineering with several biological effects. [126]–[128]. Besides a biological role, vitamin E also has a role in sustaining and adhering to two different materials: Iulian Antoniac et al. created PLA-Mg composites as filament for biomedical applications and used vitamin E to enhance the adhesion between magnesium and PLA [129]. Instead, Zahra Mahdieh et al. employed vitamin E to protect starch, a biodegradable polysaccharide with low mechanical performance, from oxidation during the blending process at elevated temperatures [130].

For soft tissues, Youyang Qu et al. prepared α-tocopherol liposome loaded in chitosan hydrogel. α-tocopherol was entrapped in a liposomal carrier, and the liposome was formulated into a chitosan-based hydrogel, with the aim of creating injectable engineered cardiac tissue capable of suppressing oxidative stress in the microenvironment, supporting and surviving cardiomyocytes [131]. Due to the hydrophobic nature of vitamin E, it is difficult to insert it into polymers that are typically hydrophilic because they need to be hydrolysable. Table 2.2 reports more in detail methods of loading vitamin E in different biomaterials for tissue engineering applications and each biological response. As it can be seen, vitamin E can be inserted within the dressing in 2 ways: directly through the solution, creating a homogenous mixture, which is then electrospinned, gelled or polymerized, or inserted within nanocarriers that are then in turn inserted within the biomaterial.

Table 2.2 Vitamin E in Tissue Engineering

Polymer Class	Polymer Name	Molecule	Structure	Method loading	Biological Response	Role of Vitamin E	Applications	Ref
Polysaccharides	Chitosan/ Alginate	αT	Hydrogel	Addition of a specified concentration of vitamin E to the already prepared chitosan/alginate solution, mixing the solution for 1 hour, addition of $CaCl_2$ to crosslink alginate and chitosan	High cell proliferation shown in vitro Acceleration of wound healing shown in vitro	Antioxidant and antinflammatory, wound healing capacity	Wound treatment	[118]
	Chitosan	αT	Hydrogel	Preparation of liposomes by thin-film hydration method, using a solution of αT, egg lectin, cholesterol, and sodium deoxycholate in ethanol. Prepared liposomes were then added into a prepared chitosan hydrogel, mixing in an ice bath.	Hydrogel improves cardiomyocytes adhesion and growth protect them from oxidative stress	Antioxidant	Cardiac tissue engineering	[131]
	cellulose acetate (CA)	αT + Vitamin A	Nanofiber scaffold	Dissolution of a specified concentration of Vitamin E or Vitamin A and CA in an acetone/DMAc mixture. Electrospinning of the prepared solution.	Not reported	Antioxidant	Wound treatment	[121]
	Hyaluronic Acid (HA)/Alginate	αT acetate + Aloe Vera	Polymeric film	Starting from 2 solutions: 1) Alginate and hyaluronate, Aloe Vera and vitamin E. 2) PEO and PVA in water. Solutions 1 and 2 were mixed to obtain homogenous mixture	Not reported	Antioxidant and antinflammatory, wound healing capacity	Wound treatment	[122]
	Starch	αT+ nanoforsterite	Scaffold	EVOH, Vitamin E, and nanoforsterite are added in a starch solution. Blending occurs after extrusion at high temperature.	Good fibroblast adhesion, High simulated body fluid (SBF) deposition,	Antioxidant to protect the polymer from oxidation during the manufacturing process.	Bone tissue engineering	[130]
	Collagen	αT	Film	Before functionalization collagen were covalently linked to the resin in order to protect terminal amino-group, to increase bioavailability. After that, functionalization was carried on adding α-Toc in collagen solution at room T for 72h.	Collagen esterified with α-tocopherol have protective activity against free radicals in rat liver microsomal membranes.	Antioxidant	Wound treatment	[123]

Polymer Class	Polymer Name	Molecule	Structure	Method loading	Biological Response	Role of Vitamin E	Applications	Ref
Polyesters	PLA-Mg	αT	Filaments	Addition of Vitamin E in a PLA-Mg solution before the extrusion process and following 3D printing of the implant	Not reported	It enhances adhesion between Mg particles and PLA	Implant devices	[129]
	PLA	αT	Polymeric film	Addition of Vitamin E into the PLA/ chloroform solution. Shaking the solution with the following addition of it in glass dishes. Evaporation of the solvent in dark conditions at room temperature.	The film has good protein adsorption and, inhibits osteoblasts, bacterial and platelets adhesion, and spreading.	Protein adsorption Antioxidant	Tissue engineering	[126]–[128]
	PLA-CL	αT, Silk Fibroin (SF), Curcumin (C)	Nanofiber scaffold	Preparation of a solution with PLACL, SF, C, and αT in HFIP. Electrospinning of the prepared solution.	The scaffold induces fibroblast proliferation/attachment and it stimulates collagen secretion.	Antioxidant, anti-inflammatory, and wound healing capacity	Wound treatment	[119]
	PLA and PCL	αT acetate	Bilayer nanofiber scaffold	Preparation of a solution with PCL PLA and Vitamin E in DCM. Electrospinning of the prepared solution.	The scaffold induces angiogenesis and cell proliferation	Antioxidant, anti-inflammatory, and wound healing capacity	Wound treatment	[120]
	P(3HB)/Bioglass	Vitamin E	Foam scaffold	Incorporation of the appropriate amounts of vitamin E and MWCNTs into the polymer solution. Sonication of the mixture before impregnating it into the preforms.	The scaffold has good biocompatibility, good protein adsorption, stimulates cell proliferation, and allows vascularization.	Protein adsorption Antioxidant	Bone tissue engineering	[125]

2.4.3 Vitamin E in drug delivery

Vitamin E as a drug

Nowadays, vitamin E has also gained particular importance due to its proven anti-carcinogenic activities, which lead it to be an interesting candidate as an adjuvant anti-cancer treatment drug or as a preventive drug. In fact, its preventive properties were discovered according to research that showed that the Mediterranean diet, known to be rich in antioxidants such as vitamins C and E, has a protective effect from certain cancers, like colon cancer [90], [132]. As the literature suggests, γ- and δ-tocopherol are more potent inducers of apoptosis than β- and α-tocopherols; in fact, despite its antioxidant power, it would seem that α-tocopherol is not cytotoxic against cancer cells [133]. In particular, among all the various forms of vitamin E, tocotrienols appear to have a stronger anti-proliferative and proapoptotic effect than tocopherols [134].

Due to its lipophilicity, vitamin E is able to cross the cell membrane but, given its insolubility in water, its bioavailability is limited. In fact, the biological mechanism of digestion of vitamin E occurs through emulsion into lipid droplets. The emulsion allows vitamin E to be transported (through micelles or vesicles) and thus to be absorbed by diffusion by the various target tissues [135], [136]. For this reason, methods to encapsulate vitamin E for use in drug delivery have been studied in the literature, using various materials such as synthetic polymers or biopolymers and different delivery systems: hydrogel, micro and nano-particles, liposomes and nano-emulsions (Table 2.3).

In literature, chitosan is widely explored as a drug delivery system to load α-tocopherol: the water solubility of chitosan is exploited to increase the bioavailability of α-tocopherol.

Majid Naghibzadeh et al. developed chitosan nanoparticles with α-tocopherol loaded by dispersing chitosan in water and dripping a solution of ethanol and α-tocopherol. The nanoparticles are obtained by placing the mixtures in an ice bath and sonicated using the ultrasonic probe [137]. With a similar approach, J. Nam et al. created a chitosan-specific micelle for tocopherol and doxorubicin delivery by grafting with a targeting ligand (anti-HER2/neu-polyethylene glycol [PEG] peptide) with the goal of having a synergistic anti-cancer effect of TP and DOX and site-specific drug delivery [138]. So, chitosan is a good biomaterial that can encapsulate tocopherol by O/W emulsion either on its own or with the help of other polymers such as zein, an amphiphilic protein found in corn, which helps create a stronger polymeric complex with chitosan. In fact, Yangchao Luo et al.

prepared and characterized the nanoparticles by first preparing a solution in ethanol of zein and tocopherol and then placing it in another solution of chitosan and acetic acid. [139].

In addition to chitosan, PCL was also investigated for drug delivery systems. Similar to that mentioned about chitosan, PCL nanoparticles loaded with tocopherol were made into O/W emulsion with successive ultrasonication methods to optimize encapsulation. Youngjae Byun, et al. formulate and characterize PCL nanoparticles loaded with tocopherol, using PCL dissolved in methylene chloride with tocopherol as an organic phase and PVA dissolved in PBS as an aqueous phase, with a subsequent ultrasonication in an ice bath [140]. Instead, Catherine Charcosset et Al. created PCL nanocapsule, using PCL dissolved in acetone with tocopherol as an organic phase and TWEEN 20 dissolved in water as an aqueous phase [141].

Another important biopolymer used in drug delivery is hyaluronic acid, a hydrophilic gel, which could be used also to enhance the water solubility of α-tocopherol. Parveen Singh et al. created a hyaluronic-acid-based β-cyclodextrin grafted copolymer to encapsulate vitamin E [142].

Moving to another area, polymeric nanoparticles obtained from thermosensitive materials received great attention in the encapsulation and controlled release of drugs. Cirley Quintero et al. has presented preparation and characterization of thermosensitive α-tocopherol-loaded polymer nanoparticles, with the shell obtained by the triblock copolymers PNIPAM-b-PCL-b-PNIPAM. The preparation of α-tocopherol loaded nanoparticles is based on the dissolution of α-tocopherol and of the corresponding copolymer in acetone, and subsequent dropping in an aqueous solution at pH 5 [143]. Likewise, Behrouz Mohammadi et al. have successfully nano-encapsulated vitamin E in stearic acid-lauric acid (SA-LA) in the form of a core-shell structure for thermo-sensitive drug delivery purpose. The synthesis process involves always the O/W emulsion with SA-LA and α-tocopherol as an organic phase and PVA, PVP, Sodium SLS as an aqueous phase [144].

From what has been said so far, we can see that in the literature typically vitamin E is encapsulated within polymeric nanoparticles. There are also cases where α-tocopherol is functionalized on metal nanoparticles such as gold, to increase the scavenging ability of the latter, for biological applications [145][146].

Vitamin E as a delivery system

Most of the approved anti-cancer drugs, such as paclitaxel, docetaxel, etc. are lipophilic, which renders it challenging for their bioavailability and thus for their uptake by the target tissues [147].

Although tocopherols and tocotrienols have a nearly amphiphilic structure, the hydrophilic part of the tocols, characterized by the hydroxyl group (-OH), is too small to spontaneously self-assemble into a micellar structure. Conversion of the phenolic component of the vitamin E to esters using acetic or succinic acid is often performed to expand the hydrophilic part and optimize the amphiphilic structure, thus creating more stable esterified compounds that can be easily used for drug delivery, such as α-tocopheryl ether-linked acetic acid (αTEA) or α-tocopherol succinate (αTOS), also discovered to be potent anti-cancer agents [133],[148],[149]. The esterification of α-tocopherol succinate (α-TOS) with polyethylene glycol (PEG) forms a new compound, D- α-tocopheryl polyethylene glycol succinate (TPGS), widely used today in drug delivery as a non-ionic surfactant and micellar stabilizer, capable of forming micelles in water at a concentration as low as 0.02 wt%. This new amphiphilic polymer has several advantages given by the physicochemical properties of PEG and vitamin E, such as high biocompatibility, improved cellular uptake of the drug and anti-tumor activity, which allowed it to be approved by the FDA as a safe adjuvant [61-63]. TPGS is widely used as surfactant and permeation enhancer (reviewed in [61]), as prodrug carrier (reviewed in [151]) and also as a copolymer with other biopolymers such as PLA and PLGA or PCL (reviewed in [152]) [153].
Another interesting synthetic polymer is formed by the esterification of α-tocopherol succinate with the glucosidic polymer, inulin (INU), creating amphiphilic compounds obtained based on inulin with hydrolyzable groups, and with a vitamin E-based radical chain, called INVITE. This novel INU-based polymer easily self-assembles into nanocarriers, thus it has been envisioned as a novel drug delivery system for the therapy of different diseases.

Delia Mandracchia et al. developed and characterized INVITE micelles, which have stability in water, low size (about 50 nm), used in different diseases, for different targets. Due to the renal passive targeting ability of inulin, INVITE results as a good candidate for drug delivery systems for target tissues such as the urinary tract [154]. It has also been tested with good results for delivery of celecoxib to the intestinal site against Caco-2 cells,[155] conjugated with several other molecules such as biotin and succinic anhydride, creating INVITEBIO and INVITESA, respectively[156][157] and loaded with

curcumin, creating INVITE C, for the treatment of diabetic retinopathy or neurodegenerative diseases [158][159]. Through the esterification of α-tocopherol succinate with hyaluronic acid, a novel amphiphilic compound was created for the tumor-targeted delivery system, exploiting the known ability of hyaluronic acid to bind to the membrane receptor CD44, a protein overexpressed by tumor cells. The created polymer's name is HA-VES and was used by Jinling Wang et al. for the release of the anti-cancer agent Doxorubicin [160].

As we can observe in Figure 2.5, vitamin E is typically bound to other biomolecules that increase amphiphilicity and optimize the drug delivery system. In contrast, Khushwinder Kaur et al. have succeeded in creating nanoparticles of pure α-tocopherol. The work suggests a method that involves an emulsion of the components with water:surfactant:oil ratio where the organic phase consists of a first surfactant TWEEN 80 and tocopherol in ethanol and the aqueous phase is water containing a second surfactant (SSL). Through this method, they were able to create stable nanoparticles for the encapsulation of curcumin as an antioxidant and benzylisothiocyanate as an anti-cancer agent [161].

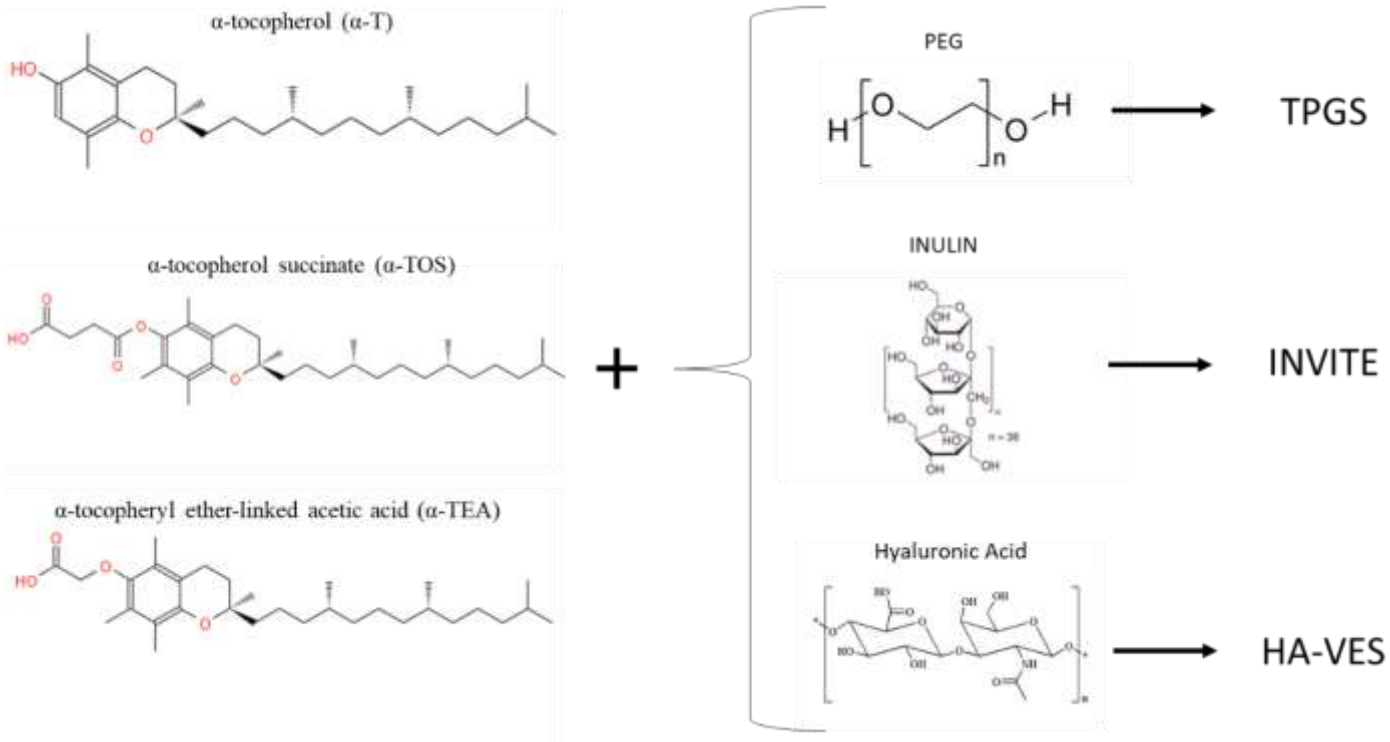

Figure 2.5 Chemical structure of different forms of vitamin E used for drug delivery systems

2.5 Methods to detect Vitamin E within materials

Vitamin E can be easily detected in different liquid media, such as in oils, serum, human milk, foods, etc. by different methods including high-performance liquid chromatography (HPLC), FTIR, RAMAN and UV-VIS spectroscopy and spectrophotometric methods. Recently, some protocols were also developed for the analysis of vitamin E incorporated into cosmetics and food packaging.

The first method usually used to allow a simple and rapid quantitative determination of α-tocopherol is HPLC. In fact, HPLC is one of the most powerful tools for the determination of fat-soluble vitamins and has been widely used for their separation and detection; different detectors can be used for vitamins such as UV-VIS, fluorescence, and mass spectrometry. In the case of vitamin E, typically the HPLC column is connected to a UV absorbance detector as the compound absorbs the ultraviolet light, particularly around 290 nm. This method is, in fact, used not only to quantitatively analyse the content of α-tocopherol in food or beverages but also in cosmetics and biological samples including human plasma and human milk [162], [163], [164], [165], [166]. Thanks to its clear absorbance peak at 290 nm, visible ultraviolet spectroscopy (UV-Vis) proved to be able to detect the presence of vitamin E even at low concentrations [167], [168].

Another way to detect α-tocopherol is FTIR. Sandra et Al. developed a rapid methodology for the analysis of α-tocopherol in vegetable oils, using FTIR-ATR as an alternative to the HPLC methods. By analyzing thirteen vegetable oils with a known content of vitamin E, a research team created a calibration curve which was then used to quantitatively measure the α-tocopherol content of the vegetable oils concerned [169]. FTIR was also used for detecting the functional groups of a hydrophobic film of vitamin E deposited on a copper substrate [170]. Along with FTIR, RAMAN is a potential alternative to HPLC methods, used to detect vitamin E in oil-water emulsions and biological samples [171], [172]. Surface-enhanced Raman spectroscopy (SERS) technology is of a high level of interest: it exploits the amplification of Raman diffusion by molecules adsorbed on a metal or metallic nanoparticles [173], [174]. Typically, most SERS techniques use metal aqueous colloids as a substrate and require that compounds to be analysed are water soluble. For water insoluble analytes, such as vitamin E, the matter is more complicated. Given the disadvantage of using colloidal Ag

nanoparticles to directly measure SERS of the analyte, Tiantian Cai et al. have successfully tried other methods to analyse vitamin E: after dissolving the compound in chloroform, the solution obtained is dripped onto the surface of a metal substrate with surface Raman activity. Another method could be to directly immerse the metal substrate in the sample solution containing vitamin E, to extract it after a certain time, and to measure it at RAMAN after the solvent has evaporated [175].

Thanks to its antioxidant properties, vitamin E can also be analysed through all those methods that exploit chemical reactions, typically redox, to develop coloured compounds that are then measured spectrophotometrically. In general, spectrophotometric methods for the determination of vitamin E use the easy oxidation of the aromatic ring of α-tocopherol to the corresponding quinone, creating tocopheryl quinone, by means of oxidising agents that finally give coloured products.

Among these methods, there is definitely the spectrophotometric assay, which uses the 1,1-diphenyl-2-picrylhydrazyl (DPPH)-2,2-diphenyl-1-picrylhydrazyl as a free radical of purple colour, which discolours when it reacts with vitamin E. Valeria M. et Al. have used the DPPH method to compare the antioxidant power of drugs containing α-tocopherol. The problem with the DPPH method is its low reproducibility due to the low stability of the radical [176].

Another such methodology is the Folin&Ciocâlteu (FC) reagent in an aqueous solution. In this case, however, given the insolubility of vitamin E in water, this methodology is not the optimal one. However, modifications have been made to the FC method to simultaneously enable the measurement of lipophilic and hydrophilic antioxidants [177].

There are many other methods using different oxidizing reagents such as Fe(III)-bathophenanthroline, Cu(II)-neocuproine, or silver nitrate, but they require a rigid control of the conditions for precise results [178]. Another method is the Emmerie and Engel colour reaction with ferric chloride: it is a precise and easy to perform the reaction, and therefore the approach of choice for a routine clinical laboratory [179].

Similarly, nitric acid can be used in a very simple way. A solution of nitric acid in ethanol is able to oxidize α-tocopherol forming the coloured red o-quinone which can be detected spectrophotometrically (Figure 2.6) [180].

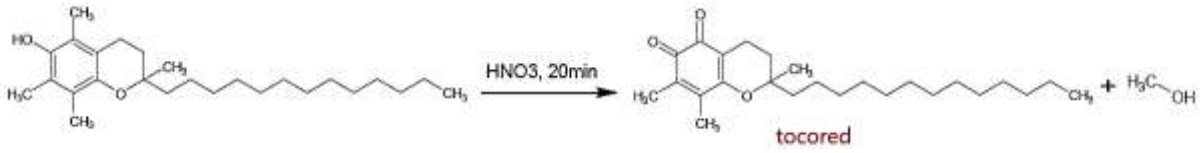

Figure 2.6 Formation of Tocored with Nitric Acid

Thanks to the vitamin E detection methods employed in various applications involving cosmetics, food packaging, and so on, it is possible to apply the above methods to the biomedical field for the detection of vitamin E when combined with different biomaterials.

Certainly, it is easy to find detection methods in the literature when vitamin E is combined with UHWMPE, as it is the most widely applied biomaterial coupled with vitamin E. With HPLC analysis, it is convenient to quantify the vitamin E content within UHMWPE, using a calibration curve produced from the areas of the HPLC peaks [181]. Instead, J. Hufen et Al.. developed an accurate method to detect the α-tocopherol content in UHWMPE using HPLC analysis to separate it and determine its concentration by UV-Vis spectroscopy, with a corresponding calibration curve [182]. However, it is also possible to use only UV-Vis in absorbance mode combined with FTIR to quantify vitamin E within UHMWPE [183]. Vitamin E blended with polyethylene induces yellowing of the sample, Martínez-Morlanes et al. exploited this characteristic using the colorimetric technique and reflectance spectroscopy, to detect the amount of vitamin E incorporated in polyethylene samples [184]. These types of methods especially HPLC are also used in drug delivery to calculate the drug encapsulation efficiency, resulting in the quantification of the vitamin E encapsulated within polymeric nanoparticles [140][142][143]. With the same object, HPLC is used in tissue engineering to quantify the vitamin E content inside the matrices or scaffolds [122], [185].

Since vitamin E is an extremely hydrophobic molecule, another important way to detect the presence of tocopherol on different substrates is definitely the measurement of the contact angle, the quickest test to evaluate a surface modification [186]. Filippo Renò et al. used the contact angle measurement on PLA blended with Vitamin E, and they discovered that the enriched with vitamin E was more easily wetted [126], [127], [48].

To get a more in-depth understanding of the chemical bonds between the substrate and the deposited molecule, the XPS technique is useful, as in the case of Elena Stoleru et al. who used XPS to have information about the bond between chitosan and vitamin E of the chitosan/vitamin E coating deposited on

a polyethylene substrate [186].

Once the characteristic peaks of vitamin E are known, the FTIR analysis is helpful, not only to detect vitamin E [120], but also to analyse the eventual shifts in the wavenumber of the peaks that denote an interaction between tocopherol and the combined biomaterials. Ahmad Salawi et Al. used the FTIR technique to analyse the interaction between a new copolymer called Soluplus and α-tocopherol for wound healing application [187], and Joana T. Martins et al. studied the physiochemical effect of the incorporation of a-tocopherol in chitosan-based films through different analysis including FTIR [188].

In the biomedical field, the DPPH test is used to analyse the radical scavenging ability of vitamin E combined with biomaterials, as Elena Stoleru et al. did on a film electrosprayed with a chitosan/vitamin E formulation [186]. DPPH was used also by Zhou Nier et al. to test the antioxidant activity of Au nanoparticles functionalized with Trolox (hydrophilic analog of α-tocopherol) [145][146].

The table (Table 2.3) reports the characterization methods used to detect vitamin E when combined with different biomaterials.

Table 2.3 Methods to detect Vitamin E

Technique	Combined Material	Molecule detected	Method	Information	Ref.
HPLC	UHWMPE	α-Tocopherol	HPLC connected to UV/Vis diode array detector at 297nm, construction of calibration curve of HPLC peak area.	Quantitative	[181]
	UHWMPE	α-Tocopherol	HPLC connected to UV/Vis diode array detector, construction of calibration curve of absorbance peak area at 290 nm.	Quantitative	[182]
	Collagen mesh	α-Tocopherol	HPLC connected to a fluorescence detector, detection at excitation wavelength of 290 nm and emission wave- length of 330 nm	Quantitative	[185]
	Alginate and hyaluronate film	α-Tocopherol acetate	HPLC connected to UV/Vis diode array detector, construction of calibration curve of absorbance peak area at 285 nm.	Quantitative	[122]
	Hyaluronic-acid-based β-cyclodextrin copolymer	α-Tocopherol	HPLC connected to UV/Vis diode array detector	Quantitative	[142]
	PNIPAM-b-PCL-b-PNIPAM copolymer	α-Tocopherol	HPLC equipped with a differential refraction index detector	Quantitative	[143]
	UHWMPE	α-Tocopherol	Construction of calibration curve of absorbance peak area at 290nm	Quantitative	[183]
UV-VIS	UHWMPE	α-Tocopherol	Analysis of reflectance spectra which presents a minimum around 290 nm and a decrease of reflectance at 400-500 nm.	Detection	[184]
	Hyaluronic acid	α- Tocopherol succinate	Construction of calibration curve of absorbance peak area at 285nm	Quantitative	[189]
	PLA+PCL	α-Tocopherol acetate	Construction of calibration curve of absorbance peak area at 284nm	Quantitative	[120]
Colorimetric Assay	UHWMPE	α-Tocopherol	The yellowing of the sample were analysed through three parameters (a,b,L) of CIELAB colour space, and a calibration curve of colour distances were constructed.	Quantitative	[184]
FTIR-ATR	UHWMPE	α-Tocopherol	Analysis of peaks. For quantitative analysis, calibration curve of these peaks is needed.	Analysis of Vitamin E transformation products in polymer samples prior to extraction and quantitative.	[181]
	Collagen	α-Tocopherol	Analysis of main peaks	Characterization of film	[123]

Technique	Combined Material	Molecule detected	Method	Information	Ref.
FTIR-ATR	Magnetite	α-Tocopheryl succinate	Analysis of main peaks	Characterization of chemically modification of nanoparticles	[149]
	Chitosan	α-Tocopherol	Analysis of peaks	Physical bonds and chemical interactions are reflected by changes in characteristic spectral peaks.	[188]
	Chitosan	α-Tocopherol	Analysis of peaks	Characterization of nanoparticles	[137]
	PCL/PLA	α-Tocopherol acetate	Analysis of peaks	Characterization of membranes	[120]
	Soluplus	α-Tocopherol	Analysis of peaks	Analysis of bonding between Soluplus/Vitamin E	[187]
XPS	Polyethylene	α-Tocopherol	Analysis of peaks from 600–4000 cm−1	Analysis of interaction between vitamin E and chitosan	[186]
	Polyethylene	α-Tocopherol	All binding energies were referenced to the C1s peak at 285 eV.	Analysis of covalent bonding	[186]
DPPH	Polyethylene	α-Tocopherol	The scavenging activity was estimated RSA (%) = (1 – (A sample/Acontrol)) × 100, measuring the adsorption at 515 nm after 30 min in dark condition.	Radical scavenging activity evaluation	[186]
	Chitosan	α-Tocopherol	The scavenging activity was estimated RSA (%) = (1 – (A sample/Acontrol)) × 100, measuring the adsorption at 517 nm after 30 min in dark condition.	Radical scavenging activity evaluation	[188]
	Collagen/chitosan	α-Tocopherol	DPPH were measured bu the adsorption at 517 nm after 30 min in dark condition. DPPH loss which is a concentration of DPPH radicals reacted with antioxidants.	Antioxidant activity	[185]
Contact Angle	Polyethylene	α-Tocopherol	Contact angle titrations were performed by measuring sets of contact angles at each pH value.	analysis of hydrophobic behaviour as pH increases	[106]
	PLA	α-Tocopherol	Static contact angle	analysis of material wettability change	[126][127] [48]

2.6 Coupling Vitamin E with Titanium Alloy

As noted, vitamin E has a number of relevant biological actions (antioxidant properties, anti-inflammatory properties, inhibition of platelet aggregation, preservation of cell membrane integrity) with positive outcomes on the immune system, bone health, skin protection, age-related diseases, and cancer. Some new fields of application are being studied in the area of biomaterials under research and have great potential impact in the future; in this regard, we can include implant coating. Interestingly, however, research on vitamin E in combination with titanium as a biomaterial has not yielded many results to date.

In fact, doing a search on Scopus and entering tocopherol, titanium, and implant as filter words, only 20 results are found from 2004 to present.

With this in mind, this part of the research wants to couple vitamin E to titanium, to better understand the controversial antibacterial activity of vitamin E in order to impart new properties to titanium alloy, in addition to those already discussed. New types of combinations with biomaterials are here explored, such as grafting the molecule onto titanium surfaces by coating or functionalization.

In particular, this chapter aims to study and compare two forms of vitamin E, α-tocopherol (αT) and its water-soluble form α-tocopherol phosphate (αTP), find suitable surface characterization analyses for each molecule, and study their cellular and bacterial properties once they are coupled to a chemically treated Ti6Al4V biomaterial.

New applications are also discussed and compared depending on the molecule chosen. α-tocopherol is chosen for a temporary implant type application, while α-tocopherol phosphate is thought for a permanent implant application.

Based on these premises, α-tocopherol is here applied for the first time as a bioactive coating to the surface of a chemically treated titanium alloy and it is fully characterized by its physical-chemical properties. Different characterizations were carried out to analyse the coating and its adhesion on the surface by means of different physical/chemical techniques such as contact angle, ζ potential, UV\Vis spectroscopy, FTIR analysis, tape test, release test, and spectrophotometric assays (DPPH). The biological characterization is focused on the adhesion and viability rate of human mesenchymal stem cells (hMSC) and biofilm formation by Gram positive and negative bacteria with the final aim to prevent the formation of excessive bone on-growth and the risk of

infection without the release of toxic elements impairing the self-healing process. The idea to modify the surface of an implantable material in order to make it not cells-friendly may sound like a paradox, but, as anticipated in the first chapter, an excessive tissue on-growth around the implant can bring complex difficulties for surgeons during the removal procedures in the case of temporary devices [190]. Therefore, massive cells' colonization should be prevented onto such implants to facilitate the work of surgeons; however, taking into consideration the short/middle period of direct contact with the tissue, it is obvious that tissue on-growth inhibition cannot be achieved by the use of toxic compounds which would compromise the healing process.

On the other side, α-tocopherol phosphate is used to develop a surface with antibacterial properties for orthopedic and dental devices. Two different strategies of surface grafting, molecular functionalization and thin coating, are explored and the divalent Ca^{2+} ion is exploited for both modes as a linker between the surface, rich in deprotonated OH groups, and the *α*TP molecule, which is also negatively charged in solution. This process was designed based on past studies by the authors that used Ca^{2+} to ensure a bond between the above surface and gallic acid or polyphenols, which easily release H_3O^+ ions in solution [191].

Finally, different characterizations were carried out to evaluate the grafting of the *α*TP molecule on the surface by means of different physical/chemical techniques such as contact angle, ζ potential, X-ray photoelectron spectroscopy (XPS), UV\Vis spectroscopy, FTIR analysis, and Kelvin probe force microscopy. The biological characterization was performed by cellular assays with human mesenchymal stem cells (hMSC), to evaluate the cytocompatibility, whereas the antibacterial activity was assessed by evaluating the ability of the coated or functionalized specimens to prevent the surface colonization of the pathogen *Staphylococcus epidermidis*.

For both works, a chemically treated titanium alloy (Ti6Al4V) substrate has been selected because its roughness and surface chemistry are suitable for an effective adhesion of the coating and a proper grafting of the molecule. The chemically treated substrate is also of interest because it has been demonstrated to have low bacterial adhesion and it can contribute to lower the risk of infection by a passive strategy (nano-topography, surface enrichment in deprotonated OH functional groups). As last, it has bioactive behaviour (precipitation of hydroxylapatite from the biological fluids), osseoconductive and osseoinductive effects and it can fast osseointegration in the case of permanent implants [27].

2.7 Materials and Method

2.7.1 Surface chemical treatment

The substrate selected for the surface modifications is the titanium alloy Ti6Al4V (ASTM B348, Gr5, Titanium Consulting and Trading, discs 10mm in diameter and 2 mm thickness). All the discs were polished with SiC papers (up to 400 grit). To clean the surface, the samples were first immersed in acetone for 5 min, then twice in ultrapure Milli-Q (MQ, Millipore) water for 10 min, in an ultrasonic bath. In order to expose a high density of hydroxyl groups and to increase the roughness for enhanced adhesion of the coating on the substrate, the samples underwent a patented chemical treatment [27], [192]. It includes a first acid etching in diluted hydrofluoric acid and subsequently controlled re-oxidation by hydrogen peroxide. Before functionalization, the treated samples were UV-C irradiated for 1 hour to reduce water content and carbon contamination and to improve the reactivity of hydroxyl groups. From now on, the samples treated as above described will be named chemically-treated (CT), while the samples polished up to 4000 grit used as control will be named mirror-polished (Ti64).

2.7.2 α-Tocopherol coating preparation

Standard α-tocopherol was purchased from Sigma Aldrich ((+)-α-tocopherol, Type V, T3634, Sigma- Aldrich) and exploited for the coating deposition. The α-tocopherol was added into ethanol (≥ 99.9 %) with a concentration of 5mg/ml and homogenized by magnetic stirring for 10 min. Each sample, previously chemically treated as described above, was immersed in 5 ml of the prepared solution for 3 hours in the dark at a constant temperature of 37°C. After incubation, the samples were washed 2 times twice in a controlled manner: the first time by rapid immersion in 15ml of ethanol and subsequent drying under a hood, the second time by immersing the samples in 15ml of MQ water 2 times, with subsequent drying under the fume hood

a-Tocopherol functionalization

In a similar manner, functionalization was also done on CT samples with the α- tocopherol molecule. After repeating all the above steps and thus withdrawing the samples from the incubator, the samples were immediately washed in ethanol 3 times, and consequently dried under hood. However, as discussed in section 2.8.2, the samples obtained in this way were not further characterized, as this type of functionalization did not reveal any effective surface modification.

2.7.3 *α*-Tocopheryl phosphate grafting preparation

First of all, the treated samples were irradiated with UV light for 1 hour. Immediately after irradiation, the samples were immersed in a solution of $CaCl_2$ (0.292 g/L) for 24 hours, minimizing sample contact with the air during the transfer, in this way divalent, positive calcium ions interact electrostatically with the acidic OH ions in the sample, as shown in Figure 2.7. α-tocopheryl phosphate (*α*TP) ((±)-α-Tocopheryl phosphate disodium salt, T2020, Sigma-Aldrich, St. Louis, MO, USA) was employed for surface functionalization. For the grafting of the molecule, a solution of α-tocopheryl phosphate (*α*TP) in TRIS-HCL with a concentration of 5 mg/mL was prepared by mixing the solution on a magnetic stirrer for 10 min, until the molecule was completely dissolved. After 24 hours, the samples immersed in the calcium solution were dried under a laminar flow hood and then immersed in the prepared αTP solution for 3 hours at 37°C.

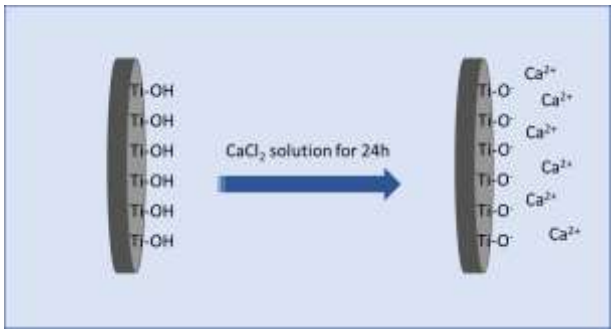

Figure 2.7 Scheme of possible interaction of Ca^{2+} ions with titanium surface

Coating

The coating method involved the following steps. Firstly, the samples taken from the solution (see 2.2) were dried for 5 minutes under a laminar flow hood, in this way, the molecule can form a continuous layer adhered to the substrate. After the layer was dried, the samples were rinsed 3 times in ultrapure water, to remove what was not adsorbed. Lastly, samples were dried again under a laminar flow hood. The coating method is represented in Figure 2.8

Functionalization

The functionalization method involved the following steps. Firstly, the samples were taken from the solution (see 2.2) and were immediately rinsed 3 times in ultrapure water, precisely with the aim of avoiding the formation of a coating and allowing the grafting of a molecular layer. Lastly, samples were dried under a laminar flow hood. The functionalization method is represented in Figure 2.8

Table 2.4 shows a list of acronym and characterization techniques used in this part of the work.

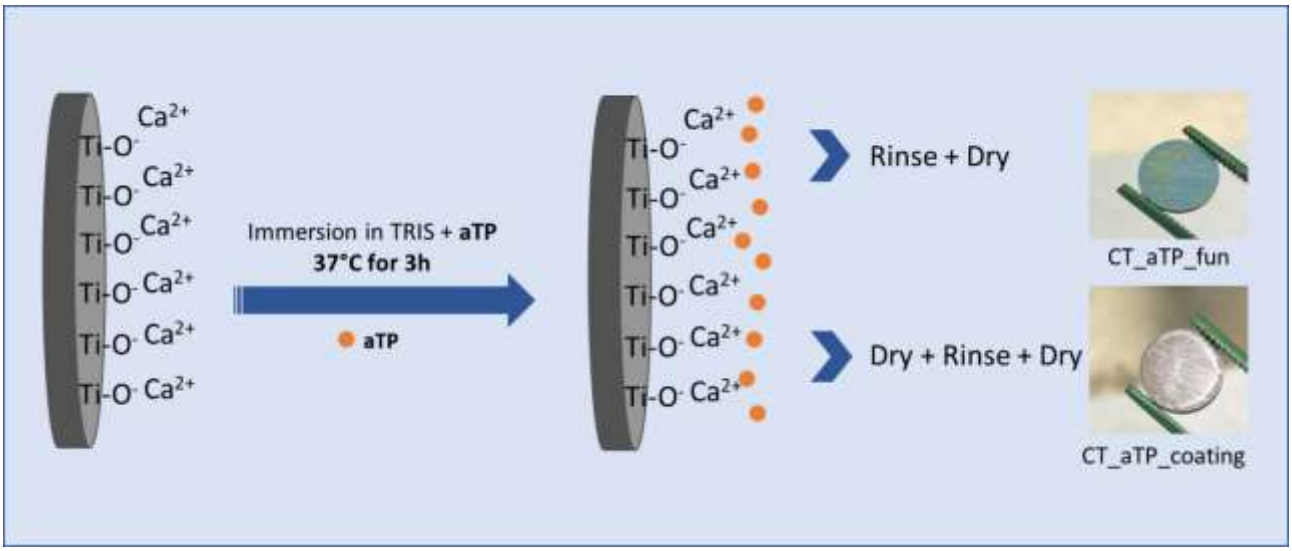

Figure 2.8 Process of functionalization and coating with αTP

Table 2.4 .Acronyms and relative samples characterization

Description	Acronym	Characterization techniques
Ti64 up 4000 grit	Ti64	Contact angle, biological tests.
Ti64 up 400grit chemically treated	CT	DPPH, UV-Vis, Zeta potential, FTIR, contact angle, biological tests.
Ti64 up 400grit chemically treated and coated with α.tocopherol (αT).	CT_aT_coating	DPPH, UV-Vis, Zeta potential, FTIR, contact angle, soaking test, tape test, biological tests, immersion in ethanol with subsequent UV-Vis spectrophotometry of the soaking solution.
Ti64 up 400grit chemically treated and functionalized with α.tocopherol (αT).	CT_aT functionalization	ζ potential
Ti64 up 400grit chemically treated and coated with α-Tocopherol after tape test	CT_aT_tape	FTIR, Optical Microscopy, immersion in ethanol with subsequent UV-Vis spectrophotometry of the soaking solution.
Ti64 up 400grit chemically treated and coated with α-Tococpheryl phosphate (αTP)	CT_aTP_coating	UV-Vis, Zeta potential, FTIR, contact angle, AFM with Kelvin Probe, XPS, biological tests.
Ti64 up 400grit chemically treated and functionalized with α-Tococpheryl phosphate (αTP)	CT_aTP_fun	UV-Vis, Zeta potential, FTIR, contact angle, AFM with Kelvin Probe, XPS, biological tests.

2.7.4 Thickness determination

For the determination of coating thickness by means of contact profiler, trenches as well defined as possible were inserted into the αT-layer and scanned with a Stylus profilometer (Veeco Tektak 150). Care was taken to ensure that the trenches extended to the layer-substrate interface. The scan length was chosen so that morphological layer changes at the edge of the trench would influence the measurement results as little as possible.

2.7.5 ζ potential titration curve

The electrokinetic measurement of the zeta potential on solid surfaces is of interest to measure the Isoelectric Point (IEP), to evidence the functional group exposed by the surface, their chemical acidic-alkaline reactivity, and the coating chemical stability at different pH [193]. The surface zeta potential of all samples (CT, CT_aT_coating, CT_aTP_fun, and CT_aTP_coating), was measured with an electrokinetic analyser (SurPASS, Anton Paar), equipped with an adjustable gap cell, by means of the streaming potential technique. Two samples were prepared for each type of titration curve (acid and basic) and the ζ potential was measured as a function of pH in a 0.001 M KCl electrolyte solution. The pH value varied by automatic titration unit, by adding HCl 0.05 M or NaOH 0.05 M starting from a pH ≈ 5.5.

2.7.6 Fourier – Transformed Infrared spectroscopy analysis

Fourier Transformed Infrared spectroscopy (FTIR, FTIR Hyperion 2000 - Tensor 27, Bruker Optics, Ettlingen, Germany) was performed in ATR mode (Attenuated Total Reflectance - FTIR Alpha, Bruker Optics, Ettlingen, Germany) for all solid samples (CT, CT_aT_coating, CT_aTP_fun, and CT_aTP_coating) using wavelengths between 400 and 4000 cm−1.

2.7.7 Contact angle measurements and surface free energy calculation

Surface wettability was assessed by measuring the contact angle with the sessile drop method. After depositing a 10 µl drop on the treated side of the sample, the contact angle was measured through Image J software after acquiring images by with a microscope (Kruss DSA 100). Measurements were performed in triplicate on each type of sample produced (CT, Ti64, CT_aT_coating, CT_aTP_fun, and CT_aTP_coating) using different media (MQ water, DMEM, and LB). MQ water is the medium used to calculate wettability, DMEM and LB (Lysogeny Broth) are media used during cellular and bacterial testing, respectively. To calculate the surface free energy (SFE) of the solid samples with and without the αT coating, the contact angle was also measured with two other solvents: hexadecane (Sigma Aldrich, St. Louis, USA) and ethylene glycol (Sigma Aldrich, St. Louis, USA). The surface energy was calculated through the Owen-Wendt-Rabel-Kaelble (OWRK) method. The experiments were done in triplicate on CT, Ti64, and CT_aT_coating samples

2.7.8 Tape Test

To evaluate the adhesion of αT coating film to the substrate, a tape test was performed according to the ASTM D 3359 standard [194] on the CT_aT_coating sample. A strip of adhesive tape was applied to the coating with constant pressure, and after removal, the coating residues were analyzed by optical microscopy and FTIR. In order to be able to analyze the degree of adhesion, one scratch was made on the coated surface before testing. To quantify the remaining α-tocopherol adhered to the surface, the sample was immersed in ethanol for 30 minutes to promote coating degradation. Afterward, the solution of the degraded coating was analyzed by UV-Vis in the full spectrum (190-750 nm), the area of the peak at 292 nm was calculated and correlated with the concentration of α-tocopherol through a calibration curve (Figure 2.9), following the procedure previously described by Hufen Julia
et al. (2008)[182]. This test was made in triplicate.

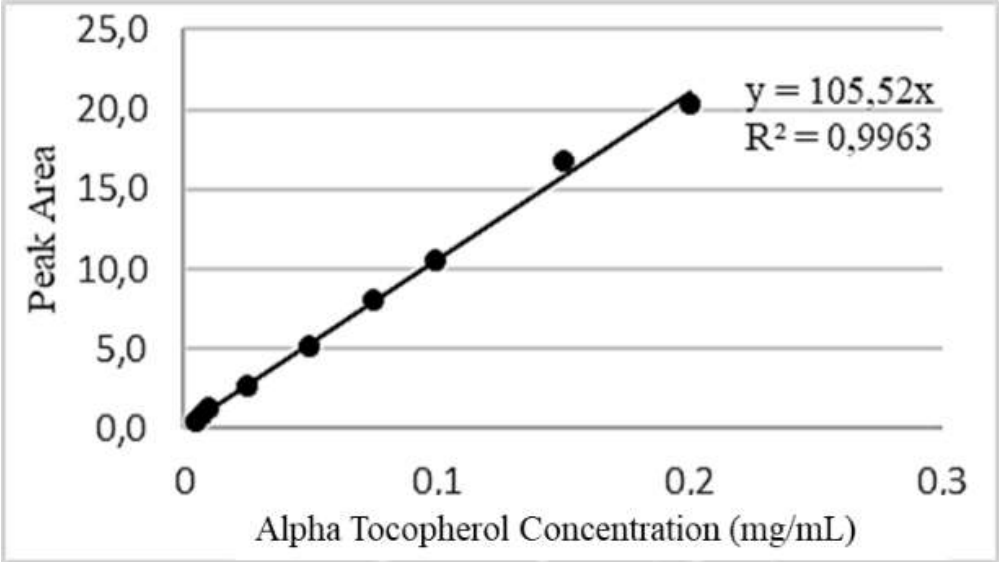

Figure 2.9 Calibration curve of UV-Vis method to quantify α- tocopherol adhered on the sample surface.

2.7.9 UV-Vis Spectroscopy

All spectrophotometric analyses were performed by means of a UV-Vis spectrophotometer (UV2600 Shimadzu). On solid samples (CT, CT_aT_coating, CT_aTP_fun, and CT_aTP_coating) reflectance spectroscopy (R%) was measured by equipping the spectrophotometer with the integrating sphere and registered in the range 190nm-750nm.
Barium sulphate ($BaSO_4$) was used as a blank for baseline correction.

2.7.10 Kelvin probe force microscopy

This is a dual-scan system in which both a topographic image and a surface potential image are obtained by a forward scan in tapping mode and a backward scan in lift mode applying a bias between the tip and the sample. To achieve this type of measurement, the atomic force microscope (Innova atomic force microscope, Bruker) was equipped with a conductive tip (Sb-doped Si, frequency 75 kHz, SCM-PIT-V2, Bruker). For this analysis, specifically samples (CT_aTP_coating and CT_aTP_fun) were prepared as here described.

The steps described in 2.7.1 were applied, then half of the sample was coated with Kapton® and the samples were coated or functionalized according to the procedure described in 2.7.3. After complete drying, the Kapton® was removed. The samples thus obtained were only half coated or functionalized with a rather narrow border with the other half of the sample. The final topography and potential images (100x100 μm) were acquired on the boundary between the functionalized and nonfunctionalized surface. The scanning parameters (scan frequency, lift height, tip-sample bias) were adjusted each time for the best results. Gwyddion software[195] was used to elaborate the images: a second-degree polynomial filter was applied to the topographical images while a matching filter was implemented for the potential images.

2.7.11 X-ray photoelectron spectroscopy (XPS)

To study the chemical composition of the uppermost layer and exposed functional groups, CT_aTP_coating, CT_aTP_fun, and CT as a reference were analyzed by X-ray photoelectron spectroscopy (XPS, PHI 5000 VERSAPROBE, PHYSICAL ELECTRONICS). All the analyses were conducted using a monochromatic Al Kα source (23.8 W) operated at 20 mA and 15 kV and a spot size of 100μm, with an energy resolution below 0.5 eV with a step interval of 0.1 eV. Survey spectra were acquired at a pass energy of 187.6 eV and a total acquisition time of 5 min. Both survey spectra (0-1200 eV), for the identification and quantification of chemical elements, and high-resolution spectra (C, O regions) for the identification of functional groups were acquired. The fitting of high resolution spectra was performed through Casa XPS software. To ensure compensation for the charge effect, the spectra were referenced by setting the C1s peak of hydrocarbons at 284.80 eV

2.7.12 Biological Evaluations of αT coating

Specimens designed for the biological characterizations were realized by using 0.22 μm filtered sterile solutions to functionalize all the surfaces of previously autoclave-sterilized (121°C) discs. Specimens were stored in sterile conditions at room temperature protected from light by aluminium foil until use.

Cells adhesion α-tocopherol coating

Human mesenchymal stem cells (hMSC) were selected to test specimen cytocompatibility and cells adhesion as cellular model due to their ability to migrate to the injured site from driving the healing process; so, they were considered as the cells trying to colonize the temporary device. Commercially available hMSC (C-12974 from PromoCell GmbH, Heidelberg, Germany, distributed by Merck, Milan, Italy) were maintained in low glucose Dulbecco Modified Eagle's Medium (DMEM, Sigma-Aldrich) supplemented with 15% fetal bovine serum and 1% antibiotics (penicillin/streptomycin) at 37°C, 5% CO_2. When cell confluence reached 80-90%, the cells were enzymatically detached by 0.25% trypsin/EDTA solution (in PBS), collected, and used for experiments. Each sample (CT, Ti64, and CT_aT_coating) was gently moved into a new 24 multi-well plate by sterile tweezers avoiding any surface damage. Then, 100 μL of medium containing $2.5x10^4$ cells/specimen was dropwise added directly onto the surface of control (Ti64) and coated (CT_aT_coating) specimens and maintained in a humidified incubator for 6 h. Afterward, the supernatant was collected for cell number count by means of Trypan blue and morphological observation using an optical digital microscope (EvosFloid, from ThermoFisher Scientific). Moreover, detached cells were seeded into a new 96 wells plate and after 24 hours their morphology and viability were visually checked by the fluorescent live/dead assay (LIVE/DEAD™ Viability/Cytotoxicity Kit from ThermoFisher Scientific) using a fluorescence microscope (TCS SP8 LIGHTNING confocal laser scanning microscope, Leica Microsystems, Wetzlar, Germany). After cells withdrawal, specimens were rinsed with 1 ml of fresh medium and incubated at 37°C; After one day, the metabolic activity of the cells adhered to the specimens' surface was further evaluated by the metabolic colorimetric Alamar blue assay (AlamarBlue®, ready-to-use solution, ThermoFisher Scientific) following Manufacturer's

instructions. The signals were evaluated by an excitation wavelength of 570 nm and an emission reading of 590 nm; The results were expressed in relative fluorescent units (RFU). The applied method is shown and schematized in Figure 2.10

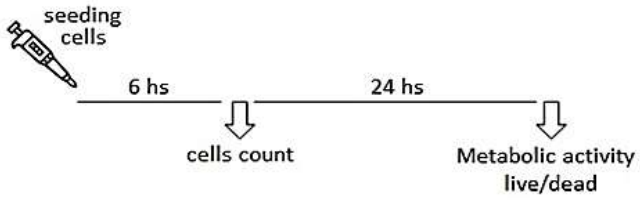

Figure 2.10 Schematic representation of the cell adhesion experimental set up

Biofilm adhesion on α-tocopherol coating

The Gram-positive *Staphylococcus aureus* (*S. aureus*, ATCC 43300) and the Gram-negative *Escherichia coli* (*E. coli*, ATCC 25922) strains were purchased from the American Type Culture Collection (ATCC, Manassas, USA) and used to test α-tocopherol antibacterial properties towards joint pathogens. Bacteria were cultivated on Trypticase Soy Agar (TSA, Sigma-Aldrich, Milan, Italy) plates and incubated at 37°C until round single colonies were formed; then, 2–3 colonies were collected and spotted into 30 ml of fresh Luria Bertani broth (LB, Sigma-Aldrich). Broth cultures were incubated overnight at 37°C under agitation (120 rpm in an orbital shaker). A fresh culture was prepared before each experiment; bacteria concentration was adjusted to $1x10^5$ cells/ml by diluting in fresh media until the optical density of 0.001 at 600 nm was reached as determined by a spectrophotometer (Spark, from Tecan Trading AG, Basel, CH) using pure LB medium as blank. Each sample (CT, Ti64, and CT_aT_coating) was gently moved into a new 24 multi-well plate by sterile tweezers avoiding any surface damage. Then, 100 µL of medium containing $1x10^5$ bacteria/specimen was drop wised directly onto the materials' surface and maintained in a humidified incubator for 2 h, allowing bacteria adhesion. Afterward, the supernatant was collected for the bacteria number count by means of the CFU assay while bacteria viability was visually checked by the fluorescent live/dead assay using a fluorescent fluorescence microscope. After cells withdrawal, specimens were rinsed with 1ml of fresh medium and incubated at 37°C; After one day, the metabolic activity of the cells adhered to

the specimens' surface was evaluated by the colorimetric Alamar blue assay. The applied method is shown and schematized in Figure 2.11.

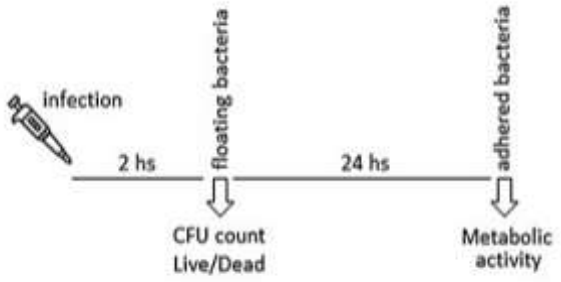

Figure 2.11 Schematic representation of the biofilm adhesion experimental set up

2.7.13 Biological Evaluations of αTP grafting

Cytocompatibility evaluation of α-tocopheryl phosphate

Specimens' cytocompatibility was evaluated towards human mesenchymal stem cells (hMSC). Cells were obtained from ATCC (PromoCell C-12974) and cultivated in low-glucose DMEM (Sigma-Aldrich) supplemented with 15% fetal bovine serum (FBS, Sigma-Aldrich) and 1% antibiotics at 37°C, 5% CO_2 atmosphere. Cells were cultivated until 80%–90% confluence, detached by a trypsin-EDTA solution (0.25% in PBS), harvested, and used for experiments. To test specimens' ability to support cells' colonization, hMSC were directly seeded onto specimens' surface (CT, Ti64, CT_aTP_fun, and CT_aTP_coating) at a defined density (2×10^4 cells/sample) and cultivated for 24-48-72 hs allowing adhesion and spreading

. Then, the viability of the cells was evaluated by means of metabolic activity using the colorimetric Alamar blue assay as prior described: moreover, the morphology of the cells adhered to the specimens' surface was visually checked by phalloidin (ab176759, AbCam, Cambridge, UK) and 4′,6-diamidino-2-phenylindole (DAPI Sigma-Aldrich, Milan, Italy) cytoskeleton and nuclei staining, respectively. Images were obtained by a fluorescent confocal microscope (TCS SP8 LIGHTNING confocal laser scanning microscope from Leica).

Antibacterial evaluation of α-tocopheryl phosphate

A commercial strain of the biofilm former pathogen *Staphylococcus epidermidis* (*S. epidermidis*, reference strain ATCC 14990) was obtained by the American Type Culture Collection (ATCC, Manassas, USA) and cultivated in Trypticase Soy Agar (TSA, Merck) at 37°C until round single colonies were observed; then, 2-3 colonies were resuspended in 20 ml of Luria Bertani broth (LB, Merck) at 37°C under agitation (90 rpm) till reaching a final concentration of $1x10^5$ cells ml^{-1}, corresponding to an optical density (OD) of 0.001 at 600 nm determined by spectrophotometer (Spark, Tecan, Switzerland).
To perform the direct infection, specimens (CT, Ti64, CT_aTP_fun, and CT_aTP_coating) were gently located into 24 multiwell plates and submerged with 1 ml of the above-mentioned bacteria suspension for 24 hours at 37°C; afterward, bacteria metabolic activity was evaluated by the colorimetric Alamar

blue assay (AlamarBlue™, Life Technologies) whereas the number of the viable colonies adhered to the specimens' surface was counted by the CFU method. Briefly, the ready-to-use Alamar solution was added to each well containing the test specimen and incubated for 4 hours in the dark; then supernatants were collected and measured via fluorimetric analysis (λex = 570 nm and λem = 590 nm). For CFU count bacteria were detached from specimens' surface by vortex and sonicator (3 times each, 30 seconds) to perform six-serial 10-fold dilutions as previously described by the Authors [65]; the final number of CFU was calculated as follows:

$$CFU=[(\text{number of colonies} \times \text{dilution factor})^{\text{serial dilution}}]$$

Finally, bacteria morphology was visually checked by scanning electron microscopy (SEM, JSM-IT510 from Jeol). Briefly, after fixation in glutaraldehyde (20 min, room temperature) specimens were dehydrated by the alcohol scale (70-90-100%, 30 min each), treated with hexamethyldisilazane and cover-sputtered with gold before collecting images at different magnifications.

2.7.14 Anti-inflammatory evaluation of α-tocopherol

Soaking test

Eight α-tocopherol coated samples were assayed by a soaking test for 4 weeks. Four samples were immersed in 10 ml of phosphate-buffered saline (PBS, pH 7.4), and the other four were immersed in 10 ml of a solution of PBS with H_2O_2 0.05 M adjusted with HCl reaching a final pH of 4.5. The first test is aimed at mimicking a physiological environment, while the second one simulates a pathological pro-inflammatory condition. Each sample was soaked in its respective solution for 28 days at 37 °C protected from light. Soaking solutions were replaced after different time points (1, 7, 14, and 28 days) and analysed by F&C test and DPPH assay. After 28 days, the solid samples were extracted and characterized as indicated in table 2.5 through UV-VIS spectroscopy, FTIR, spectrophotometric assays, as indicated in Table 2.5 Samples soaked in PBS solution are called CT_aT_PBS, and samples soaked in PBS+H2O2 solution are called CT_aT_H2O2.

Table 2.5 Acronyms and relative samples characterization for inflammatory evaluation.

Description	***Acronym***	***Characterization techniques***
Ti64 up 4000 grit	Ti64	Biological tests.
Ti64 up 400grit chemically treated	CT	DPPH, FTIR, biological tests.
Ti64 up 400grit chemically treated and coated with α-tocopherol	CT_aT_coating	DPPH, UV-VIS, soaking test, biological tets.
Ti64 up 400grit chemically treated and coated with α-tocopherol after soaking test in physiological conditions	CT_aT_PBS	DPPH, FTIR, UV-VIS
Ti64 up 400grit chemically treated and coated with α-tocopherol after soaking test in inflammatory conditions	CT_aT_H2O2	DPPH, FTIR, UV-VIS

Folin&Ciocalteu Test

The Folin Ciocalteu (F&C) reaction is an antioxidant assay based on electron transfer, which measures the reductive capacity of an antioxidant. The Folin-Ciocâlteu reagents, formed by tungsten and molibden, are reduced to oxidation numbers +4 and +5, forming a blue chromophore whose absorption maximum depends on the concentration of phenolic compounds, detectable with a spectrophotometer at 760 nm. This method works correctly with water-soluble cambions, thus capable of reacting with the reagents. To overcome problems due to the lipophilic nature of α-tocopherol, assay was performed following a modified method for measuring lipophilic antioxidant molecules [177], after the soaking test. α-tocopherol concentration in the soaking solution was estimated after incubation at room temperature for 30 min. The absorbance was evaluated at 665 nm wavelength through UV-Vis spectroscopy (UV2600 Shimadzu). Pure ethanol was used as a blank.

Radical Scavenging Activity (RSA) through DPPH Test

The DPPH test allows measuring the reducing activity of antioxidant molecules against the DPPH radical. DPPH is a radical that when free is purple and when it binds to an antioxidant, it discolours (Figure 2.12). The 2,2 diphenyl-1-picrylhydrazyl (DPPH) was purchased from Sigma Aldrich (D9132-1G) and used to measure the radical scavenging activity of tocopherol following manufacturer's instructions as previously described and explained as follow. [6]-[8]. DPPH was added to the ethanol solution with a concentration of 60 µg/ml, then diluted till an absorbance of approximately 1 at 515 nm wavelength. In triplicate, each sample (CT, CT_aT_coating, CT_aT_PBS, CT_aT_H2O2) was immersed in 3 ml of the prepared DPPH solution. Uncoated samples (CT) were used as controls. After 30 min under dark conditions at room temperature, the absorbance of the supernatants was recorded at 515 nm using a UV-vis spectrophotometer, against pure ethanol, used as a blank. The anti-oxidant activity was calculated using the following formula:

$$\textbf{RSA}\ (\%) = \frac{\text{Abs. of Blank} - \text{Abs. of Sample}}{\text{Abs. of Blank}} \times 100$$

To test the antioxidant properties of the soaking solution, the same procedure

was followed by mixing 1 ml of each sample solution with 2 ml of the DPPH solution as previously detailed.

Figure 2.12 DPPH colour, PURPLE: RSA = 0%

Biological Evaluations of anti-inflammatory response

3D Cell culture on titanium discs

Human mesenchymal stem cells (hMSC, Promo Cell C-12974 from Merck) were maintained in Dulbecco's modified Eagle's medium Low Glucose (DMEM, Euroclone), supplemented with 15% fetal bovine serum (FBS, Euroclone), 2 mM L-glutamine (Sigma-Aldrich), 1% penicillin/streptomycin (Sigma Aldrich), and cultured at 37°C in a humidified incubator with 5% CO_2. Titanium discs were placed into wells of 24-well cell culture plates in sterile conditions, and hMSC with a final density of 500.000 cells/ml of PureCol™ EZ Gel (Sigma Aldrich) ready-to-use collagen were seeded into each well, fully immersing titanium specimens. Plates were placed in the incubator for 2 hours, allowing collagen sol-gel transition, and then an additional aliquot of 200 µl of culture medium was added on top of the gel. After 24 hours, a typical spindle-shape of hMSC was observed and cells were treated with pro-inflammatory agents: TNFα/IL-1β 10 µg/ml (each) and IFNγ 20 ng/ml for 24 hours. Then, cells were recovered from gel using collagenase type I (Sigma Aldrich; 4 mg/ml) and total RNA was extracted for further analysis.

RT-qPCR

Trizol reagent (Invitrogen) was used to isolate total RNA, as indicated by the supplier. The ExcelRT™ Reverse Transcription Kit (SMOBIO) was used to synthesize cDNA from 2 mg of total RNA, following the manufacturer's instructions. Quantitative PCR (qPCR) reactions were performed by using the Excel-Taq FAST qPCR SybrGreen and a CFX96 thermocycler (Bio-Rad). Primer sequences were designed by using the online IDT PrimerQuest Tool software (IDT; https://eu.idtdna.com/pages), and sequences are reported below (Table 2.6). L34 was used as internal control, and the comparative Ct method ($^{\Delta\Delta}$Ct) was used for the relative quantification of gene expression.

Table 2.6 Primer sequences

IL1β	AAGGCGGCCAGGATATAA/GGGATT GAGTCCACATTCAG
COX2	GCCTGGTCTGATGATG/TTAGCCTGG TTGTCTGG
TGFβ1	GACATCAACGGGTTCACTAC/GTGGA GAAGCAATAGTT
IDO	CTTGGAGAAAGCCCTTCAA/CCTTTC CAGCCAGACAAATA
PGE2	TCTGGCGTCCTTTGACTA/TTGAGTC GCTTGCTGATG
IL6	CCCAGGAGATTCCAAAG/ATGCCGTC GAGGATGTA
ATF4	CCCGGAGAAGGCATCCTC/GTGGCC AAGCACTTCAAACC
ATF6	TTTGCTGTCTCAGCCTACTGTGGT/TC CATTCACTGGGCTATTCGCTGA
XBP1	AGAGAAAACTCATGGCCTTGTAGTT G/CATTCCCCTTGGCTTCCG
L34	GTCCCCGAACCCTGGTAATAGA/GGC CCTGCTGACATGTTTCTT

Evaluation of the immune response by flow cytometry

To evaluate the immune-biocompatibility of the Vitamin E-coated discs, fresh peripheral blood mononuclear cells (PBMCs) from six healthy donors were seeded at a concentration of $1x10^6$ cells/well onto sterile specimens, in a 48-well plate, for 72 hours, keeping the polished side upwards. Before staining, media was removed, and cells were washed with PBS-EDTA 0.5M. Subsequently, cells were stained with a viability dye (BD Horizon™ Fixable Viability Stain 780) to distinguish live and dead cells and then 100 µL of BD Pharmingen™ Human BD Fc Block™ solution was added to block the non-specific binding of the immunoglobulin to Fc receptors. PBMCs were stained with the following antibodies: monoclonal anti-CD45 – BUV395 human antibody (mAb) (Cat: 563792; leucocytes), anti-CD3 – BUV 496 mAb (Cat: 612940; T cells), anti-CD4 – BUV737 mAb (Cat: 612748; T helper cells), anti-CD8 – BUV805 mAb (Cat: 612889; cytotoxic T cells) anti-CD45RA – BUV563 (Cat: 612926) and anti-CD197 – BV711 mAbs (Cat: 566602; naïve, central memory (CM), effector memory cells (EM), and terminally differentiated EM cells), anti-CD25 – APC-R700 (Cat: 565106) and anti-CD127 – BV786 mAbs (Cat: 563324; regulatory T cells, Tregs), anti-CD183 – APC (Cat: 550967), anti-CD194 – PE-CF594 (Cat: 565391) and anti-CD196 – BV480 mAbs (Cat: 566130; Th1, Th2, and Th17). All reagents were purchased from BD Biosciences. The samples were acquired using FACSymphony™ A5 (BD Biosciences) flow cytometer and data were analysed using BD FACSDIVA™ software (BD Biosciences). Data were further analysed using Prism software (GraphPad, Version 9.0.0) and are shown as average ± SEM. (n=6). Ordinary One-way ANOVA or Kruskal-Wallis multiple comparisons test was used; *=p<0.05.x

2.7.15 Statistical analysis of data

Experiments were performed in triplicates of each specimen for all the presented applied assays. The physico-chemical analysis statistical analyses were performed by one-way ANOVA, with a significance level of $p < 0.05$. For biological evaluations, normal distribution and homoscedasticity were tested with Wilk-Shapiro's and Levene's tests, respectively. Samples were statistically compared by the SPSS software (v25, IBM, New York, NY, USA) using the one-way ANOVA test and Tukey's post-hoc analysis. Results were considered significant for $p < 0.05$.

2.8 Results

2.8.1 Surface samples:

The surface obtained by chemical treatment is a surface with a micro-nanoporous oxide layer about 300 nm thick, increased roughness compared to the polished one (Ra = 0.25 µm), and a high density of acidic -OH groups exposed on the surface (Figure 2.13). The resulting surface has osteogenic and bioactive properties [27] and is suitable for effective adhesion coatings and proper grafting of biomolecules.

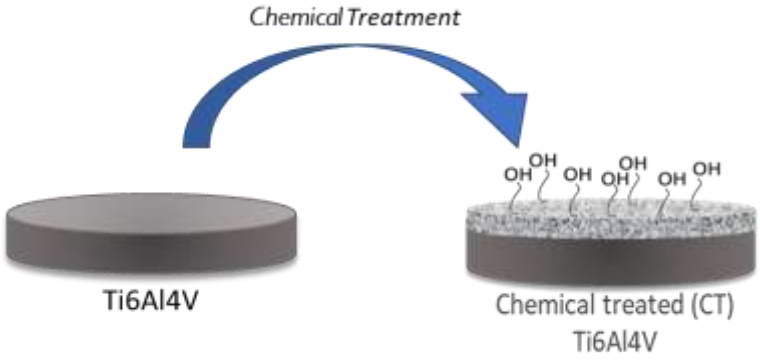

Figure 2.13 Scheme of CT surface

Figure 2.14. shows the surface of the CT samples as seen by FE-SEM.

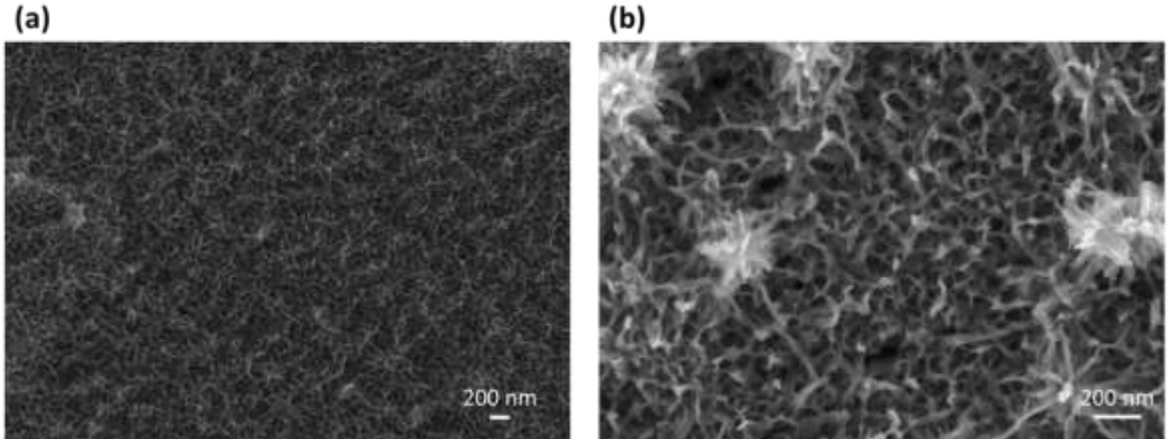

Figure 2.14 FE-SEM images of CT (a) 60k X magnitude (b) 150k X magnitude

2.8.2 Thickness determination

The thickness of the obtained αT coating measured with the stylus profilometer was found to be 1.7 µm. Accordingly, the coating can be classified as a thin film on a micrometric scale.

2.8.3 Zeta potential titration curves:

The titration curves of the CT, coated (CT, CT_aT_coating, CT_aTP_coating), and functionalized samples (CT_aTP_fun) with α-tocopherol or α-tocopheryl phosphate are shown in Figure 2.15.

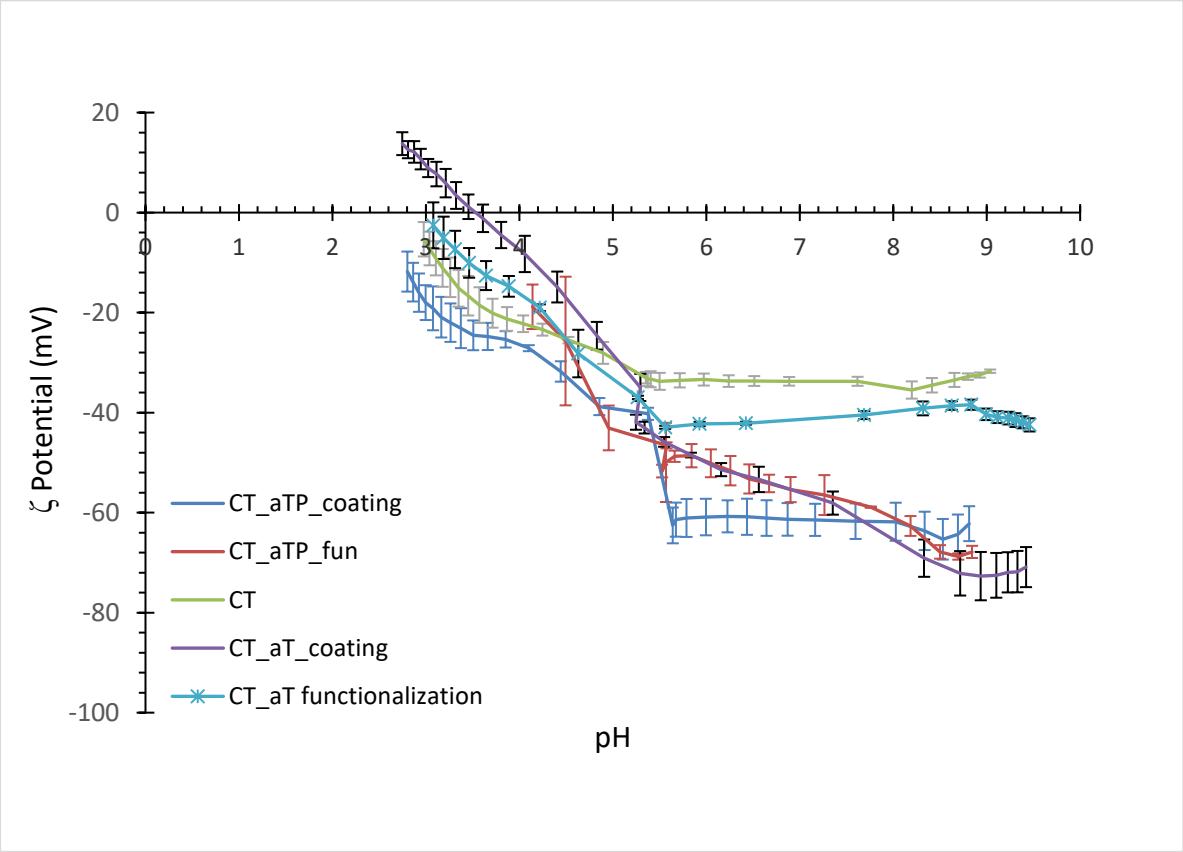

Figure 2.15 Zeta potential vs pH for CT, CT_aTP_coating, CT_aTP_fun, CT_aT_coating and CT_a T functionalization

The figure 2.15 shows the CT_aT functionalization curve representing a sample on which functionalization with α-tocopherol was performed instead of coating. As can be seen, the curve remains identical to the control CT curve (with a difference of less than 10 mV representing the instrument's sensitivity). This indicates that αT is not present on the sample surface, and the functionalization of the αT molecule does not lead to an effective surface modification.

Therefore, from now on, The surface modification chosen with the αT molecule is a surface coating, which will be characterized in detail below.

Instead, the difference between the substrate (CT) and the others modified surfaces was evident: or an IEP significantly different from CT was registered (CT_aT_coat) or the shape of the curve was different (CT_aTP_coating, CT_aTP_fun).

Although the isoelectric point value (IEP) was not always measured, due to measurement limitations, it is derived by extrapolation to be in the range of pH 2-3 for the CT and aTP coated and functionalized samples (CT_aTP_coating, CT-aTP_fun). It was due to the presence of functional groups with a strong acidic chemical reactivity: these acidic groups can be differently explained as discussed in the following.

In agreement with the measured IEPs, two curves (CT, CT-aTP_coating) exhibited a well-defined plateau for pH values above 5.5, indicating that the acidic groups had a specific acidic strength and completely dissociated above pH 5.5. In the case of CT, the acidic functional groups were bridged hydroxyls of the titanium oxide layer [196]. In the case of CT-aTP coating, the plateau values of the ζ potential were significantly lower than they were on CT. This effect can be justified by the exposure of negatively charged phosphate groups on the surface. The value of pKa reported in the literature for the complete deprotonation (from $-HPO_4^-$ to $-PO_4^{2-}$) of the phosphate group of tocopheryl phosphate is around 6 [197]. The obtained curve of CT_aTP_coating basically agrees with the literature, even if the pKa seems to be shifted to around 5 (according to the onset of the plateau). A partial exposition of OH groups of the substrate (CT) could be supposed at this stage, but it will be excluded considering the measured thickness of the coating (see paragraph 2.8.2).

Both CT and CT_aTP_coating showed high wettability. In fact, water, being strongly adsorbed by hydrophilic surfaces, hardly detached from it, making slow the replacement by OH groups from the solution even if pH is increasing. As a result of this process, the ζ potential slightly changed by changing the pH of the solution, above pH 5.5, because the functional groups of the surface did not

change their chemical state and no ions were adsorbed from the solution.
The curve obtained on CT_aT_coating was significatively different from that of CT, confirming the presence of the coating, but the acidic behaviour was also different from the surfaces containing aTP. Indeed, there was a shift of the IEP up to 3.6, slightly lower than 4, suggesting that there were only very weak, even if still acidic, groups exposed on the α-tocopherol coated surface. In fact, an IEP of 4 is expected for a surface without acidic/basic functional groups (or with a balance between them). This agrees with the chemical behaviour of the -OH groups of α-tocopherol. Indeed, α-tocopherol acts as a very weak acid (pKa = 10.8) and in an aqueous medium, it exists mainly in the non-ionized form. It is of relevance to know from the IEP that these weak functional groups are exposed on the coated surface because of their role in the antioxidant activity of α-tocopherol.

Looking at CT_aT_coating and CT_aTP_fun, it is clear that the zeta potential of the two samples was highly sensitive to pH (high slope of the curves) which is a typical behaviour of hydrophobic surfaces: water is easily substituted by hydroxyl or hydronium ions by changing the pH of the solution. In the case of CT_aT_coating, αT is expected to be a hydrophobic molecule. In the case of CT_aTP_fun, the steep slope of the curve evidenced that the hydrocarbon (phytyl) tail of the molecule was mainly exposed outwards. The absence of the plateau in the basic region can be explained by the lack of negatively charged phosphate groups exposed on this surface by αTP and by a complete covering of the CT substrate and its acidic OH groups. An electrostatic attraction between the phosphate group of αTP and the CT surface can be explained by supposing a linker action by the Ca^{2+} ions used during the functionalization (see the following). An ordered grafting of the αTP molecule can be supposed to occurred on CT_aTP_fun.

For αTP samples, the ζ potential electrokinetic measurement was also performed at constant pH to analyze surface changes in time (98 minutes) in different environments and verify the stability of the grafting (Figure 2.16). Particularly, two acid pH values (3.1 and 4.5) which correspond to the acidosis condition that stresses the cells during inflammation processes were tested. The ζ potential of the functionalized and coated CT samples is rather constant, taking also in view of the fact that a variation of 10 mV between measurements can be considered negligible. There is also a correspondence in the values of the ζ potential between the measurements made at variable pH (the titration curves before reported) and these ones. The ζ potential measured at physiological pH of 7.4, is constant too but, unlike the other two, deviates significantly from the values obtained at variable pH (-55/-60 mV vs. -80/- 85 mV). In conclusion, it can be affirmed that all procedures lead to a stable grafting of the αTP biomolecule both at physiological and inflammatory conditions.

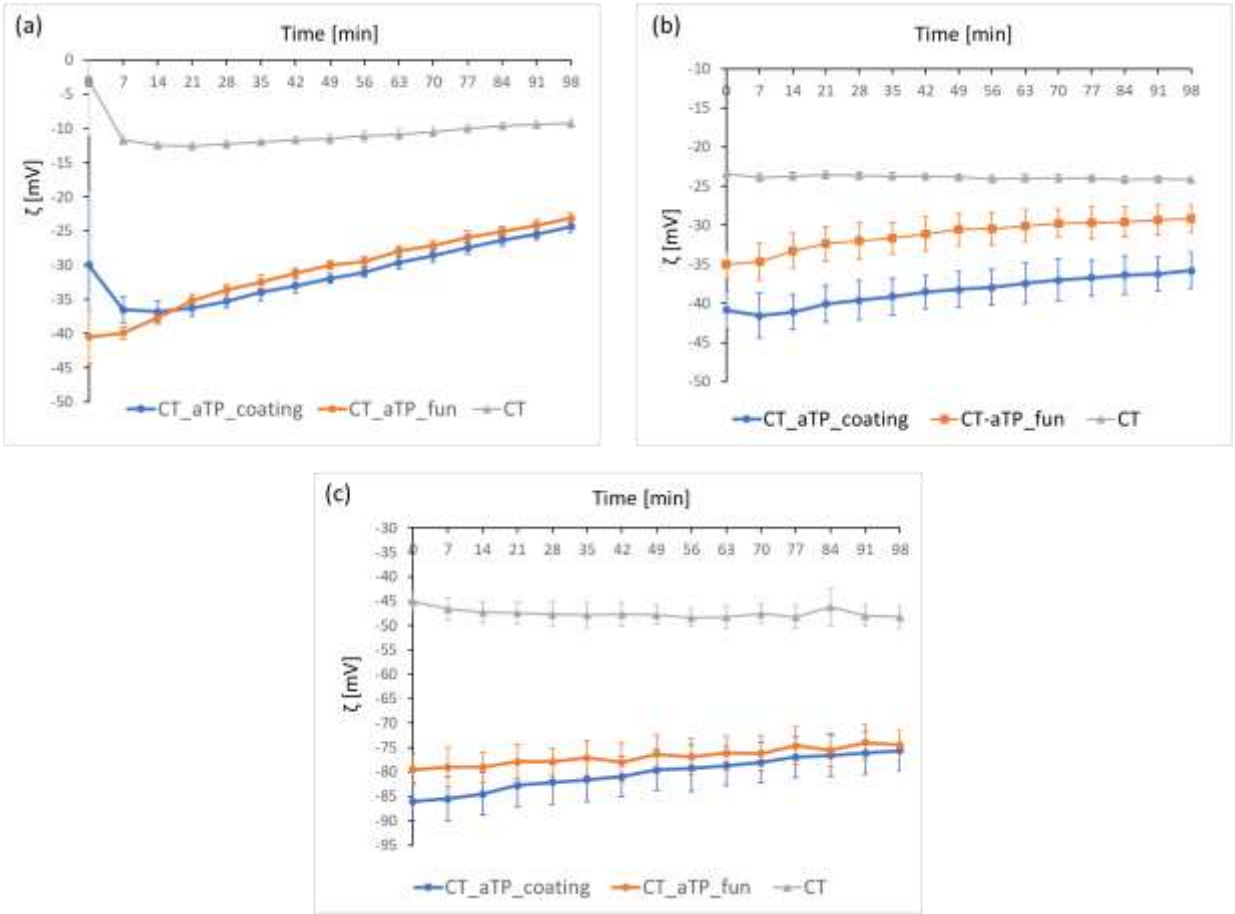

Figure 2.16 Zeta potential at pH costant over 98 min: (a) pH 3 (b) pH 4,5 (c) pH 7,4

2.8.4 Fourier – Transformed Infrared spectroscopy analysis

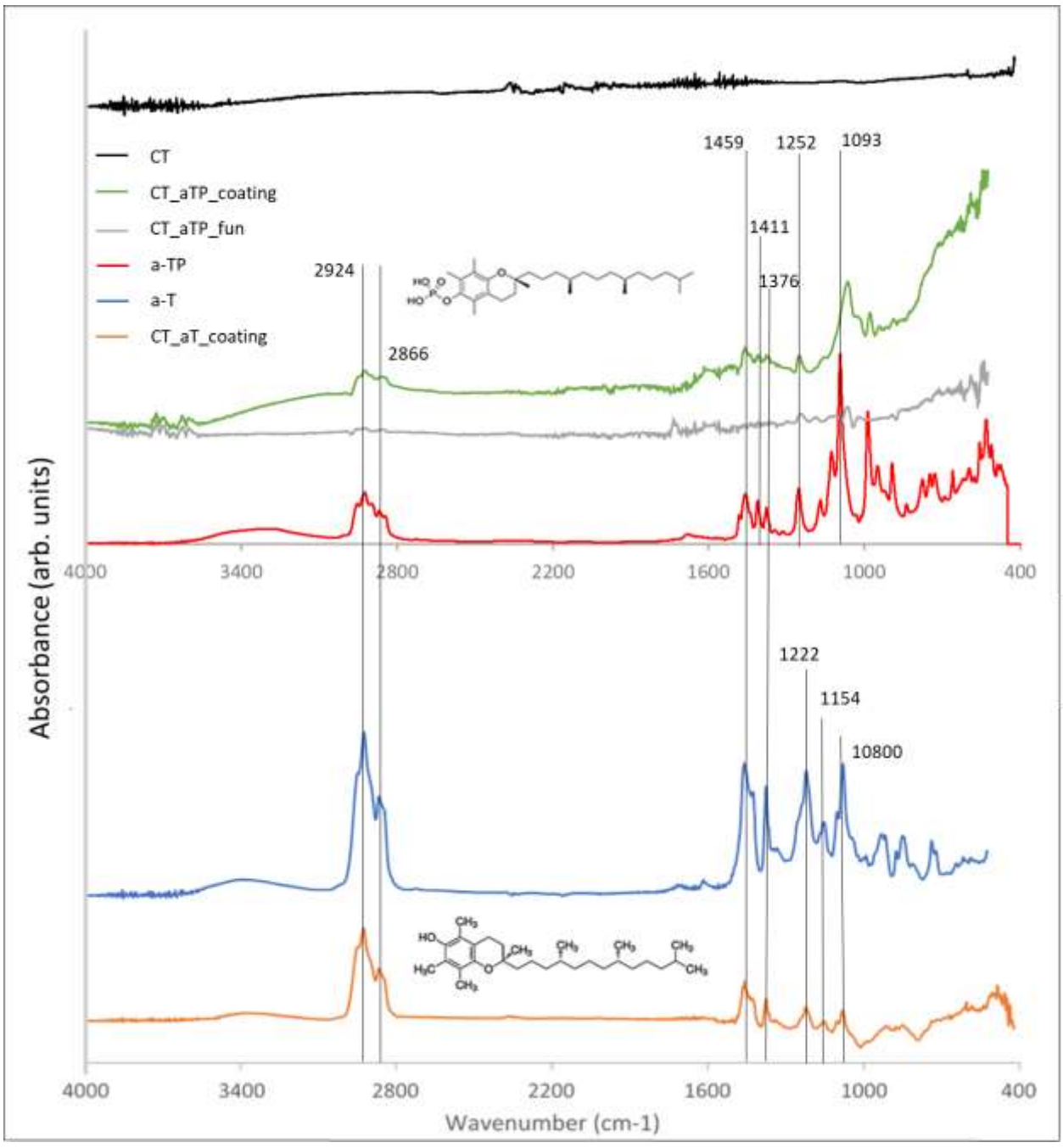

Figure 2.17 FTIR analysis of CT, CT_aT_coating, CT_aTP_coating, CT_aTP_fun, liquid αTP, and liquid αT

FTIR-ATR spectroscopy was used to confirm the presence of the molecules on the modified surfaces and to identify the exposed functional groups on the coated and functionalized surfaces. FTIR analyses were performed on a drop of a solution of αTP, αT, and a CT sample, as controls, and on the functionalized or coated samples (CT_aTP_fun, CT_aT_coating, CT_aTP_coating), respectively. The αTP and αT spectra are useful for identifying the molecular groups typical of these molecules. The spectra obtained are shown in Figure 2.17.

Having the two molecules in question (αTP and αT) common functional groups, peaks at 2924 and 2866 cm^{-1} attributed to the asymmetrical and symmetrical stretching vibrations of $-CH_3-$ and $-CH_2-$ in the long alkyl chain of the molecule [198], were clearly visible in all samples evidencing that the used procedures of surface modification were successful. These signals are stronger on CT_aT_coating than on the other samples. Other peaks that were present in both molecules are at 1459 and 1376 cm^{-1}, associated with the phenyl skeletal and CH bending, respectively [199]. These peaks were clearly visible on the CT_aTP_coating and CT_aT_coating samples, while on the functionalized one (CT_aTP_fun) they were not clearly visible, probably due to the sensitivity of the instrument. CT_aTP_coating had the highest and most defined peaks evidencing the highest amount of the molecule on the surface, compared with CT_aTP_fun.

For the samples modified with aTP, the peak at 1252 cm^{-1} was attributed to the alkyl CH vibration [200]. This peak was clearly visible in both samples (CT_aTP_coating and CT_aTP_fun), confirming the presence of the long side chain of the molecule. The peak typical of αTP, which makes the difference with α-tocopherol, is the one at 1093 cm^{-1} attributed to the phosphate group, specifically the stretching band of $-PO_4^{2-}$ [201]. This peak turned out to be slightly shifted on both the samples, probably due to the formation of a complex with Ca^{2+} ions which were adsorbed on the surface before the grafting of αTP.
On the other hand, in addition to the peaks already mentioned regarding the αT molecule, others can be found on the coated samples: 1222 cm^{-1} and 1154 cm^{-1} attributed to the -CO stretching of the phenol group, and 1080 cm^{-1} for the phenyl bending [199], [202], [203]. This led us to conclude that the spectrum of the coated αT sample, (CT_aTP_coating) clearly shows the presence of characteristic peaks of α-tocopherol.

2.8.5 Contact angle measurements and surface free energy

Considering the relevance of the wettability of a biomaterial for the biological response (protein adsorption, cells, and bacteria adhesion), contact angle measurements were performed in aqueous media both without (water) and with proteins and organic compounds (DMEM, LB). The graph showing the mean contact angle values, with their standard deviations, is reported in Figure 2.18 The liquid media used for the measure were water, DMEM (used for the cellular analysis), and LB (used for the bacterial analysis), respectively.

As expected, the wettability of the chemically treated titanium sample (CT) was significantly higher than that of the polished titanium alloy (Ti64) for all liquid media used ($p < 0.05$), as a consequence of the exposure of hydrophilic -OH groups on the titanium oxide layer [27]. Regarding surfaces with αTP, the functionalized sample (CT_aTP_fun) had the highest contact angle compared to the coated ones (CT_aTP_coating, CT_aT_coating) ($p<0,05$). This can be explained by assuming that, in the functionalized sample, the αTP molecules used the phosphate group ($-PO_4^{2-}$) to create a bonding with the previous adsorbed Ca^{2+} ions, thereby exposing outwards the long hydrophobic alkyl chain, in agreement with the previous data (zeta potential titration curves). On the other hand, the wettability of the αTP coated samples (CT_aTP_coating) is not significantly different from that of the CT sample ($p>0.05$), in agreement with the exposition of the hydrophilic phosphate group. Coated sample with α-tocopherol had significantly higher contact angles ($p < 0.05$) compared to the chemically treated (CT), polished (Ti64), and αTP coated (CT_aTP_coating) samples, due to the presence of the hydrophobic α-tocopherol which is adsorbed on the surface. The contact angles did not significantly change by varying the liquid medium in the case of CT or Ti64 ($p > 0.05$), while they change ($p < 0.05$) for all the modified samples (CT_aT_coating, CT_aTP_coating, and CT_aTP_fun), which showed slightly higher wettability if the liquid medium used was DMEM or LB with respect to water. This agrees with the presence of an organic compound on the modified surfaces.

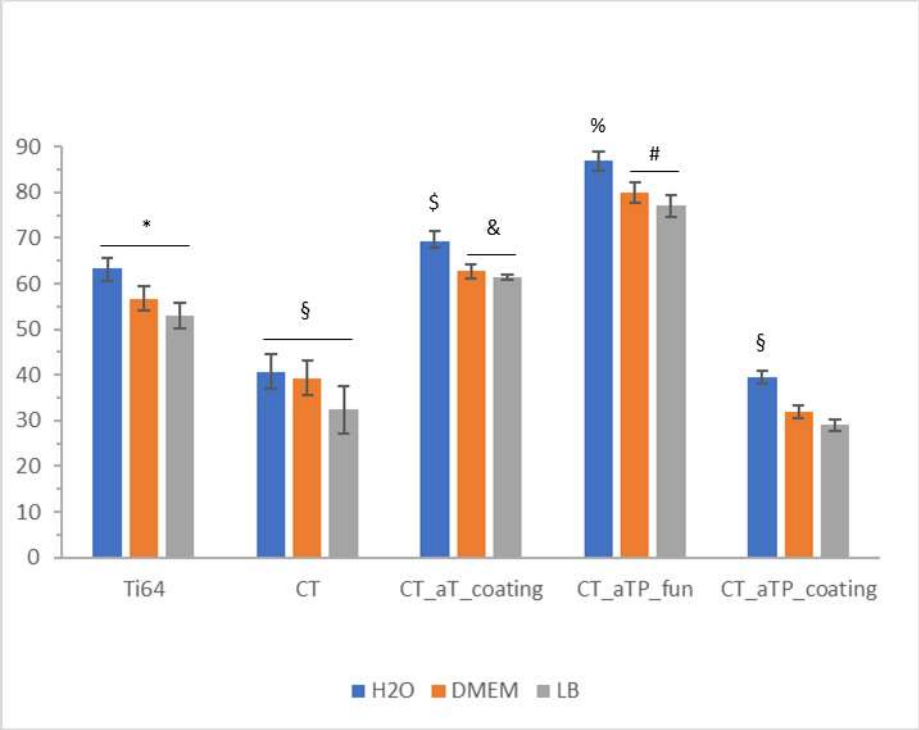

Figure 2.18 Contact angles measured by using water, DMEM, and LB on Ti64, CT, CT_aT_coating, CT_aTP_fun, and CT_aTP_coating. When the same symbol is reported on two columns it means that no statistically significant difference was registered.

Regarding the coating with α-tocopherol, a deeper investigation was performed by using hexadecane as a testing liquid medium; Ti64 and CT were used as references. The obtained results can be discussed on the basis of the surface energy (γ) of the different surfaces and liquid media. Figure 2.19 shows the surface energy of polished Ti64, CT, and CT_aT_coating samples. The surface energy (γ) of polished Ti alloy (Ti64) was 56 mN/m, it increased up to 73 mN/m after the chemical treatment (CT) and decreased to 39 mN/m after coating with α-tocopherol. Therefore, the coating had surface tension similar to some common polymers such as PVC, but lower than polystyrene commonly used for cells (44mN/m) or bacteria (46 mN/m) cultures. Polymers classified as surfaces with extremely low surface tension, such as fluoride thermoplastics, have surface tension in the range of 5-30 mN/m. This result is important for α-tocopherol coating because a general rule is often reported [204] about a threshold between the adhesive and not adhesive surfaces at the critical surface tension of 40 mN/m (aqueous contact angle around 60°), whereby surfaces with lower surface tension are not adhesive: it is interesting to note that the α-tocopherol coating is close to this threshold. Even if such a detailed investigation

was not performed on the other samples (CT_aTP_fun and CT_aTP_coating) and their values of surface energy are not exactly known, the contact angles with water are clearly lower than 60° for CT and CT_aTP_coating and larger for CT-aTP_fun: these results will be of interest for the discussion of the biological response of these surfaces.

The obtained values of surface energy can be used to discuss the contact angles obtained by using LB and DMEM. Higher wettability is expected by increasing the surface energy of a solid and decreasing the surface tension of the liquid. LB has a lower surface tension (57-60 mN/m) than DMEM (70 mN/m^2) and water (73 mN/m^2). According to this rule, the observed decreasing trend of wettability moving from CT to Ti64 and, finally, to CT_aT_coating was explainable; analogously, the slightly higher wettability of all the modified surfaces by LB can be explained. However, it is not easy to explain why the modified surfaces had higher wettability by DMEM than by water. Considering the complex formulation of the media for biological tests, it is not surprising that surface tension is not the unique key factor.

Another interesting factor is the distribution of dispersive and polar surface energy depending on the sample: on CT, it is clear that the polar surface tension was increased as the surface was enriched with acidic and polar OH groups after the chemical treatment. On the other hand, the dispersive energy increased after coating with α-tocopherol because of the presence of the long organic chain covering the surface.

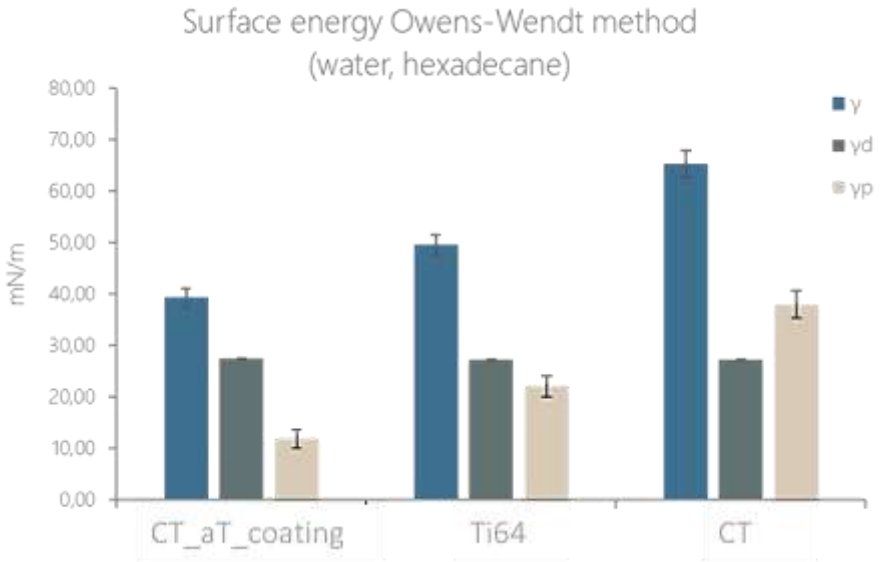

Figure 2.19 Surface Energy of CT_aT_coating, Ti64, and CT

2.8.6 Tape test

This test is useful to evidence the mechanical adhesion of the coating to the substrate; it is of relevance considering the mechanical stress and friction applied to a bone implant during surgery. Considering that it is not easy to mimic the friction applied during the surgery, this test has been considered the worst case. Since it was not possible to visualize the coating at the optical microscope, as foreseen by the protocol of the tape test to calculate the degree of adhesion of the coating to the substrate, other methods of analysis were used here.

Figure 2.20 shows the FTIR analysis of the as-prepared CT_aT_coating sample, as well as of the sample after the tape test (CT_aT_tape). This sample was selected for this test considering that FTIR and UV-Vis analyses evidenced a thicker coating on it. The comparison revealed that, as expected, the test induced a partial removal of the coating, but part of the α-tocopherol remained adherent to the surface as the principal absorption peaks of the molecule (corresponding to the CH stretch) were observable on CT_aT_tape (2924 cm^{-1} and 2866 cm^{-1}). Different areas with a different appearance at a visual glance (as reported in the insets of Figure 2.20) were analysed, obtaining a similar FTIR spectrum. It can be concluded that a layer of the coating was still present on the surface after the tape test even if it was randomly partially removed.

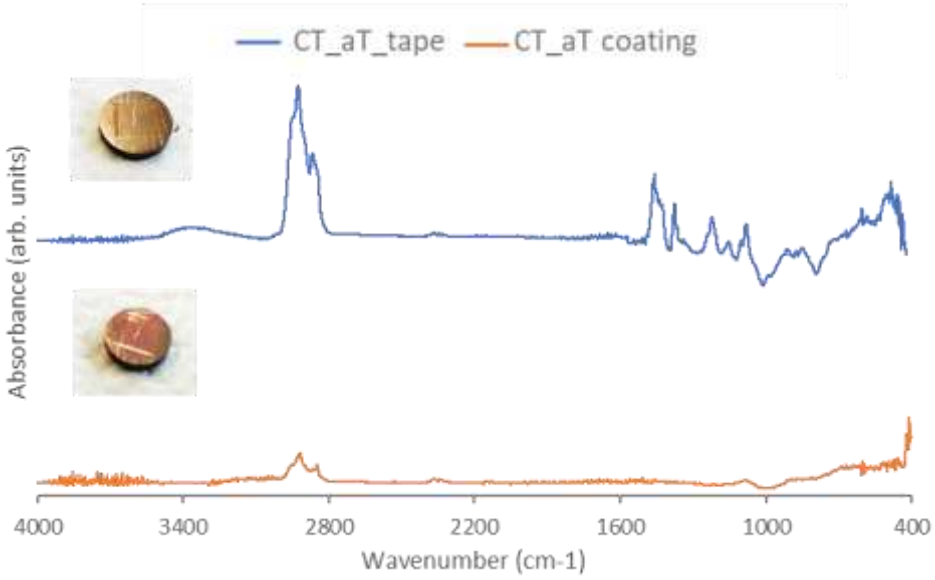

Figure 2.20 FTIR Analysis of CT, CT_aT_tape, and CT_aT_coating samples

To get a quantitative idea of the amount of the coating lost during the test, the coatings of CT_aT_coating and CT_aT_tape were dissolved in ethanol, and the solutions were analysed by UV-Vis as described in the Materials and Methods section. Table 2.7 shows the obtained values: the percentage of the coating remaining on the surface after the tape test was around 24%.

Table 2.7 Calculated values of α-tocopherol in the coating of the samples before and after the tape test

	Peak Area	***C (mg/mL)***	***αT in the coating (mg)***
CT_aT_coating	2.33±0.5	0.0221±0.013	0.221±0.13
CT_aT_tape	0.55±0.08	0.0052±0.001	0.052±0.01

2.8.7 UV-VIS Spectroscopy

The UV-Vis spectra of CT, CT_aT_coating, CT_aTP_coating, and CT_aTP_fun are shown in Figure 2.21. The CT sample had a spectrum with clear interference ripples, due to the transparent titanium oxide layer that was created on the surface by the chemical treatment: multiple reflections occurred at the interface between the transparent surface layer and the metal. The characteristics of the surface titanium oxide layer of CT have been reported elsewhere [205].

All three curves show an upward trend, probably caused by the absorption of UV light by titanium dioxide (TiO_2) [206].

The coated samples (CT_aTP_coating and CT_aT_coating) exhibited less pronounced and less extensive ripples, indicating the presence of a continuous coating masking the titanium transparent oxide layer. It was clear that the CT_aT_coating curve was flatter than the CT_aTP_coating curve, suggesting that α-tocopherol created a thicker coating than αTP on the CT surface. The spectrum of the functionalized sample (CT_aTP_fun) still showed rather pronounced ripples suggesting that the oxide layer had been only partially masked.

For all the curves, there was a flattening of the spectra of the functionalized and coated samples in the region between 250-300 nm, that is the region where the peak absorbance of αTP and α-tocopherol occurs [184]: it is most evident for the coated (CT_aTP_coating and CT_aT_coating) samples, confirming the presence of a thicker masking coating.

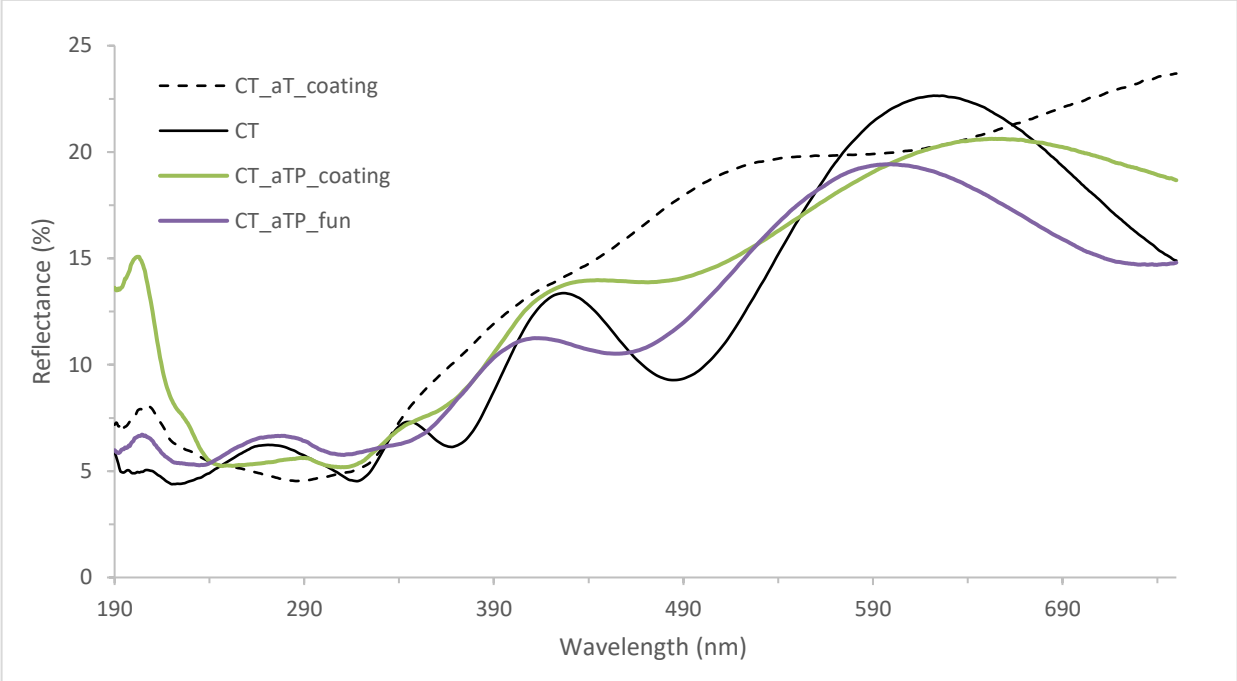

Figure 2.21 Reflectance spectra for CT, CT_aT_coating. CT_aTP_fun, and CT_aTP_coating

2.8.8 Kelvin probe force microscopy

An investigation of the distribution of αTP on CT_aTP_fun and CT_aTP_coating was performed to clarify if it was continuous or not. CT_aT_coating was not investigated by this technique because it was already clear from previous analyses (zeta potential titration curves and UV-Vis) that it was a continuous coating completely covering the CT substrate. The use of AFM equipped with a Kelvin probe allowed us to image the presence of the αTP molecule on the surface of the samples by measuring the electrical potential difference on the border between a chemically treated area and a functionalized or coated one on the same sample (Figure 2.22 a-d). Figure 2.22 shows the macro-optical image of a partially coated sample used for this analysis. Figures 2.22b and d show the electric potential of the surface as a 3D image and its absolute value along a horizontal line, respectively. The electric potential difference between the two areas was about 60 mV, with the coating having a lower potential, as expected. The electric potential was homogeneous on the coated area and this result confirmed the presence of a continuous layer of αTP on the surface of CT_aTP_coating. Despite the high electric potential difference and the coating visible to the naked eye, there is no difference between the two halves in the AFM image of the topography, as shown in Figure 2.22c, which means that the micro- and nano-textures of the CT surface were not covered by the coating. This observation is important if the osteogenic properties of the surface are to be preserved.

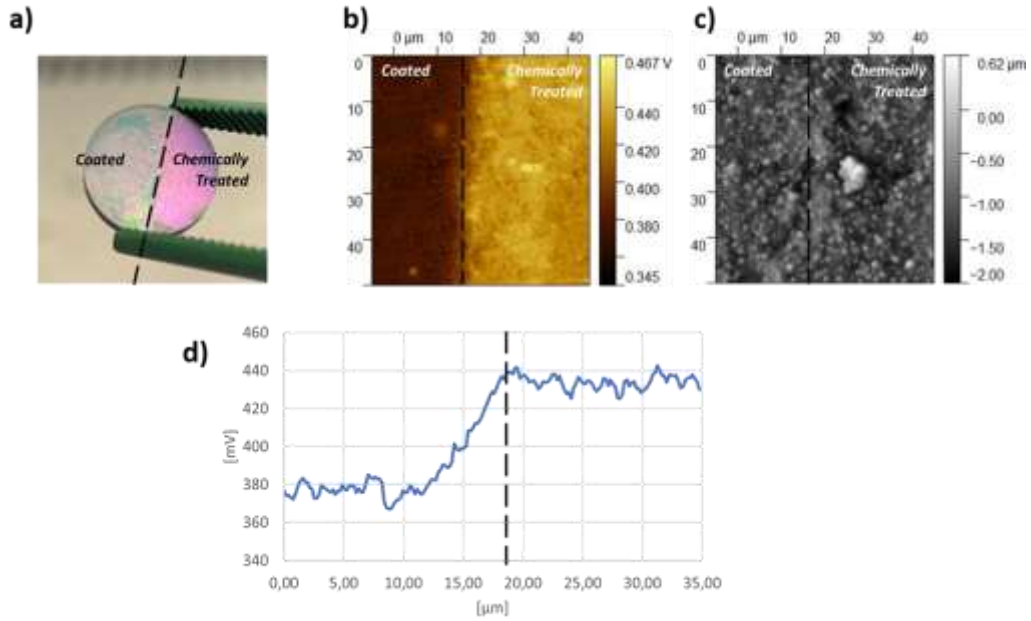

Figure 2.22 AFM and Kelvin Probe measurements on a partially aTP coated CT sample: (a) macro-optical image of the sample. (b) Image of electric potential of the sample, measured at the border between the coated and un-coated parts. (c) Topography of the sample (d) 35 µm long profile signal

Figure 2.23 shows the same images and data in the case of a partially functionalized sample. In this case, the border between the two areas of the sample was not as sharp as it was previously, and it is justifiable considering that a molecular layer of the grafted molecule was expected; a different enlargement has been consequently used for better visualization. Also, in this case, the functionalized surface appeared with a uniform electric potential. The electric potential difference between the functionalized and chemically treated areas was about 40 mV, 20 mV less than in the previous case, which can be considered a significant result in terms of the different amounts of αTP molecules on the two surfaces. Moreover, as Figures 2.23 a and c show, the difference between the two halves was not visible to the naked eye and by AFM topography imaging. It can be concluded that a thinner layer of the αTP molecule is grafted on the functionalized samples than on the coated ones, but, in both cases, the grafted molecule formed a continuous layer, and micro-and nano-topography of the surfaces (due to the chemical treatment) was preserved.

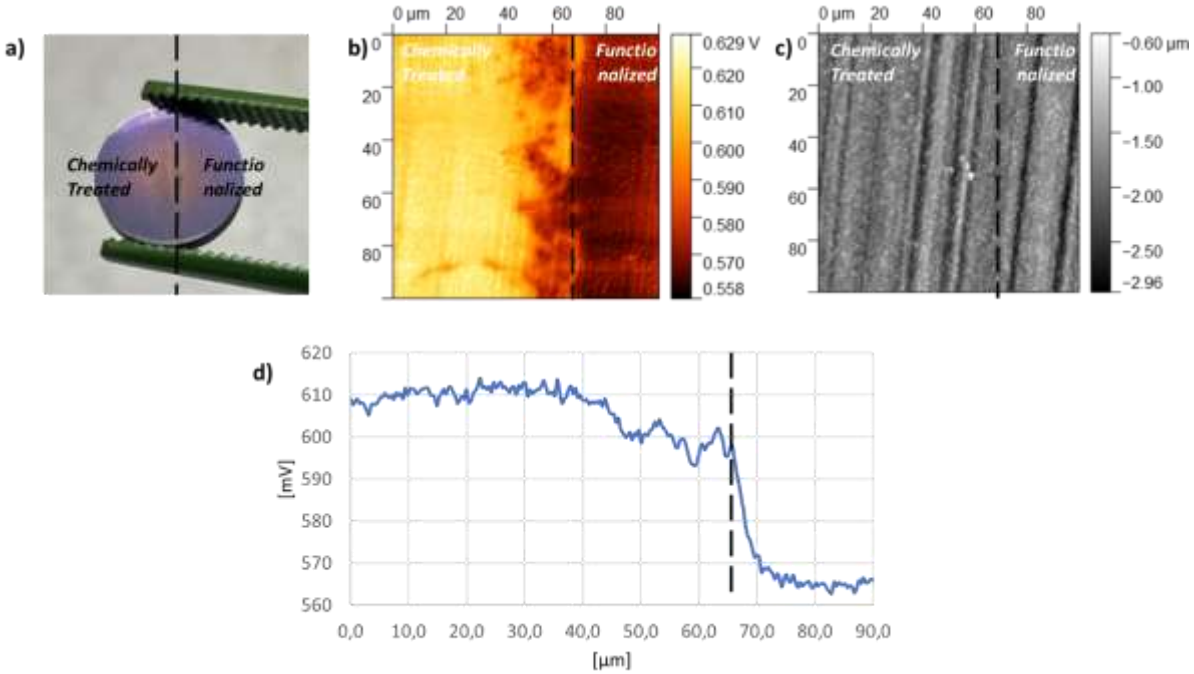

Figure 2.23 AFM and Kelvin Probe measurements on a partially αTP functionalized CT sample: (a) macro-optical image of the sample. (b) Image of electric potential of the sample, measured at the border between the coated and un-coated parts. (c) Topography of the sample (d) 90 µm long profile signal

2.8.9 X-ray photoelectron spectroscopy (XPS)

Table 2.8 Atomic percentage of the elements detected on CT_aTP_fun, and CT_aTP_coating after XPS analysis

	O	***C***	***Ti***	***P***	***Ca***	***Other***
CT	46.9	41.8	10.3	-	-	1.1
CT_aTP_fun	33.7	54.9	8	1.2	0.4	1.8
CT_aTP_coating	15.7	79.3	-	2.3	0.4	2.3

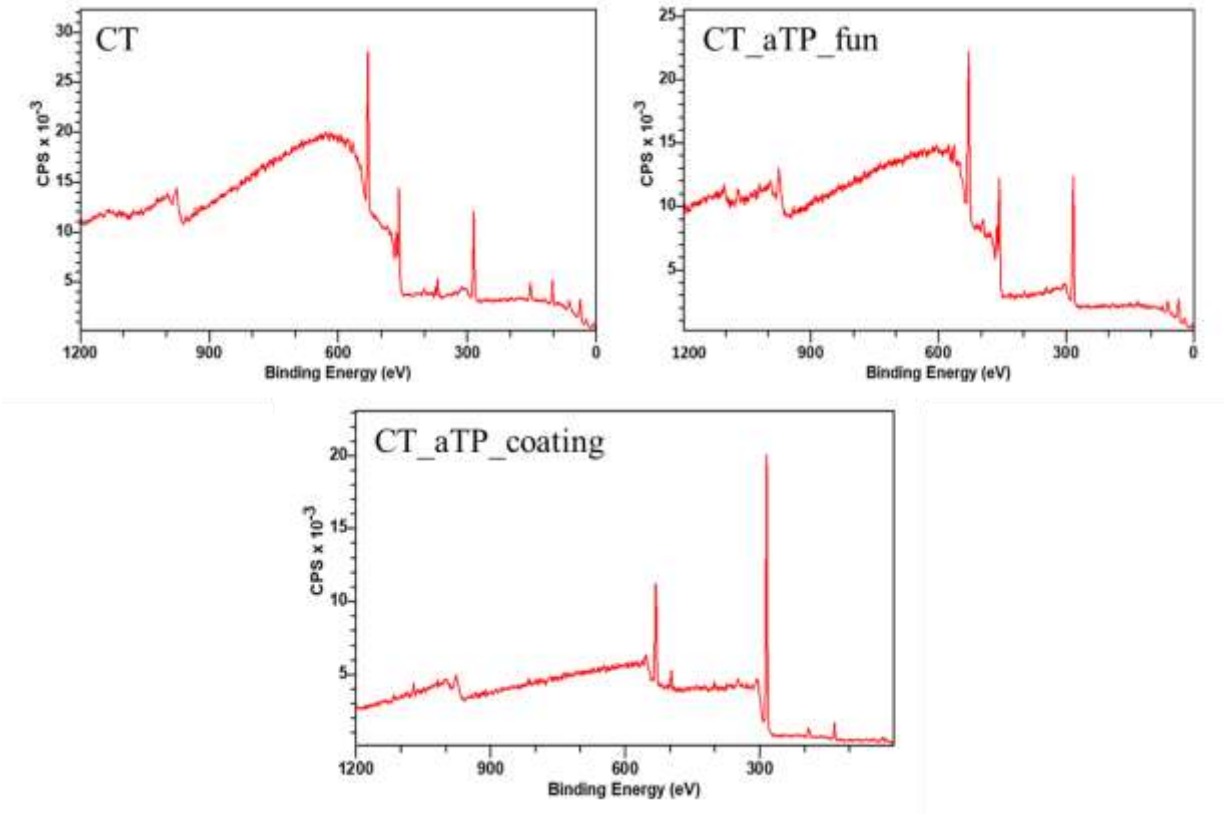

Figure 2.24 Survey spectra for CT, CT_aTP_fun and CT_aTP_coating

XPS analysis was performed on the α-tocopheryl phosphate coated and functionalized samples (CT_aTP_coating and CT_aTP_fun), and on the control sample (CT) as a reference, for a better understanding of the thickness of the grafted layers, orientation, and grafting mechanism of this molecule on the different surfaces. The atomic element percentage, as detected in the survey spectra of the different samples, is reported in Table 2.8 and survey spectra for the three samples are reported in Figure 2.24. A large amount of oxygen was detected on the CT sample, confirming the presence of an oxide layer on the surface. The Ti amount is similar for the CT and CT_aTP_fun sample, while on the coated (CT_aTP_coating) sample, the Ti alloy substrate was not detectable, supporting the previous results (UV-Vis reflectance, FTIR) that showed the presence of a thicker coating on this sample. In addition, the maximum penetration depth of the XPS analysis is around 10 nm, which indicates that the coating thickness is such that the substrate cannot be seen by the instrument. A high percentage of carbon was found on the CT since, as a common contaminant, it adsorbs very easily on titanium surfaces, but it grew considerably for CT_aTP_coating, with respect to the CT sample, because of the presence of the organic coating, whereas the percentage of oxygen decreased because of the titanium oxide layer is no more detectable. Phosphorous, the element that is characteristic of the αTP molecule, was present in small amounts on both samples (on CT_aTP_fun it was half than on CT_aTP_coating) and obviously not present on CT. Calcium was detected on both the modified surfaces in small amounts (CT_aTP_fun and CT_aTP_coating) as a result of the 24 hours immersion in a solution of $CaCl_2$.

For the determination of the chemical state and binding energy of the elements, a high-resolution analysis was performed on the oxygen and carbon regions, as shown in Figure 2.25. In the O1s region, the CT sample, as expected, had a clearly visible signal given by the bridged acidic OH groups (around 530.5-531.0 eV) and a lower signal due to the terminal basic OH groups at 531.5-532.0 eV. A large contribution around 530.4 eV attributed to Ti-O bonding was also visible and assigned to the TiO_2 oxide layer [207]. In contrast, the spectrum of the CT-coated sample (CT_aTP_coating) was significantly different: the signal attributed to the Ti-O bond disappeared (in agreement with the absence of Ti in the survey), confirming the presence of a thick coating. Instead, it showed the signals of the phosphate group at about 531 eV (-P=O) [196] and 532.5 eV (-POH) [208], confirming the findings of the ζ potential and contact angle (see next paragraph) measurements, according to which the ionic, hydrophilic phosphate group is largely exposed on the outermost layer of the coating. On the CT_aTP_fun functionalized samples, the presence of the characteristic TiO_2

peak was evident (in agreement with the presence of Ti in the survey), confirming that the αTP layer is so thin to make the oxide layer still detectable by XPS on the functionalized sample. The region of the OH group had several contributions coming from the acidic OH groups of the titanium oxide layer (around 531 eV), overlapped with the -P=O signal of the phosphate group, and the basic OH groups of the titanium oxide layer, overlapped with the -P-OH signal (around 532 eV).

Looking instead at the carbon region, the main signal was at 284.8, which is attributed to the C-C and C-H bonds that are always present on the surface of titanium due to the presence of hydrocarbon contaminants. These chemical bonds were also present in the grafted αTP molecule and, as expected, the related peak was higher on the coated CT sample (CT_aTP_coating). The other two peaks present in the carbon spectra were associated with the C-O (286.3 eV) and C-O-C (286-287 eV) bonds [209]. The spectrum of the functionalized sample (CT_aTP_fun) was slightly shifted to the right due to the detection of the C-Ca signal [210]. According to the obtained data, it can be concluded that the result of the functionalization process was the adsorption of Ca^{2+} ions by the acidic OH groups of the titanium oxide layer, linking a molecular layer of αTP, bonded to the substrate through electrostatic attraction with the phosphate group of αTP and exposing outwards the hydrocarbon tail. In the case of the coating, αTP makes a thicker coating exposing phosphate groups on the outermost layer.

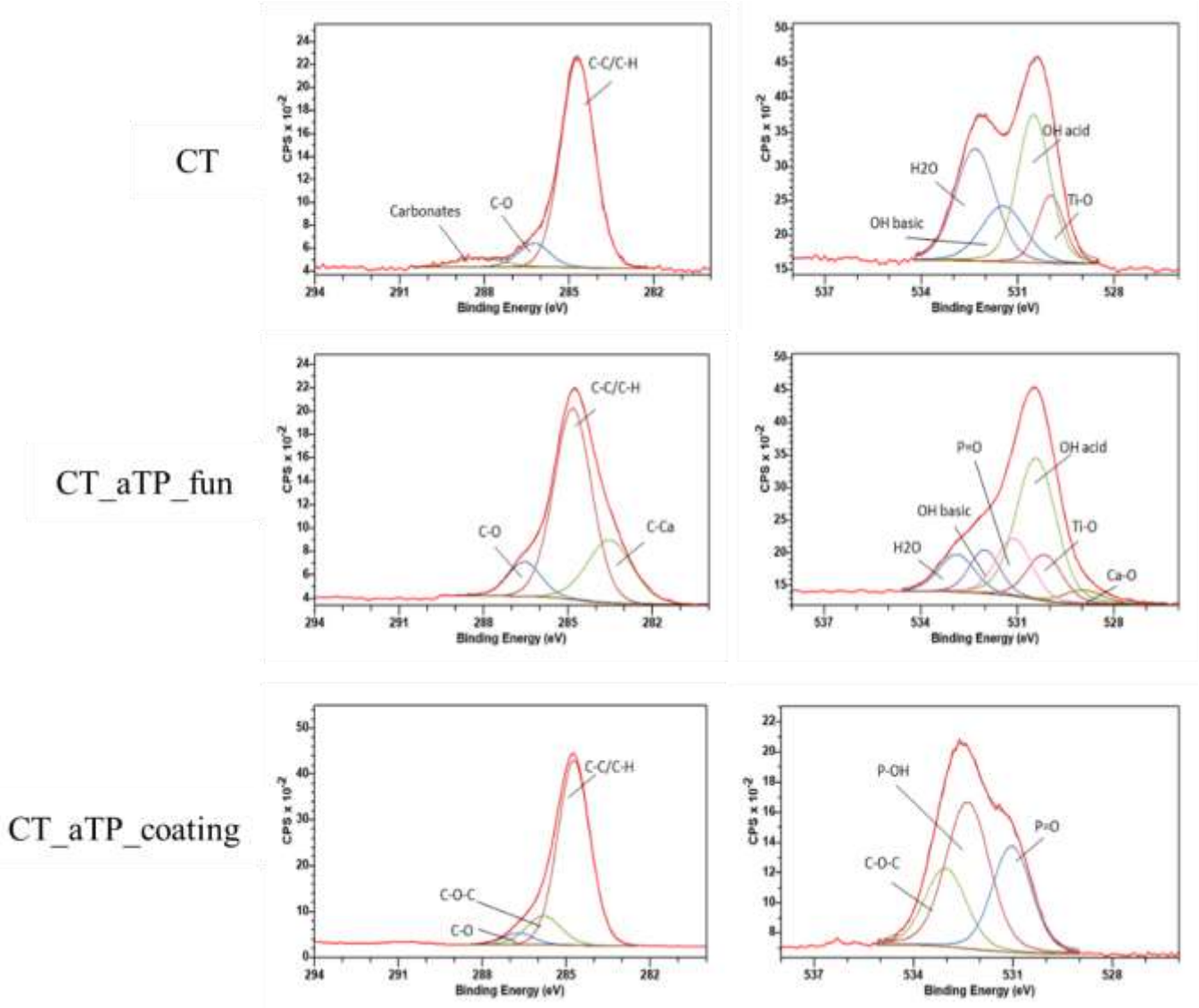

Figure 2.25 High-resolution XPS spectra of C and O1s regions of CT, CT_aTP_coating, and CT_aTP_fun

2.8.10 Biological evaluation of CT_aT_coating

Biofilm adhesion on α-tocopherol coating

The results reported in Figure 2.26 showed that the number of floating bacteria unable to adhere to CT_aT_coating after 2 h of direct infection was two orders of magnitude higher than those ones observed for the Ti64 controls ($p<0.05$, indicated by #). As a consequence, the metabolic activity evaluated by the Alamar blue assay after 24 h of direct cultivation onto control specimens resulted in values 1.8 and 1.6 times in comparison with CT_aT_coating considering E. coli and S. aureus, respectively (Figure 2.26 c, $p<0.05$ indicated by #). However, the fluorescence live/dead assay (Figure 2.26 b) applied to the floating bacteria collected from specimens' supernatants revealed that >80% of bacteria were viable (stained in green) and only a small minority was reported as dead (stained in red) for both Ti64 and CT_aT_coating thus suggesting an antifouling role of α-tocopherol rather than to an antibacterial effect. As a confirmation, images showed that bacteria aggregated with each other forming clusters (Figure 2.26 c, indicated by the arrows) that are probably representative of poor adhesion because they found an anchorage to other bacteria rather than the specimens' surface.

To verify that the antifouling activity was mainly due to the presence of aT, results were also compared to the chemically treated specimens (CT); the significant differences observed for both the CFU count (Figure 2.26 a, $p<0.05$ indicated by §) and the metabolic activity evaluation (Figure 2.26 c, $p<0.05$ indicated by §) between CT and CT_aT_coating specimens definitely suggested a specific role of the α-tocopherol coating in conferring protection from infection. Moreover, the similar behavior of the Gram+ S. aureus and the Gram- E. coli appears to exclude the role of cytoskeleton rearrangements that is normally observed for nanometric topographies that are more effective towards Gram+ species. So, the anti-adhesive effect is most likely due to the hydrophobicity degree of the α-tocopherol coating as previously described in the physico-chemical characterization (Figure 2.26).

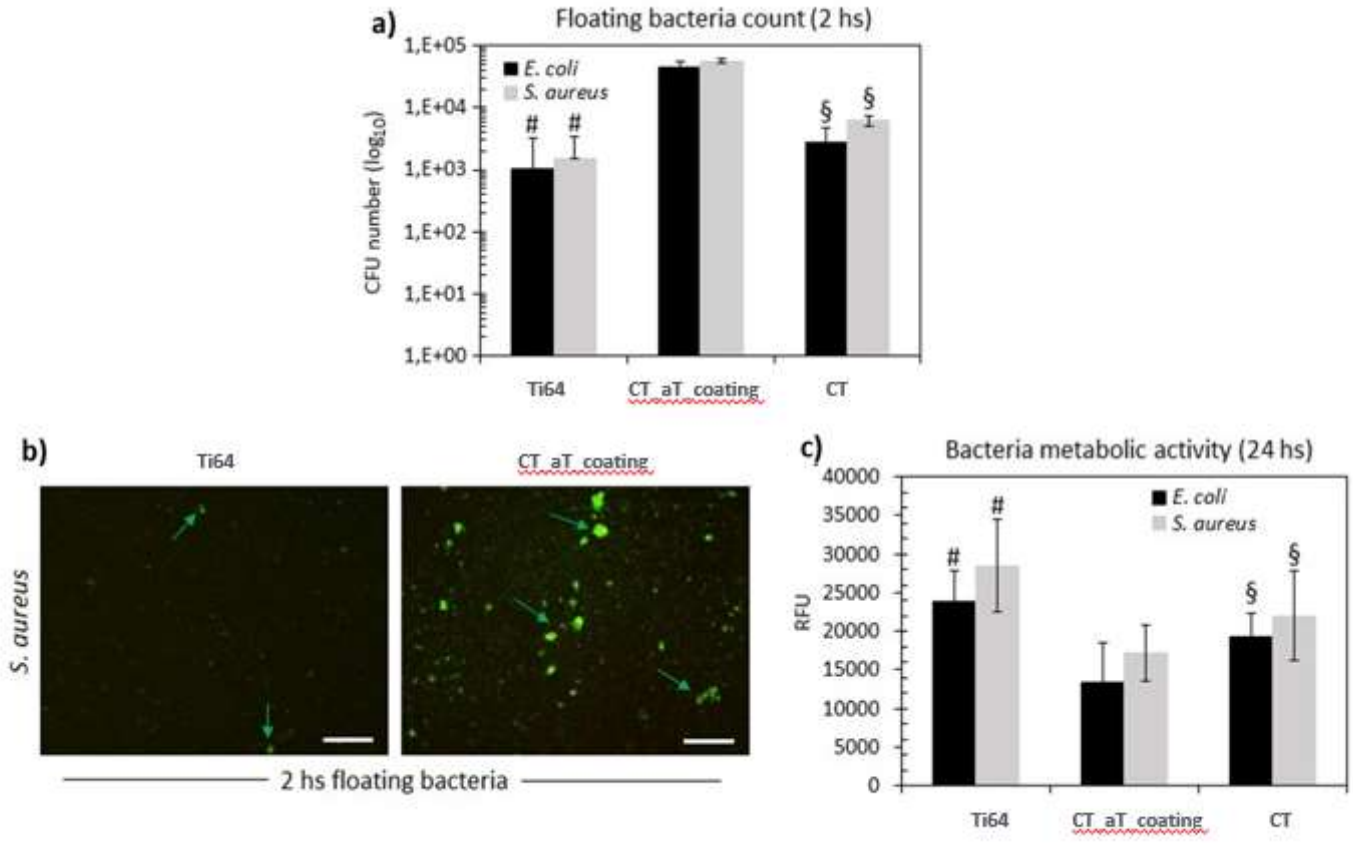

Figure 2.26 Antibacterial Assays of CT_aT_coating
(a) Floating bacteria colonies count (CFU) after 2 h of adhesion revealed that the aT coating significantly increased the number of non-adherent bacteria in comparison to Ti64 ($p<0.05$, indicated by #) and CT ($p<0.05$, indicated by §). (b) Live/Dead assay confirming that the detached cells were viable (stained in green) as well as (c) the metabolic activity of the cells cultivated onto the specimens' surface after 24 h confirmed a significant reduction of the viable colonies onto CT_aT specimens in comparison to Ti64 ($p<0.05$, indicated by #) and CT ($p<0.05$, indicated by §). Bars represent means±s.d; images bar scale =125 µm.

Cells adhesion α-tocopherol coating

After demonstrating the α-tocopherol antifouling effect towards pathogens colonizing joint implants, the possibility to obtain the same effect with human cells was then investigated. Results in Figure 2.27 showed that the number of cells detaching from CT_aT_coating was six times higher than that observed for the Ti64 controls; accordingly, the αT coating promoted a significant increase of the floating cells in comparison with both Ti64 ($p<0.05$, indicated by #) and CT ($p<0.05$, indicated by §) specimens. As a consequence, the metabolic activity evaluated by the Alamar blue assay after 24 h of direct cultivation onto the specimens was about three times higher for Ti64 controls in comparison with αT specimens (Figure 2.27). Again, the observed reduction of the metabolic activity resulted as significant between the αT coating and both Ti64 ($p<0.05$, indicated by #) and CT ($p<0.05$, indicated by §) specimens.
However, to check whether the cells detachment was due to a toxic or anti-adhesion effect coming from the α-tocopherol, the cells detached after 6 h adhesion were moved to a new polystyrene plate and incubated for 24 h; afterward, their morphology and viability were detected by the optical microscope and fluorescence live/dead assay (Figure 2.27 c-d). As expected from the results obtained by the floating cells count, much more cells were detected in the supernatant coming from the α-tocopherol specimens in comparison with the control (Figure 2.27 c, left panel). Moreover, cells mostly appeared as aggregates, forming clusters that are often representative of poor adhesion. However, after cells seeding for 24 h inside a new plate (Figure 2.27 c, right panel) their morphology was comparable to cells collected from the Ti64 controls. As a confirmation, the live/dead assay was applied (Figure 2.27 d) and >95% of cells were viable (stained in green) while only a small minority was dead (stained in red, indicated by the arrow). So, in line with the results, previously obtained from the antibacterial evaluation, it is suggested that α-tocopherol played an anti-adhesive rather than a toxic role that would have affected cell viability over the 24 h cultivation. Therefore, the hypothesis to apply αT to reduce tissue ingrowth on temporary orthopedic implants without introducing toxic was validated.

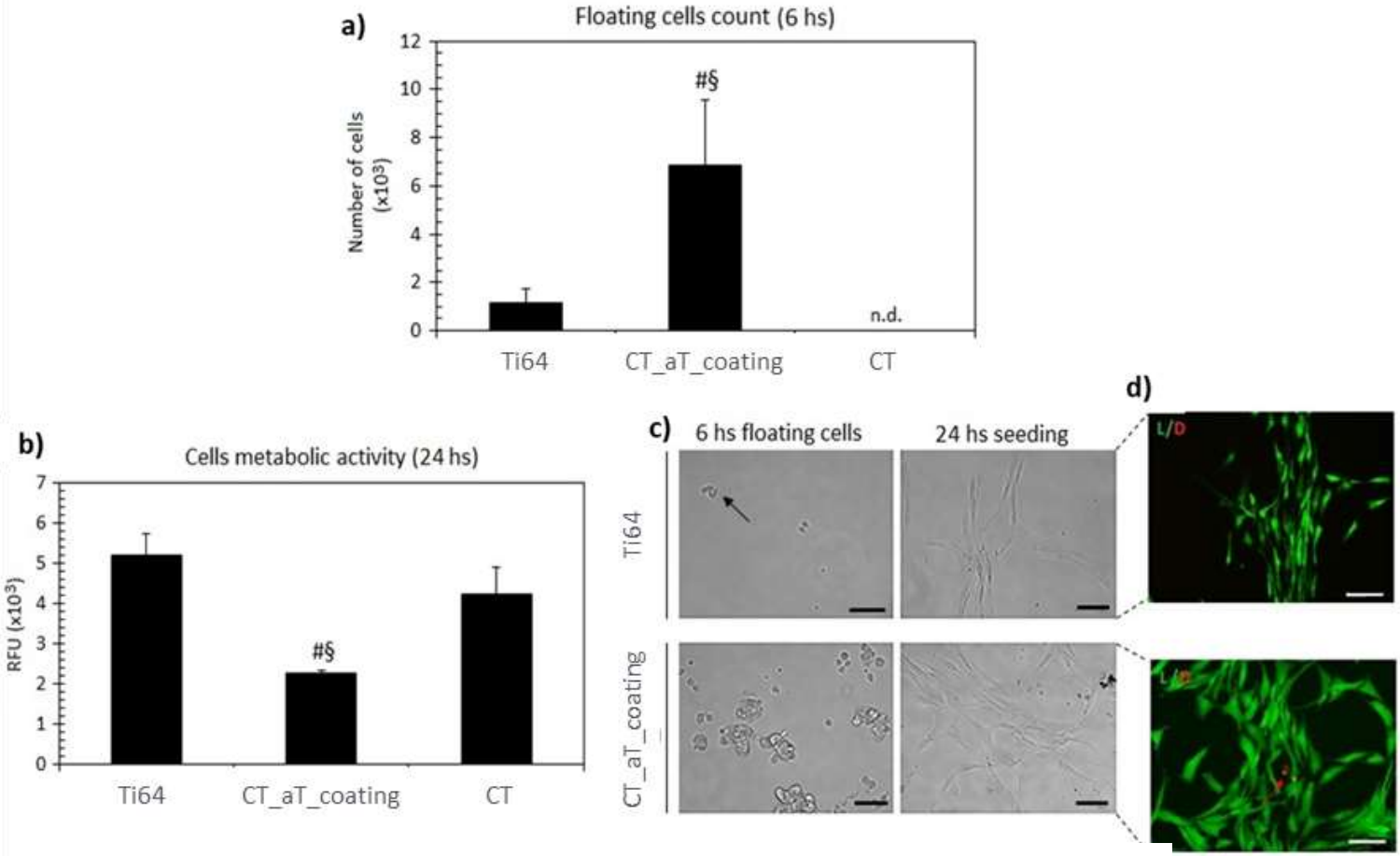

Figure 2.27 Cytocompatibility evaluation of CT_aT_coating

(a) Floating viable cells count after 6 h adhesion revealed that α-tocopherol coating significantly increased the number of non-adherent cells in comparison to Ti64 ($p<0.05$, indicated by #) and CT ($p<0.05$, indicated by §). (b) The metabolic activity of cells cultivated onto specimens' surface after 24 h confirmed a significant reduction of the viable cells onto CT_aT_coating in comparison to Ti64 ($p<0.05$, indicated by #) and CT ($p<0.05$, indicated by §) whereas (c) optical microscope and (d) live/dead assay confirmed that detached cells were viable (stained in green) and more numerous for the CT_aT specimens. Bars represent means±dev.st.; images bar scale=125 μm

2.8.11 Biological Evaluations of αTP grafting

Antibacterial evaluation of α-tocopheryl phosphate

Taken into consideration that bone represents the target tissue for the titanium coated and functionalized specimens, Staphylococcus epidermidis (S. epidermidis) was considered as a reference strain due to its common involvement in orthopaedic and dental implant contamination [211], [212]. Moreover, the selected strain (ATCC 14990) is certified as a pathogen and biofilm former, so it was selected to verify the ability of the coating to prevent surface colonization and subsequent 3D biofilm-like formation. Accordingly, specimens were processed with a direct infection of the surface to simulate bacterial colonization of the exposed implant. Results in Figure 2.28 showed the metabolic activity of bacteria grown for 24 hs onto the mirror-polished and treated samples as control (Ti64 and CT, respectively) and on functionalized and coated samples (CT_aTP_fun and CT_aTP_coating, respectively). Results are expressed in RFU (relative fluorescent units), and the Ti64 specimens are considered as the control material. The process used to create the αTP surface layer resulted as a key-point for the molecule efficacy: in fact, only the coating (CT_aTP_coating) was effective in reducing the metabolic activity of bacteria in a significant manner in comparison to Ti64, CT samples, and the functionalized ones (Figure 2.28, $p>0.05$indicated by #). A such inhibitory activity resulted in a 93(±6) % reduction of bacterial viability (Figure 2.28) when S. epidermidis colonies were seeded onto CT_aTP_coating surfaces in comparison to the Ti64 control. As a confirmation of the inhibitory activity determined by αTP after coating, when the number of viable colonies (CFU) adhered to the specimens' surface was counted, a reduction larger than 3 logs was observed between CT_aTP_coating and Ti64 control specimens (Figure 2.26, $p<0.05$ indicated by #). CT_aTP_fun prevented bacterial proliferation (the starting infection number is indicated by the dashed line in Figure 2.28), but reduced the final number of ≈1 log, thus failing an irrefutable antibacterial effect. Finally, SEM imaging was used to investigate bacterial morphology and aggregation (Figure 2.28). As expected, from the previous results, the Ti64 and CT surfaces showed a high degree of bacterial colonization and a frequent appearance of 3D biofilm-like aggregates (appreciable in the higher magnification images). On the opposite, the CT_aTP_coating surfaces reported a low degree of contamination and only rare aggregates. The CT_aTP_fun

results as less contaminated than the Ti64 and CT ones, but more colonies (mostly single cells) were detected in comparison with the coated ones. Therefore, SEM imaging basically confirmed the Alamar and CFU results, confirming the very promising efficacy of αTP deposited by the coating method in preventing bacteria colonization of implantable metal devices.

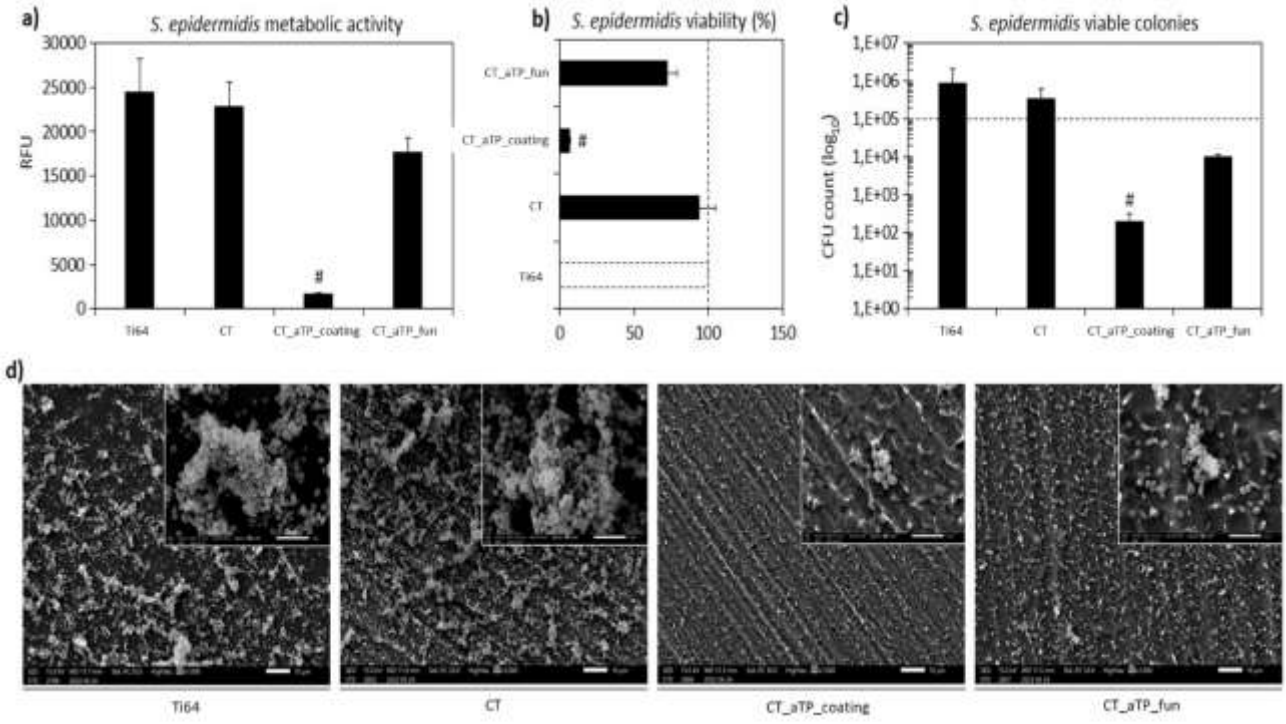

Figure 2.28 Antibacterial activity of CT_aTP_coating and CT_aTP_fun

(a) The αTP coating method resulted as highly effective by significantly reducing the metabolic activity of adhered bacteria in comparison to the other specimens (#=p<0.05). (b) The efficacy of the coating method determined a viability reduction of 93(±6) % with respect to the Ti64 controls. (c) The count of the viable colonies (CFU) revealed a > 3 log reduction between the CT_aTP_coating and the Ti64 controls. (d) SEM images confirmed the lower bacterial colonization degree for the CT_aTP_coating surfaces as well as the reduction of biofilm-like 3D aggregates. Bars represent means±dev.st of replicates=3. SEM images: low magnification=1000x, bar scale=10μm; high magnification=5000x, bar scale=1μm.

Cytocompatibility evaluation of α-tocopheryl phosphate

Tissue growth in tight contact with the device should be expected after the implantation of permanent bone implants; progenitor and mesenchymal cells play a pivotal role in the formation of such tissue-device connections by firstly migrating to the injured site and then by differentiation into the mature bone lineage [213]. In fact, the first tissue-device sealing is crucial for the correct osteointegration avoiding tissue micro-fracture due to scaffold micro-displacements. Therefore, the implanted device should improve or at least not impair the migration and the following colonization of such cells. Following this principle, human mesenchymal stem cells (hMSC) were used to evaluate the cytocompatibility of the test materials coated or functionalized by αTP. Figure 2.29 shows the viability of hMSC cultured directly onto the surface of controls (Ti64 and CT), functionalized, and coated samples (CT_aTP_fun and CT_aTP_coating, respectively) after 24 (Figure 2.29 a), 48 (Figure 2.29 b) and 72 hours (Figure 2.29 c) by means of their metabolic activity evaluation that was expressed as RFU. The results showed an increase in viability at the different time points for the control samples (Ti64 and CT), while the cells seeded onto CT_aTP_fun and CT_aTP_coating showed a significant decrease in comparison to the controls from day 2 of cultivation (Figure 2.29 # and § $p<0.05$ vs Ti64 controls). However, looking at the results reported as lines in function of time in Figure 2.29 d, it can be speculated that the cells onto the αTP doped surfaces were not induced to an apoptotic phase, since the values did not decrease with respect to the first time-point of 24 hours, as it can be expected by a cytotoxic effect. It looked pretty that they were slower to grow with respect to the Ti64 and CT controls where the increase in terms of metabolism was faster (appreciable already at 48 hours, Figure 2.29 d) and continuous over days.
Moreover, an important difference between the coated and functionalized samples can be observed by analyzing the images obtained from fluorescence staining of the cytoskeleton and nuclei (Figure 2.29 e). The morphology of the cells seeded onto the CT_aTP_coating sample resulted as elongated and flat, thus being comparable to the ones adhered and spread onto Ti64 control and CT as well. In fact, the deposition of lamellipodia through the processes of actin filament polymerization and branching was also clearly visible on the coated surface. On the other hand, the cells found on CT_aTP_fun sample did not display a correct morphology: in fact, they were small, rounded, and not interconnected to each other. These results were in line with what was expected:

cells resulted as more prone to adhere to the hydrophilic CT_aTP_coating surfaces, whereas, on the opposite, they did not successfully colonize surfaces with a contact angle greater than 60°, as it was for the functionalized surfaces of the CT_aTP_fun specimens.

Thus, taking into account the objective of this preliminary assessment aimed at determining the safety of doped surfaces, results related to the coating specimens can be considered promising even if further evaluations are still necessary to verify if the specimens will be able to confirm the same cytocompatibility in a real physiological environment in contact with bone (in vivo).

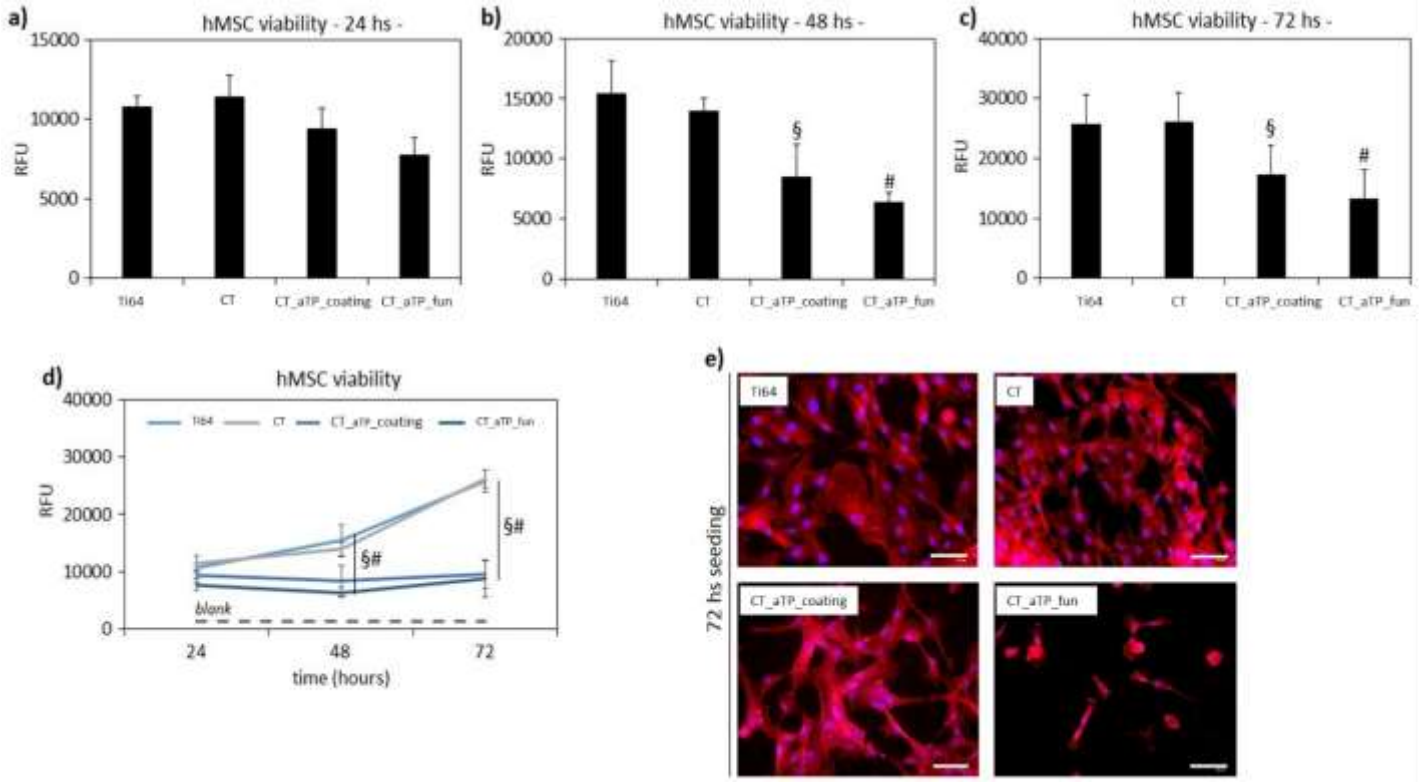

Figure 2.29 Cytocompatibility evaluation of CT_aTP_coating and CT_aTP_fun
(a-c) hMSC metabolic activity was significantly reduced over time by the presence of the αTP in both CT_aTP_fun or CT_aTP_coating with respect to Ti64 and CT controls ($p<0.05$ indicated by § and #). (d) However, results reported as lines in function of time suggested mostly a delayed proliferation rather than a toxic effect since values did not decrease over time in CT_aTP_fun and CT_aTP_coating. (e) Fluorescent images revealed that cells cultivated onto CT_aTP_coating hold a morphology comparable to the Ti64 and CT controls even if with a lower density, whereas cells were mostly round shaped on CT_aTP_fun. Bars represent means±dev.st of replicates=3. Fluorescence images: red=cytoskeleton (phalloidin), blue=nuclei (DAPI), bar scale=100μm.

2.8.12 Anti-inflammatory evaluation of α-tocopherol

The following work is intended to be focused primarily on the anti-inflammatory and immunomodulatory properties of α-tocopherol. As mentioned above, several studies have shown that α-tocopherol has anti-inflammatory effects as it acts on the immune system, enhancing the immune response and increasing resistance against various pathogens. The anti-inflammatory and immune-stimulating properties of α-Tocopherol appear to be related not only to its antioxidant activity, but also to a set of factors associated with modulating signal transduction, altering cytokine production and thus the proliferation of certain cells. [81], [87], [214], [72]
The idea, therefore, is to study in more detail the antioxidant properties of α-tocopherol once the anti-adhesive coating is created on the titanium surface (see paragraph 2.8.9) and its effect on the immune system in vitro.

UV-Vis spectroscopy on the coating before and after soaking

Soaking tests were performed to check the stability of the the αT coating in contact with fluids. Two solutions were used: PBS to mimic a physiological environment and the same solution with the addition of hydrogen peroxide and with a pH of 4.5 to mimic an inflammatory condition. UV-VIS spectroscopy was used to check that the coating was not destroyed and that it remained continuous and homogeneous after the soaking period. With this purpose, testing was done on CT and CT_aT_coating samples, used as controls, and CT_aT_PBS and CT_aT_H2O2 samplesafter the soaking period. The UV-Vis spectra of CT, CT_aT_coating, CT_aT_PBS, and CT_aT_H2O2 are shown in Figure 2.30.
As already discussed (see paragraph 2.8.6), the presence of the coating is identified by less pronounced ripples, due to a continuous coating masking the substrate surface. The important result was the fact that CT_aT_coating, CT_aT_PBS, and CT_aT_H2O2 had comparable UV- Vis spectra. The clear similarity between these spectra indicates the presence of a stable coating on the surface, even after 28 days of soaking, evidencing that α-tocopherol is not significantly released even after a long soaking at both physiological or pro-inflammatory conditions.

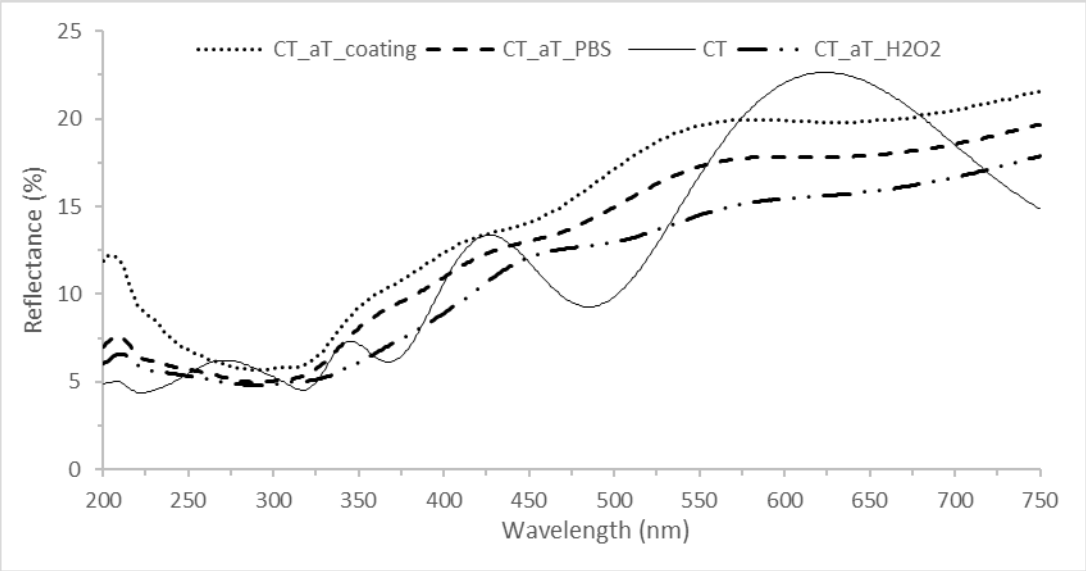

Figure 2.30 Reflectance spectra of samples with (CT_aT_coating) and without the coating (CT), and after the soaking tests (CT_aT_PBS, CT_aT_H2O2)

FTIR-ATR spectroscopy on the coating before and after soaking

In this case, FTIR-ATR was used to identify peaks of the coating that remained after soaking. Figure 2.31 shows the FTIR spectra of coated samples after 28 days of soaking (CT_aT_PBS; CT_aT_H2O2) and of liquid α-tocopherol, as a reference. Samples with and without the coating (CT, CT_aT_coating) are used as references. The samples analysed after 28 days of soaking in PBS, showed peaks identical to the coated sample before soaking, evidencing that the coating is still on the surface even after a long time at physiological conditions (PBS, pH 7.4). A slight shift in the peak corresponding to the CO stretching from 1222 cm^{-1} to 1216 cm^{-1}can be evidenced.

Instead, some significative differences could be evidenced in the spectrum of the sample soaked for 28 days in pro-inflammatory conditions (CT_aT_H2O2). The spectrum showed both the signals of α -and oxidized tocopherol, that is a quinone (α-TOQ), and can be identified by the characteristic C=O absorbance at 1650 cm^{-1}. This result showed that partial oxidation of tocopherol occurred in presence of hydrogen peroxide. On the basis of the literature, the hypothesis is that a hemiketal intermediate compound α-TOQ(OH) was created, which became α-TOQ as a long-term oxidation product. [11]

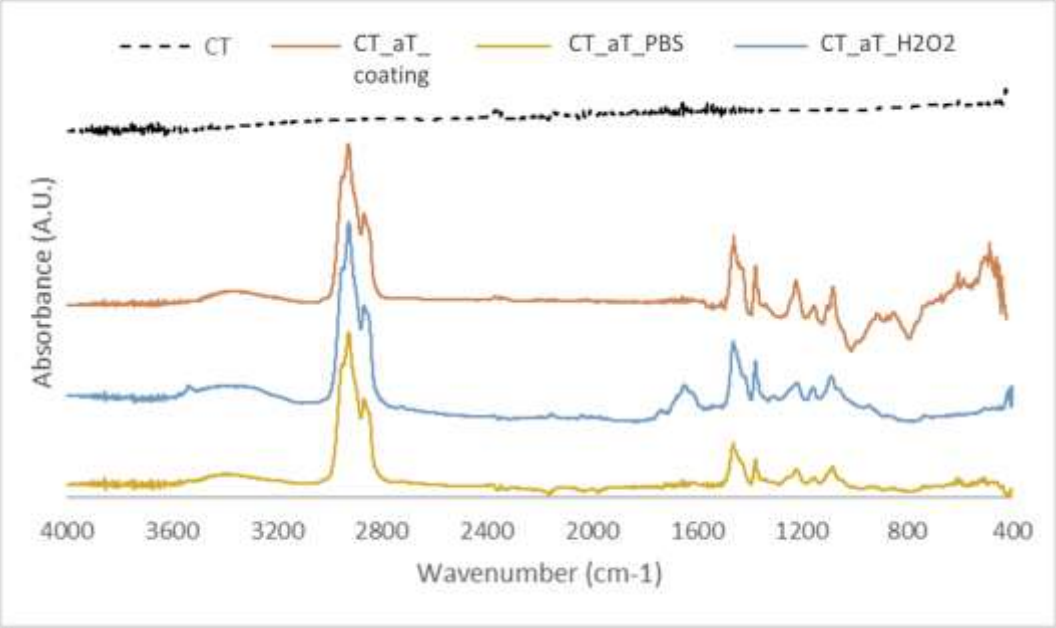

Figure 2.31 FTIR spectroscopy of samples with and without coating (CT_aT_coating, CT) and after release test (CT_aT_PBS, CT_aT_H2O2)

DPPH test on the coating before and after soaking

In this case, the DPPH test aimed at understanding whether the very high scavenging property of αT was lost during the release tests. It was performed on specimens after 28 days of soaking at physiological (PBS, pH 7.4) or pro-inflammatory (PBS+H2O2) conditions. α-tocopherol, since it is a fat-soluble molecule, it is very soluble in ethanol. This allows it to react immediately with the free radical of DPPH and thus give RSA (radical scavenging activity) values, indicated in Figure 2.32. Values of the substrate with and without the coating (CT, CT_aT_coating) are reported as references. The RSA of the original coating (CT_aT_coating) was very high (about 80%) evidencing a high antioxidant ability of α-tocopherol within the coating. After 28 days of immersion in PBS and in PBS+H2O2, RSA was still evident, but it significantly decreased ($p < 0,05$) by 30% in physiological conditions and by 40% in the pro-inflammatory one. Given the strong dependence between concentration and absorbance value in spectrophotometric assays, results can be ascribed to a partial release or degradation of the tocopherol during soaking.

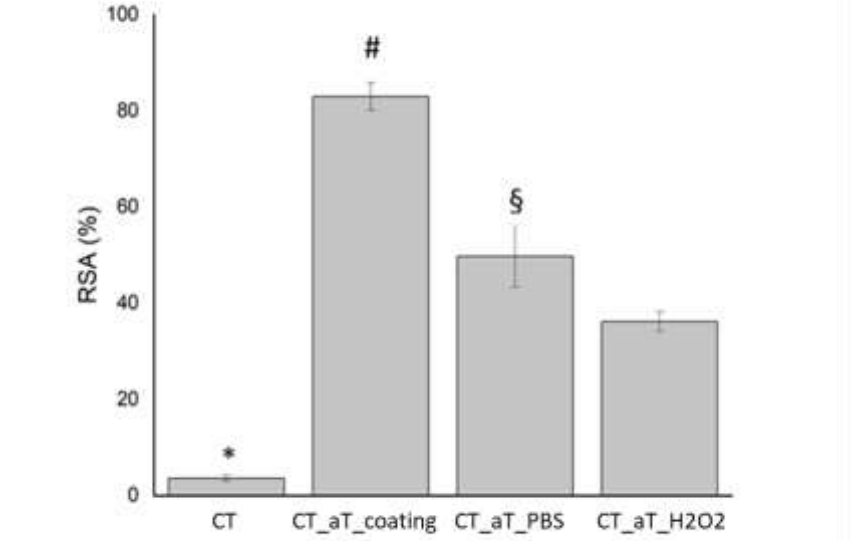

Figure 2.32 Radical Scavenging Activity measured through DPPH assay, before and after release test, p<0,05.

DPPH and F&C test of the soaking solutions

When measuring the α-tocopherol concentration in the soaking solutions by the modified F&C and DPPH assays, after specific periods, the absorbance values of both assays were always below the detection limit (that is 0.001 Abs), regardless of the elapsed time. These results, coupled with the UV-Vis and FTIR-ATR spectra, allowed to exclude of a significant release of α-tocopherol in favour of a partial degradation/oxidation of the molecule during the soaking, especially in the pro-inflammatory environment in presence of hydrogen peroxide [12],[13].

In conclusion, CT_aT_coating showed several features of potential interest in view of a chemical and biological anti-inflammatory action. The αT coating was not removed by soaking for 28 days in inorganic physiological or inflammatory-like solutions even if it was partially oxidised by the last one. No release of αT occurred. The radical scavenging ability is very high on the as-prepared sample and partially maintained after a long soaking.

Biological Evaluations of anti-inflammatory response

Anti-inflammatory properties evaluation

As described in the paragraph 1.3, implanted biomaterials can cause an inflammatory response, known as foreign body response (FBR). Despite inflammation playing an important role in the early stages of wound healing processes, excessive and chronic inflammation cause hostile conditions for tissue regeneration and repair [218]. To test anti-inflammatory properties of titanium discs treated with aT, hMSC were cultured in 3D conditions in the presence of the described biomaterials under physiological or pro-inflammatory conditions, mimicked by the treatment with pro-inflammatory cytokines such as TNFα/IL1β or IFNγ. To this aim, the cell response was evaluated by measuring the expression levels of both pro-inflammatory (IL1β and IL6) and anti-inflammatory (IDO, COX2, PGE2, TGFβ1) markers. Data shown in Figure 2.33 indicate a slight upregulation of IL1β expression in hMSC cultured in the presence of the discs coated with αT compared to control materials (CT and Ti64), which was further enhanced in the case of the addition of pro-inflammatory cytokines. On the contrary, IL6 expression was downregulated by both αT and CT, compared to control (Ti64), under physiological conditions. However, no differences were evidenced in presence of pro-inflammatory conditions. The analysis of anti-inflammatory markers evidenced a coherent upregulation of all markers (IDO; COX2, and TGF-b1) except for PGE2, in cells exposed to αT and CT, compared to control in physiological conditions. The PGE2 pathway was recently described to promote an anti-inflammatory neutrophil phenotype and to determine the outcome of inflammation resolution in vivo[219].

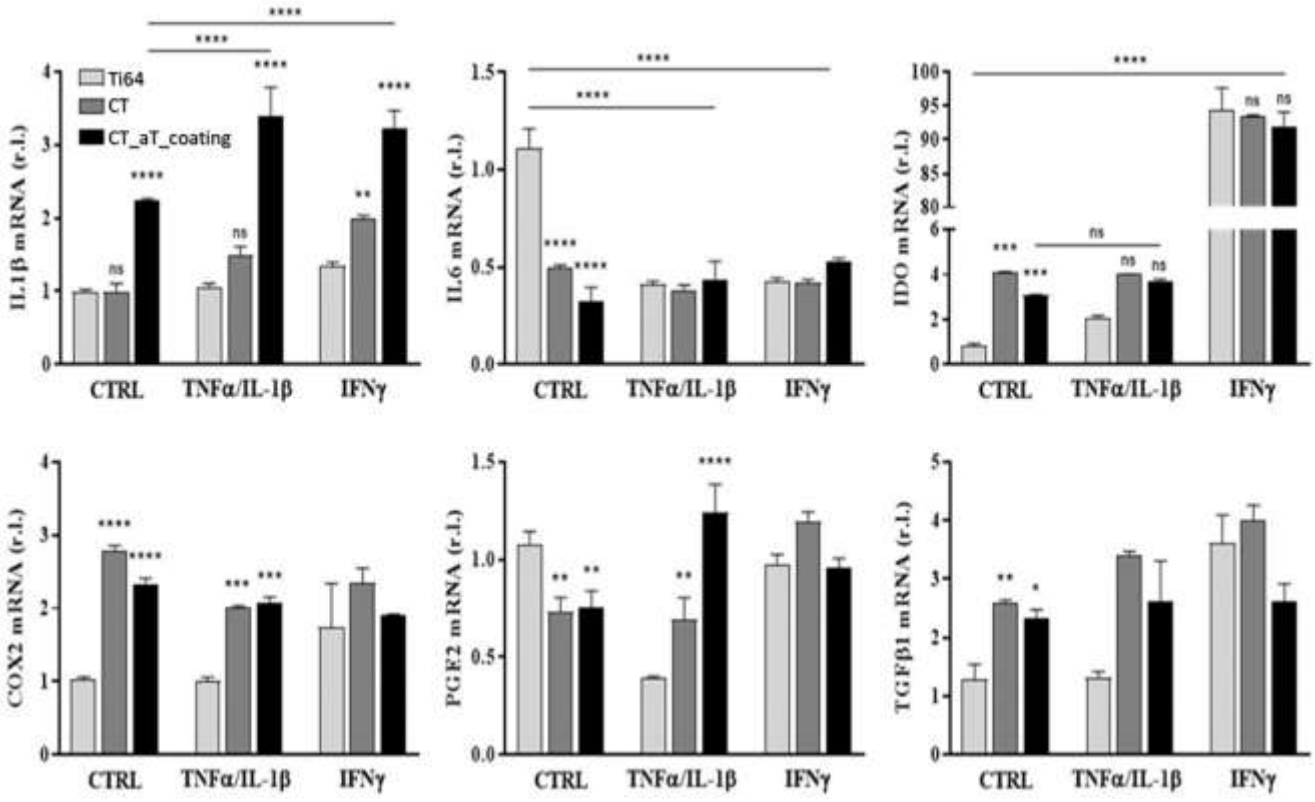

Figure 2.33 Pro- and anti-inflammatory markers expression in hMSC cultured in the presence CT_aT_coating

*The mRNA levels of inflammation mediators were evaluated using RT-qPCR. Expression levels of IL1β, IL6, PGE2, TGFβ1, COX2, and IDO were compared between hMSC cultured in the presence of titanium discs coated with αT (CT_aT_coating) and two control materials with a chemically treated (CT) or mechanically polished surface (Ti64), in pro-inflammatory conditions induced by two different pro-inflammatory mediators - TNFα/IL1β and IFNγ or not treated cells (CTRL). L34 was used as an internal control. Data are represented as 'fold over control' (r.l. = relative levels). Bars represent means ± s.d. * p<0.05; ** p<0.01; *** p<0.001; **** p<0.0001.*

A similar approach was used to test the effect of the presence of chemically treated (CT), coated (CT_aT_coating), and control (Ti64) samples on the biological stress condition on bone marrow-derived mesenchymal stem/stromal cells. The endoplasmic reticulum (ER) stress response is induced by the accumulation of unfolded or misfolded proteins. Upon ER stress induction, cell activate adaptive mechanisms, known as unfolded protein response (UPR), which is aimed to compensate for damage and can eventually trigger cell death if ER stress is severe or chronic. Components of UPR regulate numerous processes, including cholesterol metabolism, energy homeostasis, and cell differentiation [220], [221] Importantly, growing evidence also indicates a key role of ER stress and UPR in host inflammation responses[222]. New observations suggest that UPR initiates activation of the 'central mediator' of inflammation NFκB, that results in increased leukocyte recruitment and T-cell activation, leading to increased inflammation[221], [223]. Therefore, to better define the cells' response to modified titanium, the levels of the well-characterized UPR markers. [224]TF4, ATF6, and XBP1 were evaluated in hMSC cultured in the presence of bioactive titanium, in the same experimental conditions reported above. Results shown in Figure 2.35 indicate no clear modulation of both ER stress and downstream UPR by the modified titanium, at least in the experiments reported above.

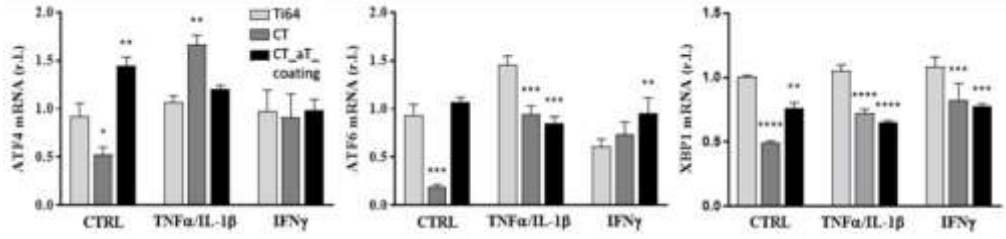

Figure 2.34 Unfolded protein response markers expression in hMSC cultured in presence of CT_aT_coating

*The mRNA levels of UPR markers were evaluated using RT-qPCR. Expression levels ATF4, ATF6, and XBP1 were compared between BMSC cultured in the presence of CT coated with αT (CT_aT_coating) and two control materials with a chemically treated (CT) or mechanically polished surface (Ti64), in pro-inflammatory conditions induced by two different pro-inflammatory mediators - TNFα/IL1β and IFNγ or not treated cells (CTRL). L34 was used as an internal control. Data are represented as 'fold over control' (r.l. = relative levels). Bars represent means ± s.d. * p<0.05; ** p<0.01; *** p<0.001; **** p<0.0001.*

Immuno-biocompatibility evaluation

Analogously, the effect of the presence of the chemically treated (CT) or coated (CT_aT_coating) titanium vs the control (Ti64) was tested on PBMC (human Peripheral Blood Mononuclear Cells) which include lymphocytes (T cells, B cells, and NK cells), monocytes, and dendritic cells. After 72h of culture in contact with the coated discs and the respective controls, the immunophenotype of the harvested PBMCs was evaluated by flow cytometry. Among the several lymphocyte subsets analysed, no differences were found between the CT_aT_coating specimens and either CT or Ti64, except regarding Tregs. In this case, a significant decrease was observed in the presence of CT and CT_aT_coating. However, since no differences were found when comparing the aT-coated discs with the uncoated specimens, we conclude that the αT coating did not impact the phenotype of the immune cells and that this treatment has high biocompatibility and can be implanted without affecting the immune response (Figure 2.34).

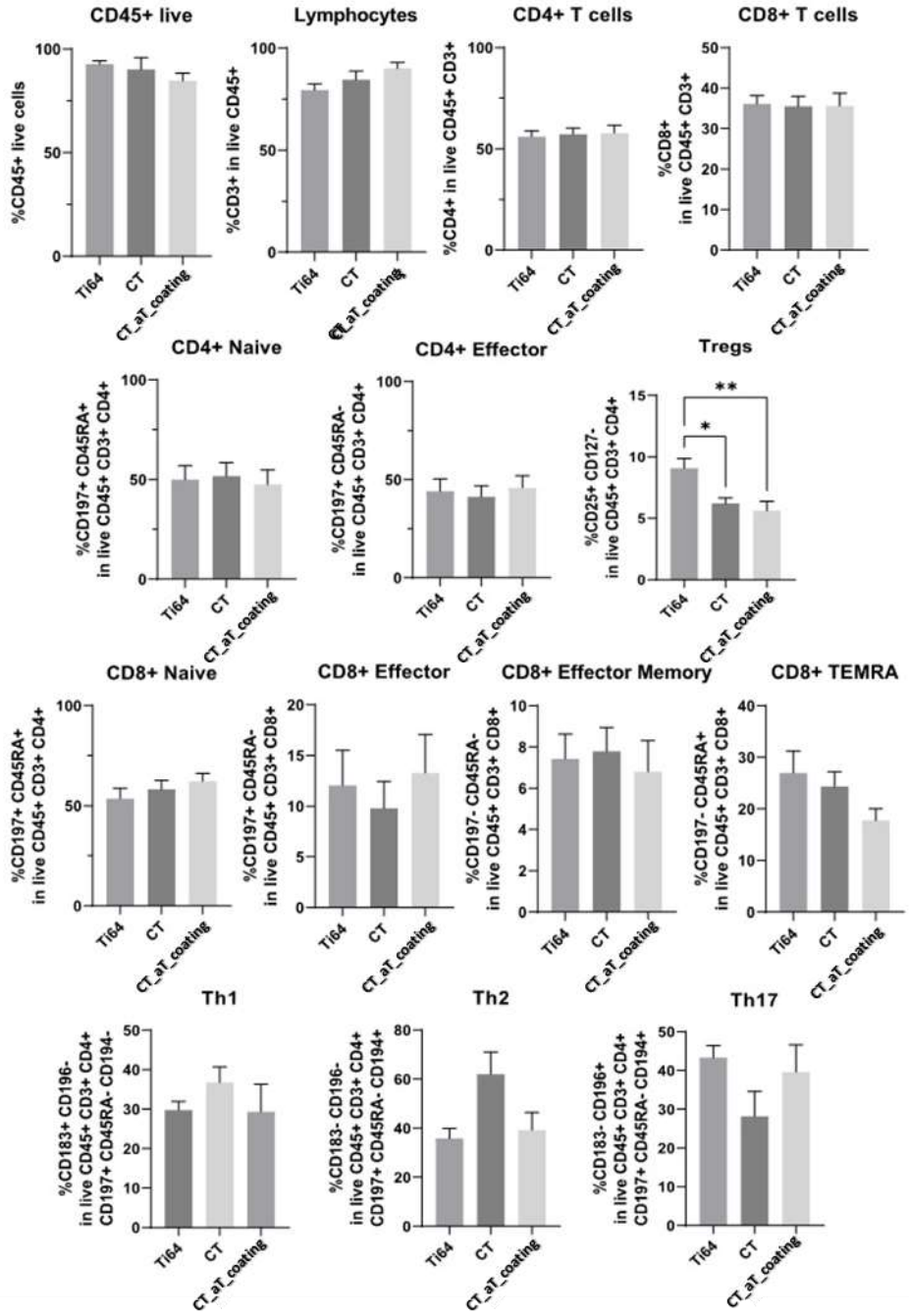

Figure 2.35 Immuno-biocompatibility assay with CT_aT_coating
*Multiparametric flow cytometry analysis of PBMCs stained with the following antibodies: monoclonal anti-CD45 human antibody (mAb) (leucocytes), anti-CD3 mAb (T cells), anti-CD4 mAb (T helper cells), anti-CD8 mAb (cytotoxic T cells) anti-CD45RA and anti-CD197 mAbs (naïve, central memory (CM), effector memory cells (EM), and terminally differentiated EM cells), anti-CD25 and anti-CD127 mAbs (regulatory T cells, Tregs), anti-CD183, anti-CD194 and anti-CD196 mAbs (Th1, Th2, and Th17). The samples were acquired using FACSymphony TM A5 (BD Biosciences) flow cytometer and data were analysed using FACSDIVA software (BD Biosciences) and Prism (GraphPad, Version 9.0.0)). Data are shown as mean ± SEM. (n=6). Ordinary One-way ANOVA or Kruskal-Wallis multiple comparisons test were used. *p<0.*

3. Chapter: Polyphenols

3.1 Introduction

Polyphenols are a diverse group of phytochemicals found in fruits, vegetables, nuts, and other plant-based foods. They have potent antioxidant properties and have been shown to have anti-inflammatory effects on the body [225].

In addition to their antioxidant properties, polyphenols also have anti-inflammatory effects on the body. Indeed, polyphenols have gained great interest in different industrial fields [226] due to their antioxidant, antibacterial, and anticarcinogenic capabilities. Polyphenols are molecules that can be extracted from a large number of natural products, including waste products, economically and sustainably, representing an important approach to the sustainable use of resources.

This chapter includes a bibliographic part, with particular attention on green tea catechins, a family group of polyphenols, including structure, properties, and biological roles. The second part concerns a surface functionalization protocol optimized to graft tea polyphenols onto a treated titanium surface, previously made bioactive (*in vitro* precipitation of hydroxyapatite) and antibacterial through a specific heat treatment and loading of iodine ions. For functionalization, a specific focus is on the selection of the solvent medium and pH, the effect of Ca^{2+} ions in the solution on the grafting mechanism, and the

concentration of the polyphenols source solution. A preliminary characterization of the functionalized surfaces was performed using the Folin–Ciocalteu photometric test and XPS (X-ray Photoelectron Spectroscopy) analysis, to verify the presence and activity of the grafted polyphenols. *In vitro* bioactivity and antibacterial activity, cytocompatibility, and antioxidant capacity were evaluated on the functionalized samples. Accordingly, the formation of apatite was observed, the ability to prevent the surface colonization from the pathogen *Escherichia coli* was verified, and the antioxidant activity was confirmed by the possibility to protect human cells from toxic active species in a pro-inflammatory environment by a scavenger mechanism.

Part of this chapter is included in a published manuscript (F. Gamna et Al. "Conferring antioxidant activity to an antibacterial and bioactive titanium surface through the grafting of a natural extract", 2023, Nanomaterials).

3.2 Polyphenols classifications:

Foods of plant origin contain polyphenols; these compounds have a wide range of complex structures. The famous representatives of polyphenols, such as resveratrol in red wine, epigallocatechin gallate in green tea, chlorogenic acid in coffee, and anthocyanins in colored fruits, have gained great interest not only in food science and nutrition but also in many other disciplines, including the biomedical field. The polyphenol family counts more than 8000 phenolic molecules, which must contain at least one aromatic nucleus and one or more -OH groups and contain both monomers and polymerized rings. All polyphenols are classified into 2 main categories, depending on the number and the type of phenolic ring: flavonoids and non-flavonoids, which include phenolic acids, stilbenes, and lignans (Figure 3.1) [227]–[229]

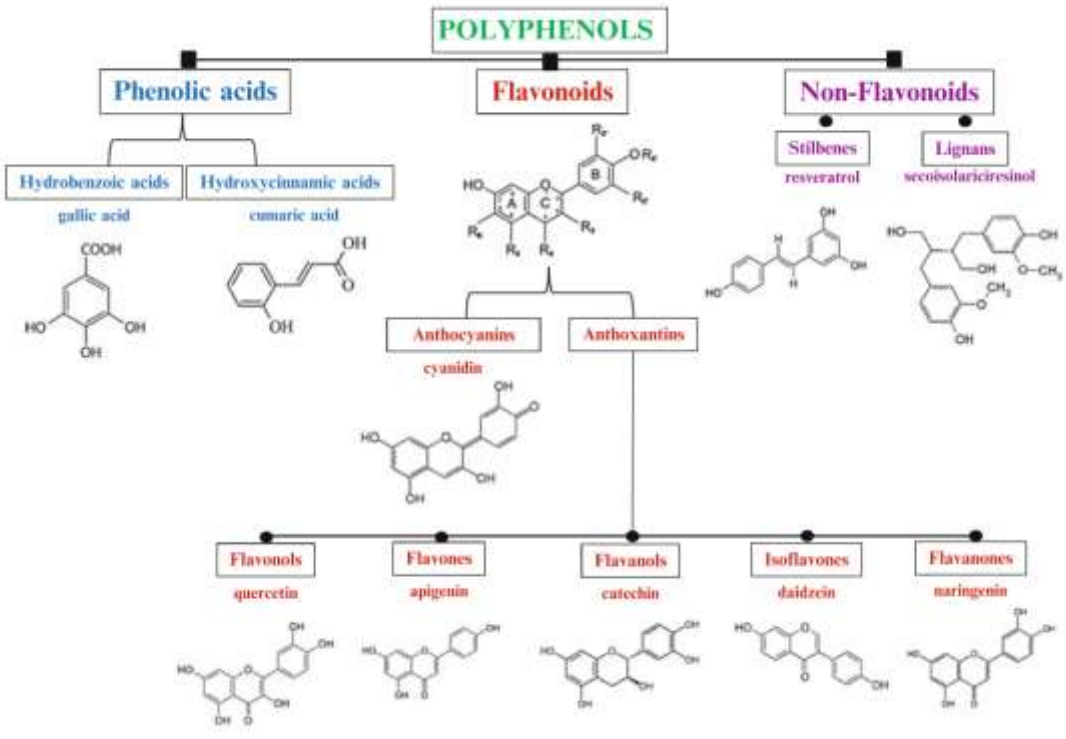

Figure 3.1 Classification of polyphenols [226]

As Figure 3.1 shows, non-flavonoids are divided into 3 groups:

Stilbenoids are a subclass of non-flavonoid compounds, and one of the most representatives is resveratrol. They occur naturally, especially in grapes, and result from a reaction between cinnamic acid and malonyl coenzyme. Being very rich in grapes, they are found in abundance in wine. Red wines usually contain higher concentrations than rosé or white wines because the contact of the must with the skins during fermentation is longer.[230]

Lignans are dimers or oligomers present in ferns, gymnosperms, and angiosperms, in particular, they are localized in woody stems and seeds and play a role as insect deterrents [231].

Phenolic acids are abundant in plants and are divided into 2 classes: Hydroxycinnamic acids and hydroxybenzoic acids, which are characterized by the presence of a carboxyl group substituted on a phenol. The most representative polyphenol of this class is gallic Acid, which is a hydroxybenzoic acid. Among the various polyphenols, gallic acid has been listed as one of the most powerful antioxidants and has been used as a reference for all other classes of polyphenols [232].

A class of non-flavonoids polyphenols is represented by hydrolysable tannins so defined because their structure is based on a carbohydrate as a core (glucose or quinic acid) with the hydroxyl groups partially or totally esterified with phenolic groups such as gallic acid (gallotannins) or ellagic acid (ellagitannins). They hydrolyse into glucose and ellagic acid or gallic acid in the presence of strong acids at high temperatures. Gallotannins are extracted from galls (Quercus infectoria and Rhus semialata), sumac fruits (Rhus coriaria), and tare fruits (Caesalpinia spinosa). Tannic acid is one of them. They react with molecular oxygen helping to preserve musts and wines from oxidation and act as free radical acceptor molecules and are also responsible for the deproteinization of the wine thanks to the bonds they can establish with proteins, causing their flocculation. Ellagitannins are instead present in oak wood (Quercus robur, Quercus petraea, and Quercus alba), chestnut (Castanea sativa), and mirabolan (Terminalia chebula).

Flavonoids are characterized by a C6-C3-C6 structure. Among all the flavonoids, flavonols are the most diffused in the human diet and the most representative is quercetin.

Flavonoids have a number of biological activities in plants, animals, and

bacteria. In plants, flavonoids are responsible for the color and aroma of flowers and fruits, as well as pollination, seedling growth and development. They protect plants from various external environmental stresses and UV radiation and also function as signal molecules and antimicrobial defensive compounds [233]. They have miscellaneous favourable biochemical and antioxidant effects associated with various diseases such as cancer, Alzheimer's disease (AD), atherosclerosis, etc

Flavanols are another subclass of flavonoids and exist in two forms, the monomer form named catechins and the polymer one named proanthocyanidins The proanthocyanidins are polymers of catechins that are bound together to form condensed tannins. Catechins are present in green tea, chocolate, red wine, and fruits and are further discussed in the next paragraph.

3.3 Catechins in Tea

As already mentioned, catechins are part of the flavonoid family and are very abundant especially in green tea, responsible for its well-known and renowned beneficial effects, including the antioxidant capacity. Tea is a very ancient beverage, initially drunk in China for more than 5,000 years until the present, and now exported and consumed all over the world. The tea drink is made by soaking the leaves of Camellia sinensis in hot water [234]. The most widely consumed tea is black tea, followed by green, oolong, and white tea. The difference between black tea and other teas is fermentation: the fresh black tea leaves are dried and crushed to achieve fermentation before final processing. In the fermentation step, some catechins combine to form complex theaflanins and other flavonoids, with the help of the enzyme polyphenol oxidase, which gives black tea a distinctive flavor and color. Polyphenol oxidase is a thermolabile enzyme, and its activity is reduced by steam heating during fermentation. In fact, to make green tea, polyphenol leaves are heated after harvest to inactivate the polyphenol oxidase enzyme [235]. This also leads to green tea has better antioxidant properties than black tea [236].Catechins make up 30 % wt of tea leaves [237]. The trend of catechins for all types of tea is represented in Figure 3.2

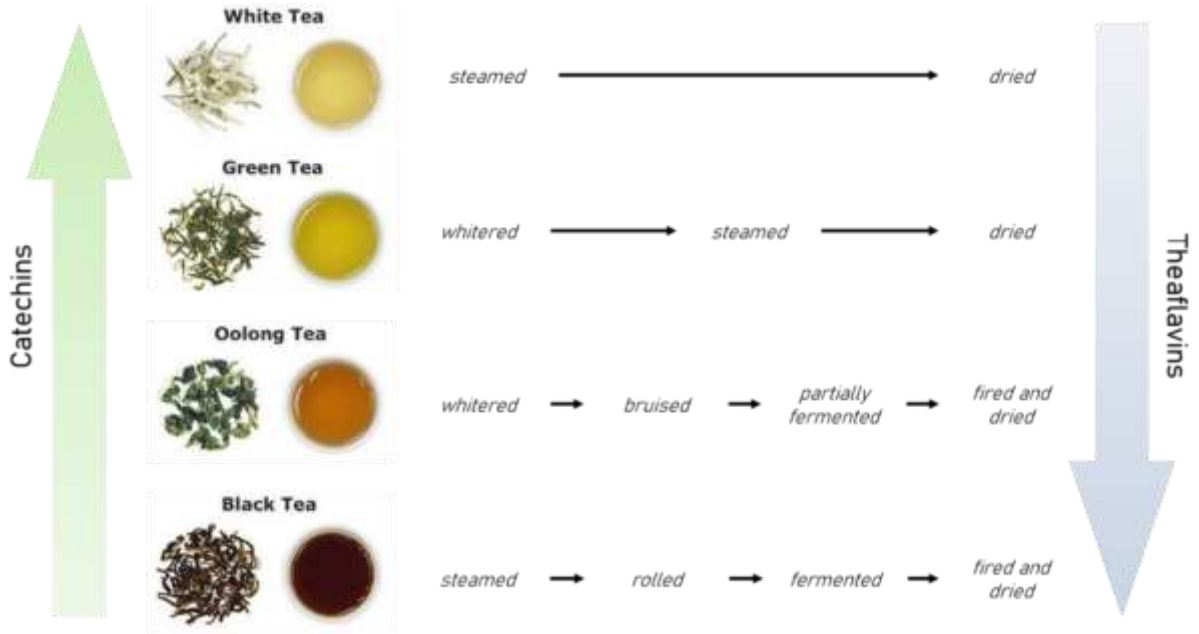

Figure 3.2 Catechin and flavin trends depending on the type of tea

Catechins are subdivided into several subclasses: epicatechin (EC), (-)-epigallocatechin (EGC), (-)-epicatechin gallate (ECG), (-)-epigallocatechin gallate (EGCG), which vary according to the substituents (Figure 3.3).

In large part, the benefits of green tea have been attributed to the high concentration of catechins with the main components being (-)-epigallocatechin-3-gallate (EGCG), representing approximately 59% of the total content, followed by (-)-epigallocatechin (EGC) (approximately 19%), (-)-epicatechin-3-gallate (ECG) (approximately 13.6%); and (-)-epicatechin (EC) (approximately 6.4%) ., [238]

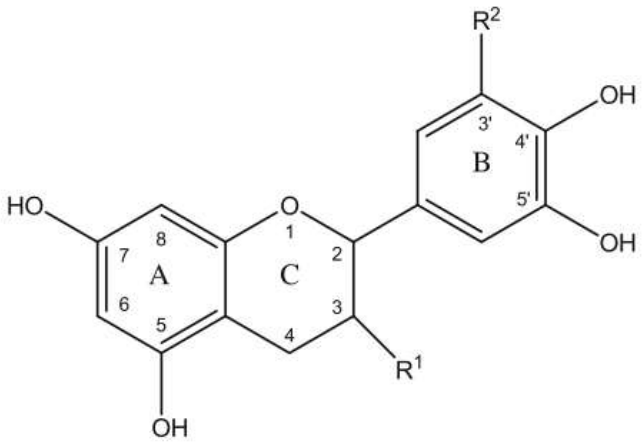

Name	Substitution
(+)-catechin	3S –OH
(+)-gallocatechin	3S –OH; 3´–OH
(+)-catechin gallate	3S –gallate
(+)-gallocatechin gallate	3S –gallate; 3´–OH
(-)-epicatechin	3R –OH
(-)-epigallocatechin	3R –OH; 3´–OH
(-)-epicatechin gallate	3R –gallate
(-)-epigallocatechin gallate	3R –gallate; 3´–OH

Figure 3.3 Structure of catechins [226]

3.4 The biological role of polyphenols

3.4.1 Antioxidant activity and anticancer activity:

The primary biological role of polyphenols is surely linked to their antioxidant power.

The antioxidant action is strictly connected to the removal of radical oxygen species, and it resolves into an anti-inflammatory behaviour in a biological environment.

As mentioned above, ROS generation is inevitable in aerobic organisms. Under normal circumstances, ROS levels are balanced by cells with antioxidants. When this balance is disrupted, cellular defenses can be overwhelmed and the cell suffers damage, eventually resulting in cell death or tumor generation.

One of the main mechanisms by which polyphenols exert their antioxidant effects is by redox chemical action and scavenging free radicals. Free radicals are highly reactive molecules that can cause damage to cells and contribute to the development of chronic diseases such as cancer and heart disease. Polyphenols act as antioxidants and neutralize these free radicals, thereby preventing cellular damage [239], [240].

Due to their chemical structure, polyphenols can interact with the cytoplasmic membrane and nonpolar compounds present in the hydrophobic layer of the membrane. In particular, certain flavonoids, including catechins, present in the hydrophobic core of the membrane can prevent access to oxidants and protect membrane structure and function [68].

The antioxidant activity of polyphenols can be direct or indirect. In a direct way, polyphenols react with reactive oxidative species (ROS) to form relatively stable phenolic oxygen radicals, thus eliminating free radicals. Two main mechanisms of antioxidation have been proposed. The first is based on the ability of the phenolic functional group to donate a hydrogen atom to a free radical R·. In this case, polyphenols act as chain-breaking antioxidants and the antioxidant phenol (ArOH·) itself becomes a free radical. The second mechanism is the transfer of a single electron from ArOH to a free radical R· with the formation of a stable radical cation ArOH·+.[241] (Figure 3.4)

In addition to directly scavenging free radicals, polyphenols also protect the body from oxidative damage by regulating different types of oxidase and antioxidant enzyme activities.

For example, in this way, tea polyphenols act by preventing the activity of certain oxidative enzymes such as Nicotinamide adenine dinucleotide phosphate oxidase (NADPH), lipoxidase, and cyclic oxidase, thus reducing the production of free radicals

Similarly, tea polyphenols regulate the expression of some antioxidant enzymes, such as superoxide dismutase (SOD), and glutathione s-transferase (GSH), which protect mitochondria from oxidative stress[236]

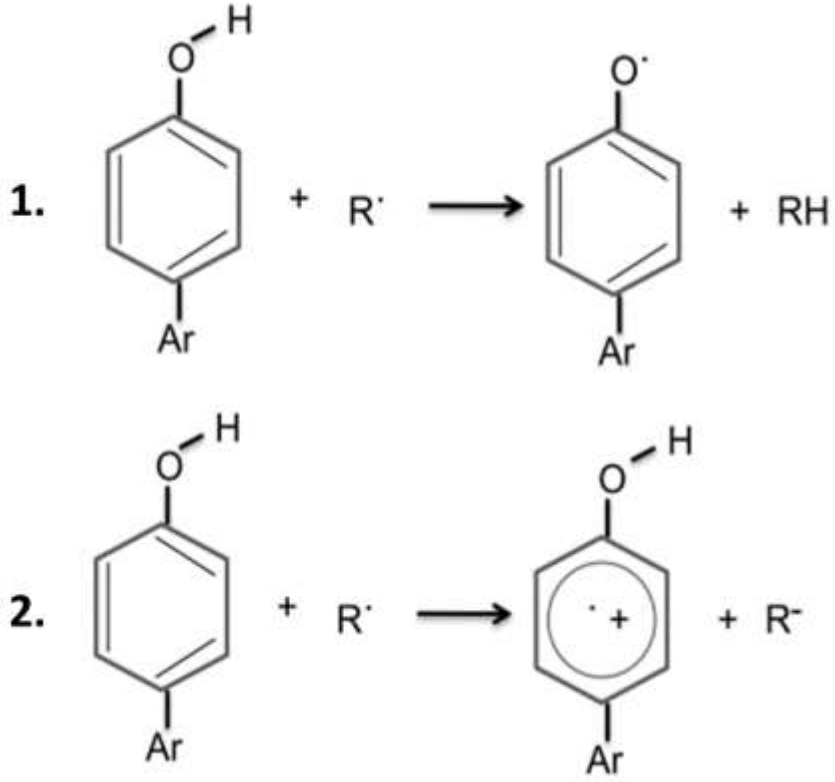

Figure 3.4 Mechanisms of direct antioxidant activity of Polyphenols.[230]

Polyphenols are also known for their anticancer activity, and their effect is definitely related to two main actions:

1. Antioxidant ability
2. Interference with key elements in signal transduction pathways related to cellular functions. (apoptosis, cell cycle, angiogenesis, metastasis). [242]

In fact, in addition to the antioxidant aspect, polyphenols can interrupt or reverse the process of carcinogenesis by acting on molecules in the intracellular signaling network involved in cancer initiation and/or promotion.[243]
Basic cellular functions such as apoptosis, proliferation, and differentiation are extremely important factors to inhibit tumor initiation and propagation.

Polyphenols have been shown to have an effect on apoptosis and proliferation in human myeloid and lymphoid leukemia cell lines, and, in particular, they have antitumor activity against leukemic cells with differentiated effects depending on the chemical structure of the molecule.[244]

Another important phenomenon in tumor growth is angiogenesis, as malignant cells are in search of nutrient supply. Polyphenols could have an anti-angiogenesis effect, through a shared and multi-targeted mechanism consisting of the inhibition of COX-2 enzyme expression and metalloproteinases such as MMP9, enzymes that degrades extracellular matrix components allowing endothelial cells to penetrate and reshape the connective tissue.[245]

The green tea extract has been subjected to numerous studies and has been shown to have several antitumoral properties. In particular, the combination of EGCG, EGC, and ECG, has been shown to have antitumor preventive activity and to have an antiproliferative and proapoptotic effect on prostate cancer cells[246]. Harakeh et al, on the other hand, demonstrated similar effects in HTLV-1-positive and negative leukemia cells [247]. It has also been reported that EGCG controls and promotes IL-23-dependent DNA repair, enhances cytotoxic T-cell activities, and blocks cancer development by inhibiting cancer signal transduction pathways [248]. It also modulates and inhibits several biological pathways, including, overexpression of cyclooxygenase, proteasome activity, and insulin-like factors [249]. As can be seen, ECGC has a variety of effects on modulating cancer cell growth, metastasis, angiogenesis, and other aspects of cancer progression by affecting different mechanisms and interfering with different molecules and enzymes (Figure 3.5)[250].

Figure 3.5 Mechanism of action of Green Tea [240]

3.4.2 Antimicrobial Activity

The antimicrobial activity of polyphenols has been extensively studied in the literature and hundreds of papers have been published recently on the antimicrobial activity of polyphenols. In an era of increasing antibiotic resistance, the development of new strategies to combat bacteria is welcome. Polyphenolic compounds, including flavonoids and flavonols, hydroxybenzoic acid, and derivatives from various plants, have shown potent antimicrobial activities against pathogens in food, sometimes to a similar extent as standard antibiotics [251].

Phenolic extracts of tea, especially catechins, have been found to have great antimicrobial properties. Their antibacterial activity was discovered more than a hundred years ago by an experiment conducted by J. G. McNaught, who studied the antibacterial property of tea and observed that the number of Bacillus typhosus decreased sharply when immersed in cold tea.[252]. The mechanism of the antibacterial action of catechins has been widely discussed and 2 different hypotheses have been proposed:

1. Mechanism of expansion: due to their charge, catechins accumulate in the bacterial membrane, increasing the space between lipids and altering the permeability of the membrane, disrupting it.
2. Mechanism of H_2O_2 formation: Catechins react with oxygen and produce hydrogen peroxide through autoxidation, which can damage the bacterial cell [253] (Figure 3.6).

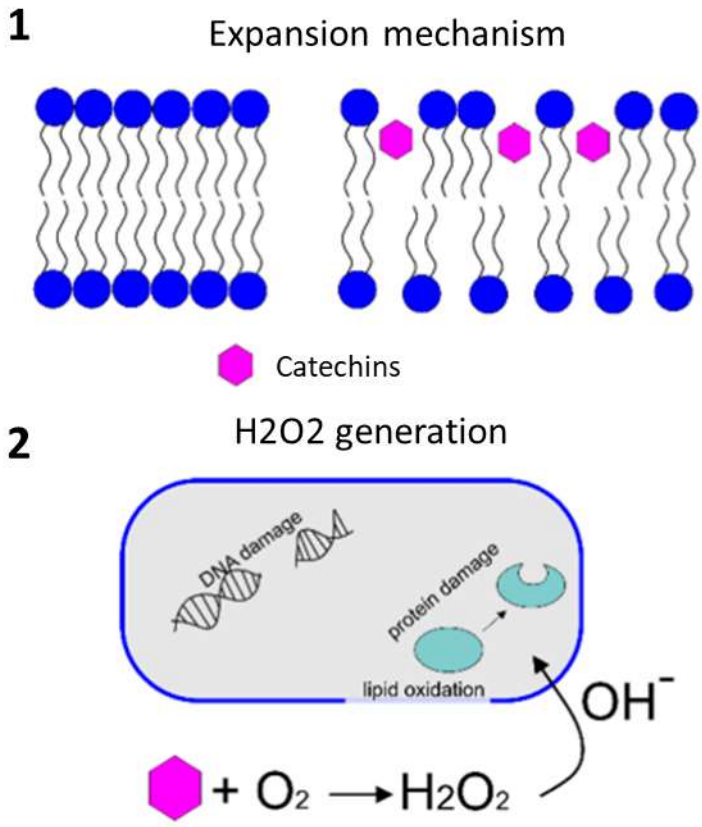

Figure 3.6 Antibacterial mechanisms of catechins[243]

Among all catechins, special attention has been paid to EGCG as the main molecule found in green tea. Xin Xu et Al. Demonstrated that some catechins from green tea, especially epigallocatechin gallate (EGCG), are able to inhibit the growth and glucosyltransferases activity of S. mutans. They found that EGCG can inhibit S. mutans planktonic cells' growth at a MIC of 31.25 µg/ml and inhibit biofilm formation at 15.6 µg/ml [254]. Hara K and al have studied the effect of EGCG on oral health and discovered that EGCG is effective in inhibiting the formation of caries, interacts with salivary proteins, and has an antimicrobial effect against the periodontal bacterium Aggregatibacter actinomycetemcomitans. [255] Similarly, in a study by Jieqiong Hu et al., EGCG was incorporated into a glass ionomer cement for dental application and, in addition to having an antibacterial effect, EGCG was able to improve mechanical properties [256]

Since EGCG is excreted in urine at a high enough concentration to be potentially effective as an antimicrobial agent, Wanda Reygaert et al. even suggest that green tea ingestion could potentially have antimicrobial effects on infections caused by E. coli [257].

Other studies have demonstrated the effective antimicrobial activity of EGCG against E. coli. Diego O. Serra et Al. have shown that the molecule is an effective agent against biofilms by interfering with the assembly of curli-subunits into amyloid fibres [258]. In addition to its ability to inhibit biofilm formation, EGCG has also been shown to alter extracellular AI2 activities, and swarm motility, and to impair infectivity by reducing the transcription of key virulence genes of E.Coli [259]. Moreover, Yoshiko Sugita-Konishi et Al. indicated a capacity of inhibition of extracellular release of Vero toxin from E. Col.[260] In addition to having an antibacterial effect against E.Coli, EGCG has demonstrated the ability to inhibit the growth of P. Aeruginosa at a MIC level of 200~400 μg/ml and has been proposed as an adjuvant for infections resistant to traditional antibiotic therapies [261]. Speaking of antibiotic-resistant bacteria: Acetinobacter is a bacterium that is often resistant to antibiotics, and N. Hosseini Jazani et al. showed that the water-soluble green tea extracts have a bactericidal effect against the bacterial isolate, which is resistant to several groups of antibiotics [262]. Again, the antibacterial effect of tea polyphenols extracted from Korean green tea was investigated against clinical isolates of methicillin-resistant Staphylococcus aureus (MRSA) and, in particular, protein expression in MRSA after exposure to tea polyphenols. This study showed that exposure to TPP dramatically affected the expression of several important proteins in MRSA.[263] Up to this point, it is clear that polyphenols not only have a bactericidal effect but also intervene in protein and gene expression and generally in the life cycle of bacteria. Indeed, EGCGs have been shown to interfere with the quorum sensing of bacteria, which is crucial for the stage of biofilm formation, in particular by interfering with AHL-mediated signaling of bacterial strains such as Pseudomonas putida and Burkholderia cepacia[264]. Literature works on the antibacterial effect of Tea polyphenols are summarized in Table 3.1

Table 3.1 Antibacterial effect of Tea Polyphenols extract

Molecule	**Concentration**	**Effect**	**Bacteria/Fungi**	**Ref**
EGCG	31.25 µg/mL 15.6 µg/mL	Inhibition of planktonic cells growth and inhibition of biofilm formation	Streptococcus mutans	[254]
EGCG	>0.5 mg/mL	Bactericidal	Aggregatibacter actinomycetemcomitan	[255]
EGC	500 µg/mL	Inhibition of the growth of infection in the urinary tract	E. Coli in the urinary tract	[257]
EGCG	>12.5 µg/ml	Inhibition of biofilm formation	E.Coli	[258]
Green tea extract	-	Bactericidal	Acinetobacter	[262]
Green tea polyphenols	50 to 180 µg/mL	Downregulation of several proteins expressed in the bacteria	S. Aureus (MRSA)	[263]
EGCG	25 µg/ml	Reduction of transcription of the major virulence gene and inhibition of biofilm formation	E.Coli O157:H7	[259]
Tea Polyphenols	-	Inhibition of biofilm formation and quorum sensing	Pseudomonas putida and Burkholderia cepacia	[264]
EGCG	300 to 650 µg\ml	Bactericidal	Klebsiella pneumoniae	[264]
EGCG and GCG	-	Inhibition of the extracellular release of Shiga toxin	E.Coli	[260]
EGCG	>0,4 mg/mL	Inhibition of bacteria growth	P. aeruginosa and E.Coli	[261]

3.4.3 Bone Health

As already mentioned in chapter 1, the process of bone remodeling is influenced by the effect of cytokines such as RANKL, OPG, and nuclear factor κB (NF-κB) which regulate the balance between osteoclastogenesis and osteoblastogenesis.

Osteoporosis is a progressive medical condition in which bone mineral density (BMD) slowly decreases with advancing age. Osteoclasts release free radicals such as reactive oxygen species (ROS) that induce the apoptosis of osteoblasts and osteocytes, favoring osteoclastogenesis and inhibiting mineralization and osteogenesis. The strong antioxidants, by counteracting the action of free radicals, contribute to inhibiting the activity of osteoclasts and therefore the process of bone resorption.[265]

The effects of polyphenols on bones in animal experiments have been widely examined with a broad and heterogeneous spectrum of findings [266]. The bone-protective capacity is certainly due to their antioxidant properties, although flavonoids and their metabolites have been shown to act on cells independently of their antioxidant capacity, interacting with specific proteins involved in intracellular signaling pathways[267]

Green tea polyphenols seem to have special properties to improve bone density and reduce the risk of fractures by attenuating the phenomenon of bone resorption. In addition, they could counteract the development of osteoclasts thanks to their good antioxidant properties, which act on inflammation and promote osteoclast apoptosis. Catechins therefore may have a direct effect on osteoclasts or an indirect effect through the modulation and activation of various cytokines that influence the process of osteoclastogenesis [268]. It has also been found that green tea catechins have a direct cellular effect on mesenchymal cells. EGCG has stimulating effects on the activity of ALP and cellular mineralisation, further confirming its positive influences on osteogenesis [269]. A hypothetical mechanism of influence on osteogenesis is illustrated in Figure 3.7

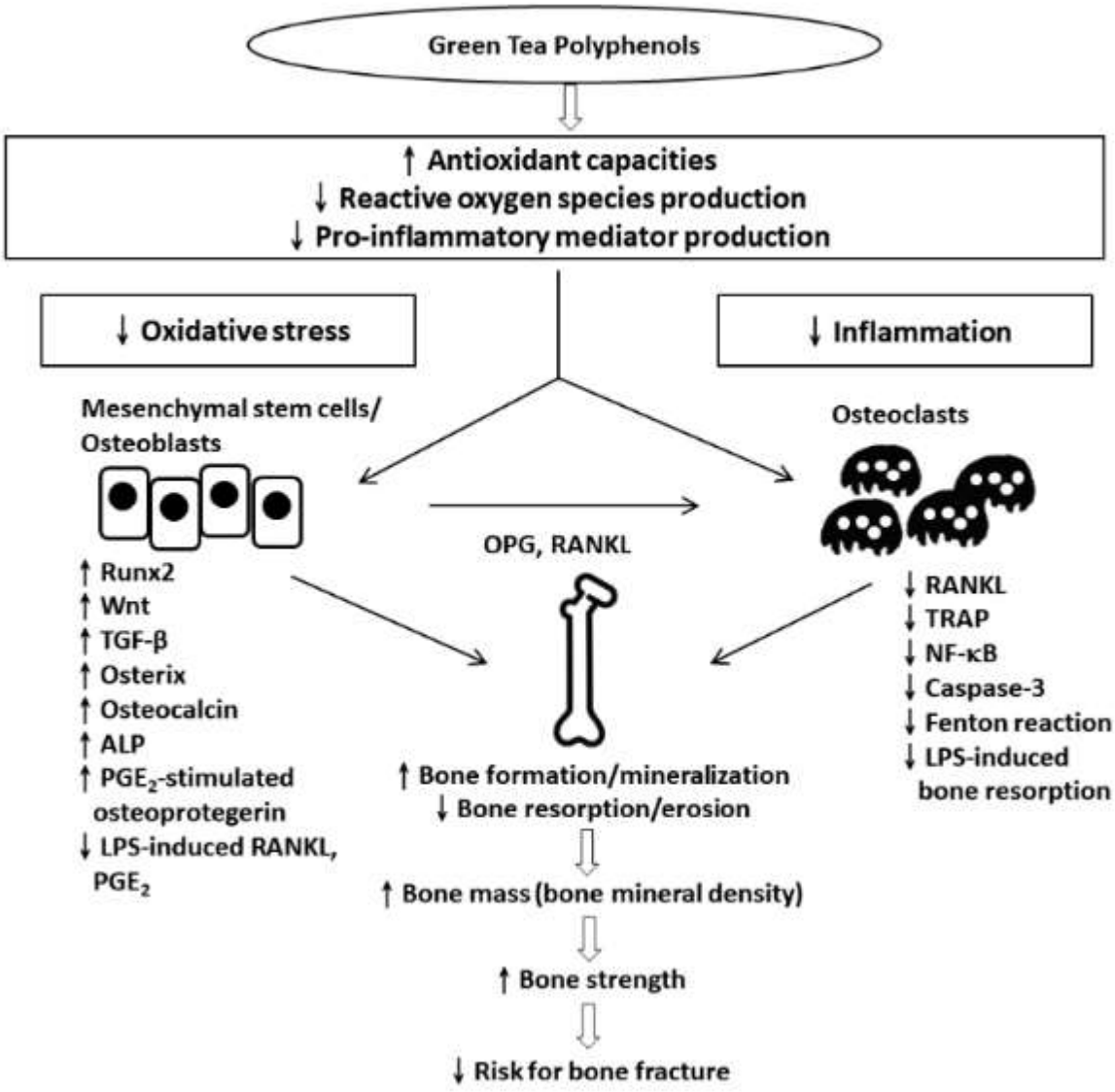

Figure 3.7 Green tea polyphenols in bone health[258]

3.4.4 Chemical stability of polyphenols

Polyphenols, given their structure and very reactive groups, may have problems with chemical stability: Epi-merization and autoxidation, for example, are reactions that can cause polyphenols to lose their stability. These reactions could affect their structural variations even without the presence of external factors such as temperature, light, pH, and so on.

Epimerization is one of the most important mechanisms leading to the instability of polyphenols and occurs due to external factors, particularly the temperature; it affects ECGC and takes place, for example, during tea processing. It involves the conversion of ECGC to GCG, in which the 2,3-cis bond of the EGCG is converted into a 2,3-trans bond in GCG (Figure 3.8) [270], [271].

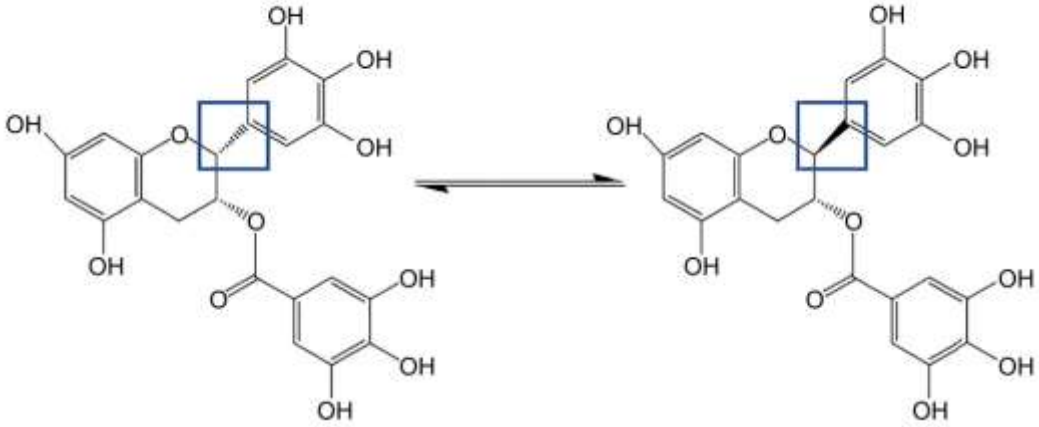

Figure 3.8 Conversion of EGCG to GCG through epimerization [260]

Autoxidation is another reaction that causes the instability of polyphenols and can occur in presence of oxygen (Figure 3.9)[272]

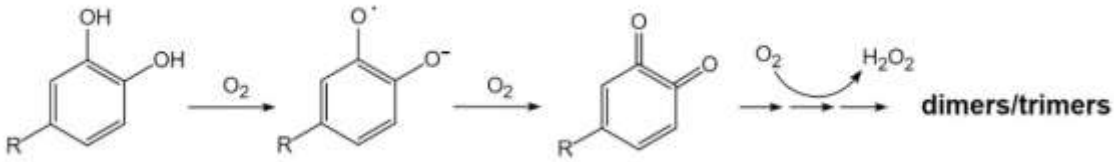

Figure 3.9 Autoxidation of polyphenols[262]

3.5 Biomedical applications of polyphenols

Thanks to their properties, polyphenols are found in the literature to be used in various biomedical applications in combination with different biomaterials. It is possible to use them to improve the mechanical properties of biomaterials, as in the case of collagen. In this case, polyphenols were used as cross-linkers to stabilise the material in dental tissue engineering. They can be used as enzyme inhibitors, as in the case of matrix metalloprotease (MMP-2) when used in dentin or remineralisation of root caries. They can be used in wound healing as antimicrobials to improve the wound healing process or grafted with polymers for antidiabetic scaffolds [273].

Their properties also make it possible to improve the surfaces of biomaterials and make them bioactive, with antibacterial, antioxidant, or osteogenic properties. Polyphenols are applied to the surface in different ways, either by coating or by immobilisation and functionalisation. They also have the ability to reduce metal ions, which makes them good alternatives for the formation of nanoparticles, such as silver nanoparticles. Finally, they are used for drug delivery, either as drugs or to form hydrogels [274].

3.5.1 Coupling of polyphenols with titanium alloys

This section is intended to present the biomedical applications of polyphenols in combination with titanium as a biomaterial, which is the biomaterial used in this thesis.

Many different applications of polyphenols with titanium are found in the literature, with different purposes and properties. Riccucci et al. used polyphenols extracted from red grape pomace to functionalize a chemically treated and nano-textured titanium surface. The research group investigated molecular grafting by physical/chemical characterisation and found that a good, homogeneous, and stable layer was formed on the surfaces. [210],[275]. The same substrates were used to produce grafting with gallic acid, using Ca^{2+} as a crucial linker for the binding mechanism. In this study, Ferraris et al. explored also the role of pH and ionic composition on the graft ability of gallic acid. [276]. Also in this case, they found a physical/chemical characterization protocol that revealed a good adhesion of the layer to the substrate [191]. As for the biological effect of the surface modified with polyphenols, several studies confirm that polyphenols have the ability to promote osteointegration. Cazzola et al. have shown that Ti6Al4V samples functionalised with green tea polyphenols have the ability to exhibit osteoinductive behaviour using KUSA A1 cells[277].

Although polyphenols are said to have an antimicrobial effect, they seem to lose their effect when they are deposited on the surface. Weber et al. have done extensive research on this and found no significant inhibition of C. albicans growth and biofilm formation, suggesting that the release of the active molecules from the coatings does not reach relevant inhibitory concentrations [278]. The same dubious effect was found in a study by Douglas et Al. who prepared a coating on titanium substrates with polyphenols and chitosan. Antibacterial studies showed that both chitosan and polyphenols did not inhibit Methicillin-resistant *Staphylococcus aureus* (MRSA) growth. [279] Polyphenols have also been combined with other molecules to create coatings with additional properties. Phenolic enriched fibrillar collagen was used to create a coating on titanium alloy that promoted osteogenic activities while reducing inflammation in vitro. Cells appeared to attach and spread well on the coatings, and the presence of polyphenols significantly reduced gene expression of inflammation markers. Furthermore, the expression of markers of osteoclast activation may be directly dependent on polyphenol concentration [280]. The ability of polyphenols to complex metal ions has also been exploited to bind

silver ions, agents with renowned antibacterial properties, to the metal substrate. H. Zhang et Al. used tannic acid with polydopamine to introduce Ag into a coating on a titanium substrate. In order to load Ag ions, the already prepared titanium samples coated with polydopamine/tannic acid were immersed in a solution of $AgNO_3$ for 1 day at 20°C. Dopamine was used here to allow the self-polymerisation of the tannic acid, resulting in the coating [281]. S. Lee et al. instead, created a metal-polyphenol network between Mg^{2+} as a metal ion and EGCG as a polyphenol. They tried the osseointegration of EGCG-Mg^{2+} coating in a rabbit tibia model and found positive behaviour of hMSCs and hADSCs cells and saw enhanced osteogenic differentiation in hADSCs cultured on EGCG-Mg^{2+}-coated Ti, rather than with either element, confirming the synergy between EGCG and Mg^{2+}.[282]

The table below (Table 3.2) shows a collection of research on polyphenols combined with titanium.

Table 3.2 Polyphenols combined with titanium and its alloy

Molecules	**Material**	**Deposition method**	**Applications**	**Effects of Polyephnol**	**Ref.**
Polyphenols from red grape pomace	Chemical treated Ti6Al4V	Functionalization	Orthopedic/dental implants	Successful grafting	[210]
Polyphenols from red grape pomace	Nano-Textured Ti	Functionalization	Orthopedic/dental implants	Successful grafting	[275]
Gallic Acid	Chemical treated Ti6Al4V	Functionalization	Orthopedic/dental implants	Successful grafting	[276] [191]
Tannic Acid and pyrogallol	Ti	Coating	Prevention of fungal colonization in dental implants.	No inhibition to the growth of C.Albicans	[278]
Phenolic enriched collagen	Titanium	Coating	Increase the osseointegration of titanium implants.	Reduction of the inflammatory response, promotion of osteoblast and fibroblast adhesion.	[280]
Green Tea Polyphenols	Chemically-treated Ti6Al4v	Functionalization	Increase the osseointegration of titanium implants.	Enhancement of cell differentiation and stimulation of biological mineralization.	[277]
Ag-Incorporated Polydopamine/Tannic Acid	Titanium	Coating	Orthopedic implants	Complex with metal ions and graft of Ag ions onto the surface	[281]
EGCG-Mg2+	Ti6Al4V	Coating	Increase the osseointegration of titanium implants.	Osteogenic differentiation, antiosteoclastogenesis, osseointegration	[282]
Polyphenols and Chitosan	Titanium	Coating	Bone contact application	No marked increase or decrease in Hela cell number or antibacterial action	[279]

The following section is intended to present my experimental research in which green tea polyphenols are chosen to functionalize a titanium surface for bone implant applications. In this work, a surface functionalization protocol has been optimized to graft tea polyphenols onto a treated titanium surface, previously made bioactive (*in vitro* precipitation of hydroxyapatite) and antibacterial through a specific heat treatment and loading of iodine ions.
This reasearch aims to improve an already extensively studied titanium surface that already showed exceptional osseointegration capacity and antimicrobial properties by incorporating the renowned anti-inflammatory properties of tea polyphenols to create a multifunctional surface with antimicrobial, anti-inflammatory, and osseointegration capabilities.[283], [284]

3.6 Materials and methods

3.6.1 Polyphenols Extraction

Green tea leaves (Longjing) were imported from Hangzhou, China, and dried in an oven at 60°C for 36 hours and ground to a powder in a ceramic mortar. Conventional solvent extraction with a 20:80 water-to-ethanol solution ratio was used. The solid-liquid ratio used was 1:50 (g:mL) [226]. The dried and ground tea leaves were placed in the extraction solvents in a glass bottle covered with aluminum to protect the tea from UV light and kept for 1 hour at 60°C shaking in a thermal bath. The solution was then filtered and placed in an incubator at 37°C overnight to ensure total evaporation of ethanol. Finally, the extracts were collected and suspended in double-distilled water and freeze-dried (Figure 3.10). The extracted natural polyphenols were named TPH.

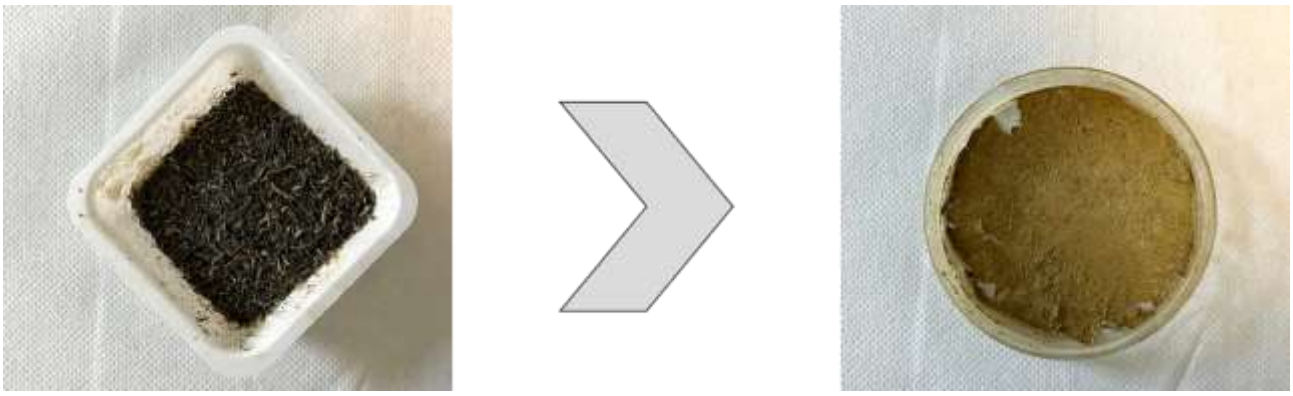

Figure 3.10 Extraction of polyphenols. Left: minced tea leaves, Right: lyophilized extract of tea leaves

3.6.2 Surface Treatment

Commercially pure titanium (Ti) samples of rectangular shape (10x10x1 mm^3) were polished with a 400-grain diamond plate. After being cleaned with acetone, 2-propanol, and ultrapure water in an ultrasonic bath for 30 min each, they were dried at 40 ◦C in an incubator overnight. Following this, a thermal-chemical surface treatment was performed, obtaining a calcium titanate surface layer. Briefly, the samples were initially immersed in an aqueous solution of NaOH 5 mol/L at 60 ◦C for 24 hours, and then in $CaCl_2$ 100 m mol/L at 40 ◦C for 24 hours in a shaking oil bath at 120 rpm. The samples were then heated to 600 ◦C for 1 hour. To introduce iodine ions on the surfaces, some samples were immersed in an iodine-containing solution of 10 mM/L ICl_3 and then placed in an oil-shaking bath at 80°C for 24 hours. Other samples were placed in water at 80°C for 24 hours and used as controls. For bacterial tests, however, the treatments were conducted in the same way as described above, but the samples have a larger size (25 x 25 x 1 mm^3).
Prepared samples were named Ti_Ca+I and Ti_Ca, respectively.

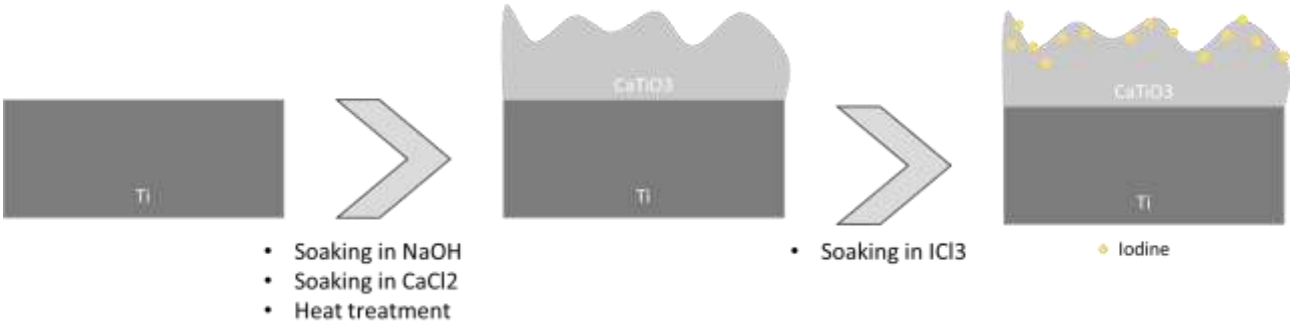

Figure 3.11 Treatment for the samples Ti_Ca and Ti_Ca+I

3.6.3 Surface functionalization

Ti_Ca and Ti_Ca+I samples were then functionalized in clean conditions with TPH, depositing a 100 µL/10mm^2 drop of TPH solution on the surfaces for 3 h at 37 ◦C in dark conditions. The TPH solution for functionalization was obtained with a concentration of 1 mg/mL by dissolving TPH in TRIS/HCl at 7.4 pH and stirring for 1 h. After the solution was prepared and the polyphenols were well dissolved, the solution was filtered with a syringe and 0.2 µm filter to avoid bacterial contamination. The filtered solution was used for functionalization, which lasted 2 hours. Finally, the samples were rinsed with double-distilled water twice and dried under a fume hood. The functionalized samples were named Ti_Ca+TPH and TI_Ca+I+TPH. The method of surface functionalization is illustrated in Figure 3.12.

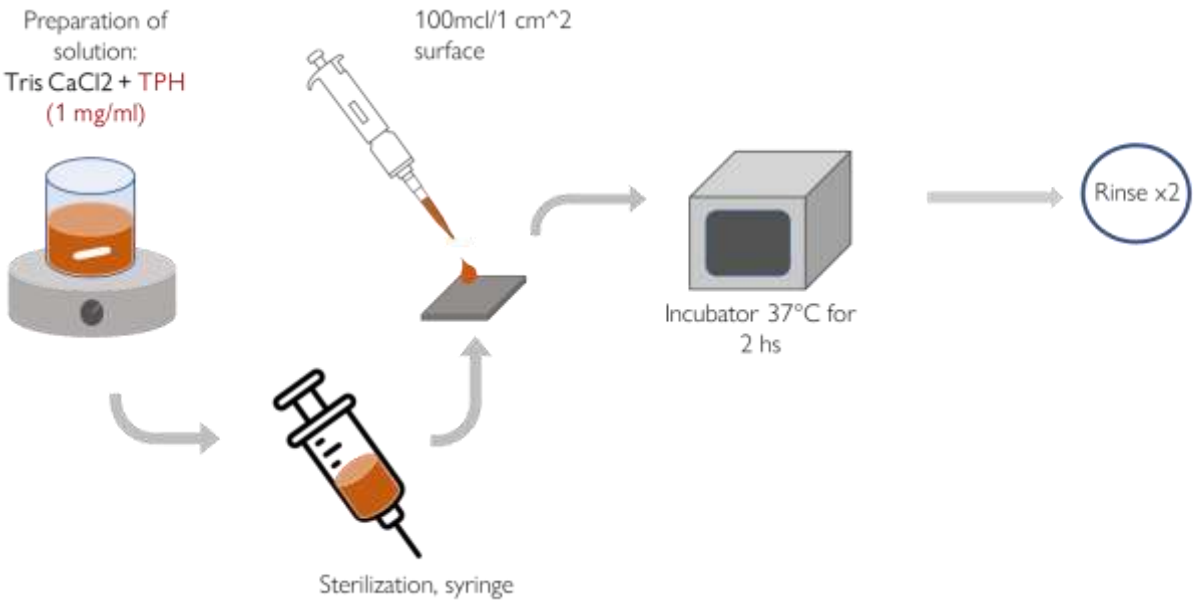

Figure 3.12 Method of functionalization with the TPH solution

3.6.4 X-ray Photoelectron Spectroscopy

The surface chemical composition of the functionalized and non-functionalized samples (Ti_Ca+I+TPH and Ti_Ca+I) were analyzed using X-ray photoelectron spectroscopy (XPS, PHI 5000 Versaprobe II, ULVAC-PHI, Inc., Kanagawa, Japan), with an Al-Kα beamline as the X-ray source at a take-off angle of 45◦. The binding energy of the observed spectra was calibrated by referring to the C1s peak of the CH_2 groups on the substrate, which occurs at 284.8 eV.

3.6.5 Zeta Potential Measurements

The zeta potential titration curve was measured by an electrokinetic analyzer (SurPASS, Anton Paar GmbH, Graz, Austria) for both functionalized and non-functionalized samples (Ti_Ca+I+TPH and Ti_Ca+I). Two samples were prepared for each type of titration curve (acid and basic) and the ζ potential was measured as a function of pH in a 0.001 M KCl electrolyte solution. and the pH value (which starts at approximately 5.5) was varied by adding 0.05 M HCl or 0.05 M NaOH using the automatic titration unit of the instrument. The isoelectric point (IEP) was established as the intercept of the titration curve with the x-axis (zeta potential = 0 mV).

3.6.6 Ion Release

To measure the release of Iodine from Ti_Ca+I and Ti_Ca+I+TPH samples, the mentioned samples were immersed in 2 ml of PBS under continuous shaking (50 rpm) at 36.5 °C in dark conditions. After the planned periods (for 1 h, 6 h, 24 h, 5 days, and 1 week), the concentrations of iodine ions were measured by inductively coupled plasma emission spectroscopy (ICP, SPS3100, Seiko Instruments Inc., Chiba, Japan). The measurement was done in triplicate and average and standard deviations were calculated.

3.6.7 Hydroxyapatite Formation

Ti_Ca+I+TPH and Ti_Ca+I were soaked in 24 mL of SBF with ion concentrations close to those of human blood plasma, according to the work of Kokubo [285], for 1, 3 days and 1 week at 36.5 ◦C. After these periods, the SBF was removed and apatite formation on the substrate was observed at FE-SEM.

3.6.8 SEM

The surfaces of the prepared titanium samples soaked in SBF, Ti_Ca+I and Ti_Ca+I+TPH were observed under a scanning electron microscope (FE-SEM, S-4300, Hitachi Co., Tokyo, Japan) at an acceleration voltage of 15 kV.

3.6.9 Polyphenols quantification and distribution on surfaces

Fluorescence microscopy

To observe the distribution of surface-grafted polyphenols, their fluorescent property was exploited [286]. To observe the red fluorescence, a confocal microscope (LSM 900, ZEISS) with a red filter and an excitation wavelength (573 nm) with a 1-second exposure time and a magnification of 100X was used. The test was used to observe the surfaces of Ti_Ca+I and Ti_Ca+I+TPH.

Spectrophotometric analysis

A modified Folin - Ciocalteu method was used to verify and evaluate the amount of polyphenols grafted onto the surface samples (Ti_Ca+I+TPH and Ti_Ca+TPH). The samples were soaked for 2 hours under dark conditions in a solution with 8 ml of water, 0.5 ml of Folin - Ciocalteu reagent, and 1.5 ml of 20% (w/V) Na_2CO_3 solution [287]. After this time, photometric measurement was performed at 760 nm. To quantify the polyphenol amount, a standard calibration curve was previously prepared using solutions with different gallic acid concentrations (i.e., 0.0025, 0.005, 0.01, 0.02, 0.03, and 0.04 mg/ml) as

described in [288].

3.6.10 Biological evaluation

Antibacterial Activity Test:

The antibacterial activity of untreated titanium (Ti), Ti_Ca+TPH, Ti_Ca+I, Ti_Ca+I+TPH against Escherichia coli (E. coli; IFO3972) was estimated according to the ISO22196 standard [289]. Drops of bacterial cell suspensions (100 µL) in RPMI 1640 broth were injected onto the 25 × 25 × 1 mm^3 sized samples and covered with a 20 × 20 mm^2 sterile flexible polypropylene film so that the solutions were firmly in contact with the substrate. The samples thus prepared were stored in Petri dishes in an incubator with controlled humidity and temperature (95% and 35°C, respectively) for 24 hours. After 24 hours, the samples were removed from the incubator and rinsed with 10 mL of soybean casein digestion bar containing lecithin and polyoxyethylene sorbitan monooleate (SCDLP) to collect bacteria grown during incubation. Finally, the number of bacterial cells was calculated using the dilution factor and the number of colonies counted on the Petri dish.

Cytocompatibility evaluation

Biological characterizations were performed using square specimens (10 × 10 × 1 mm^3) sterilized by UV light (2 hours). Specimens' cytocompatibility was tested in vitro towards Human bone marrow-derived stem cells (hMSC); cells were obtained from Merck (Promo Cell C-12974) and cultivated in low-glucose Dulbecco's modified Eagle Medium (DMEM, Sigma Aldrich, Milan, Italy) supplemented with 15% fetal bovine serum (FBS, Sigma Aldrich, Milan, Italy) and 1% antibiotics (penicillin/streptomycin) at 37°C, 5% CO_2 atmosphere. Cells were cultivated until 80-90% confluence, detached by a trypsin-EDTA solution (0.25% in PBS), harvested, and used for the experiments.

For cytocompatibility studies, specimens were gently located into a p24 multiwell plate and cells were dropwise seeded in a defined number ($1x10^4$ cells/specimen) onto the specimens' surface and allowed to adhere for 4 hours at 37°C before being submerged with 1 ml of medium. After 24 hours of cultivation in direct contact with the specimens' surface, the cells' viability was evaluated in function of their metabolic activity by the colorimetric metabolic

alamar blue assay (alamarBlue™, ready-to-use solution from Life Technologies, Milan, Italy). Briefly, after introducing the alamar solution the plate was incubated in the dark for 4 hours at 37°C; then, supernatants were collected and the fluorescence signals were evaluated with a spectrophotometer (Spark®, Tecan Trading AG, Zürich, Switzerland) using the following set-up: fluorescence excitation wavelength 570 nm, fluorescence emission reading 590 nm. Moreover, cells adhered to the specimens' surfaces were investigated for their viability by the fluorescent Live/Dead assay (LIVE/DEAD, from Invitrogen, Milan, Italy); briefly, after washing with PBS the solution was added to each specimen and then incubated for 45 min. After incubation specimens were washed with PBS and fluorescent images were collected by a confocal microscope (Leica SP8 confocal platform, Leica Microsystems, Germany).

Antioxidant properties evaluation

Specimens' ability to act as antioxidants by a scavenger activity was evaluated towards their ability to protect cells' survival in a pro-inflammatory environment. Accordingly, the inflammation was chemically induced by adding hydrogen peroxide (H_2O_2, 3 hours, 300 mM) in the medium with the aim to generate oxidative stress by toxic active species as previously shown by the Authors [290]. Accordingly, H_2O_2 was added before the cells' seeding to resemble a pre-implant inflammation or after the seeding to simulate a post-operative inflammation. Afterward, cells' metabolic activity was evaluated by the alarm blue assay as previously detailed. Moreover, to demonstrate that the toxic effect was due to the internalization of toxic active species, the specific CellRox reagent (CellROX™ Deep Red Reagent kit, from Thermo Fisher Scientific, Milan, Italy) was used to visualize the species in the intracellular compartment; cells were further co-stained with phalloidin (Alexa Fluor 488 Phalloidin, from Thermo Fisher Scientific, Milan, Italy) and 4,6-diamidino-2-phenylindole (DAPI, Sigma Aldrich, Milan, Italy) to visualize cytoskeleton F-actin filaments and nuclei, respectively. Cells cultivated in the regular medium were considered as a positive control.

3.7 Results and discussion

The first part of the research has been devoted to verifying the effective presence of both polyphenols and iodine ions on the functionalized surface and to their characterization. The Ti_Ca+I surface has already been characterized in [283] and it is here used as a reference.

This substrate is extensively characterized in previous works and its osseointegration ability is already verified. In fact, in vivo mechanical and histological experiments are performed on the specimens, confirming a high long-term sustainable bone-bonding capacity [284], [291].

3.7.1 X-ray Photoelectron Spectroscopy

The atomic percentages of the elements are shown in Table 3.3 as detected by XPS on the surfaces before and after functionalization. The functionalized samples showed a reduction in the atomic percentage of titanium with respect to Ti_Ca+I, evidencing that a layer, attributable to polyphenols, covered the titanium oxide surface. In addition, the functionalized samples (Ti_Ca+I+TPH) showed a 60 % reduction in the atomic percentage of iodine. One explanation is that the organic molecules covered the surface, thus also covering the surface-exposed iodine ions as it occurred for titanium. A second explanation could be that the functionalization method led to an ionic release at the interface between the sample surface and the drop of the polyphenols solution, thus leading to a possible decrease of iodine on the functionalized surface. The ratio between the titanium and iodine percentages was similar on both surfaces (respectively 21 on TiCa+I+TPH and 18 on Ti_Ca+I) suggesting that the first explanation was more reliable and the iodine release during the functionalization was quite limited.

Confirming this, the analysis survey also showed an important increase in the percentage of carbon, the main element that composes polyphenols. Oxygen, on the other hand, did not change drastically because, polyphenols, being OH-rich, exposed oxygen on the functionalized surface as the titanium oxide did before functionalization. As last, both surfaces contained calcium. This can be explained considering that the chemical treatment used for obtaining Ti_Ca+I induced a calcium enrichment of the titanium oxide layer as well as the

functionalization with polyphenols was performed in a solution with Ca^{2+} ions.

Table 3.3 The atomic percentages of the elements detected on the surface of samples Ti_Ca+I+TPH and Ti_Ca+I.

Atomic percentage					
	C1s	O1s	Ca2p	Ti2p	I3d5
Ti_Ca+I+TPH	41.24	45.28	1.75	11.2	0.53
Ti_Ca+I	13.79	59.49	1.57	23.79	1.36

To identify the specific chemical groups exposed on the surfaces, the high-resolution spectra of carbon and oxygen (C1s and O1s) were measured, as shown in Figure 3.13, which represent the main elements that characterize polyphenols.

After TPH grafting, different contributions can be detected in the carbon region (Figure 3.13b). In particular, although the peak of C-C and C-H bonds at 284.7 is the highest in both cases, the peak related to C-O at 287.5 eV [27] became more intense after functionalization, as expected when polyphenols are compared to adventitious organic contaminations (mainly hydrocarbons). Moreover, a new signal can be observed, at about 288 eV. This can be attributed to C=O bonds, already detected on surfaces functionalized with polyphenols [277] and explained by partial oxidation of the molecule creating a quinone bond. The presence of a peak due to carbonates can be due to some impurities.

In the oxygen region, the difference between the functionalized and nonfunctionalized samples is clearer and more visible. (Figure 3.13a). Three peaks were present on the Ti_Ca+I sample at 530.44 eV, 531.5, and 532.5 eV and can be correlated with the Ti-O bond of the titanium oxide, with the –OH acid (OH_a) and basic (OH_b) groups exposed by the surface titanium oxide layer after the treatment, respectively [284], [292]. In the spectrum of the Ti_Ca+I+TPH sample, these peaks were still present, but a new peak was visible at 533.8 eV, related to the OH aromatic band that was attributable to polyphenols [292]. It is of interest that the ratio between the area of the peaks related to OH_b and OH_a is almost the same before and after functionalization (OH_b/OH_a is 3 after functionalization, and 4 before it), confirming that these functional groups belong to the titanium oxide layer. Analogously, the ratio between the area of the peak related to TiO and the sum of the peaks related to OH_b and OH_a does not significantly change before and after functionalization ($TiO/(OH_a+OH_b)$ is 0.4 after functionalization and it is 0.3 before it). Both these ratios shown in Table 3.4, confirm that the OH groups of the polyphenols are related to the

phenolic signal while the others belong to the titanium oxide layer. In both cases, a signal related to Ca-O is evidenced: it is due to the calcium titanate on Ti_Ca+I and to the Ca^{2+} ions linking the polyphenols on Ti_Ca+I+TPH.

Table 3.5 The ratio of the peak area of the XPS curves for the Ti_Ca+I+TPH and Ti_Ca+I samples.

	OH_a/OH_b	$TiO/(OH_a+OH_b)$
Ti_Ca+I+TPH	3	0.4
Ti_Ca+I	4	0.3

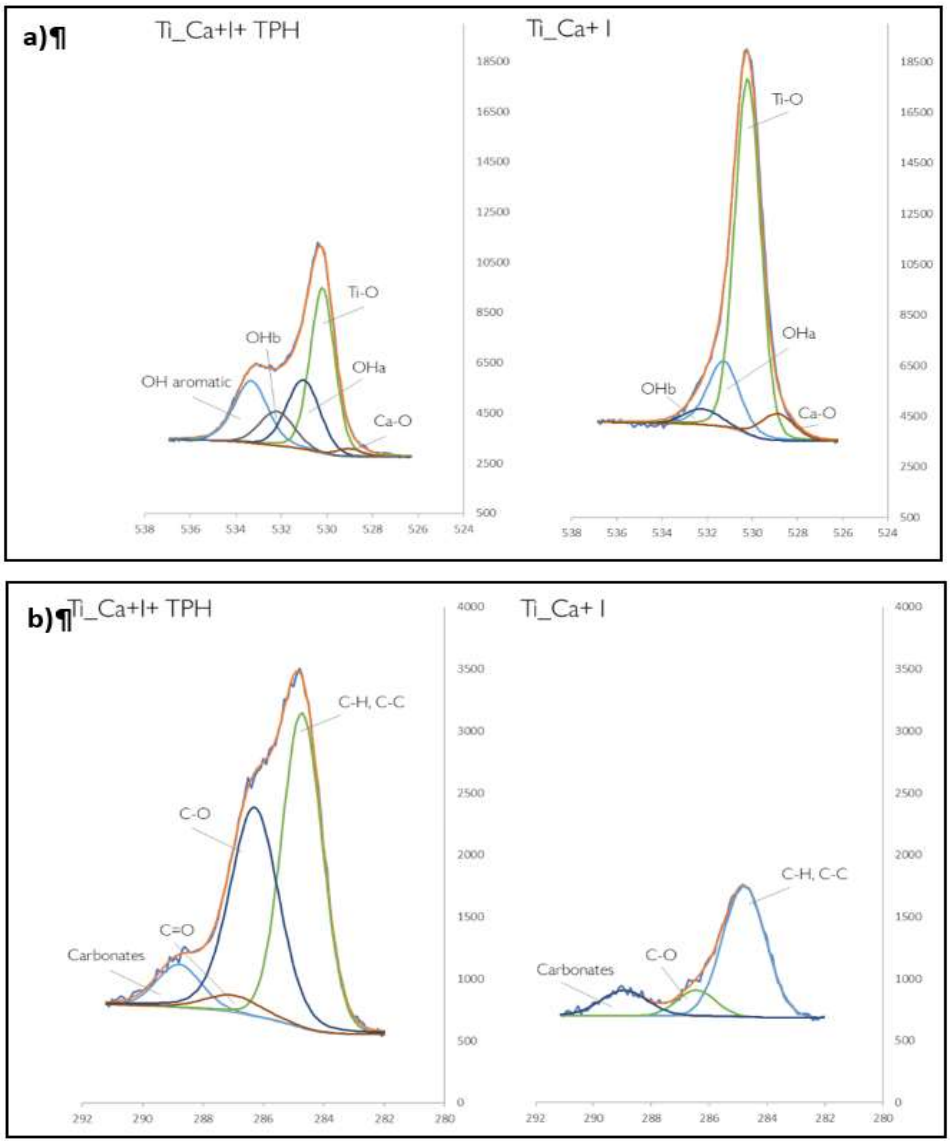

Figure 3.13 XPS high resolution (HR) spectra of (a) O1s and (b) C1s of the samples Ti_Ca+I+TPH and Ti_Ca+I. X-Asis: (eV binding)

3.7.2 Zeta Potential Measurements

Figure 3.14 shows the zeta potential titration curves of titanium samples with (Ti_Ca+I+TPH) and without polyphenols (Ti_Ca+I). The surface before functionalization had an isoelectric point (IEP) at about 5.3 and it was negatively charged at physiological pH (about -34 mV at pH = 7.4). The curve shows an evident plateau in the acidic range (with positive zeta potential values), which can be explained by the presence of basic functional groups (supposedly basic OH). The beginning of the acidic plateau is at pH ≈ 4 and indicates that the functional groups behave as a very strong base, in fact, they protonate at a low pH value. On the other hand, the surface was also rich in acid functionalities (presumably OH acid groups), confirmed by the presence of a plateau in the basic range beginning at pH 8.5. In fact, surface treatment, in addition to creating basic groups, created some acidic groups, but they acted as a weak acid and are deprotonated only at very high pH. The prevalence of the basic groups in determining the surface charge and zeta potential, because of the stronger reactivity, was evidenced by a shift of the IEP towards a higher value (5.3) with respect to untreated titanium (expected IEP at pH 4). A contribution by basic and acidic functionalities due to iodine (HOI as an amphoteric functional group) may also be supposed [293]. The presence of acidic and basic groups are confirmed also by XPS (see paragraph 3.7.1).

On the other hand, looking at the curve of the functionalized sample (Ti_Ca+I+TPH), the shift of the isoelectric point toward the acidic range and disappearance of the plateau at acidic pH can be explained by the polyphenols covering the surface and basic functional groups of Ti_Ca+I while the functionalized surface exposed many more acidic OHs, characteristic of polyphenols molecules. This fact also led to the appearance of a much more pronounced plateau from the pH value of 4.5, indicating that the acidic OHs behave as a strong acid. This is expected for some of the OH groups of polyphenols (EGCG, in particular) which have a pKa value lower than 7 [294]. The standard deviation of the zeta potential was very small for the entire measurements (the error bars are hardly visible in the graph), both for the reference and functionalized sample, demonstrating the good surface chemical stability [295] and the efficacy of polyphenol grafting on the surface.

Looking at the XPS data and comparing them with the zeta potential curves, we can say with certainty that the acidic and basic functional groups of the Ti_Ca+I samples are given by the basic and acidic OH groups exposed on the

surface as a result of the treatment.

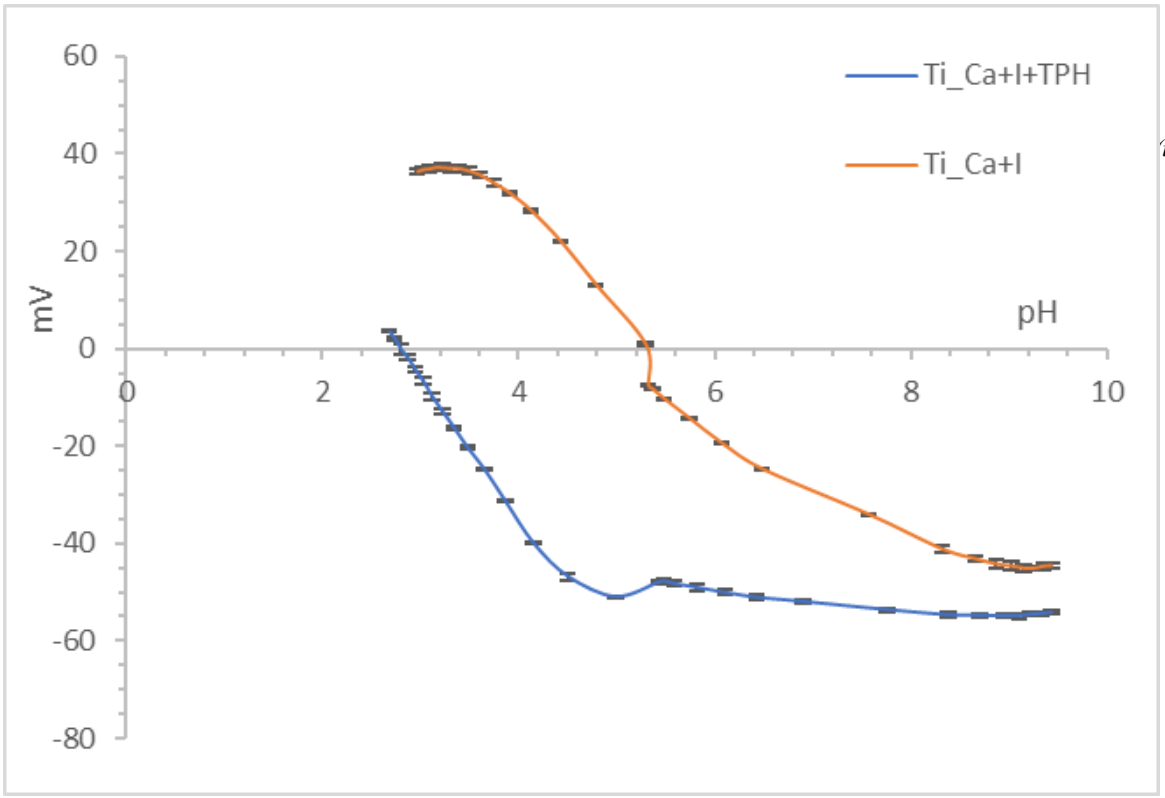

Figure 3.14 Zeta Potential titration curve of Ti_Ca+I and Ti_Ca+I+TPH

3.7.3 Ion Release

Figure 3.15 shows the concentration of iodine released from the treated Ti_Ca+I and Ti_Ca+I+TPH samples as a function of immersion time in PBS. The graph shows that the treated Ti_Ca+I initially released 4.0 ppm of iodine within 6 hours and then slowly released another 1.6 ppm over one week. In contrast, the functionalized sample (Ti_Ca+I+TPH) showed a significant decrease in the ionic release, about half the amount of the reference sample, indicating that the functionalization mode probably reduces the kinetic of the ion release and slightly reduces the amount of iodine available on the sample surface, as confirmed by XPS. Interestingly, the presence of polyphenols did not alter the mechanism of the ion release: the release trend remains the same even if with a lower absolute value in terms of concentration. The standard deviation was also lowered after the functionalization evidencing a lower but probably more stable release.

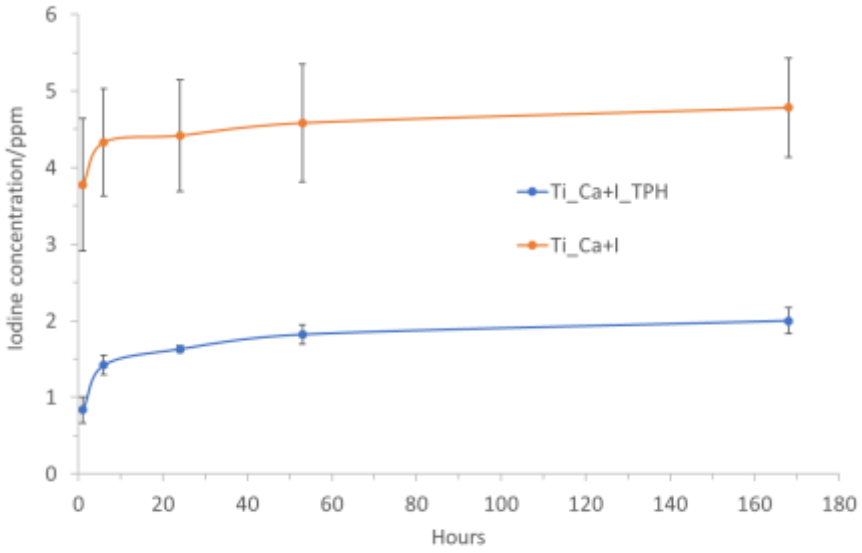

Figure 3.15 Iodine concentration released from Ti_Ca+I and Ti_Ca+I+TPH as a function of the soaking time in PBS (in hours).

3.7.4 Hydroxyapatite Formation

Figure 3.16a shows the formation of apatite on the functionalized samples (Ti_Ca+I+TPH) after 1, 3, and 7 days. After immersion in SBF, the samples formed numerous spherical particles on their surface, which on day 7 covered almost the entire surface. In contrast, Figure 3.16b shows the formation of apatite on a reference sample (Ti_Ca+I) after 3 days. Polyphenols would seem to slow the growth of hydroxyapatite, as it is clear that after 3 days fewer and smaller particles are found on the functionalized sample. In fact, in general, polyphenols interact with hydroxyapatite by binding to the surface of the apatite crystals. This binding can affect the nucleation and growth of the apatite crystals, leading to changes in the size, morphology, and shape of the crystals [296], [297]. In any case, the surfaces had a remarkable ability to induce hydroxyapatite precipitation during soaking in simulated body fluid, as it appeared after 7 days of soaking.

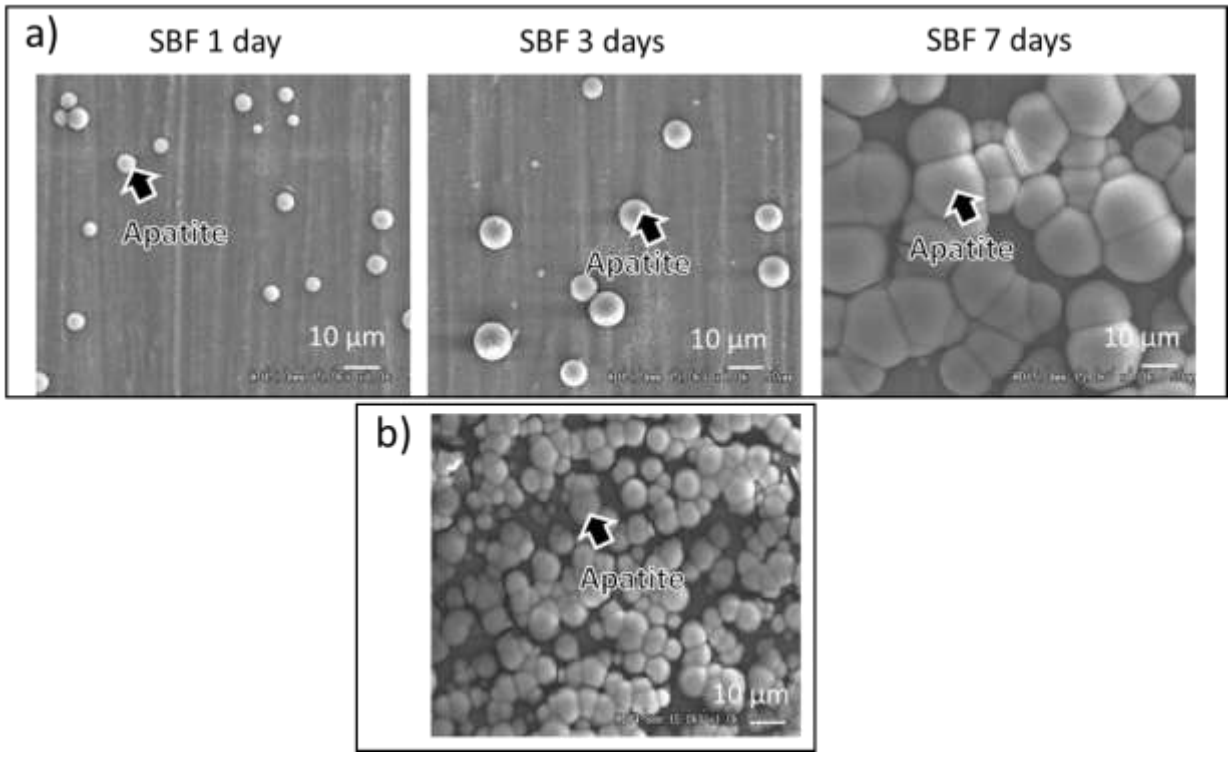

Figure 3.16 FE-SEM images of the surfaces soaked in SBF of (a)Ti_Ca+I+TPH for 1, 3, and 7 days, (b) Ti_Ca+I for 3 days

3.7.5 Polyphenols quantification and distribution on surfaces

The distribution of polyphenols on the sample surface was studied by exploiting the autofluorescent abilities of polyphenols. Figure 3.17a shows the fluorescence microscope observations on the Ti_Ca+I sample before and after functionalization. On the surface of the reference sample (Ti_Ca+I), the fluorescent signal was absent, confirming that the surface itself was not fluorescent. On the other side, the surface of the functionalized sample (Ti_Ca+I+TPH) showed a uniform intensity of the emitted fluorescent signal, due to the grafted polyphenols with a uniform distribution on the surface of the material, forming a thin but homogeneous layer. It is also important to note from the SEM images of the functionalized and reference surfaces, Ti_Ca+I-TPH and Ti_Ca+I, respectively (Figure 3.17b), that although polyphenols were uniformly present on the sample surface, they did not alter the nanotextural morphology created by the treatment, which is important for osseointegration.

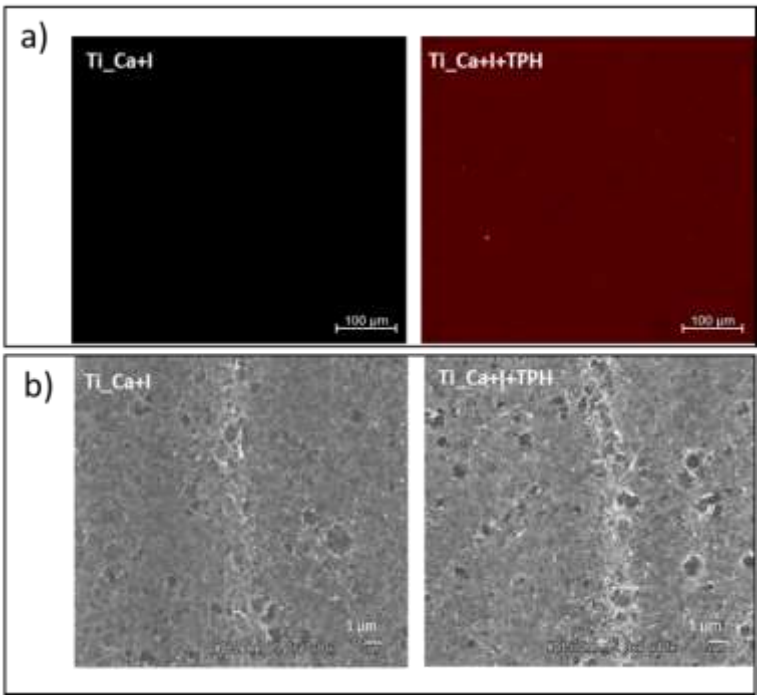

Figure 3.17 Morphology of Ti_Ca+I and Ti_Ca+I+TPH samples a) Fluorescence microscopy observations on the surfaces, b) Surface FE-SEM images.

Quantification of surface polyphenols, on the other hand, was studied by exploiting the antioxidant capacity of polyphenols, using spectrophotometric methods such as the Folin-Ciocolteau analysis test modified to be applied to surfaces As shown in Figure 3.18, the absorbance at 760 nm was around 0.07, evidencing a redox activity of surface polyphenols equivalent to a solution with a gallic acid concentration of 0.003 mg/ml (GAE). Considering a "calibration curve" of TPH, an absorbance of 0.07 corresponded to a concentration of TPH of 0.0038 mg/ml, which was close to the one obtained in terms of GAE. This result evidenced also that the grafted polyphenols maintained their redox chemical activity after grafting.

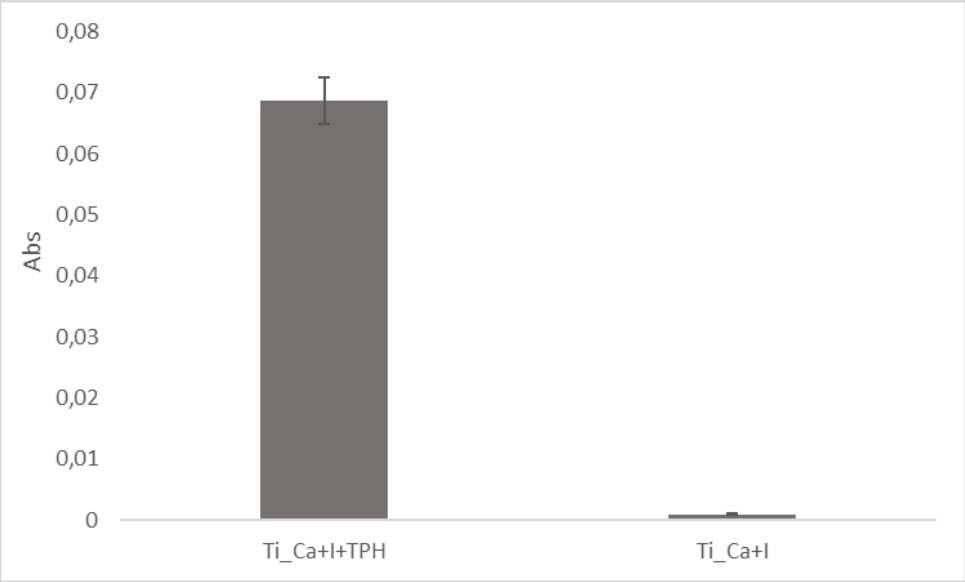

Figure 3.18 Redox activity of polyphenols grafted on the surfaces, measured through the Folin – Ciocalteu modified method, of Ti_Ca+I+TPH and Ti_Ca+I samples.

3.7.6 Biological evaluation

Antibacterial effect

The antibacterial effect of iodine is well known and has been already studied in previous works [284]. The antibacterial test was carried out according to ISO22196 standard on Ti, Ti_Ca+TPH, Ti_Ca_I+TPH, and Ti_Ca_I samples. A larger set of samples (with also Ti_Ca+TPH) has been used for this test to understand whether the presence of polyphenols affected the antibacterial effect of iodine. Figure 3.19 shows that functionalized and reference samples, without iodine ions on the surface (Ti and Ti_Ca+TPH), had no antibacterial effect against *E.Coli*, being free of the antibacterial agent. It was also evident that the presence of polyphenols on the surface did not inhibit bacterial colonization, showing no antibacterial effect. Samples with iodine on the surface (Ti_Ca+I and Ti_Ca+I+TPH), on the other hand, did not show colony formation either before or after functionalization, indicating a potent antibacterial activity of iodine on *E. Coli* (with a percentage reduction > 99%), as shown in Table 3.5 The presence of polyphenols, therefore, did not inhibit the antibacterial capacity of iodine, which remained intact, even if the ion release was reduced.

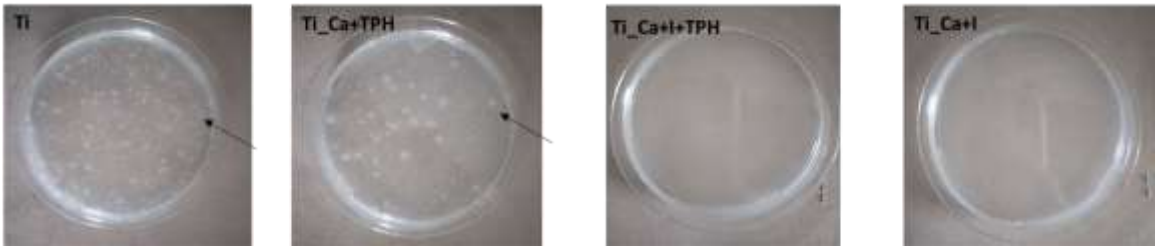

Figure 3.19 Optical images of colony formation on Ti, Ti_Ca+TPH, Ti_Ca+I+TPH, and Ti_Ca+I

Table 3.6 Antibacterial activity value of Ti_Ca+TPH, Ti_Ca+I+TPH, Ti_Ca+I and Ti against E.Coli

Average of E.Coli Count/CFU			
Ti	Ti_Ca+TPH	Ti_Ca+I+TPH	Ti_Ca+I
9.40E+06	5.07E+06	<20	<20

Cytocompatibility evaluation

To exclude any toxic effect, cytocompatibility was verified before moving to the antioxidant properties evaluation. Given the potential application of the here developed specimens for bone repair, human mesenchymal stem cells (hMSC) were considered as a target model in view of their pivotal role in the healing process. Moreover, cells were seeded in direct contact with the control and functionalized surfaces to study their ability to properly adhere, spread, and exploit metabolic activity, thus simulating possible colonization of the device after implantation by the cells recruited from the neighbor tissue towards the injury site [298].

The metabolic activity was considered the parameter to determine the viability of the cells adhered to the specimens' surface after 24 hours of cultivation; results are reported in Figure 3.20. None of the treated surfaces (Ti_Ca+I or Ti_Ca+I+TPH) determined a reduction of the hMSC metabolic activity in comparison to the untreated Ti control ($p>0.05$) that was considered as a positive control given the large literature demonstrating its biocompatibility [299]. On the opposite, the presence of polyphenols (TPH) determined an increase (≈15%) in the metabolism in comparison to the Ti control that was assumed as 100% as prior discussed (Figure 3.20b). It can be hypothesized that the bioactivity of the functionalized specimens was improved thus being hypothetically able to improve/speed up the healing process. Similar pro-regenerative results were obtained in literature by using for example resveratrol and curcumin; Prakoeswa et al. [300] demonstrated that resveratrol can boost hMSC to release growth factors in non-healing wounds whereas Chen et al. [301] showed that curcumin improves hMSC BMP-2 and TGF-β production ameliorating osteogenesis in a pro-inflammatory environment. On the opposite, the iodine contribution appeared insignificant in terms of hMSC metabolism boost (≈5% improvement in comparison to Ti control); however, no previous literature reported a significant pro-regenerative or pro-healing activity of iodine towards stem cells.

It is mostly recognized as a strong antioxidant compound [302] as well as a potential antibacterial agent as previously demonstrated in this work, too. Finally, to give a visual confirmation of the specimens' successful colonization, Live/Dead fluorescent imaging (Figure 3.20c) was applied to confirm that cells were viable (stained in green) showing a correct fibroblast-like morphology and comparable surface density between the control and functionalized samples.

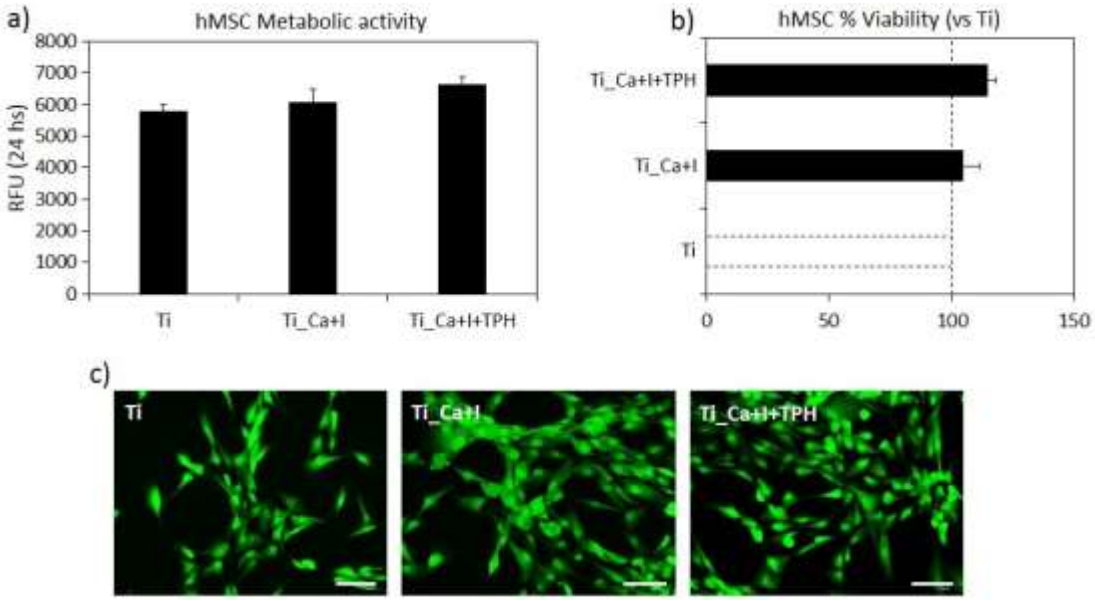

Figure 3.20 Cytocompatibility evaluation of Ti Ca+I and Ti Ca+I+TPH

Surface functionalization with iodine (Ti_Ca+I) and polyphenols (Ti_Ca+I+TPH) did not decrease hMSC metabolic activity in comparison to the Ti controls (a, p>0.05) giving a positive boost of ≈5% and ≈15%, respectively. Live/dead images confirmed that cells were viable (stained in green) with a proper morphology and comparable surface density. Bars represent means±dev.st, replicates=3. Images bar scale=125μm

Antioxidant properties evaluation

We imposed an oxidative stress to the hMSC seeded onto the control (Ti) and functionalized specimens (Ti_Ca+I and Ti_Ca+I+TPH) by the generation of active species through a medium doped with H_2O_2 to verify if any scavenger action was performed by the surfaces. In the first experimental set-up, the pro-inflammatory environment was induced before the cells' seeding to verify if the functionalization was effective in reducing the amount of free toxic active species affecting the cells migrating towards the implant site; the protocol was first validated using polystyrene as a gold standard substrate for cells' cultivation.

Results related to the specimens' test are reported in Figure 3.21. As expected, the lowest value in terms of cells' metabolic activity was registered by the untreated Ti controls (Figure 3.21a); the lack of any protective effect determined a toxic environment driving cells mostly to the apoptotic stage as clearly seen by the SEM images (Figure 3.21b) where they appeared mostly in the typical apoptotic round-shape. On the opposite, iodine (Ti_Ca+I) provided first protection showing a significant improvement in comparison to the Ti control (Figure 3.21a, $p<0.05$ indicated by §), but the best results were achieved by the combination of iodine + polyphenols (Ti_Ca+I+TPH) that were significant towards both controls and iodine (Figure 3.21a, $p<0.05$ indicated by § and #, respectively). SEM images (Figure 3.21b) confirmed that cells seeded onto such functionalized surfaces were able to adhere, spread, and maintain a proper fibroblast-like morphology as well as their metabolism was the highest when the Alamar blue assay was applied. So, it can be hypothesized that iodine and polyphenols worked in synergy to maximize the capture of the active species thus protecting cells from their toxic effect. To confirm this hypothesis, the specific fluorescent assay CellRox was applied to visualize the active species internalized by the cells. As displayed in Figure 3.21c, most of the cells cultivated onto Ti were positive to the red color of the dye (indicated by the red arrows) whereas the number of positive cells decreased when iodine and iodine + polyphenols surfaces were analyzed. Moreover, as previously observed by SEM, cells onto Ti controls displayed mostly a round-shaped morphology forming clusters. On the opposite, cells cultivated onto Ti_Ca+I+TPH specimens showed the highest density, proper morphology, and lowest number of red-positive signals thus giving a clear demonstration of the starting hypothesis.

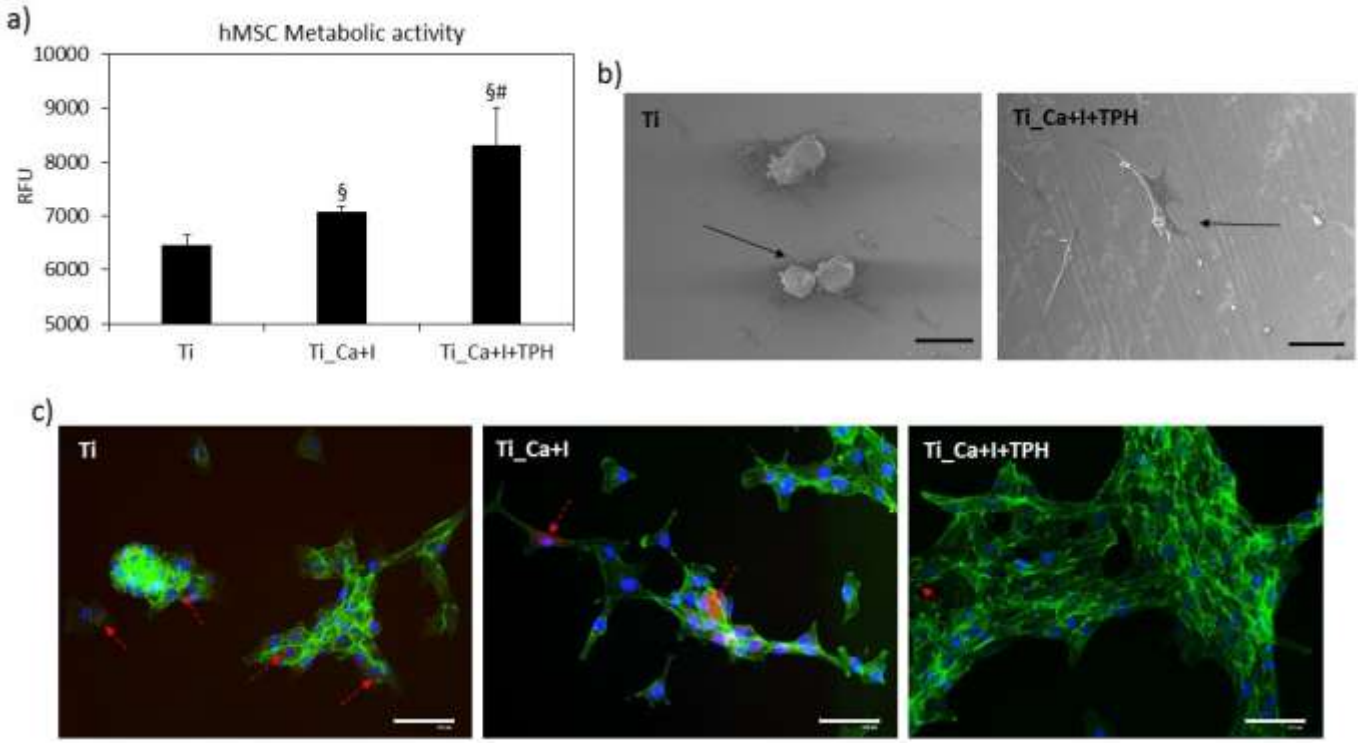

Figure 3.21 Pre-inflammatory evaluation of Ti_Ca+I and Ti_Ca+I+TPH

When the inflammatory environment was generated before the cells' seeding, the presence of iodine + polyphenols (Ti_Ca+I+TPH) protected cells by oxidative stress showing the highest metabolism (a, $p<0.05$ in comparison with Ti and Ti_Ca+I, indicated by § and #, respectively) and a proper morphology at SEM images (b). The toxic effect was due to the active species internalization as shown in the CellRox staining (c, positive cells stained in red) where most of the cells resulted as protected by the iodine and polyphenols. Bars represent means±dev.st, replicates=3. SEM images: 180x magnification, bar scale=100µm; fluorescent images bar scale = 125µm.

In a very similar way to the first experimental set-up, the lowest value in terms of cells' metabolic activity was reported by the untreated Ti controls (Figure 3.22a); however, in this second pro-inflammatory condition only the functionalization based on the iodine + polyphenols reported significant results in comparison to both Ti controls and Ti-Ca+I iodine functionalized (Figure 3.22a, $p<0.05$ indicated by § and #, respectively). Probably, the presence of the cells seeded prior to the H_2O_2 administration reduced the scavenger activity of the surfaces by "screening" some of the surface-exposed iodine ions and polyphenols; therefore, only the combination was effective in protecting the cells from oxidative stress. So, it was confirmed the very promising protective effect of the iodine + polyphenols combination that allowed cells to maintain the correct morphology as seen by the SEM images (Figure 3.22b) and minimize the toxic effect of the internalization of active species as confirmed by the CellRox fluorescent dye (Figure 3.22c).

The results agree with the literature. Iodine has been largely demonstrated to hold an intrinsic antioxidant activity that can be exploited to reduce inflammation in situ upon implantation for tissue engineering purposes. In fact, iodine is internalized by a facilitated diffusion system that is evolutionary conserved and it directly neutralizes free radicals, induces the expression of type II antioxidant enzymes, or inactivates proinflammatory pathways [302]. Moreover, iodine was here combined with polyphenols, molecules conferring strong antioxidant activity to the functionalized surfaces as previously demonstrated also by the authors [303], [304]. In fact, polyphenols have been shown as a very promising chemical improving tissue repair under pro-inflammatory conditions; dealing with bone repair, representing the target of this study, polyphenols have been found to stimulate bone formation, mineralization, as well as the proliferation, differentiation, and survival of osteoblasts by a protective effect against oxidative stress and inflammatory cytokines [273]. In addition, polyphenols inhibit the differentiation of the osteoclast cells thus favoring bone repair over resorption[273].

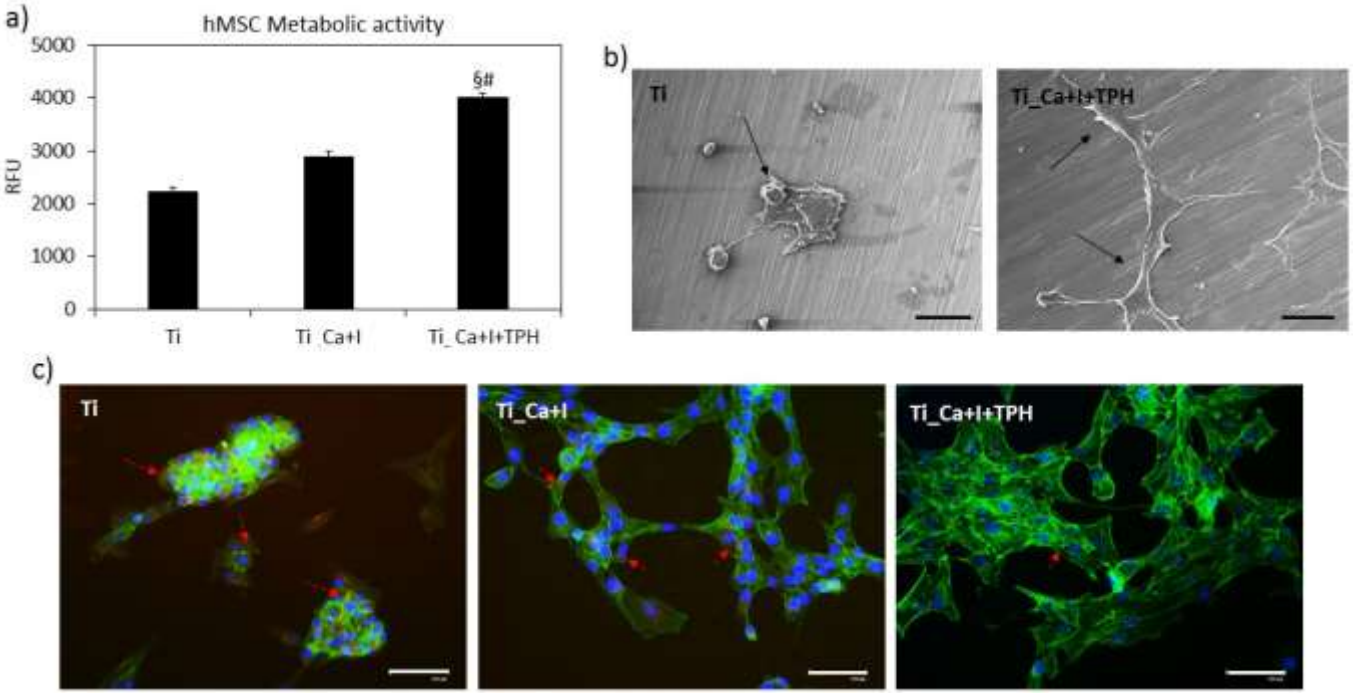

Figure 3.22 . Pro-inflammatory evaluation of Ti_Ca+I and Ti_Ca+I+TPH

When the inflammatory environment was generated after the cells' seeding, the presence of iodine + polyphenols (Ti_Ca+I+TPH) protected cells by oxidative stress showing the highest metabolism (a, $p<0.05$ in comparison with Ti and Ti_Ca+I, indicated by § and #, respectively) and a proper morphology at SEM images (b). The toxic effect was due to the active species internalization as shown in the CellRox staining (c, positive cells stained in red) where most of the cells resulted as protected by the iodine and polyphenols. Bars represent means±dev.st, replicates=3. SEM images: 180x magnification, bar scale=100µm. fluorescent images bar scale = 125µm.

4. Chapter: Peptoids

4.1 Introduction

Antimicrobial peptides (AMPs) have gained great interest in scientific research in recent years, particularly in biomedical applications such as drug delivery and orthopaedic applications. The main limitation of AMPs concerns their easy degradation in the physiological environment, which is rich in proteolytic enzymes. Recently, scientific research is attempting ways to make AMPs more stable, as easy degradation may be a problem when the antimicrobial agent is desired to have a longer-term effect.

My experimental research involved a collaboration with the EU project PREMUROSA where functionalization with the polypeptide nisin was successfully performed on a chemically treated titanium surface [305]. The experimental results are reported in Appendix A, because they were not the focus of my Ph.D. thesis.

Peptoids are synthetic oligomers of N-substituted glycines that mimic the structure of peptides, they were created more than fifteen years ago and, in this time, research on them is greatly increased due to their biological capabilities, so today there is a very rich database of tested and proven peptoids. In fact, peptoids, not having the peptide bond, have a structure that does not allow proteolytic degradation, making them much more stable, while maintaining

antimicrobial activity. In addition, this structure brings many advantages to the molecule, including greater diversity and specificity, making them more suitable for biological applications.

This chapter includes a bibliographic part, with particular attention on antimicrobial peptides (AMPs), with a brief overview of their biomedical applications and their limitations which lead to an introduction to peptoids. The second part concerns a surface functionalization protocol optimized to graft a peptoid onto a treated titanium surface. A preliminary characterization of the functionalized surfaces was performed using the contact angle measurement and ζ potential titration curves. Finally, the ability to prevent surface colonization and biofilm formation by the pathogen *Escherichia coli* and S. epidermidis was verified.

4.2 Peptides

Peptides are short chains of amino acids that are joined together by peptide bonds, usually with a molecular weight of 500-5000 Da.[306] The peptide bond is a covalent bond that forms between the carboxyl group (-COOH) of one amino acid and the amino group ($-NH_2$) of another amino acid. It is formed through a dehydration reaction, in which a water molecule is removed, leaving a peptide bond and a dipeptide (two amino acids joined together) (Figure 4.1). The peptide bond is a strong and stable bond that is essential for the formation of protein structures. Indeed, the backbone of a protein is made up of a long chain of amino acids joined together by peptide bonds, with the side chains of the amino acids extending out from the backbone. The sequence of amino acids in a protein, as determined by the order of peptide bonds, is known as its primary structure. The properties of the peptide bond, such as its strength and rigidity, are determined by the nature of the chemical bonds involved in the chemical surrounding and geometry of the bond. It has a partial double bond character, which restricts its rotation and gives it a planar geometry. This planar geometry is important for the formation of secondary structures in proteins, such as alpha helices and beta sheets [307][308].

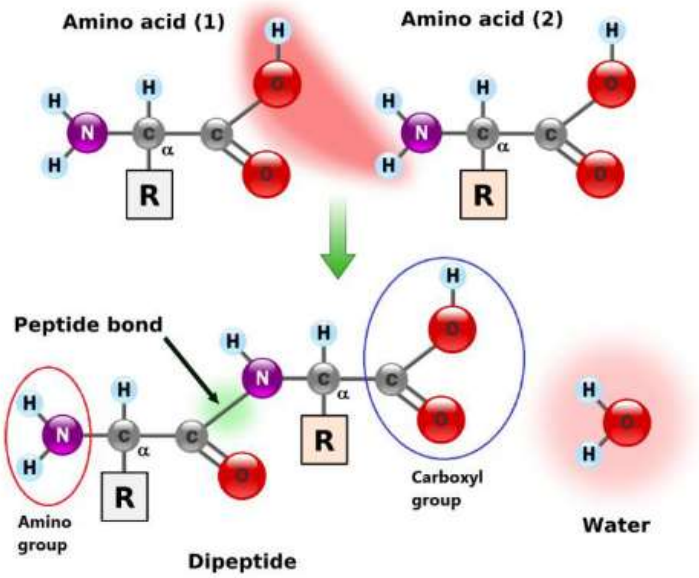

Figure 4.1 Amino acid structure and peptide bond [308]

There are 20 common amino acids that are used to synthesize proteins, each with a unique chemical structure and set of properties. The R group, also known as the side chain, is a unique component of each amino acid that differentiates from other amino acids. The R group can vary in size, shape, polarity, and charge, and it determines the chemical properties of the amino acid. The sequence and arrangement of the amino acids in a protein, and the properties of their R groups, ultimately determine the protein's overall structure and function. Amino acids are classified based on the properties of their R group, which can be nonpolar, aromatic, polar, basic, or acid.

Nonpolar amino acids, like valine and alanine, are hydrophobic and stabilize protein structures through hydrophobic interactions. Proline is also hydrophobic and reduces peptide chain flexibility due to its cyclic side chains. Aromatic amino acids, such as phenylalanine and tryptophan, have nonpolar and hydrophobic R groups.

On the other side, tyrosine has a polar OH group that can deprotonate at high pH (weak acid) and is a fluorophore residue in proteins. Polar amino acids, like serine and threonine, have hydrophilic R groups with polar moieties. Cysteine contains sulfhydryl groups responsible for disulfide bonds. Asparagine and glutamine have amide groups. Basic amino acids, like lysine, histidine, and arginine, are positively charged at neutral pH due to their N-containing R groups. Acidic amino acids, like aspartic acid and glutamic acid, have a prevalence of negatively charged carboxyl groups at physiological pH. Basic and acidic amino acids are the most hydrophilic [308],[309], [310].

In general, there is a wide variety of peptides with different structures, functions, and properties. This diversity makes peptides an important area of research for drug discovery and other applications [311].

Here are some of the important properties and functions of peptides:

1. Protein building blocks: Peptides are the basic building blocks of proteins. The sequence of amino acids in a peptide or protein determines its unique structure and function [312].
2. Signaling: Many peptides act as signaling molecules in the body, transmitting information between cells and tissues [313]. Examples include neuropeptides like endorphins and the hormone insulin that regulates the blood glucose level.
3. Antibacterial activity: Some peptides, such as antimicrobial peptides (AMPs), have antibacterial properties and can kill or inhibit the growth of microorganisms [314]

Peptides with functions like these described above are called bioactive peptides

and can have specific physiological functions, potentially benefiting human health and protecting against the development of various diseases. There are several sources of bioactive peptides which can be broadly classified as endogenous or exogenous. Endogenous bioactive peptides are naturally occurring peptides that are produced by the body, whereas exogenous bioactive peptides are derived from external sources, such as food or supplements [315].

In this thesis, we will focus on a specific type of bioactive peptides, antimicrobial peptides (AMPs)

4.2.1 AMPs

AMPs are ancient host defense molecules that are well-preserved in eukaryotes. They are a component of the innate immune system and are produced faster and more efficiently than antibodies. AMPs also act faster than immunoglobulins and are particularly important in organisms that lack a lymphocyte-based immune system, such as insects. AMPs have been found in a wide range of organisms, including microorganisms, plants, invertebrates, fish, amphibians, reptiles, birds, and mammals [316].

AMPs are typically short peptides, typically consisting of 10-50 amino acids, and they have a broad spectrum of activity against microorganisms [317]. In contrast, bacteria produce AMPs in order to kill other bacteria competing for the same ecological niche [317].

AMPs can kill bacteria by disrupting their membranes or penetrating them. The positively charged AMPs have a strong attraction for the negatively charged components of bacterial and fungal membranes, leading to their destruction [304],[306].

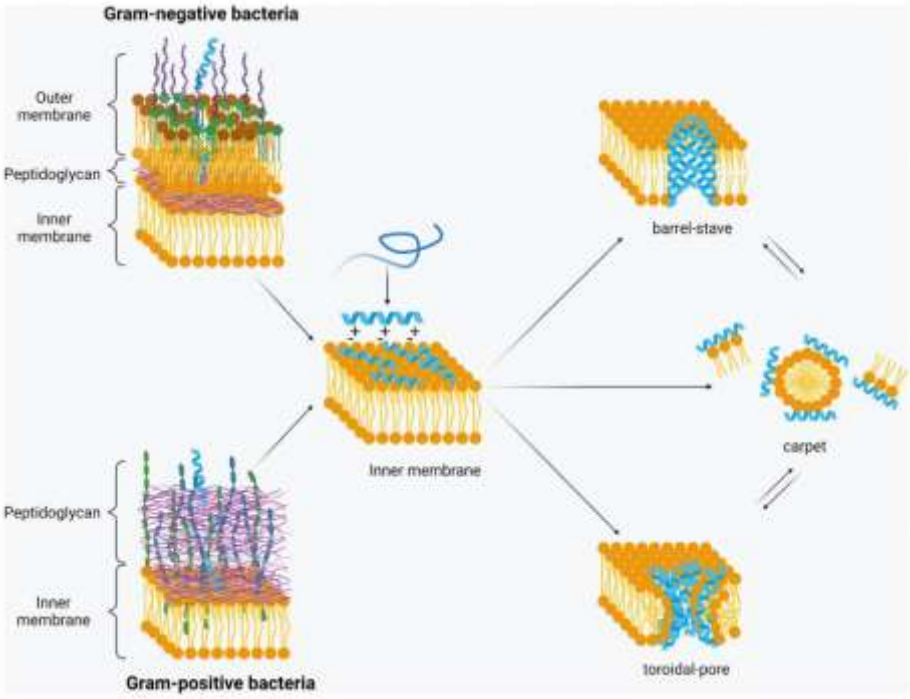

Figure 4.2 Interaction between AMPs and bacterial membrane [308]

In particular, AMPs could insert themselves into the bacterial membrane through hydrophobic and electrostatic interactions and they are believed to form pores in the inner membrane with two different modes of action: toroidal pore and barrel stave [319](Figure 4.2).

AMPs have a broad range of effects on membranes and intracellular components, making it difficult for bacteria to develop resistance to them. This makes AMPs an attractive option for combating antibiotic resistance.[320]
Recent studies have shown that AMPs not only have direct antimicrobial activity but also possess immunomodulatory and wound healing properties [321]. AMPs can modulate the host immune system by regulating the production of cytokines, chemokines, and growth factors [322]. Moreover, some AMPs can stimulate angiogenesis,[323] have anticancer activity [324], anti-inflammatory effects, and accelerate wound closure [325]. These additional properties of AMPs make them promising therapeutic candidates for the treatment of various infectious and inflammatory diseases.

Table (4.1) shows the different and potential activities of AMPs selected from the Antimicrobial Peptide Database (APD)

Table 4.1 AMPs from APD with their potential activity [315]

Activity AMP	Selected Examples of AMPs	Total No.
Antibacterial peptides	Abaecin; andropin; bombinin; [1] bBD-1-13; cecropin A, B, C, D, P; cryptdin; drosocin; esculentin-1-2; dermaseptin-B2-B5, B6, S1-S4; [2] hBD-26,27; LL-37; magainin; melittin; nisin; protegrin 1; pyrrhocoricin; temporin A, B, C, E, F, G, K, L; thanatin; tritrpticin	2678
Antibiofilm peptides	BMAP-27,28; citropin 1.1; colistin A; Dhvar4; gramicidin S; hBD-3; holothuroidin 1; indolicidin; LL-37; nisin A; polymyxin B; protegrin 1; SMAP-29 (Ovispirin); tachyplesin III; temporin B; temporin-1CEb	57
Anticancer peptides	Alloferon 1,2; aurein 1–3; buforin II; gomesin; indolicidin; lactoferricin B; LL-37; magainin 2; mastoparan B; melittin; nisin A,Z; tritrpticin	237
Anti-diabetic peptides	Amolopin; brevinin-1E, 2EC; esculentin-1, 1B; magainin-AM2	15
Antifungal peptides	Androctonin; antifungal protein; aurein 1–3; cecropin 2, A, B; dermaseptin-S1-S5; HD-2-6; HNP-1-6; indolicidin; lactoferricin B; magainin 2; melittin; protegrin 1–5; ponericin G1-G4; G7, W1-W5; thanatin; tritrpticin	1142
Anti-HIV peptides	Aurein 1.2; cecropin A; dermaseptin-S1,S4, S9; hBD-2,3; HNP-1-4; indolicidin; lactoferricin B; LL-37; melittin; protegrin 1	109
Anti-inflammatory peptides	Allomyrinasin; cathelicidin-PY; coprisin; defensin DEFB126; lucilin; papiliocin	20
Anti-MRSA peptides	Acipensin 1,2; BMAP-27,28; CAP18, citropin 1.1; clavanin A; cryptdin-4; [4] Dhvar5; esculentin-1,2 ISa-ISb; hBD-3; hedistin; [3] HNP-1; hominicin; imcroporin; indolicidin; LL-37; micasin-1; omega76; SMAP-29; plectasin; pleurocidin; protegrin 1; ubiquicidin	165
Antiparasitic peptides	Batroxicidin; cecropin A; dermaseptin-S1-S5; kalata B2, B5-B7; LL-37; magainin 2; melittin; temporin A, B, F, L;	116
Anti-sepsis peptides	Apidaecin IA; bactenecin 7; buforin II; cathelicidin-PY; cecropin 2, P1; drosocin; [5] HD-5; HNP-1; lactoferricin B; LL-37; melittin; polymyxin B; protegrin 1; pyrrhocoricin; SMAP-29; tachyplesin I; temporin L; thanatin	75
Anti-toxin peptides	hBD-1-4; HNP-1-5; retrocyclin-1-3	15
Anti-tuberculosis peptides	Griselimycin; hBD consensus; hBD10; human granulysin; lassomycin; laterosporulin10; LL-37; micrococcin P1; pantocin wh-1; RNase 7; Teixobactin; VpAmp1.0, 2.0	13
Antiviral peptides	Alloferon 1,2; antiviral protein Y3; aurein 1.2; BMAP-27,28; dermaseptin-S1, S4; hBD-1-3; HNP-1-6; indolicidin; lactoferricin B; LL-37; magainin 2; melittin; mucroporin; protegrin 1–5; thanatin; temporin A, B	189
Wound-healing peptides	AH90; AG-30; AG-30/5C; bactenecin; coprisin; epinecidin-1; hBD-2, 3; HD-5; HNP-1; IDR-1018; indolicidin; LL-37; lucifensin; magainin 2; nisin A; temporin A	22

[1] bBD: bovine beta defensin; [2] hBD: human beta-defensin; [3] HNP: human neutrophil peptide; [4] Dhvar: human Histatin; [5] HD: human defensin.

4.2.2 Nisin

Nisin is a 34 amino acid polypeptide produced by the bacterium Lactococcus Lactis that contains three unusual amino acids: lanthionine (Lan), methyllanthionine (MeLan), and dehydroalanine (Dha). These unusual amino acids are formed by post-translational modification of specific residues during biosynthesis, which gives nisin its unique structure and stability. The presence of lanthionine and methyllanthionine residues in the peptide's structure is believed to contribute to its stability by forming a network of intramolecular hydrogen bonds that help to maintain the peptide's secondary structure. The peptide is divided into five distinct regions and structures involving disulfide bridges.: A, B, C, D, and E, each of which has a specific role in the peptide's antimicrobial activity (Figure 4.3)[326],[327].

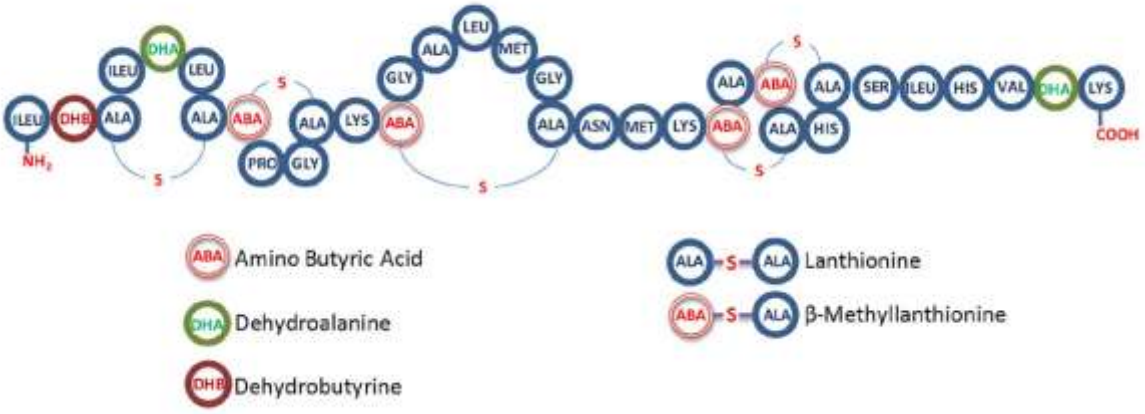

Figure 4.3 Structure of nisin [316]

Nisin exhibits potent antimicrobial activity against a broad range of Gram-positive bacteria, including many foodborne pathogens such as Listeria monocytogenes, Staphylococcus aureus, and Bacillus cereus which makes it an attractive antimicrobial agent for use in the food industry as a food preservative [328], [329].

Like all the other AMPs, it works by disrupting the bacterial cell membrane, leading to cell death. In particular, it exerts its biocidal activity through both the pore formation in the membrane and disruption of the cell wall biosynthesis by

binding to lipid II, which is an essential intermediate in peptidoglycan biogenesis[330].

It has been shown to exhibit synergistic activity with other antimicrobial agents, including organic compounds, such as carvacrol, eugenol, cinnamic acid, and thymol [331] essential oils [332] other AMPs, or antibiotics [333] which may enhance its antimicrobial activity.

However, the effectiveness of nisin is often affected by environmental factors such as pH and temperature. It seems stable at high temperatures, but its antibacterial activity was reduced to 25% under treatment at 160°C [327]. Moreover, nisin is most stable at a pH range of 4.5 to 5.5. At pH values above 7.0, nisin can be rapidly degraded and loses its antimicrobial activity and solubility. This is because the structure of nisin is dependent on the presence of unsaturated amino acids Dhb2, Dha5, and Dha3 residues that can be negatively affected by high pH values.[334]

4.2.3 Biomedical application of AMPs

Due to their properties, AMPs today find many types of biomedical applications. Wound healing and drug delivery are two fields in which AMPs find great applications. In the wound healing field, amphiphilic antimicrobial peptides such as Jelleine-1 could self-assemble into hydrogels having at the same time antimicrobial activity against both Gram-positive and Gram-negative bacteria [335]. They also could be used as molecules encapsulated in nanoparticles in biodegradable polymers for drug delivery systems. In this case, AMPs are used as a drug with anti-biofilm properties.[336]
AMPs are often conjugated with biomaterials. In particular, peptides are often covalently immobilized on a biopolymer through various immobilization techniques for different applications [337]. For example, chitosan is a biopolymer widely used thanks to its biodegradability and amino-hydroxyl functional groups and it is suitable to create a covalent bonding with antimicrobial peptides [338]. Moreover, PEG, another biodegradable biopolymer, has been extensively used to functionalize peptides [339].

AMPs are also conjugated with metal surfaces to create antibacterial coatings to prevent biomaterial-related infections. Two different approaches are used for surface modification: covalent binding or non-covalent immobilization, even if the covalent bindings are preferred, exploiting the functional groups of the peptide [340]. There are three ways studied in the literature to pursue a peptide coating. One requires a binding sequence incorporated into the peptide for ensuring a bonding with the substrate. The second requires coating the substrates firstly with linker layers that offer different functional groups for covalent coupling of peptides. The third one provides that peptides are immersed in a material matrix (nanotubes or porous surface) from which they should be released over time (Figure 4.4) [341].

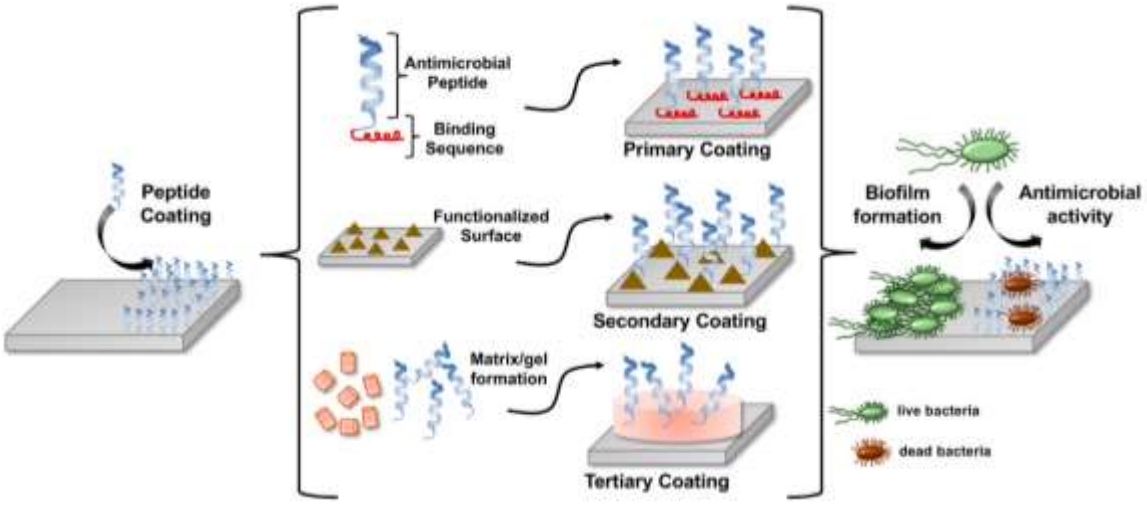

Figure 4.4 Coating of medical devices through 3 different techniques [341]

Coupling AMPs with titanium and its alloys

Although the biomedical applications are diverse and biomaterials conjugated to AMPs that have been found in the literature are multiple, this section wants to focus on the AMPs in combination with titanium and its alloys. Functionalization of AMPs onto titanium surfaces can be achieved through various methods, such as covalent bonding [342]–[346], [346]–[356] or physical adsorption[357]–[359]. Once the AMPs are functionalized onto the titanium surface, they can provide a potent antimicrobial barrier against bacterial infections.

The most popular method to combine AMPs with titanium is the covalent immobilization method. Different covalent coating methods have been used and explored and they are briefly illustrated in Figure 4.5.

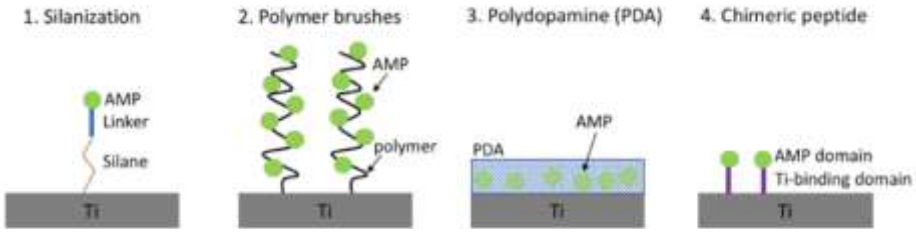

Figure 4.5 Covalent immobilization of AMPs on titanium surfaces [340]

The most popular covalent bonding method is the use of silane coupling agents, which can covalently bind titanium surfaces and form a stable chemical bond with the AMPs. For example, LL-37, a human cathelicidin-derived AMP, has been functionalized onto titanium surfaces and demonstrated effective antimicrobial activity against Escherichia coli [355]. In another study, GL13K was functionalized onto titanium surfaces and inhibited the biofilm formation of P. gingivalis, a putative pathogen of peri-implantitis [351].

Although the covalent immobilization method is the most widely used, it has been reported that the immobilization process on the surface of the implant may hinder the antimicrobial activity of the AMP. It's assumed that the incorporated AMPs don't reach the target microorganisms because they're released with difficulty.In addition, altering the stereochemistry or orientation of the peptide molecule resulted in lower antimicrobial efficacy than in the solution [356].

Physical adsorption involves the absorption of AMPs onto the titanium surface without the use of chemical linkers or covalent bonding, it is a simple method that is highly dependent on the composition and morphology of the titanium surface [360]. An example of physical adsorption is the loading of AMP Tet213 onto a Ca-P coating on a titanium surface for the prevention of implant-associated infections [358]. Although the non-covalent interactions are weaker than covalent bonds, the formed films can be stable, depending on the peptide-surface system and experimental conditions [361].

4.3 Peptoids

As we have seen so far, AMPs have become increasingly important in biomedical applications due to their different and multiple abilities. However, AMPs are not without limitations, particularly with regard to their stability. One of the major limitations of peptides in biomedical applications is proteolytic degradation. Peptides can be rapidly degraded by proteases in the body, which can result in a short half-life and reduced bioavailability [362].

Proteases are enzymes found in the body that catalyze the breakdown of peptide bonds, leading to the fragmentation of peptides. When peptides are administered for therapeutic purposes, proteases can quickly degrade them, resulting in a reduction in their therapeutic effectiveness. Additionally, certain tissues in the body, such as the liver and kidneys, contain high levels of proteases that can rapidly degrade administered peptides, further limiting their half-life and bioavailability [363].

Other limitations regard chemical reactions, such as oxidation, hydrolysis, and racemization which can affect the AMPs' stability and functionality [364], [365]. Moreover, some peptides have poor solubility in water or biological fluids, which can limit their bioavailability and efficacy [366]. Additionally, peptides can be sensitive to temperature changes, which can affect their stability and functionality [367]. Another limitation of peptides in biomedical applications is their potential for immunogenicity. Some peptides can be recognized by the immune system as foreign bodies, leading to an immune response that can limit their effectiveness and cause adverse reactions [364].

To overcome these limitations, efforts are being made to develop new strategies focused on the improvement of peptides' stability. For these reasons, peptoids have been introduced as an alternative to peptides. Peptides and peptoids are two classes of molecules that are similar in structure but differ in several key features. As we have already seen, peptides are short chains of amino acids that are linked together by peptide bonds. Peptoids, on the other hand, are synthetic molecules that resemble peptides but have their side chains (R) attached to the nitrogen atoms instead of the alpha-carbon atoms. (Figure 4.6)

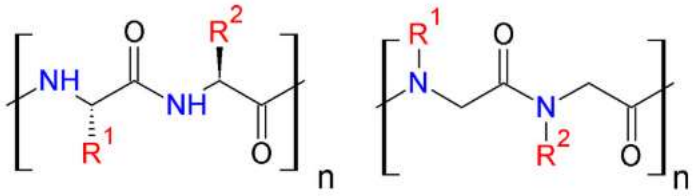

Figure 4.6 Chemical structure of peptides (left) and peptoids (right)

This difference in structure gives peptoids several advantages over peptides, including increased stability, diversity, and specificity. Peptoids are more stable than peptides because the side chains are not susceptible to cleavage by protease or acid hydrolysis, they are more bioavailable and have more stability to salt and pH variations [368]. These properties make peptoids more suitable for use in biological applications that require long-term stability, such as drug development.

Moreover, peptoids are highly diverse and can be synthesized with a wide range of side chains. This diversity allows for the creation of large libraries of peptoids that can be screened for specific biological activities. Peptoids have a high degree of specificity due to their unique structure [369], [370].

Current peptoid syntheses are not unique and involve a trade-off between sequence specificity and scalability.

The synthesis used for peptoids obviously mimics that implemented for peptides and can be of different methodologies: solution synthesis (CSS), solid-phase synthesis (SPS) and liquid-phase synthesis (LPS). [371]

Solid phase synthesis of peptoids is the most widely used method. It offers high specificity, easy purification, precise sequence control and can be automated [372] It is the synthesis also used to create the peptoid used in my work and typically involves the use of resin. The resin is a non-soluble, polymer-based material, which is prefunctionalized so the starting building block can easily bind. The building blocks are generally protected once they are added onto the resin, and they can be easily deprotected and treated with the next desired building block in solution. Once the desired peptoid has been synthesized, it can easily be cleaved from the resin.

4.3.1 Role of Lysine and Tryptophane

Lysine and tryptophan are important amino acids for the design of antibacterial peptoids. These amino acids can be incorporated into peptoids to enhance their antimicrobial activity against a range of bacterial pathogens. Lysine residues are positively charged at physiological pH and can interact with the negatively charged bacterial cell membranes. In addition, lysine residues can also interact with bacterial DNA and could lead to the inhibition of bacterial replication [373]. Tryptophan (Trp), on the other hand, is a hydrophobic amino acid that can insert into the bacterial membrane and disrupt its structure. Tryptophan-containing peptoids can also induce the formation of pores in the bacterial membrane, causing the leakage of cellular contents and ultimately leading to bacterial death [374].

Based on these considerations and given the paucity of scientific research on peptoids used in combination with biomaterials for bone-contact applications, in the next section a peptoid is used to functionalize a chemically treated titanium surface for antibacterial purposes. The peptoid was chosen from a library of novel N-substituted glycines designed by Biljana et al. in which they analyzed for each peptoid the direct effect of hydrophobicity on the antimicrobial activity and cytotoxicity of the peptoid [375].

4.4. Materials and methods

4.4.1. Peptoid synthesis:

The peptoid GN2-Npm9 was synthesized using solid-phase Fmoc chemistry with amidation at the carboxyl end and purified by reversed-phase HPLC using a C18 column (Higgins Analytical Inc. 10 µm 250x10 mm) and a water/acetonitrile gradient. The correct mass and purity > 95% were verified by Dionex Ultimate 3000 RP-UHPLC (C18 Kinetex 100 x 2.1 mm, 100 Å) electrospray ionization mass spectrometry (Finnigan LTQ). The selected peptoid had already been synthesised and tested for its antibacterial activity and cytocompatibility [375]–[377] and it is formed by lysine and tryptophan as the 2 main amino acids. (Figure 4.7).

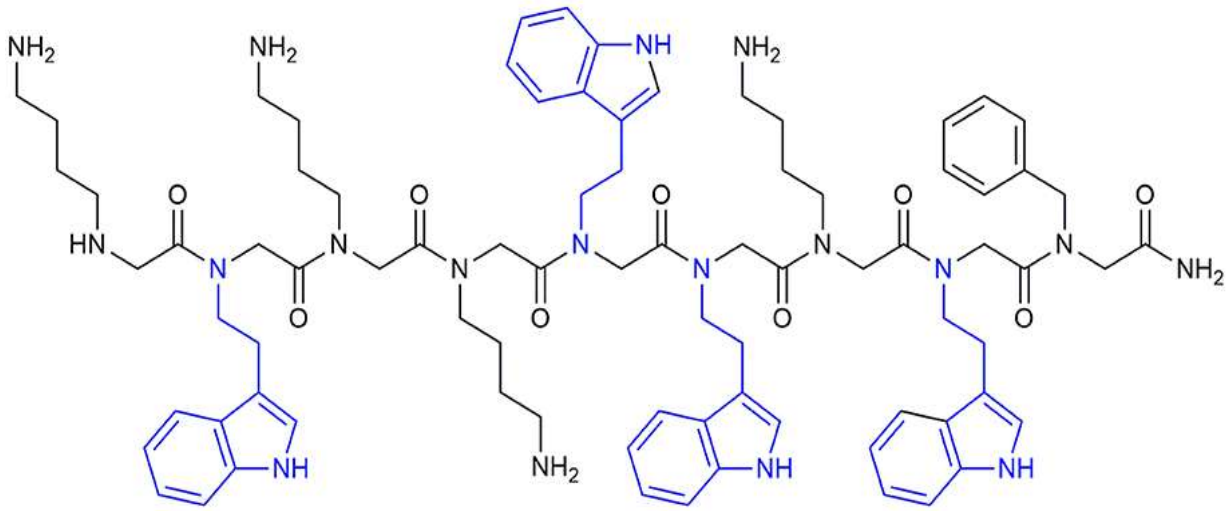

Figure 4.7 GN2-Npm9

4.4.2. Surface treatment

The substrate chosen for the surface modifications is titanium alloy Ti6Al4V (ASTM B348, Gr5, Titanium Consulting and Trading, 10 mm diameter discs). All discs were polished with SiC paper (up to 400 grit). To clean the surface, the samples were first immersed in acetone for 5 minutes and then twice for 10 minutes in high purity Milli-Q (MQ, Millipore) water in an ultrasonic bath. To expose a high density of acidic hydroxyl groups and increase roughness to improve the adhesion of the coating to the substrate, the samples were subjected to a patented chemical treatment [24], [187] involving initial acid etching in dilute hydrofluoric acid followed by controlled reoxidation with hydrogen peroxide. Before functionalisation, the treated samples were irradiated with UV light for 1 hour to reduce the water content and carbon impurity and to improve the reactivity of the hydroxyl groups. From now on, the samples treated as described above will be referred to as chemically treated (CT), while the samples polished to a grain size of 4000, which served as a control, will be referred to as mirror polished (Ti64).

4.4.3. Surface functionalization

A solution of PBS and GN2_Npm9 1mg/mL was previously prepared by stirring the molecule in PBS for 5 minutes and then filtering through a 0.2µ filter to leach out bacterial contamination. With the solution prepared, the CT samples were withdrawn from UV irradiation and placed on a Petri dish. A 100-µl drop of the solution was dropped onto the sample so that the entire surface of the sample was covered, taking care not to break the drop. The samples were left in an incubator at 37°C for 2 hours. The samples were then rinsed in double distilled water to remove the non-adherent peptoid on the surface and dried under a hood. From now on, functionalized samples will be named CT_GN2-Npm9. Figure 4.8 shows the functionalization method of the sample.

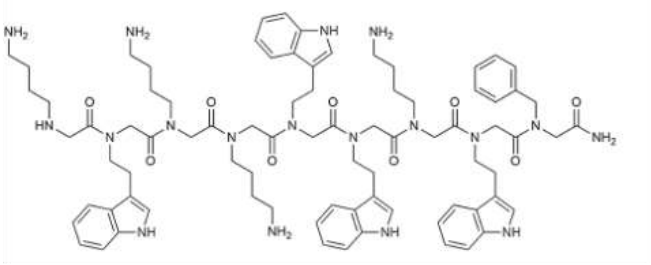

pI Lysin 9,8 → positive at pH < 9,8

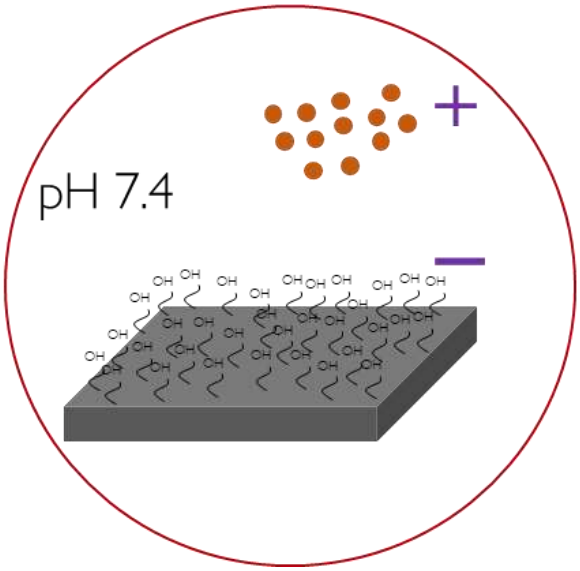

Figure 4.8 functionalization method

4.4.4.UV-Vis Spectroscopy

The spectrophotometric analyses were performed by means of a UV-Vis spectrophotometer (UV2600 Shimadzu). A solution of water and Gn2-Npm9 at a concentration of 1mg/ml was analyzed and its absorbance was measured in a wavelength range of 200 to 600 nm, and the absorption peak of peptoid was plotted using Versa Studio software.

4.4.5. Zeta Potential Measurements:

The zeta potential titration curve was measured by an electrokinetic analyzer (SurPASS, Anton Paar GmbH, Graz, Austria) equipped with an adjustable gap cell for both functionalized and non-functionalized samples (CT and CT_GN+Npm9). The Zeta potential was determined as a function of pH in an electrolyte solution of 0.001 M KCl, for two different couple of samples and the pH value (which starts at approximately 5.5) was varied by adding 0.05 M HCl or 0.05 M NaOH using the automatic titration unit of the instrument. The isoelectric point (IEP) was established as the intercept of the titration curve with the x-axis (zeta potential = 0 mV).

4.4.6. Contact Angle measurement

Surface wettability was assessed by measuring the contact angle with the sessile drop method. After depositing a 10 µl drop of water on the treated side of the sample, the contact angle was measured through Image J software after acquiring images with a microscope (Kruss DSA 100). The contact angle was measured on CT, CT_GN2-Npm9, and CT_ PBS.

4.4.7.Biological evalutation

Cytocompatibility evaluation

Specimens were sterilized by UV-light exposure (30 minutes) before biological experiments. To test specimens' cytocompatibility, human bone marrow-derived stem cells (hMSC) were obtained from Merck (Promo Cell C-12974) and cultivated in low-glucose Dulbecco's modified Eagle Medium (DMEM, Merck) supplemented with 15% fetal bovine serum (FBS, Merck) and 1% antibiotics (penicillin/streptomycin, Merck) at 37°C, 5% CO_2 atmosphere. Cells were cultivated until 80-90% confluence, detached by a trypsin-EDTA solution (0.25% in PBS, from Merck), harvested, and used for the experiments. Cells were directly dropwise seeded onto specimens' surface at a defined concentration (2.5 x10^4 cells/specimens) and cultivated for 1 and 2 days; at each time-point, the viability of the cells has been deduced in the function of their metabolic activity by the colorimetric assay alamar blue (alamarBlue™, ready-to-use solution from Invitrogen™) following Manufacturer's instructions: accordingly, fluorescence signals were evaluated with a spectrophotometer (Spark®, Tecan Trading AG, CH) using excitation wavelength 570 nm, fluorescence emission reading 590 nm. Results are expressed in relative fluorescence units (RFU). Untreated mirror-polished Ti specimens were considered as a positive control (100% viability).

To verify cells' spreading and confluence onto specimens' surface, on day 2 specimens were washed with PBS, fixed with 4% paraformaldehyde (20 min, room temperature), permeabilized for 20 minutes with Triton (0.5% in PBS), and then stained with Texas Red™-X Phalloidin (Thermo Scientific; Invitrogen: T7471) and 4,6-diamidino-2-phenylindole (DAPI, Sigma, Aldrich) to visualize f-actins cytoskeleton filaments and nuclei, respectively. Images were collected by a confocal microscope (Leica SP8 confocal platform, Leica Microsystems, Germany).

Finally, to better appreciate the adaptation of cells to the surfaces' morphology, scanning electron microscopy (SEM) was applied; accordingly, cells were fixed with 2.5% glutaraldehyde, dehydrated by the alcohol scale (50%, 70%, 90%, and 100%, 2 h each) and finally treated with hexamethyldisilazane (from Alfa Aesar, Waltham, MA, USA). Then, specimens were mounted onto aluminum stubs, surface metalized by gold, and observed with an SEM-EDS JEOL JSM-IT 500.

Antibacterial properties

Specimens' ability to prevent surface bacterial infection was verified towards the Gram-positive *Staphylococcus epidermidis (S. epidermidis)* and the Gram-negative *Escherichia coli (E. coli)* pathogens. Strains were obtained from the American Type Culture Collection (*S. epidermidis* ATCC 14990, *E. coli* ATCC 25922) and cultivated following the manufacturer's instructions. Fresh broth cultures were prepared before each experiment in order to test bacteria in their exponential growth phase; the final number of bacteria was adjusted to $1x10^5$ bacteria/ml by optical density (0.001 at 600 nm).

Specimens' infection was performed according to the ISO 22196 standard; so, an aliquot of 100 µl of the above-mentioned bacterial suspensions was gently seeded onto the specimens' surface, covered with a sterile polyethylene film, and placed in an incubator at 35°C for 24 h. Then, the cover film was gently removed, specimens were washed 3 times with PBS to remove non-adherent bacteria, and alamar blue was applied to determine bacterial viability in the function of the metabolic activity as prior detailed. Moreover, SEM imaging was applied to check the formation of biofilm-like 3D aggregates in the function of the surfaces' properties.

Selectively targeted activity

Specimens' ability to preserve cells from infection was evaluated by a cell-bacteria co-culture assay as prior reported by the Authors[65]. Briefly, 2.5×10^4 cells/specimen of hBMSC were seeded onto the specimens' surface and allowed to adhere and spread for 24 hours. The day after, specimens were infected with 1 ml of antibiotics-free DMEM containing 1×10^3 *S. epidermidis* colonies. After 48 hours of infection, specimens were collected, and surface-adhered cells and bacteria were detached by trypsin digestion; viable cells were counted by a Bürker chamber and trypan blue stain to determine the viable number, while bacteria were evaluated by the colonies forming unit (CFU) by seeding them into Luria Bertani semi-solid agar plates after serial dilutions. The final number of CFU was calculated according to Harrison et al.[378] by the following formula:

CFU = [(number of colonies × dilution factor)^(serial dilution)]

4.4.8.Statistical Data Analysis

Biological evaluations were performed using triplicates. Results were analyzed by using SPSS software (v25, IBM, New York City, NY, USA) by means of one-way ANOVA followed by Tukey's test as post hoc analysis. The significance level was set at $p < 0.05$

4.5. Results and discussions

4.5.1. UV-Vis Spectroscopy

The peptoid solution (1 mg/ml) was analyzed by UV–Vis spectroscopy before performing functionalization on CT samples (Figure 4.9). This characterization of the solution was made to verify the success of the purification process and make a qualitative measurement of the concentration of the peptoid by measuring the UV absorption at 280 nm. As the figure below shows, a single strong peak can be observed in the spectrum, which is due to the absorption of the tryptophan residues (commonly referred to as A280). This proves the proper purification of the peptoid, which can then be used for the functionalization of the sample and physicochemical and biological characterizations.

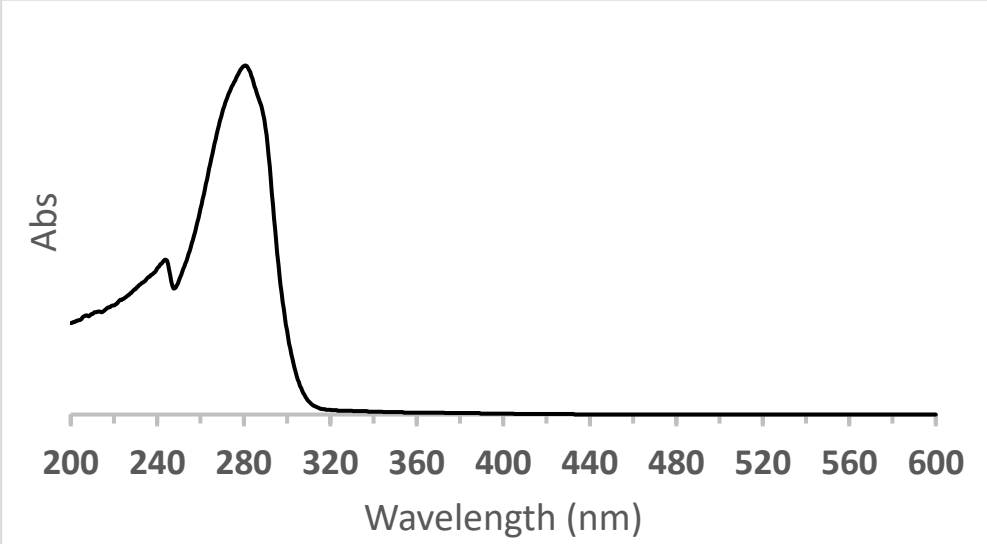

Figure 4.10 UV-VIS absorpion peak of the peptoid water solution (1 mg/ml)

4.5.2. Zeta Potential Measurements:

The Figure 4.10 displays the titration curves of the CT and functionalized samples (CT, CT_GN2-Npm9). At a glance, the curve of CT_GN2-Npm9 appears considerably different from that of CT confirming the effectiveness of the functionalization process. This is the first key information from this measurement.

The CT curve has an IEP at a very low pH (≈ 3), a low slope in the acid range of the titration, and a stable plateau (around -45 mV), with an onset at a pH value of about 5.5, in the basic range. These features are due to the CT surface's chemistry. The CT sample, after undergoing the chemical treatment, acquired a hydrophilic surface with a high density of OH groups. The hydroxyl groups were exposed and exhibited a highly acidic behavior, being deprotonated at pH values as low as 3-5.5. An IEP at around 4 is expected for a surface without acidic/basic functional groups or a balance of them, while a shift towards lower values is expected in presence of acidic functional groups: the prevalence of the negatively charged OH functional groups on the surface justified the low IEP of CT. Water molecules adhered firmly to the hydrophilic CT surface and were not easily replaced by ions in the solution as the pH changed: this was the origin of the low slope of the curve in the acidic range of the titration. The OH groups became completely deprotonated at pH values higher than 5.5: this justified the presence of the plateau.

The IEP of the functionalized surface shifted towards more basic values, reaching a pH of around 6, which confirmed the presence of the grafted molecule on the CT substrate. As will be explained below, the isoelectric point we expect should be more basic, indicating that the molecule does not form a continuous layer on the substrate, since the surface has a zero potential at an average pH between the surface CT and the peptoid. However, this shift was likely due to the positive surface charges (amine groups): a shift of the IEP towards values higher than 4 is expected when basic groups are prevalent on the surface. The peptoid's IEP point is expected to have a value higher than 4, because of the following considerations.

Firstly, we can think of the analogous peptide. Lysine has an IEP of 9.7, the pKa of the alpha carboxylic group is 2.2, that of the ammonium group is 8.9, and that of the side chain is 10.5 [379]. Tryptophan has an IEP of 5.9, the pKa of the alpha carboxylic group is 2.5, and that of the ammonium group is 9.4; it

has an apolar and hydrophobic side chain. The expected titration curves of the monomers are reported in Figure 4.10 (a) and (b). The IEP of the dipeptide lysine-tryptophan is expected to be at pH 10 and it moves towards higher values by increasing the length of the peptide (see Figures 4.10 (c) and (d)) because more carboxylic groups are engaged into the peptide bond by adding more units, and are not available for deprotonation, while the number of the basic side chain of lysine increases and they are all available for protonation.

The titration curve is not expected to change by changing the sequence of the monomers inside the chain.

The titration curve of the peptide can be described as follows. A high and constant value of the zeta potential occurs at very low pH, due to the exposition of the protonated ammonium groups: it increases as the number of lysine monomers in the chain increases, in this specific dipeptide. A small decrease of the zeta potential is expected in the titration curve of the dipeptide when the dissociation of the carboxylic terminal groups occurs. A first plateau is reached when they are completely dissociated. At last, the second larger decrease of the zeta potential occurs when the ammonium groups dissociate, the second plateau is reached when dissociation is completed. This second decrease is larger by increasing the number of lysine monomers in the chain while a minor contribution is due to the ammonium terminal groups.

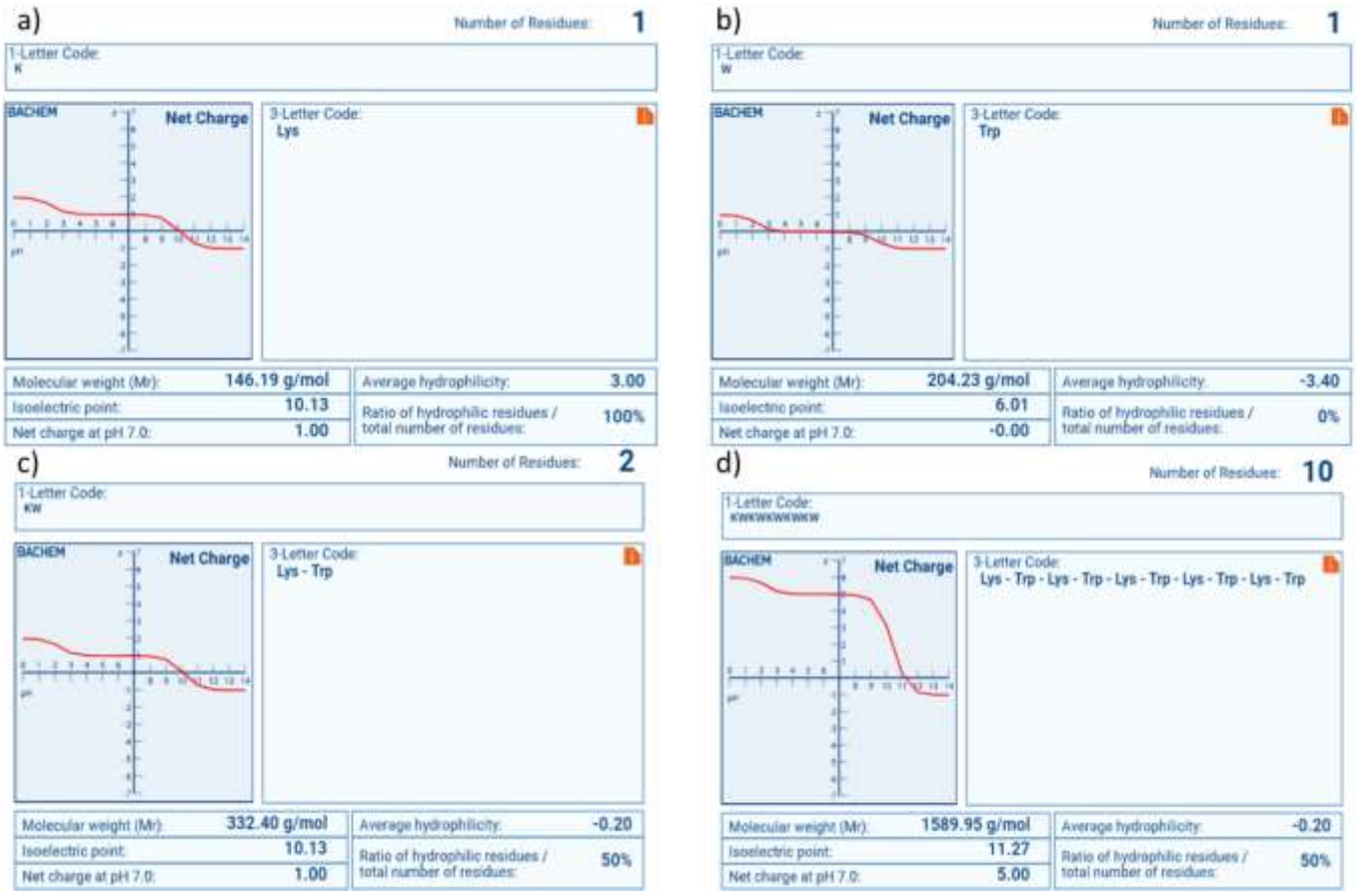

Figure 4.11 Expected titration curves of (a) Lysine residue (b) Tryptophane residue (c) dipeptide Lys-Trp and (d) with 10 residues

Moving from the peptide to the peptoid, the absolute value of the expected features of the titration curve can change because of the position of the side chains was moved from the alpha carbon to the nitrogen and the pKa values can change. In any case, a similar trend is expected.

Some evident differences can be observed in the measured titration curve of the grafted peptoid with respect to what was expected. The IEP of the grafted peptoid was significantly lower (close to pH 6) than expected: a minor contribution of the side chain of lysine could be deduced and a preferential (not unique) exposition of tryptophan could be supposed. Some terminal carboxy groups were exposed: this is different from what was expected based on the supposed structure). The curve did not reach a plateau at high values of pH.: it could mean that a variety of ammonium groups are exposed with different acid-basic strengths. At this stage, these hypotheses need confirmation from other techniques or zeta potential measurements such as the suspension of the peptoid,

peptoid grafted to a hydrophobic substrate, and a comparison among different peptoids grafted to the same substrate).

At the pH value chosen for the functionalization process (7.4), the CT substrate had a negative surface charge with completely deprotonated -OH groups, whereas the peptoid has an overall positive charge. Based on these conditions, it can be predicted that there will be an electrostatic attraction between the substrate and the biomolecule.

The difference in slope between the titration curves of the functionalized surface and CT can be attributed to the higher hydrophobicity of the grafted peptoid, despite its hydrophilic nature in solution. This phenomenon can be explained by examining the structure of the peptoid, which has a hydrophilic, charged section composed of lysine and a hydrophobic, neutral part composed of tryptophan. In this case, it can be assumed that the hydrophilic section of the peptoid, which should be attracted to the substrate surface, was facing the surface, while the hydrophobic portion was facing the solution. This agreed with the measured IEP.

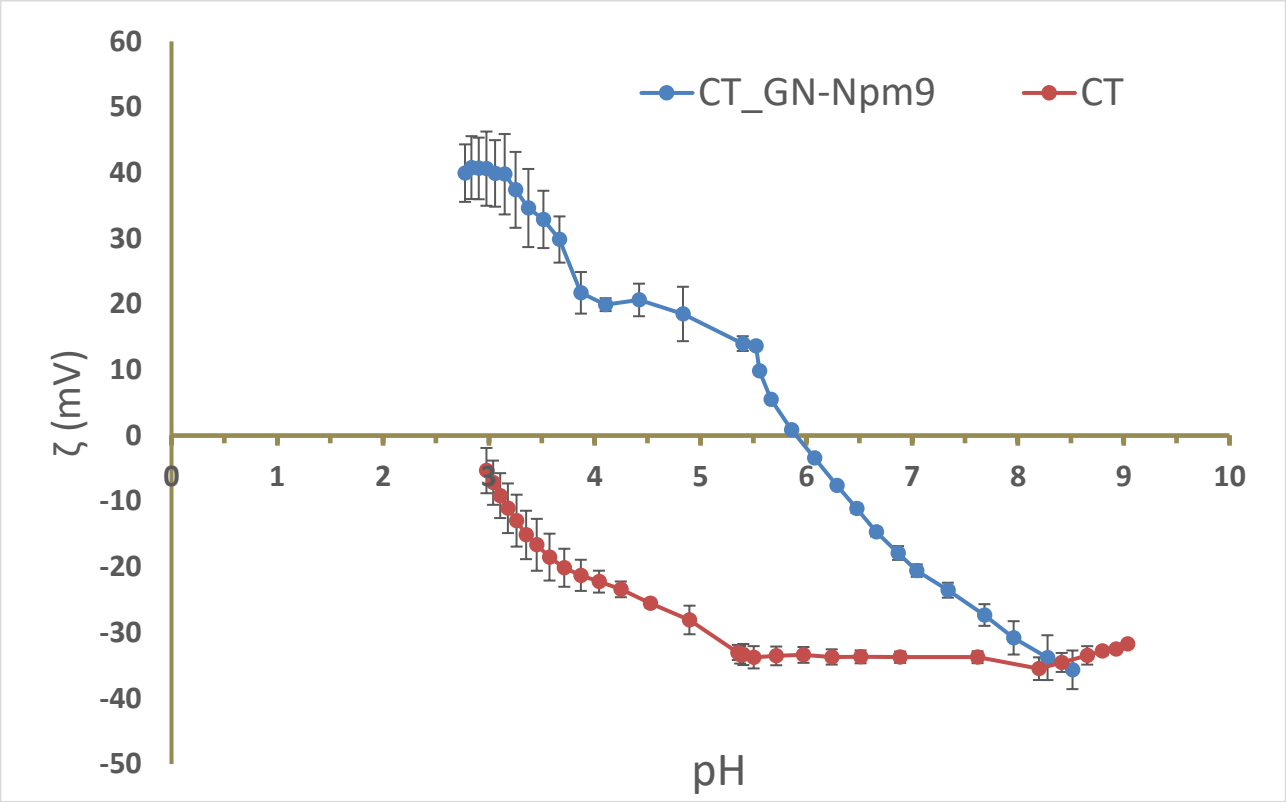

Figure 4.12 ζ Potential titration curve of CT and CT_GN2-Npm9

4.5.3. Contact Angle measurement

The surface properties of functionalized samples were expected to differ from the control sample (CT) due to the presence of various functional end groups on their surfaces. Figure 4.12 illustrates the water contact angles measured on CT, surface-functionalized titanium (CT_GN2-Npm9), and a reference sample (CT_PBS) onto which a drop of PBS (without the addition of the peptoid) was placed using the same functionalization method and conditions used for CT_GN2-Npm9. The CT sample exhibited a contact angle of approximately 40°, indicating a hydrophilic surface, as supported by the Z-potential curve and the expected high density of OH groups. The functionalized sample demonstrated a more hydrophilic behavior than the CT control sample. The CT_PBS sample had a contact angle of approximately 5°. It appeared that functionalization caused the sample to adsorb PBS (that means mainly phosphate groups) on its surface, leading to a superhydrophilic behavior. Comparing the CT_PBS and CT_GN2-Npm9 samples, the presence of the peptoid was confirmed by the different contact angles. Thus, it can be inferred that the CT_GN2-Npm9 sample exhibited a hydrophilic behavior, owing to the contemporary adsorption of PBS and the peptoid (exposing hydrophobic moieties) and the exposure of the molecule significantly increased the contact angle, reaching values of approximately 30°, which was statistically different from the controls ($p<0.05$).

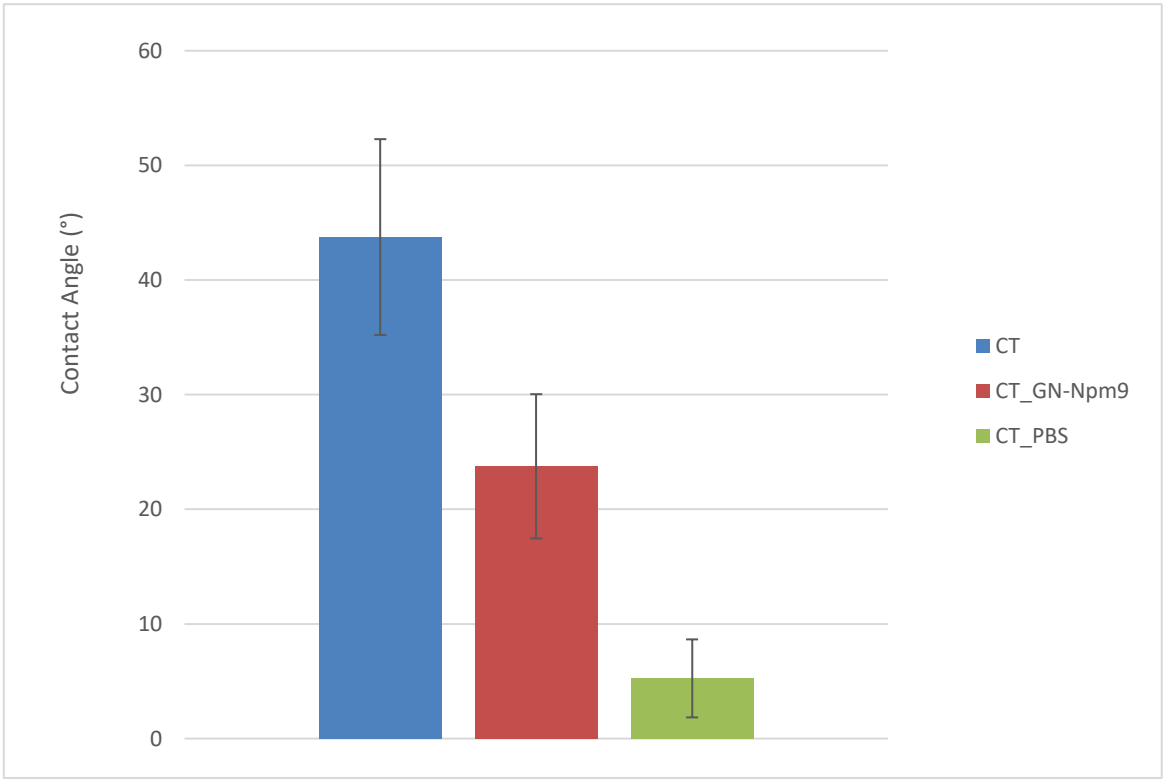

Figure 4.13 Contact angle of CT, CT_GN2-Npm9, and CT_PBS

4.5.4.Biological evaluation

Cytocompatibility evaluation

Cytocompatibility evaluation was performed on mesenchymal stem cells as they represent a frequent and consolidated pattern to test *in vitro* the ability of an implantable device to support the recruitment and colonization from the progenitor cells migrating towards the injured site. Bulk titanium has been considered a positive control due to the large literature, including clinical revisions, suggesting its biocompatibility and successful osteointegration after months upon implantation. Accordingly, it has been considered as 100% viability to rank the results coming from CT and CT_GN2-Npm9 specimens. Results are reported in Figure 4.13.

In general, the presence of the peptoid did not impair the ability of the hMSC to colonize specimens' surface, thus being metabolically active at both 1 or 2 days after seeding as demonstrated by the alamar blue assay (Figure 4.13) where the reported RFU were not significantly reduced comparing the CT and the CT_GN2-Npm9 with the Ti64 control ($p>0.05$). So, the % of viable cells was always >90% as reported in Figure 4.13b. As a confirmation of the presence of viable cells, SEM imaging (Figure 4.13c) showed that cells were able to adapt to the CT_GN2-Npm9 surface in a similar manner to the untreated Ti64 controls reporting a similar morphology despite the presence of the coating and the microtopography due to CT pre-treatment. Fluorescence staining of cells' cytoskeleton and nuclei (Figure 4.13 d) provided further evidence of the cells-friendly behavior of the test CT_GN2-Npm9 surfaces; in particular, the density of the DAPI-stained nuclei demonstrated a comparable cellular confluence between the Ti64 control and the CT_GN2-Npm9 thus confirming the ability of the test specimens to support the colonization of progenitor cells, albeit with all the limitations relating to an in vitro experiment.

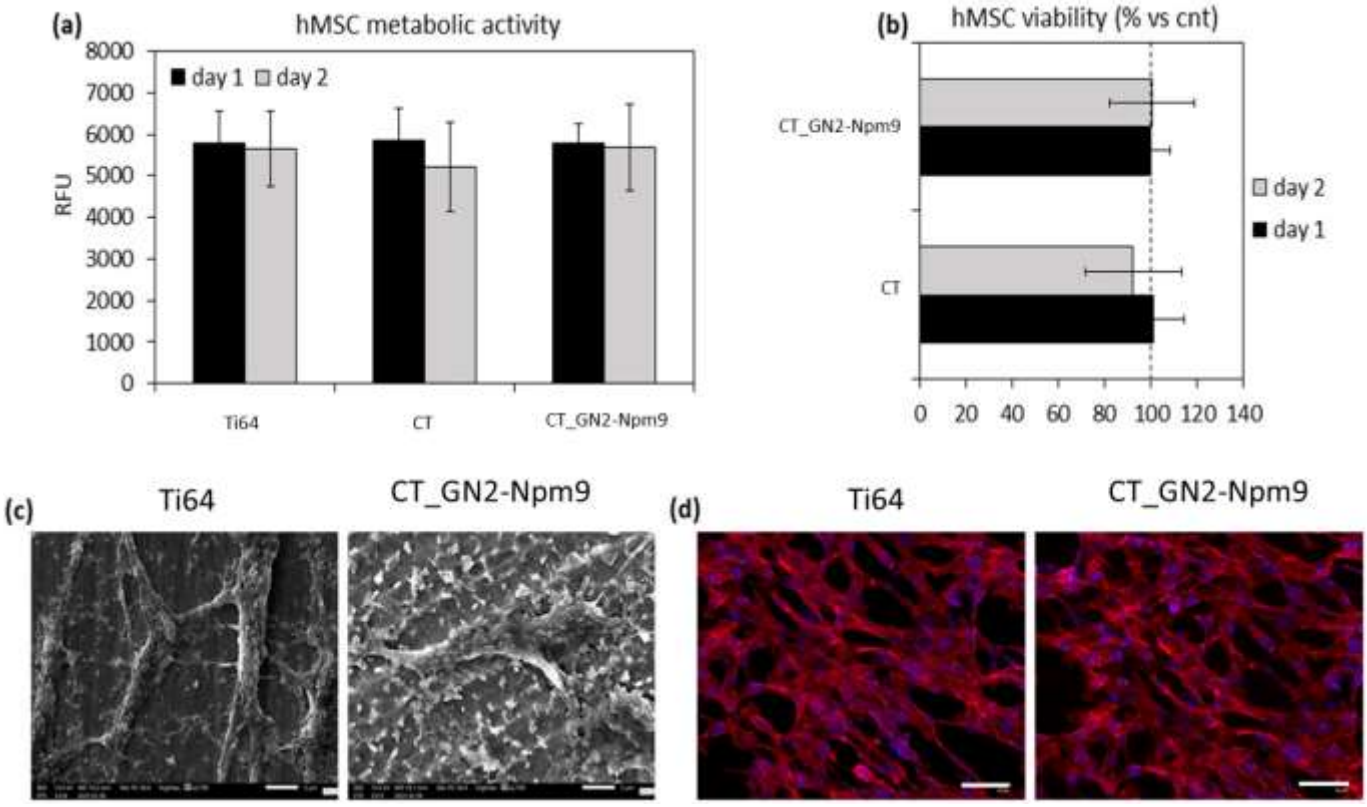

Figure 4.14 Cytocompatibility evaluation of CT, Ti64 and CT_GN2-Npm9
(a) Cells seeded onto peptoid-doped surfaces (CT_GN2-Npm9) reported a comparable metabolic activity in comparison to the Ti64 control and the CT ones ($p>0.05$). (b) Accordingly, the viability ranged between 90 and 100% in comparison with Ti64 controls. (c) SEM images confirmed the ability of cells to adapt onto the CT_GN2-Npm9 surface as well as (d) fluorescent staining demonstrated a comparable cell density between test and control specimens. Bars represent mean±sdev.st; replicates n=3. SEM bar scale=5µm (2700x); fluorescence bar scale=125µm.

Antibacterial properties

Beyond their recognized biocompatibility, Ti and its alloys are also known to be easily colonized by bacteria as they do not hold intrinsic antibacterial properties unless an antibacterial element is specifically added to the alloys. When an infection occurs, it represents a devasting event since it is extremely complicated to mechanically remove bacteria from the device upon implantation as well as most of the bacteria related to clinical infections are drug resistant, thus making pharmacological administration of common antibacterial practically useless. So, it is of worthy importance to confer antibacterial properties to the materials per se in order to prevent bacterial colonization and the evolution into a 3D biofilm-like structure representing a sort of "shield" where bacteria shelter from drugs.

Here, peptoids have been applied to coat the surface of oxidized Ti (named CT) that was previously demonstrated by the authors being able to reduce bacterial adhesion due to the obtained nanotopography; in fact, such nano-porous like structures reduce the anchorage point for bacteria in comparison to the smooth polished surfaces thus preventing massive first colonization[205]. Moreover, the surface irregularities provided by the random nano-pores force bacteria to stretch the cytoskeleton in an attempt to fit the surface; this forcing often results in a deadly event for bacteria due to irreversible pores formation occurring when the cytoskeleton is mechanically stressed too much. The presence of the peptoids is hypothesized to add a second further antibacterial bioactive element; in fact, literature report about the ability of different peptoids to act as strong antibacterial active principles with a broad range of activity including both Gram-negative and Gram-positive pathogens.

Based on these promises, specimens were infected by *S. epidermidis* (Gram-negative) and *E. coli* (Gram-positive); they are often involved in orthopedics infections as well as both the Gram species.

Results are reported in Figure 4.14.

In general, the CT nanotopography reduced the metabolic activity of both pathogens but only E. coli was significant in comparison with Ti64 controls (Figure 4.14 a-c, $p<0.05$ indicated by #). This is a predictable difference as the Gram-positive strains are expected to be more sensitive to the surface morphology due to the membrane thickness and the relative difficulty of modifying the cytoskeleton based on topography.

The presence of the peptoids improved significantly the ability of the CT specimens to reduce the colonization; in fact, CT_GN2-Npm9 resulted as significant towards both Ti64 control and CT for *S. epidermidis* and *E. coli* (Figure 4.14a-c), thus confirming their bioactivity and their broad-range activity. As a consequence, bacterial viability was reduced by ≈77% for *S. epidermidis* (Figure 4,14b) and by ≈89% for *E. coli* (Figure 4,14d).

Finally, SEM images (Figure 4.14e, representative for the *S. epidermidis* strain) validated results obtained by the metabolic assay; while Ti64 reported a highly colonized surface with bacteria aggregated into dense and thick biofilm-like 3D structures, only a few colonies mostly arranged in small aggregates were observed onto CT_GN2-Npm9 specimens.

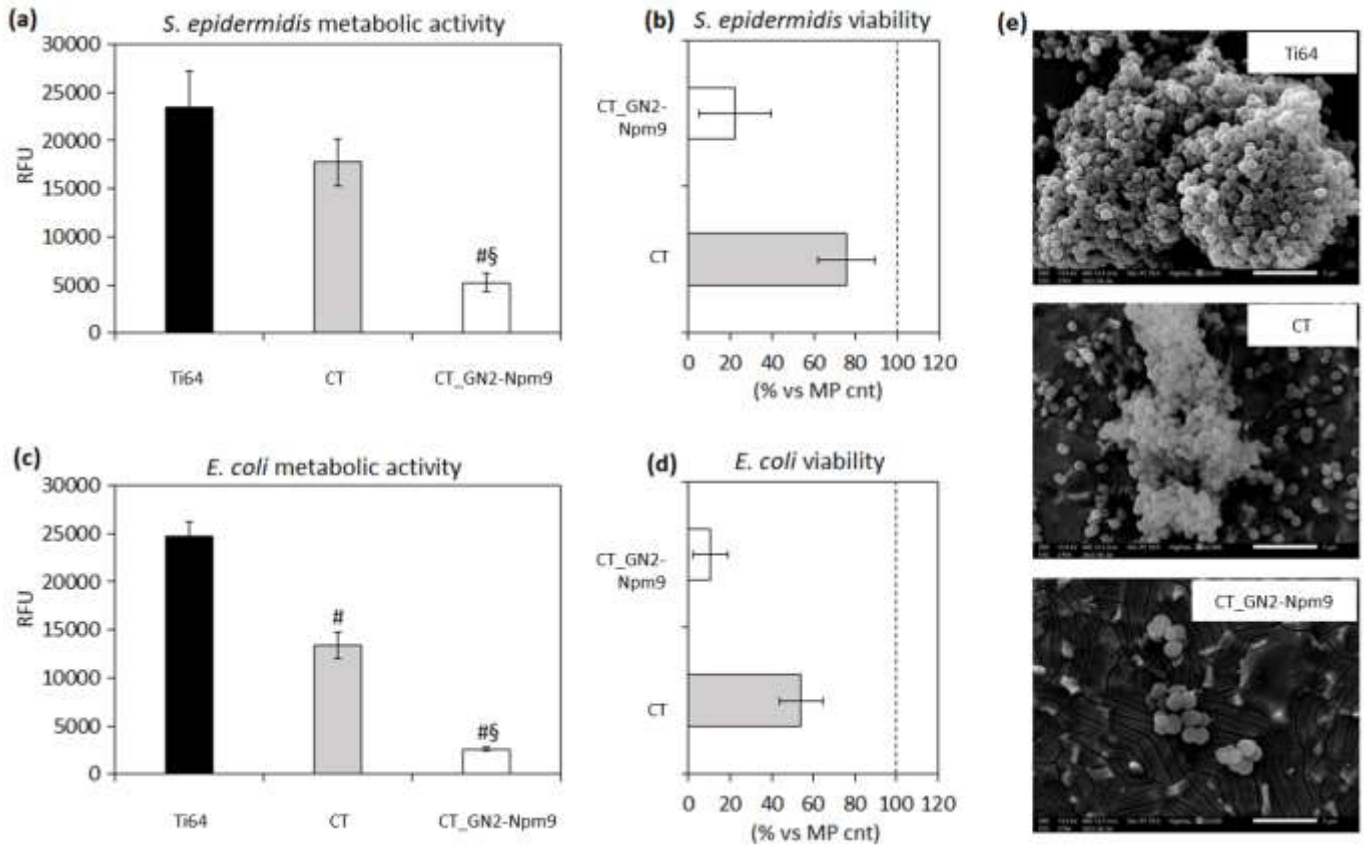

Figure 4.16 Antibacterial properties of CT, Ti64 and CT_GN2-Npm9
The nanotopography of the CT specimens determined a significant reduction of E. coli metabolic activity (c, $p<0.05$ indicated by #) but only the introduction of peptoids significantly decreases bacterial metabolic activity in comparison to both Ti64 controls (a-c, $p<0.05$ indicated by #) and CT (a-c, $p<0.05$ indicated by §). This led to a reduction of bacterial viability ranging between 70 and 90% in comparison with Ti64 controls (b-d). SEM images confirmed the strong reduction of colonies into the CT_GN2-Npm9 surfaces as well as the prevention of dense 3D biofilm-like aggregates (e, representative for S. epidermidis). Bars represent mean±sdev.st; replicates n=3. SEM bar scale=5µm (5000x).

Selectively targeted activity

After demonstrating peptoids-doped CT specimens' cytocompatibility and antibacterial activity, the co-culture method previously reported by the Authors was applied to verify whether the effect was selective towards bacteria preserving cells' viability in an environmental competition between hMSC and *S. epidermidis*.

Results are reported in Figure 4.15

In general, such experiments confirmed previous findings. In fact, in absence of any antibacterial tool, bacteria proliferated and infected the Ti64 controls; so, the number of viable cells decreased by ≈47% (Figure 4.15a), while, on the contrary, the number of bacteria increased by >2 logs (Figure 4.15b). SEM images (Figure 4.15c) confirmed the presence of bacterial aggregates (indicated by the red circle) in proximity to apoptotic cells (indicated by the black arrows). The CT specimens reported mostly a bacteriostatic effect since the number of viable bacteria increased by <1 log (Figure 4.15b) and the number of viable cells was reduced (Figure 4.15a). SEM images reported the presence of cells with a proper morphology, but also the accumulation of biofilm aggregates overhanging cells' cytoskeleton (indicated by the red circles). Finally, the presence of peptoids was effective in reducing the number of viable bacteria of ≈ 1 log (Figure 415b) as well as the number of cells increased by ≈ 17% with respect to the starting number. SEM images (Figure 4.15c) confirmed the presence of cells displaying regular morphology and only a few bacterial colonies which appear not to interact with cells. So, the CT_GN2-Npm9 surfaces seem to be a very promising combination of nano-topography and bioactive compound selectively preventing bacterial infection while preserving cells' ability to colonize the device in view of tissue engineering applications.

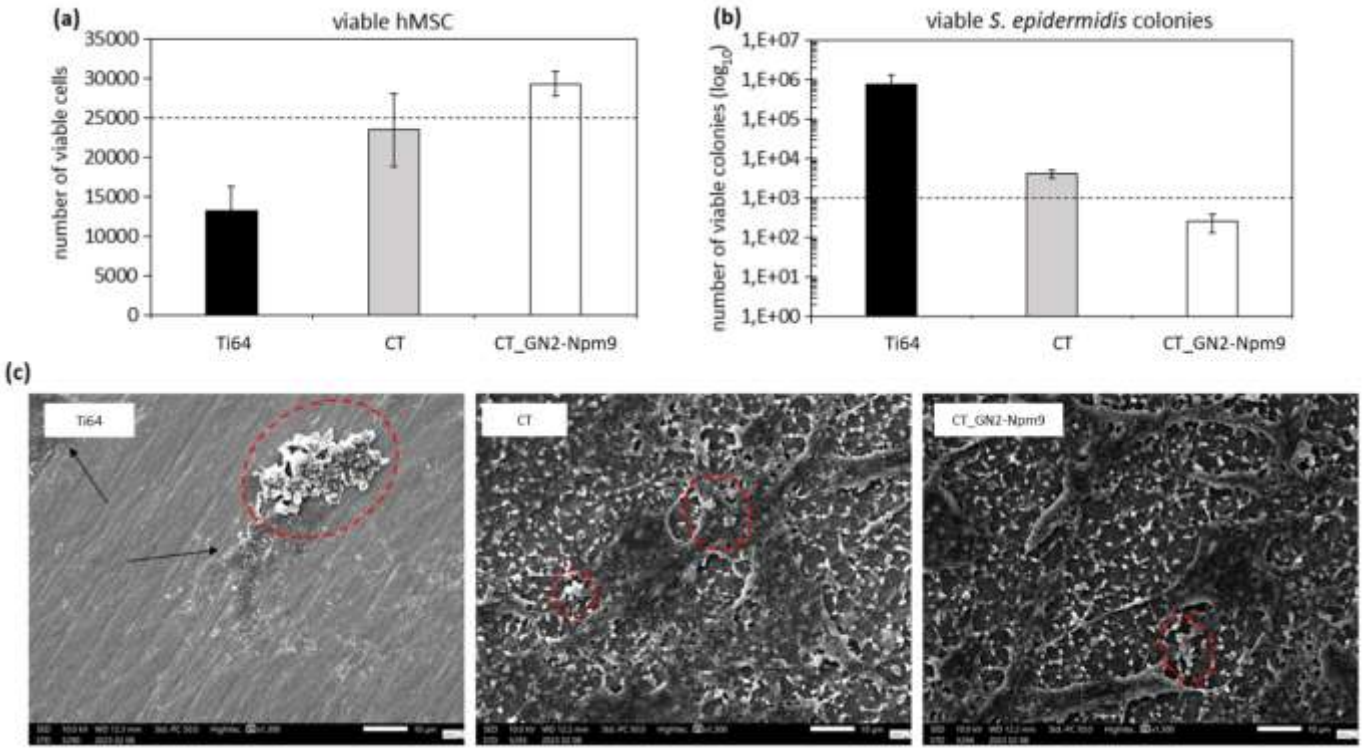

Figure 4.18 Peptoid's selective targeted activity.
The peptoid doping allowed for a parallel increase of the cells seeded onto the surface (a, the dashed line indicates the starting number of cells) and a decrease of bacteria colonizing the surface (b, the dashed line indicates the starting number of bacteria) in this competition model. Bars represent mean±sdev.st; replicates n=3. SEM bar scale=10µm (1300x).

Conclusions and future perspectives

Resuming the conclusions, the protocols of functionalization of a bioactive titanium alloy with the two forms of Vitamin E (alpha tocopheryl phosphate and alpha tocopherol), green tea polyphenols, and a synthetic peptoid were successfully designed and tailored.

Alpha tocopherol was used for the first time as a coating on a chemically treated Ti6Al4V and creates a thin (1.7 μm), compact, and continuous coating. The coating strongly adhered to the substrate, it was chemically stable in a wide range of pH, it had a large negative surface potential, and exposed -OH groups acted as a weak acid. The coating had low surface energy, even if it was not highly hydrophobic, and imposed properties in the anti-adhesive range. Biological investigation revealed a strong antifouling and anti-adhesive effect owing to the alpha tocopherol coating being able to prevent surface colonization both by human cells and bacterial pathogens without the release of toxic elements. This investigation opens a new scenario of coatings and surfaces which are both not adhesive and not cytotoxic and are promising for temporary bone implants thanks to the possibility to prevent unintended osseointegration, in addition to reducing the risk of implant-associated infections.

Alpha tocopheryl phosphate was used to create both a thin coating (<0.2 μm thick) and functionalized molecular layer on chemically treated Ti6Al4V for permanent bone contact applications. Physico-chemical characterizations of the functionalized and coated samples were carried out in parallel to study their similarities and differences and to understand which one might be more successful in a future medical application. The studies performed demonstrated

the presence of the αTP molecule as a continuous layer that does not cover the topography of the substrate, thus not altering its pro-osteogenic properties, on both surfaces. It is a thinner and hydro-phobic molecular layer on the functionalized surface, while it is thicker, hydrophilic, and rich in phosphate groups in the outermost layer when a coating is formed. The biological tests confirmed very promising anti-bacterial properties of αTP and the lack of evident toxic effects in both cases, at least at this preliminary in vitro stage in direct contact with human mesenchymal stem cells. In particular, the coating appeared to be more promising due to its higher antibacterial effect and cell adhesion. In this sense, the coating can be thought for permanent implant applications, with antibacterial properties. However, a more in-depth study on the stability of the coating and its release kinetics needs to be carried out in the future as well as the delayed cell growth should be considered to render such surfaces more cells friendly.

Green tea polyphenols have been successfully grafted onto the surface of titanium on which a heat chemically treatment introducing iodine ions with an antibacterial effect has been previously performed. Specifically, physicochemical characterization was performed, and the presence, amount, distribution, and release of the grafted polyphenols were evaluated. The reported results show a stable molecular grafting, uniform on the surface, and allowing hydroxyapatite precipitation. The polyphenols showed a good antioxidant effect in the biological environment and did not alter the antibacterial effect of iodine or the morphology of the surface, thus succeeding in obtaining a multifunctional surface with anti-inflammatory, antibacterial, and osseointegration capabilities. Finally, cell assays confirmed that the functionalization was cytocompatible towards human mesenchymal stem cells as well as the combination of iodine + polyphenols demonstrated a strong ability to protect cells from chemically-induced oxidative stress thus representing a promising strategy to provide support to the healing process under pro-inflammatory conditions.

Finally, GN2-Npm9 was used to functionalize Ti6Al4V, a preliminary physical-chemical characterization shows a hydrophilic surface, suitable for cell proliferation and adhesion, and a stable functionalization that coated the surface while changing its reactivity, as shown by the ζ potential and contact angle. Antibacterial tests showed a strong antibacterial action of the adsorbed peptoid activity without showing any cellular cytotoxicity, as coculture models evidenced. The functionalized surface seemed to be a very promising combination of nano-topography and bioactive compound selectively preventing bacterial infection while preserving cells' ability to colonize the device in view of permanent bone contact applications. A more in-depth physical-chemical analysis is required to better understand the orientation of the grafted peptide on the surface, study its exposed groups, and image its distribution on the surface, whether homogenous or not. The study of the release

kinetics is also required to study how and whether the molecule is released from the surface.

The surfaces created in this work, depending on the type of molecule used, have different physicochemical properties. The physical and chemical characterizations chosen vary according to the molecule used, and research work has been done on the right characterization so that an appropriate protocol is chosen for each molecule. Finally, each molecule gives different biological responses leading to different biomedical applications, briefly illustrated and collected in the table below.

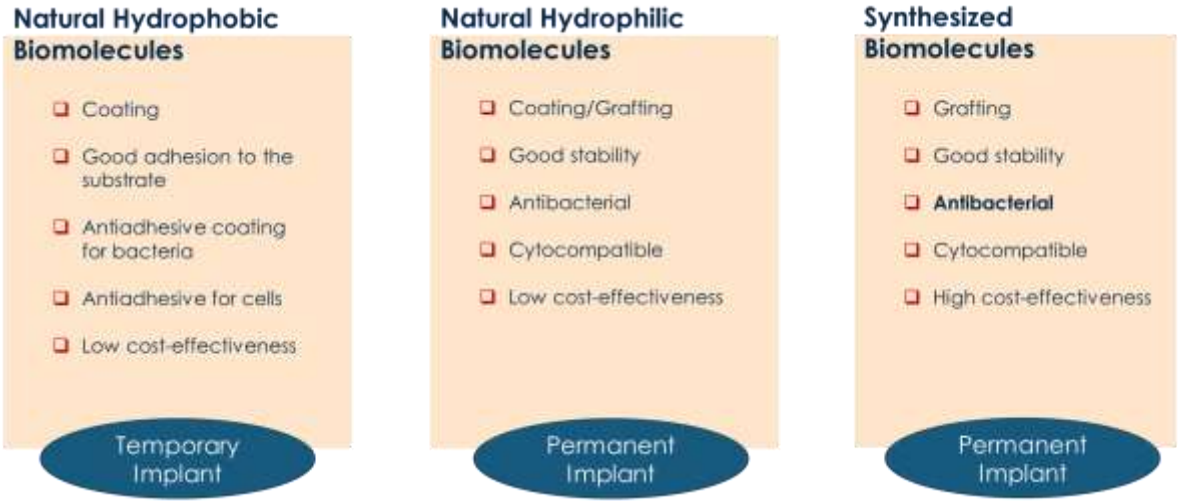

References

[1] R. Brånemark, P. I. Brånemark, B. Rydevik, and R. R. Myers, "Osseointegration in skeletal reconstruction and rehabilitation: A review," *J. Rehabil. Res. Dev.*, vol. 38, no. 2, pp. 175–181, 2001.

[2] M. B. Zaid, R. J. O'Donnell, B. K. Potter, and J. A. Forsberg, "Orthopaedic Osseointegration: State of the Art," *J. Am. Acad. Orthop. Surg.*, vol. 27, no. 22, pp. E977–E985, 2019, doi: 10.5435/JAAOS-D-19-00016.

[3] H. Takayanagi, "Osteoimmunology: Shared mechanisms and crosstalk between the immune and bone systems," *Nat. Rev. Immunol.*, vol. 7, no. 4, pp. 292–304, 2007, doi: 10.1038/nri2062.

[4] B. Corradetti, "The immune response to implanted materials and devices: The impact of the immune system on the success of an implant," *Immune Response to Implant. Mater. Devices Impact Immune Syst. Success an Implant*, pp. 1–241, 2016, doi: 10.1007/978-3-319-45433-7.

[5] C. Guder, S. Gravius, C. Burger, D. C. Wirtz, and F. A. Schildberg, "Osteoimmunology: A Current Update of the Interplay Between Bone and the Immune System," *Front. Immunol.*, vol. 11, no. January, pp. 1–19, 2020, doi: 10.3389/fimmu.2020.00058.

[6] T. R. Kyriakides, *Molecular Events at Tissue-Biomaterial Interface*. Elsevier Inc., 2015.

[7] B. D. Ratner, *The Biocompatibility of Implant Materials*. Elsevier Inc., 2015.

[8] P. Koppolu and L. A. Swapna, "Osseointegration in Implants : A Review Osseointegration in Implants : A Review," no. February, 2016, doi: 10.13140/RG.2.1.2306.2806.

[9] L. F. Cooper, "Biologic determinants of bone formation for osseointegration: clues for future clinical improvements.," *J. Prosthet. Dent.*, vol. 80, no. 4, pp. 439–449, 1998, doi: 10.1016/S0022-3913(98)70009-5.

[10] T. Albrektsson and C. Johansson, "Osteoinduction, osteoconduction and osseointegration," *Eur. Spine J.*, vol. 10, pp. S96–S101, 2001, doi: 10.1007/s005860100282.

[11] M. Haga *et al.*, "Detailed process of bone remodeling after achievement of osseointegration in a rat implantation model," *Anat. Rec.*, vol. 292, no. 1, pp. 38–47, 2009, doi: 10.1002/ar.20748.

[12] A. S. da S. Mello, P. L. dos Santos, A. Marquesi, T. P. Queiroz, R. Margonar, and A. P. de Souza Faloni, "Some aspects of bone remodeling around dental implants," *Rev. Clínica Periodoncia, Implantol. y Rehabil. Oral*, pp. 1–9, 2016, doi: 10.1016/j.piro.2015.12.001.

[13] C. Steffi, Z. Shi, C. H. Kong, and W. Wang, "Modulation of osteoclast interactions with orthopaedic biomaterials," *J. Funct. Biomater.*, vol. 9, no. 1, 2018, doi: 10.3390/jfb9010018.

[14] S. L. Truesdell and M. M. Saunders, "Bone remodeling platforms: Understanding the need for multicellular lab-on-a-chip systems and predictive agent-based models," *Math. Biosci.*

Eng., vol. 17, no. 2, pp. 1233–1252, 2020, doi: 10.3934/mbe.2020063.

[15] B. Boyce, Z. Yao, and L. Xing, "Osteoclasts have multiple roles in bone in addition to bone resorption," *Crit. Rev. Eukaryot. Gene Expr.*, vol. 19, no. 3, pp. 171–180, 2009, doi: 10.1615/CritRevEukarGeneExpr.v19.i3.10.

[16] P. Castrogiovanni, F. M. Trovato, M. A. Szychlinska, H. Nsir, R. Imbesi, and G. Musumeci, "The importance of physical activity in osteoporosis. From the molecular pathways to the clinical evidence," *Histol. Histopathol.*, vol. 31, no. 11, pp. 1183–1194, 2016, doi: 10.14670/HH-11-793.

[17] N. Udagawa *et al.*, "Osteoclast differentiation by RANKL and OPG signaling pathways," *J. Bone Miner. Metab.*, vol. 39, no. 1, pp. 19–26, 2021, doi: 10.1007/s00774-020-01162-6.

[18] D. N. R. Vootla and D. K. V. Reddy, "Osseointegration- Key Factors Affecting Its Success-An Overview," *IOSR J. Dent. Med. Sci.*, vol. 16, no. 04, pp. 62–68, 2017, doi: 10.9790/0853-1604056268.

[19] S. Parithimarkalaignan and T. V. Padmanabhan, "Osseointegration: An update," *J. Indian Prosthodont. Soc.*, vol. 13, no. 1, pp. 2–6, 2013, doi: 10.1007/s13191-013-0252-z.

[20] R. Krishna Alla, K. Ginjupalli, N. Upadhya, M. Shammas, R. Krishna Ravi, and R. Sekhar, "Surface roughness of implants: A review," *Trends Biomater. Artif. Organs*, vol. 25, no. 3, pp. 112–118, 2011.

[21] L. Le Guéhennec, A. Soueidan, P. Layrolle, and Y. Amouriq, "Surface treatments of titanium dental implants for rapid osseointegration," *Dent. Mater.*, vol. 23, no. 7, pp. 844–854, 2007, doi: 10.1016/j.dental.2006.06.025.

[22] X. Liu, P. K. Chu, and C. Ding, "Surface modification of titanium, titanium alloys, and related materials for biomedical applications," *Mater. Sci. Eng. R Reports*, vol. 47, no. 3–4, pp. 49–121, 2004, doi: 10.1016/j.mser.2004.11.001.

[23] G. Conterno, L. Pazos, M. B. Parodi, D. A. Egidi, and P. Corengia, "Surface treatment on biomaterials : acid etching on titanium surfaces," no. October 2014.

[24] Y. Iwaya *et al.*, "Surface properties and biocompatibility of acid-etched titanium," *Dent. Mater. J.*, vol. 27, no. 3, pp. 415–421, 2008, doi: 10.4012/dmj.27.415.

[25] A. Biswas, P. V. S. Srikant, I. Manna, U. K. Chatterjee, and J. Dutta Majumdar, "Chemical oxidation of Ti-6Al-4v for improved wear and corrosion resistance," *Surf. Eng.*, vol. 24, no. 6, pp. 442–446, 2008, doi: 10.1179/174329408X286097.

[26] H. Guleryuz and H. Cimenoglu, "Oxidation of Ti-6Al-4V alloy," *J. Alloys Compd.*, vol. 472, no. 1–2, pp. 241–246, 2009, doi: 10.1016/j.jallcom.2008.04.024.

[27] S. Ferraris *et al.*, "Surface modification of Ti-6Al-4V alloy for biomineralization and specific biological response: Part I, inorganic modification," *J. Mater. Sci. Mater. Med.*, vol. 22, no. 3, pp. 533–545, 2011, doi: 10.1007/s10856-011-4246-2.

[28] S. Ferraris, A. Venturello, M. Miola, A. Cochis, L. Rimondini, and S. Spriano, "Antibacterial and bioactive nanostructured titanium surfaces for bone integration," *Appl. Surf. Sci.*, vol. 311, pp. 279–291, 2014, doi: 10.1016/j.apsusc.2014.05.056.

[29] S. Ferraris, A. Bobbio, M. Miola, and S. Spriano, "Micro- and nano-textured, hydrophilic

and bioactive titanium dental implants," *Surf. Coatings Technol.*, vol. 276, pp. 374–383, 2015, doi: 10.1016/j.surfcoat.2015.06.042.

[30] T. Kokubo and S. Yamaguchi, "Novel bioactive materials developed by simulated body fluid evaluation: Surface-modified Ti metal and its alloys," *Acta Biomater.*, vol. 44, pp. 16–30, 2016, doi: 10.1016/j.actbio.2016.08.013.

[31] L. Sun, C. C. Berndt, K. A. Gross, and A. Kucuk, "Material fundamentals and clinical performance of plasma-sprayed hydroxyapatite coatings: A review," *J. Biomed. Mater. Res.*, vol. 58, no. 5, pp. 570–592, 2001, doi: 10.1002/jbm.1056.

[32] C. Ning, "Biomaterials for Bone Tissue," 2016, doi: 10.1007/978-1-84882-664-9.

[33] D. Bartolini *et al.*, "Alpha-tocopherol metabolites (the vitamin E metabolome) and their interindividual variability during supplementation," *Antioxidants*, vol. 10, no. 2, pp. 1–16, 2021, doi: 10.3390/antiox10020173.

[34] J. D. Jackson, *Chapter 3 - Immunology: Host Responses to Biomaterials*. Elsevier Inc., 2016.

[35] K. A. G. Kinnari A. Bhadang, "Influence of fluorapatite on the properties of thermally sprayed hydroxyapatite coatings," *Biomaterials*, vol. 25, pp. 4935–4945, 2004, doi: 10.1016/j.biomaterials.2004.02.043.

[36] L. T. De Jonge, S. C. G. Leeuwenburgh, J. G. C. Wolke, and J. A. J. Jansen, "Expert Review Organic – Inorganic Surface Modifications for Titanium Implant Surfaces," *Pharm. Res.*, vol. 25, no. 10, 2008, doi: 10.1007/s11095-008-9617-0.

[37] U. Fischer, U. Hempel, D. Becker, S. Bierbaum, and D. Scharnweber, "Transforming growth factor b 1 immobilized adsorptively on Ti6Al4V and collagen type I coated Ti6Al4V maintains its biological activity," *Biomaterials*, vol. 24, pp. 2631–2641, 2003, doi: 10.1016/S0142-9612(03)00068-1.

[38] C. Du, G. B. Schneider, R. Zaharias, C. Abbott, D. Seabold, and C. Stanford, "Apatite / Amelogenin Coating," *Biomater. Bioeng.*, pp. 1070–1074, 2005.

[39] A. Merolli and P. T. Leali, *Using bone repair materials in orthopaedic surgery*, no. 2. Woodhead Publishing Limited.

[40] R. H. Palmer, "E x t e r n a l F i x a t o r s an d M i n i m a l l y Invasive Osteosynthesis in Small A n i m a l Vet e r i n a r y M e d i c i n e," *Vet. Clin. NA Small Anim. Pract.*, vol. 42, no. 5, pp. 913–934, 2012, doi: 10.1016/j.cvsm.2012.06.001.

[41] Z. Knochen-, U. Knochenschrau-, and D. Metallstife, "Fixateur-externe- Osteosynthese," pp. 192–200, 2010, doi: 10.1007/s00132-009-1523-6.

[42] P. Thomsen, "Titanium in medicine Material Science , Surface Science , Engineering , Biological Responses," 2001.

[43] A. Ristorto, "Rivestimenti Antibatterici e Antiadesivi per Dispositivi di Fissazione Temporanea," pp. 1–255, 2019.

[44] L. Tian *et al.*, "Hybrid fracture fixation systems developed for orthopaedic applications: A general review," *J. Orthop. Transl.*, vol. 16, pp. 1–13, 2019, doi: 10.1016/j.jot.2018.06.006.

[45] A. Merolli *et al.*, "Biodegradable Mg alloys for orthopedic implants – A review," *Acta*

Biomater., vol. 8, no. 2, pp. 349–377, 2017, doi: 10.1533/9781845696610.3.349.

[46] J. S. Hayes and R. G. Richards, "Surfaces to control tissue adhesion for osteosynthesis with metal implants: In vitro and in vivo studies to bring solutions to the patient," *Expert Rev. Med. Devices*, vol. 7, no. 1, pp. 131–142, 2010, doi: 10.1586/erd.09.55.

[47] J. Espiritu, M. Meier, and J. M. Seitz, "The current performance of biodegradable magnesium-based implants in magnetic resonance imaging: A review," *Bioact. Mater.*, vol. 6, no. 12, pp. 4360–4367, 2021, doi: 10.1016/j.bioactmat.2021.04.012.

[48] L. K. Choudhary, "Magnesium alloys for temporary implant applications : stress corrosion cracking and biocompatible coating Lokesh Kumar Choudhary," 2013.

[49] M. Peron, R. Bertolini, and S. Cogo, "On the corrosion, stress corrosion and cytocompatibility performances of ALD TiO2 and ZrO2 coated magnesium alloys," *J. Mech. Behav. Biomed. Mater.*, vol. 125, no. October 2021, 2022, doi: 10.1016/j.jmbbm.2021.104945.

[50] S. Kamrani and C. Fleck, "Biodegradable magnesium alloys as temporary orthopaedic implants: a review," *BioMetals*, vol. 32, no. 2, pp. 185–193, 2019, doi: 10.1007/s10534-019-00170-y.

[51] M. Leigheb, M. Veneziano, R. Tortia, M. Bosetti, L. Rimondini, and F. A. Grassi, "Osteosynthesis devices in absorbable Magnesium alloy in comparison to standard ones : a Systematic Review on effec- tiveness and safety," vol. 92, no. 4, 2021, doi: 10.23750/abm.v92i3.11757.

[52] X. Dominguez-benetton, "Biocomplexity and Bioelectrochemical Influence of Biofilms in Carbon Steel Deterioration A Transmission Lines Approach for Electrochemical Impedance Analysis Xochitl Dominguez Benetton Doctor of Science," no. December 2007, 2014.

[53] S. J. Mcconoughey, R. Howlin, J. F. Granger, M. M. Manring, and H. Jason, "Biofilms in periprosthetic orthopedic infections," vol. 9, no. 8, pp. 987–1007, 2015, doi: 10.2217/fmb.14.64.Biofilms.

[54] T. Roger, M. Bhakoo, and Z. Zhang, "Bacterial adhesion and biofilms on surfaces," vol. 18, pp. 1049–1056, 2008, doi: 10.1016/j.pnsc.2008.04.001.

[55] H. C. Flemming and J. Wingender, "The biofilm matrix," *Nat. Rev. Microbiol.*, vol. 8, no. 9, pp. 623–633, 2010, doi: 10.1038/nrmicro2415.

[56] N. Høiby, T. Bjarnsholt, M. Givskov, S. Molin, and O. Ciofu, "International Journal of Antimicrobial Agents Antibiotic resistance of bacterial biofilms," vol. 35, pp. 322–332, 2010, doi: 10.1016/j.ijantimicag.2009.12.011.

[57] M. Jamal and S. Andleeb, "Bacterial Biofilm : Its Composition , Formation and Role in Human Infections Research & Reviews : Journal of Microbiology and Bacterial Biofilm : Its Composition , Formation and Role in Human," *Res. Rev. J. Microbiol. Biotechnol.*, vol. 4, no. 3, pp. 1–14, 2015.

[58] M. Simões, L. C. Simões, and M. J. Vieira, "A review of current and emergent biofilm control strategies," *Lwt*, vol. 43, no. 4, pp. 573–583, 2010, doi: 10.1016/j.lwt.2009.12.008.

[59] J. Yu, M. Zhou, L. Zhang, and H. Wei, "Antibacterial Adhesion Strategy for Dental

Titanium Implant Surfaces: From Mechanisms to Application," *J. Funct. Biomater.*, vol. 13, no. 4, 2022, doi: 10.3390/jfb13040169.

[60] C. L. Romanò, S. Scarponi, E. Gallazzi, D. Romanò, and L. Drago, "Antibacterial coating of implants in orthopaedics and trauma: A classification proposal in an evolving panorama," *J. Orthop. Surg. Res.*, vol. 10, no. 1, pp. 1–11, 2015, doi: 10.1186/s13018-015-0294-5.

[61] H. Chouirfa, H. Bouloussa, V. Migonney, and C. Falentin-Daudré, "Review of titanium surface modification techniques and coatings for antibacterial applications," *Acta Biomater.*, vol. 83, pp. 37–54, 2019, doi: 10.1016/j.actbio.2018.10.036.

[62] H. Tsuchiya *et al.*, "Innovative antimicrobial coating of titanium implants with iodine," *J. Orthop. Sci.*, vol. 17, no. 5, pp. 595–604, 2012, doi: 10.1007/s00776-012-0247-3.

[63] I. A. J. van Hengel, M. W. A. M. Tierolf, L. E. Fratila-apachitei, I. Apachitei, and A. A. Zadpoor, "Antibacterial titanium implants biofunctionalized by plasma electrolytic oxidation with silver, zinc, and copper: A systematic review," *Int. J. Mol. Sci.*, vol. 22, no. 7, 2021, doi: 10.3390/ijms22073800.

[64] Y. Z. Wan, S. Raman, F. He, and Y. Huang, "Surface modification of medical metals by ion implantation of silver and copper," *Vacuum*, vol. 81, no. 9, pp. 1114–1118, 2007, doi: 10.1016/j.vacuum.2006.12.011.

[65] A. Cochis *et al.*, "Competitive surface colonization of antibacterial and bioactive materials doped with strontium and/or silver ions," *Nanomaterials*, vol. 10, no. 1, pp. 1–19, 2020, doi: 10.3390/nano10010120.

[66] S. Ferraris *et al.*, "Natural Coatings on Titanium Surfaces to Improve Their Biological Response †," *Mater. Proc.*, pp. 1–8, 2020, doi: 10.3390/CIWC2020-06835.

[67] Y. Zheng *et al.*, "Perceiving the connection between the bone healing process and biodegradation of biodegradable metal implants through precise bioadaptability principle," *J. Mater. Sci. Technol.*, vol. 147, pp. 132–144, 2023, doi: 10.1016/j.jmst.2022.12.004.

[68] T. Hussain, B. Tan, Y. Yin, F. Blachier, M. C. B. Tossou, and N. Rahu, "Oxidative Stress and Inflammation: What Polyphenols Can Do for Us?," *Oxid. Med. Cell. Longev.*, vol. 2016, 2016, doi: 10.1155/2016/7432797.

[69] P. A. Mouthuy *et al.*, "Biocompatibility of implantable materials: An oxidative stress viewpoint," *Biomaterials*, vol. 109, pp. 55–68, 2016, doi: 10.1016/j.biomaterials.2016.09.010.

[70] J. Gallo, M. Holinka, and C. S. Moucha, *Antibacterial surface treatment for orthopaedic implants*, vol. 15, no. 8. 2014.

[71] S. Rizvi, S. T. Raza, F. Ahmed, A. Ahmad, S. Abbas, and F. Mahdi, "The role of Vitamin E in human health and some diseases," *Sultan Qaboos Univ. Med. J.*, vol. 14, no. 2, pp. 157–165, 2014.

[72] S. S. Mohd Mutalip, S. Ab-Rahim, and M. H. Rajikin, "Vitamin E as an antioxidant in female reproductive health," *Antioxidants*, vol. 7, no. 2, pp. 1–15, 2018, doi: 10.3390/antiox7020022.

[73] M. L. Colombo, "An update on vitamin E, tocopherol and tocotrienol-perspectives,"

Molecules, vol. 15, no. 4, pp. 2103–2113, 2010, doi: 10.3390/molecules15042103.

[74] Q. Jiang, "Natural forms of vitamin E: Metabolism, antioxidant, and anti-inflammatory activities and their role in disease prevention and therapy," *Free Radic. Biol. Med.*, vol. 72, pp. 76–90, 2014, doi: 10.1016/j.freeradbiomed.2014.03.035.

[75] K. Nishio *et al.*, "α-Tocopheryl phosphate: Uptake, hydrolysis, and antioxidant action in cultured cells and mouse," *Free Radic. Biol. Med.*, vol. 50, no. 12, pp. 1794–1800, 2011, doi: 10.1016/j.freeradbiomed.2011.03.021.

[76] K. N. Engin, "Alpha-tocopherol: Looking beyond an antioxidant," *Mol. Vis.*, vol. 15, no. November 2008, pp. 855–860, 2009.

[77] X. Wang and P. J. Quinn, "The location and function of vitamin E in membranes (Review)," *Molecular Membrane Biology*, vol. 17, no. 3. pp. 143–156, 2000, doi: 10.1080/09687680010000311.

[78] Y. Gilgun-Sherki, E. Melamed, and D. Offen, "Oxidative stress induced-neurodegenerative diseases: The need for antioxidants that penetrate the blood brain barrier," *Neuropharmacology*, vol. 40, no. 8, pp. 959–975, 2001, doi: 10.1016/S0028-3908(01)00019-3.

[79] A. Lloret, D. Esteve, P. Monllor, A. Cervera-Ferri, and A. Lloret, "The effectiveness of vitamin E treatment in alzheimer's disease," *Int. J. Mol. Sci.*, vol. 20, no. 4, 2019, doi: 10.3390/ijms20040879.

[80] M. Schubert *et al.*, "Long-chain metabolites of vitamin E: Metabolic activation as a general concept for lipid-soluble vitamins?," *Antioxidants*, vol. 7, no. 1, pp. 1–20, 2018, doi: 10.3390/antiox7010010.

[81] E. Reitera, Q. Jiang, and S. Christen, "Anti-inflammatory properties of α- and γ-tocopherol," *Bone*, vol. 23, no. 1, pp. 1–7, 2014, doi: 10.1016/j.mam.2007.01.003.Anti-inflammatory.

[82] D. Wu, M. G. Hayek, and S. N. Meydani, "Symposium: Molecular mechanisms of protective effects of vitamin E in atherosclerosis: Vitamin E and macrophage cyclooxygenase regulation in the aged," *J. Nutr.*, vol. 131, no. 2, pp. 382–388, 2001, doi: 10.1093/jn/131.2.382S.

[83] G. Y. Lee and S. N. Han, "The role of vitamin E in immunity," *Nutrients*, vol. 10, no. 11, pp. 1–18, 2018, doi: 10.3390/nu10111614.

[84] D. M. Hardbower, T. de Sablet, R. Chaturvedi, and K. T. Wilson, "Chronic inflammation and oxidative stress: The smoking gun for helicobacter pylori-induced gastric cancer?," *Gut Microbes*, vol. 4, no. 6, pp. 475–481, 2013, doi: 10.4161/gmic.25583.

[85] M. G. Traber and J. Atkinson, "Vitamin E, antioxidant and nothing more," *Free Radic. Biol. Med.*, vol. 43, no. 1, pp. 4–15, 2007, doi: 10.1016/j.freeradbiomed.2007.03.024.

[86] M. Keen and I. Hassan, "Vitamin E in dermatology," *Indian Dermatol. Online J.*, vol. 7, no. 4, p. 311, 2016, doi: 10.4103/2229-5178.185494.

[87] A. S. Nazrun, M. Norazlina, M. Norliza, and S. I. Nirwana, "The anti-inflammatory role of vitamin e in prevention of osteoporosis," *Adv. Pharmacol. Sci.*, vol. 2012, 2012, doi: 10.1155/2012/142702.

[88] S. K. Wong, N. V. Mohamad, N. 'Izzah Ibrahim, K. Y. Chin, A. N. Shuid, and S. Ima-Nirwana, "The molecular mechanism of Vitamin E as a bone-protecting agent: A review on current evidence," *Int. J. Mol. Sci.*, vol. 20, no. 6, 2019, doi: 10.3390/ijms20061453.

[89] M. F. Rossato, C. Hoffmeister, R. Tonello, A. P. de Oliveira Ferreira, and J. Ferreira, "Anti-inflammatory Effects of Vitamin E on Adjuvant-Induced Arthritis in Rats," *Inflammation*, vol. 38, no. 2, pp. 606–615, 2015, doi: 10.1007/s10753-014-9967-1.

[90] C. Constantinou, A. Papas, and A. I. Constantinou, "Vitamin E and cancer: An insight into the anticancer activities of vitamin E isomers and analogs," *Int. J. Cancer*, vol. 123, no. 4, pp. 739–752, 2008, doi: 10.1002/ijc.23689.

[91] L. Capuron *et al.*, "Vitamin E status and quality of life in the elderly: Influence of inflammatory processes," *Br. J. Nutr.*, vol. 102, no. 10, pp. 1390–1394, 2009, doi: 10.1017/S0007114509990493.

[92] S. R. Tintino *et al.*, "Original article : ACTION OF CHOLECALCIFEROL AND ALPHA-TOCOPHEROL ON," *EXCLI J.*, vol. 15, pp. 315–322, 2016.

[93] D. Abd, A. Kader, and F. M. Aziz, "Antibacterial Effects of Vitamin E : in Vito Study Antibacterial Effects of Vitamin E : in Vitro Study ﻪﺑ داﺿﻤﻟا ﻞﻠﺒﻜﺗﺮﻳا : ﺪﺳﺎﻗ ﺦﻳاﺮﺟ ﻻﺎﻜﺋﺎﻨﻟا ﻻﺎﺤﻳ نيماتيف ريثأت," no. January, 2013.

[94] M. M. Naguib and M. A. Valvano, "Vitamin E Increases Antimicrobial Sensitivity by Inhibiting Bacterial Lipocalin Antibiotic Binding," *mSphere*, vol. 3, no. 6, pp. 1–14, 2018, doi: 10.1128/msphere.00564-18.

[95] J. C. Andrade *et al.*, "Enhancement of the antibiotic activity of aminoglycosides by alpha-tocopherol and other cholesterol derivates," *Biomed. Pharmacother.*, vol. 68, no. 8, pp. 1065–1069, 2014, doi: 10.1016/j.biopha.2014.10.011.

[96] F. Vergalito *et al.*, "Vitamin E for prevention of biofilm-caused Healthcare-associated infections," *Open Med.*, vol. 15, no. 1, pp. 14–21, 2020, doi: 10.1515/med-2020-0004.

[97] D. L. Williams, J. Vinciguerra, J. M. Lerdahl, and R. D. Bloebaum, "Does Vitamin E-blended UHMWPE Prevent Biofilm Formation?," *Clin. Orthop. Relat. Res.*, vol. 473, no. 3, pp. 928–935, 2015, doi: 10.1007/s11999-014-3673-z.

[98] E. Ogru *et al.*, "Vitamin E phosphate: an endogenous form of vitamin E," *Medimond Srl*, no. May 2015, pp. 127–132, 2003.

[99] M. Eskin NA, "Vitamin E and the Role of Water-soluble α- Tocopheryl Phosphate," *Vitam. Miner.*, vol. 03, no. 01, 2014, doi: 10.4172/2376-1318.1000e123.

[100] Y. Negis, J. M. Zingg, E. Ogru, R. Gianello, R. Libinaki, and A. Azzi, "On the existence of cellular tocopheryl phosphate, its synthesis, degradation and cellular roles: A hypothesis," *IUBMB Life*, vol. 57, no. 1, pp. 23–25, 2005, doi: 10.1080/15216540500058980.

[101] J. M. Zingg, M. Meydani, and A. Azzi, "α-Tocopheryl phosphate-An activated form of vitamin E important for angiogenesis and vasculogenesis?," *BioFactors*, vol. 38, no. 1, pp. 24–33, 2012, doi: 10.1002/biof.198.

[102] A. Munteanu *et al.*, "Modulation of cell proliferation and gene expression by α-tocopheryl phosphates: Relevance to atherosclerosis and inflammation," *Biochem. Biophys. Res.*

Commun., vol. 318, no. 1, pp. 311–316, 2004, doi: 10.1016/j.bbrc.2004.04.028.

[103] J.-M. Zingg, "Molecular and Cellular Activities of Vitamin E Analogues," *Mini-Reviews Med. Chem.*, vol. 7, no. 5, pp. 545–560, 2007, doi: 10.2174/138955707780619608.

[104] B. M. Rezk, G. R. M. M. Haenen, W. J. F. Van Der Vijgh, and A. Bast, "The extraordinary antioxidant activity of vitamin E phosphate," *Biochim. Biophys. Acta - Mol. Cell Biol. Lipids*, vol. 1683, no. 1–3, pp. 16–21, 2004, doi: 10.1016/j.bbalip.2004.03.005.

[105] S. Nakayama, E. M. Katoh, T. Tsuzuki, and S. Kobayashi, "Protective effect of α-tocopherol-6-O-phosphate against ultraviolet B-induced damage in cultured mouse skin," *J. Invest. Dermatol.*, vol. 121, no. 2, pp. 406–411, 2003, doi: 10.1046/j.1523-1747.2003.12351.x.

[106] R. A. Harper *et al.*, "Soft, adhesive (+) alpha tocopherol phosphate planar bilayers that control oral biofilm growth through a substantive antimicrobial effect," *Nanomedicine Nanotechnology, Biol. Med.*, vol. 14, no. 7, pp. 2307–2316, 2018, doi: 10.1016/j.nano.2017.12.024.

[107] A. Bidossi *et al.*, "In vitro comparison between α-tocopheryl acetate and α-tocopheryl phosphate against bacteria responsible of prosthetic and joint infections," *PLoS One*, vol. 12, no. 7, pp. 1–12, 2017, doi: 10.1371/journal.pone.0182323.

[108] P. Bracco and E. Oral, "Vitamin E-stabilized UHMWPE for total joint implants: A review," *Clin. Orthop. Relat. Res.*, vol. 469, no. 8, pp. 2286–2293, 2011, doi: 10.1007/s11999-010-1717-6.

[109] S. M. Kurtz, P. Bracco, L. Costa, E. Oral, and O. K. Muratoglu, *17 Vitamin E-Blended UHMWPE Biomaterials*, Third Edit. Elsevier Inc., 2002.

[110] C. Wolf, T. Krivec, J. Blassnig, K. Lederer, and W. Schneider, "Examination of the suitability of α-tocopherol as a stabilizer for ultra-high molecular weight polyethylene used for articulating surfaces in joint endoprostheses," *J. Mater. Sci. Mater. Med.*, vol. 13, no. 2, pp. 185–189, 2002, doi: 10.1023/A:1013834113967.

[111] Y. Takahashi, K. Yamamoto, and G. Pezzotti, "Effects of vitamin e blending on plastic deformation mechanisms of highly crosslinked ultrahigh molecular weight polyethylene (HXL-UHMWPE) in total hip arthroplasty," *Acta Biomater.*, vol. 15, pp. 227–236, 2015, doi: 10.1016/j.actbio.2014.12.022.

[112] E. Oral and O. K. Muratoglu, "Vitamin E diffused, highly crosslinked UHMWPE: A review," *Int. Orthop.*, vol. 35, no. 2, pp. 215–223, 2011, doi: 10.1007/s00264-010-1161-y.

[113] M. Satué, J. M. Ramis, and M. Monjo, "Cholecalciferol synthesized after UV-activation of 7-dehydrocholesterol onto titanium implants inhibits osteoclastogenesis in vitro," *J. Biomed. Mater. Res. - Part A*, vol. 103, no. 7, pp. 2280–2288, 2015, doi: 10.1002/jbm.a.35364.

[114] M. Satué, M. Monjo, H. J. Ronold, S. P. Lyngstadaas, and J. M. Ramis, "Titanium implants coated with UV-irradiated vitamin D precursor and vitamin E: in vivo performance and coating stability," *Clin. Oral Implants Res.*, vol. 28, no. 4, pp. 424–431, 2017, doi: 10.1111/clr.12815.

[115] A. B. Lovati *et al.*, "Vitamin E phosphate coating stimulates bone deposition in implant-related infections in a rat model," *Clin. Orthop. Relat. Res.*, vol. 476, no. 6, pp. 1324–1338, 2018, doi: 10.1097/01.blo.0000534692.41467.02.

[116] P. H. Wang, B. S. Huang, H. C. Horng, C. C. Yeh, and Y. J. Chen, "Wound healing," *J. Chinese Med. Assoc.*, vol. 81, no. 2, pp. 94–101, 2018, doi: 10.1016/j.jcma.2017.11.002.

[117] V. Kanikireddy, K. Varaprasad, T. Jayaramudu, C. Karthikeyan, and R. Sadiku, "Carboxymethyl cellulose-based materials for infection control and wound healing: A review," *Int. J. Biol. Macromol.*, vol. 164, pp. 963–975, 2020, doi: 10.1016/j.ijbiomac.2020.07.160.

[118] A. Ehterami *et al.*, "Chitosan/alginate hydrogels containing Alpha-tocopherol for wound healing in rat model," *J. Drug Deliv. Sci. Technol.*, vol. 51, no. February, pp. 204–213, 2019, doi: 10.1016/j.jddst.2019.02.032.

[119] C. Gandhimathi, J. R. Venugopal, V. Bhaarathy, S. Ramakrishna, and S. D. Kumar, "Biocomposite nanofibrous strategies for the controlled release of biomolecules for skin tissue regeneration," *Int. J. Nanomedicine*, vol. 9, no. 1, pp. 4709–4722, 2014, doi: 10.2147/IJN.S65335.

[120] S. Zahid *et al.*, "Bi-layered α-tocopherol acetate loaded membranes for potential wound healing and skin regeneration," *Mater. Sci. Eng. C*, vol. 101, no. March, pp. 438–447, 2019, doi: 10.1016/j.msec.2019.03.080.

[121] P. Taepaiboon, U. Rungsardthong, and P. Supaphol, "Vitamin-loaded electrospun cellulose acetate nanofiber mats as transdermal and dermal therapeutic agents of vitamin A acid and vitamin E," *Eur. J. Pharm. Biopharm.*, vol. 67, no. 2, pp. 387–397, 2007, doi: 10.1016/j.ejpb.2007.03.018.

[122] G. G. Pereira, S. S. Guterres, A. G. Balducci, P. Colombo, and F. Sonvico, "Polymeric films loaded with vitamin e and aloe vera for topical application in the treatment of burn wounds," *Biomed Res. Int.*, vol. 2014, 2014, doi: 10.1155/2014/641590.

[123] S. Trombino, R. Cassano, T. Ferrarelli, B. Isacchi, A. R. Bilia, and N. Picci, "Collagen α-tocopherulate for topical applications: Preparation, characterization, and antioxidant activity evaluation," *Macromol. Res.*, vol. 20, no. 9, pp. 939–943, 2012, doi: 10.1007/s13233-012-0129-8.

[124] K. Krafts, "Tissue Repair," *Encycl. Toxicol. Third Ed.*, pp. 577–583, 2014, doi: 10.1016/B978-0-12-386454-3.00355-9.

[125] S. K. Misra *et al.*, "Poly(3-hydroxybutyrate) multifunctional composite scaffolds for tissue engineering applications," *Biomaterials*, vol. 31, no. 10, pp. 2806–2815, 2010, doi: 10.1016/j.biomaterials.2009.12.045.

[126] V. Aina, S. Gatti, M. Cannas, and F. Reno, "Effect of vitamin E addition to poly (D , L) - lactic acid on surface properties and osteoblast behaviour," vol. 26, pp. 5594–5599, 2005, doi: 10.1016/j.biomaterials.2005.02.015.

[127] G. Paul, M. Rizzi, G. Gatti, L. Marchese, and F. Ren, "Poly (D , L) Lactic Acid Blending with Vitamin E Increases Polymer Hemocompatibility : An Hydrophilic Effect," pp. 1527–

1533, 2013, doi: 10.1002/app.38841.

[128] D. Campoccia *et al.*, "Bacterial adhesion to poly-(D,L)lactic acid blended with vitamin E: Toward gentle anti-infective biomaterials," *J. Biomed. Mater. Res. - Part A*, vol. 103, no. 4, pp. 1447–1458, 2015, doi: 10.1002/jbm.a.35284.

[129] I. Antoniac, D. Popescu, A. Zapciu, A. Antoniac, F. Miculescu, and H. Moldovan, "Magnesium filled polylactic acid (PLA) material for filament based 3D printing," *Materials (Basel).*, vol. 12, no. 5, pp. 1–13, 2019, doi: 10.3390/ma12050719.

[130] Z. Mahdieh, R. Bagheri, M. Eslami, M. Amiri, M. A. Shokrgozar, and M. Mehrjoo, "Thermoplastic starch/ethylene vinyl alcohol/forsterite nanocomposite as a candidate material for bone tissue engineering," *Mater. Sci. Eng. C*, vol. 69, pp. 301–310, 2016, doi: 10.1016/j.msec.2016.06.043.

[131] Y. Qu, J. Tang, L. Liu, L. L. Song, S. Chen, and Y. Gao, "α-Tocopherol liposome loaded chitosan hydrogel to suppress oxidative stress injury in cardiomyocytes," *Int. J. Biol. Macromol.*, vol. 125, pp. 1192–1202, 2019, doi: 10.1016/j.ijbiomac.2018.09.092.

[132] G. Grosso *et al.*, "Mediterranean diet and cancer: Epidemiological evidence and mechanism of selected aspects," *BMC Surg.*, vol. 13, no. SUPPL.2, p. S14, 2013, doi: 10.1186/1471-2482-13-S2-S14.

[133] C. M. Neophytou and A. I. Constantinou, "Drug delivery innovations for enhancing the anticancer potential of vitamin e isoforms and their derivatives," *Biomed Res. Int.*, vol. 2015, 2015, doi: 10.1155/2015/584862.

[134] B. B. Aggarwal, C. Sundaram, S. Prasad, and R. Kannappan, "Tocotrienols, the vitamin E of the 21st century: Its potential against cancer and other chronic diseases," *Biochem. Pharmacol.*, vol. 80, no. 11, pp. 1613–1631, 2010, doi: 10.1016/j.bcp.2010.07.043.

[135] P. Borel, D. Preveraud, and C. Desmarchelier, "Bioavailability of vitamin E in humans: An update," *Nutr. Rev.*, vol. 71, no. 6, pp. 319–331, 2013, doi: 10.1111/nure.12026.

[136] E. Reboul, "Vitamin e bioavailability: Mechanisms of intestinal absorption in the spotlight," *Antioxidants*, vol. 6, no. 4, 2017, doi: 10.3390/antiox6040095.

[137] M. A. Faramarzi, M. Naghibzadeh, A. Amani, M. Amini, E. Esmaeilzadeh, and N. Mottaghi-Dastjerdi, "An insight into the interactions between-tocopherol and chitosan in ultrasound-prepared nanoparticles," *J. Nanomater.*, vol. 2010, no. January, 2010, doi: 10.1155/2010/818717.

[138] J. P. Nam, K. J. Lee, J. W. Choi, C. O. Yun, and J. W. Nah, "Targeting delivery of tocopherol and doxorubicin grafted-chitosan polymeric micelles for cancer therapy: In vitro and in vivo evaluation," *Colloids Surfaces B Biointerfaces*, vol. 133, pp. 254–262, 2015, doi: 10.1016/j.colsurfb.2015.06.018.

[139] Y. Luo, B. Zhang, M. Whent, L. L. Yu, and Q. Wang, "Preparation and characterization of zein/chitosan complex for encapsulation of α-tocopherol, and its in vitro controlled release study," *Colloids Surfaces B Biointerfaces*, vol. 85, no. 2, pp. 145–152, 2011, doi: 10.1016/j.colsurfb.2011.02.020.

[140] Y. Byun *et al.*, "Formulation and characterization of α-tocopherol loaded poly e{open}-

caprolactone (PCL) nanoparticles," *LWT - Food Sci. Technol.*, vol. 44, no. 1, pp. 24–28, 2011, doi: 10.1016/j.lwt.2010.06.032.

[141] C. Charcosset and H. Fessi, "Preparation of nanoparticles with a membrane contactor," *J. Memb. Sci.*, vol. 266, no. 1–2, pp. 115–120, 2005, doi: 10.1016/j.memsci.2005.05.016.

[142] P. Singh *et al.*, "Hyaluronic-acid-based β-cyclodextrin grafted copolymers as biocompatible supramolecular hosts to enhance the water solubility of tocopherol," *Int. J. Pharm.*, vol. 586, no. February, 2020, doi: 10.1016/j.ijpharm.2020.119542.

[143] C. Quintero, R. Vera, and L. D. Perez, "α-Tocopherol loaded thermosensitive polymer nanoparticles: Preparation, in vitro release and antioxidant properties," *Polimeros*, vol. 26, no. 4, pp. 304–312, 2016, doi: 10.1590/0104-1428.2324.

[144] B. Mohammadi, H. Shekaari, and M. T. Zafarani-Moattar, "Synthesis of nanoencapsulated vitamin E in phase change material (PCM) shell as thermo-sensitive drug delivery purpose," *J. Mol. Liq.*, vol. 320, 2020, doi: 10.1016/j.molliq.2020.114429.

[145] Z. Nie *et al.*, "Enhanced radical scavenging activity by antioxidant-functionalized gold nanoparticles: A novel inspiration for development of new artificial antioxidants," *Free Radic. Biol. Med.*, vol. 43, no. 9, pp. 1243–1254, 2007, doi: 10.1016/j.freeradbiomed.2007.06.011.

[146] A. Konopko, J. Kusio, and G. Litwinienko, "Antioxidant activity of metal nanoparticles coated with tocopherol-like residues—the importance of studies in homo-and heterogeneous systems," *Antioxidants*, vol. 9, no. 1, 2020, doi: 10.3390/antiox9010005.

[147] S. Dubey and S. P. Vyas, "Original Article EMULSOMES FOR LIPOPHILIC ANTICANCER DRUG DELIVERY : DEVELOPMENT , OPTIMIZATION AND IN VITRO DRUG RELEASE KINETIC STUDY," vol. 13, no. 2, 2021.

[148] C. Weber *et al.*, "Vitamin E succinate is a potent novel antineoplastic agent with high selectivity and cooperativity with tumor necrosis factorrelated apoptosis-inducing ligand (Apo2 ligand) in vivo," *Clin. Cancer Res.*, vol. 8, no. 3, pp. 863–869, 2002.

[149] A. Angulo-Molina *et al.*, "Magnetite nanoparticles functionalized with α-tocopheryl succinate (α-TOS) promote selective cervical cancer cell death," *J. Nanoparticle Res.*, vol. 16, no. 8, 2014, doi: 10.1007/s11051-014-2528-6.

[150] Y. Guo, J. Luo, S. Tan, B. O. Otieno, and Z. Zhang, "The applications of Vitamin e TPGS in drug delivery," *Eur. J. Pharm. Sci.*, vol. 49, no. 2, pp. 175–186, 2013, doi: 10.1016/j.ejps.2013.02.006.

[151] C. Yang, T. Wu, Y. Qi, and Z. Zhang, "Recent advances in the application of vitamin E TPGS for drug delivery," *Theranostics*, vol. 8, no. 2, pp. 464–485, 2018, doi: 10.7150/thno.22711.

[152] Z. Zhang, S. Tan, and S. S. Feng, "Vitamin E TPGS as a molecular biomaterial for drug delivery," *Biomaterials*, vol. 33, no. 19, pp. 4889–4906, 2012, doi: 10.1016/j.biomaterials.2012.03.046.

[153] J. Zhang *et al.*, "An Injectable Hydrogel Prepared Using a PEG/Vitamin E Copolymer Facilitating Aqueous-Driven Gelation," *Biomacromolecules*, vol. 17, no. 11, pp. 3648–

3658, 2016, doi: 10.1021/acs.biomac.6b01148.

[154] D. Mandracchia, G. Tripodo, A. Latrofa, and R. Dorati, "Amphiphilic inulin-d-α-tocopherol succinate (INVITE) bioconjugates for biomedical applications," *Carbohydr. Polym.*, vol. 103, no. 1, pp. 46–54, 2014, doi: 10.1016/j.carbpol.2013.11.056.

[155] D. Mandracchia *et al.*, "pH-sensitive inulin-based nanomicelles for intestinal site-specific and controlled release of celecoxib," *Carbohydr. Polym.*, vol. 181, no. July 2017, pp. 570–578, 2018, doi: 10.1016/j.carbpol.2017.11.110.

[156] D. Mandracchia *et al.*, "Design, synthesis and evaluation of biotin decorated inulin-based polymeric micelles as long-circulating nanocarriers for targeted drug delivery," *Nanomedicine Nanotechnology, Biol. Med.*, vol. 13, no. 3, pp. 1245–1254, 2017, doi: 10.1016/j.nano.2017.01.001.

[157] G. Tripodo, S. Perteghella, P. Grisoli, A. Trapani, M. L. Torre, and D. Mandracchia, "Drug delivery of rifampicin by natural micelles based on inulin: Physicochemical properties, antibacterial activity and human macrophages uptake," *Eur. J. Pharm. Biopharm.*, vol. 136, no. December 2018, pp. 250–258, 2019, doi: 10.1016/j.ejpb.2019.01.022.

[158] G. Rassu *et al.*, "Polymeric nanomicelles based on inulin D α-tocopherol succinate for the treatment of diabetic retinopathy," *J. Drug Deliv. Sci. Technol.*, vol. 61, no. November 2020, p. 102286, 2021, doi: 10.1016/j.jddst.2020.102286.

[159] G. Tripodo *et al.*, "Mesenchymal stromal cells loading curcumin-INVITE-micelles: A drug delivery system for neurodegenerative diseases," *Colloids Surfaces B Biointerfaces*, vol. 125, pp. 300–308, 2015, doi: 10.1016/j.colsurfb.2014.11.034.

[160] J. Wang *et al.*, "The effect of dual-functional hyaluronic acid-vitamin E succinate micelles on targeting delivery of doxorubicin," *Int. J. Nanomedicine*, vol. 11, pp. 5851–5870, 2016, doi: 10.2147/IJN.S113882.

[161] K. kaur, J. kaur, R. Kumar, and S. K. Mehta, "Formulation and physiochemical study of α-tocopherol based oil in water nanoemulsion stabilized with non toxic, biodegradable surfactant: Sodium stearoyl lactate," *Ultrason. Sonochem.*, vol. 38, pp. 570–578, 2017, doi: 10.1016/j.ultsonch.2016.08.026.

[162] M. Romeu-Nadal, S. Morera-Pons, A. I. Castellote, and M. C. López-Sabater, "Determination of γ- and α-tocopherols in human milk by a direct high-performance liquid chromatographic method with UV-vis detection and comparison with evaporative light scattering detection," *J. Chromatogr. A*, vol. 1114, no. 1, pp. 132–137, 2006, doi: 10.1016/j.chroma.2006.02.049.

[163] P. Lampen, W. Pittermann, H. M. Heise, M. Schmitt, H. Jungmann, and M. Kietzmann, "Penetration studies of vitamin E acetate applied from cosmetic formulations to the stratum corneum of an in vitro model using quantification by tape stripping, UV spectroscopy, and HPLC," *J. Cosmet. Sci.*, vol. 54, no. 2, pp. 119–131, 2003.

[164] M. M. Delgado Zamarreño, A. Sanchez Ferez, M. Sanchez Rodriguez, M. C. Gomez Ferez, and J. Hernandez Mendez, "Determination of fat-soluble vitamins in yogurt by HPLC with electrochemical detection," *Talanta*, vol. 43, no. 9, pp. 1555–1563, 1996, doi:

10.1016/0039-9140(96)01939-X.

[165] M. A. Campanero, B. Calahorra, E. Garcia-Quetglas, J. Honorato, and J. J. Carballal, "Determination of cisapride in human plasma by high-performance liquid chromatography," *Chromatographia*, vol. 47, no. 9–10, pp. 537–541, 1998, doi: 10.1007/BF02467491.

[166] O. Korchazhkina, E. Jones, M. Czauderna, S. A. Spencer, and J. Kowalczyk, "HPLC with UV detection for measurement of vitamin E in human milk," *Acta Chromatogr.*, no. 16, pp. 48–57, 2006.

[167] O. Jović, I. Habinovec, N. Galić, and M. Andrašec, "Maceration of extra virgin olive oil with common aromatic plants using ultrasound-assisted extraction: An uv-vis spectroscopic investigation," *J. Spectrosc.*, vol. 2018, 2018, doi: 10.1155/2018/7510647.

[168] X. Li, D. Chen, G. Wang, and Y. Lu, "Investigation on the interaction between bovine serum albumin and 2,2-diphenyl-1-picrylhydrazyl," *J. Lumin.*, vol. 156, pp. 255–261, 2014, doi: 10.1016/j.jlumin.2014.08.025.

[169] S. D. Silva, N. F. Rosa, A. E. Ferreira, L. V. Boas, and M. R. Bronze, "Rapid determination of α-tocopherol in vegetable oils by fourier transform infrared spectroscopy," *Food Anal. Methods*, vol. 2, no. 2, pp. 120–127, 2009, doi: 10.1007/s12161-008-9047-y.

[170] R. Fuchs-Godec and G. Zerjav, "Corrosion resistance of high-level-hydrophobic layers in combination with Vitamin E - (α-tocopherol) as green inhibitor," *Corros. Sci.*, vol. 97, pp. 7–16, 2015, doi: 10.1016/j.corsci.2015.03.016.

[171] K. Wang, D. W. Sun, Q. Wei, and H. Pu, "Quantification and visualization of α-tocopherol in oil-in-water emulsion based delivery systems by Raman microspectroscopy," *Lwt*, vol. 96, no. January, pp. 66–74, 2018, doi: 10.1016/j.lwt.2018.05.017.

[172] J. R. Beattie *et al.*, "The use of Raman microscopy to determine and localize vitamin E in biological samples," *FASEB J.*, vol. 21, no. 3, pp. 766–776, 2007, doi: 10.1096/fj.06-7028com.

[173] M. Y. Lv *et al.*, "A rapid method to authenticate vegetable oils through surface-enhanced Raman scattering," *Sci. Rep.*, vol. 6, no. February, pp. 1–7, 2016, doi: 10.1038/srep23405.

[174] Q. Tu *et al.*, "Multi-phase detection of antioxidants using surface-enhanced Raman spectroscopy with a gold nanoparticle-coated fiber," *Talanta*, vol. 206, no. July 2019, p. 120197, 2020, doi: 10.1016/j.talanta.2019.120197.

[175] T. Cai, H. Gu, X. Yuan, and F. Liu, "Normal Raman and SERS spectroscopy of the vitamin E," *J. Phys. Conf. Ser.*, vol. 277, no. 1, 2011, doi: 10.1088/1742-6596/277/1/012010.

[176] V. M. Di Mambro, A. E. C. S. Azzolini, Y. M. L. Valim, and M. J. V. Fonseca, "Comparison of antioxidant activities of tocopherols alone and in pharmaceutical formulations," *Int. J. Pharm.*, vol. 262, no. 1–2, pp. 93–99, 2003, doi: 10.1016/S0378-5173(03)00333-8.

[177] K. I. Berker, F. A. Ozdemir Olgun, D. Ozyurt, B. Demirata, and R. Apak, "Modified Folin-Ciocalteu antioxidant capacity assay for measuring lipophilic antioxidants," *J. Agric. Food Chem.*, vol. 61, no. 20, pp. 4783–4791, 2013, doi: 10.1021/jf400249k.

[178] E. Tütem, R. Apak, E. Günaydi, and K. Sözgen, "Spectrophotometric determination of vitamin E (α-tocopherol) using copper(II)-neocuproine reagent," *Talanta*, vol. 44, no. 2, pp.

249–255, 1997, doi: 10.1016/S0039-9140(96)02041-3.

[179] R. G. MARTINEK, "Method for the Determination of Vitamin E (Total Tocopherols) in Serum.," *Clin. Chem.*, vol. 10, pp. 1078–1086, 1964, doi: 10.1093/clinchem/10.12.1078.

[180] C. Golumbic and H. A. Mattill, "the Oxidation of Vitamin E," *J. Biol. Chem.*, vol. 134, no. 2, pp. 535–541, 1940, doi: 10.1016/s0021-9258(18)73212-2.

[181] K. Doudin and S. Al-Malaika, "Vitamin E-stabilised UHMWPE for orthopaedic implants: Quantitative determination of vitamin E and characterisation of its transformation products," *Polym. Degrad. Stab.*, vol. 125, pp. 59–75, 2016, doi: 10.1016/j.polymdegradstab.2015.11.028.

[182] T. Gmbh, T. Llc, and I. K. Analytik, "HPLC Method to Determine the Alpha-Tocopherol Content in UHMWPE," vol. 13, no. 2316, p. 2316, 2008.

[183] Rowell S, Oral E, and M. Ok, "Detection of Vitamin E in Irradiated UHMWPE by UV-Visible Spectroscopy," *Chem Pharm Bull*, vol. 25, no. 2, pp. 2434–2439, 2004.

[184] M. J. Martínez-Morlanes, A. Terriza, F. Yubero, and J. A. Puértolas, "Characterization of highly crosslinked polyethylenes by colorimetry," *Polym. Test.*, vol. 31, no. 6, pp. 841–847, 2012, doi: 10.1016/j.polymertesting.2012.06.005.

[185] S. Y. Gim, J. Jung, Y. J. Kwon, M. J. Kim, G. H. Kim, and J. H. Lee, "Effects of chitosan and collagen containing α-tocopherol on the oxidative stability in bulk oil and oil-in-water emulsion," *Food Sci. Biotechnol.*, vol. 27, no. 4, pp. 947–956, 2018, doi: 10.1007/s10068-018-0345-x.

[186] E. Stoleru *et al.*, "Polyethylene materials with multifunctional surface properties by electrospraying chitosan/vitamin E formulation destined to biomedical and food packaging applications," *Iran. Polym. J. (English Ed.*, vol. 25, no. 4, pp. 295–307, 2016, doi: 10.1007/s13726-016-0421-0.

[187] A. Salawi and S. Nazzal, "The rheological and textural characterization of Soluplus®/Vitamin E composites," *Int. J. Pharm.*, vol. 546, no. 1–2, pp. 255–262, 2018, doi: 10.1016/j.ijpharm.2018.05.049.

[188] J. T. Martins, M. A. Cerqueira, and A. A. Vicente, "Influence of α-tocopherol on physicochemical properties of chitosan-based films," *Food Hydrocoll.*, vol. 27, no. 1, pp. 220–227, 2012, doi: 10.1016/j.foodhyd.2011.06.011.

[189] Q. Sun *et al.*, "Hyaluronic acid-targeted and pH-responsive drug delivery system based on metal-organic frameworks for efficient antitumor therapy," *Biomaterials*, vol. 223, no. September, p. 119473, 2019, doi: 10.1016/j.biomaterials.2019.119473.

[190] J. S. Hayes, U. Seidenglanz, A. I. Pearce, S. G. Pearce, C. W. Archer, and R. G. Richards, "Surface polishing positively influences ease of plate and screw removal," *Eur. Cells Mater.*, vol. 19, no. 0, pp. 117–126, 2010, doi: 10.22203/eCM.v019a12.

[191] M. Cazzola, S. Ferraris, E. Prenesti, V. Casalegno, and S. Spriano, "Grafting of gallic acid onto a bioactive Ti6Al4V alloy: A physico-chemical characterization," *Coatings*, vol. 9, no. 5, pp. 1–17, 2019, doi: 10.3390/coatings9050302.

[192] S. Spriano, S. Ferraris, and E. Vernè, "EUROPEAN PATENT SPECIFICATION 2214732,"

vol. 1, no. 19, pp. 1–12, 2013.

[193] S. Ferraris, M. Cazzola, V. Peretti, B. Stella, and S. Spriano, “Zeta potential measurements on solid surfaces for in Vitro biomaterials testing: Surface charge, reactivity upon contact with fluids and protein absorption,” *Front. Bioeng. Biotechnol.*, vol. 6, no. MAY, pp. 1–7, 2018, doi: 10.3389/fbioe.2018.00060.

[194] C. Coatings, R. C. Products, E. Applica-, S. Tape, T. Paint, and R. Materials, “Standard Test Methods for Measuring Adhesion by Tape Test 1,” no. July, pp. 1–8, 2012, doi: 10.1520/D3359-09E02.2.

[195] D. Nečas and P. Klapetek, “Gwyddion: An open-source software for SPM data analysis,” *Cent. Eur. J. Phys.*, vol. 10, no. 1, pp. 181–188, 2012, doi: 10.2478/s11534-011-0096-2.

[196] P. G. Rouxhet and M. J. Genet, “XPS analysis of bio-organic systems,” *Surf. Interface Anal.*, vol. 43, no. 12, pp. 1453–1470, 2011, doi: 10.1002/sia.3831.

[197] M. Birringer, “Analysis of vitamin E metabolites in biological specimen,” *Mol. Nutr. Food Res.*, vol. 54, no. 5, pp. 588–598, 2010, doi: 10.1002/mnfr.200900457.

[198] W. Wainipee, D. J. Weiss, M. A. Sephton, B. J. Coles, C. Unsworth, and R. Court, “The effect of crude oil on arsenate adsorption on goethite,” *Water Res.*, vol. 44, no. 19, pp. 5673–5683, 2010, doi: 10.1016/j.watres.2010.05.056.

[199] Y. B. Che Man, W. Ammawath, and M. E. S. Mirghani, “Determining α-tocopherol in refined bleached and deodorized palm olein by Fourier transform infrared spectroscopy,” *Food Chem.*, vol. 90, no. 1–2, pp. 323–327, 2005, doi: 10.1016/j.foodchem.2004.05.059.

[200] A. TermehYousefi, S. Bagheri, K. Shinji, J. Rouhi, M. Rusop Mahmood, and S. Ikeda, “Fast Synthesis of Multilayer Carbon Nanotubes from Camphor Oil as an Energy Storage Material,” *Biomed Res. Int.*, vol. 2014, 2014, doi: 10.1155/2014/691537.

[201] D. Krilov, M. Kosović, and K. Serec, “Spectroscopic studies of alpha tocopherol interaction with a model liposome and its influence on oxidation dynamics,” *Spectrochim. Acta - Part A Mol. Biomol. Spectrosc.*, vol. 129, pp. 588–593, 2014, doi: 10.1016/j.saa.2014.03.087.

[202] X. Ma, Y. Liu, L. Fan, and W. Yan, “Ethyl cellulose particles loaded with α-tocopherol for inhibiting thermal oxidation of soybean oil,” *Carbohydr. Polym.*, vol. 252, no. September 2020, p. 117169, 2021, doi: 10.1016/j.carbpol.2020.117169.

[203] P. Bracco, V. Brunella, M. Zanetti, M. P. Luda, and L. Costa, “Stabilisation of ultra-high molecular weight polyethylene with Vitamin E,” *Polym. Degrad. Stab.*, vol. 92, no. 12, pp. 2155–2162, 2007, doi: 10.1016/j.polymdegradstab.2007.02.023.

[204] J. O. Hollinger, *AN INTRODUCTION*. 2022.

[205] S. Ferraris *et al.*, “Cytocompatible and Anti-bacterial Adhesion Nanotextured Titanium Oxide Layer on Titanium Surfaces for Dental and Orthopedic Implants,” *Front. Bioeng. Biotechnol.*, vol. 7, no. May, pp. 1–12, 2019, doi: 10.3389/fbioe.2019.00103.

[206] H. Li, S. Yin, and T. Sato, “Persistent deNOx Ability of CaAl2O4:(Eu, Nd)/TiO2-xNy Luminescent Photocatalyst,” *Nanoscale Res. Lett.*, vol. 6, no. 1, pp. 1–4, 2011, doi: 10.1007/s11671-010-9750-7.

[207] M. Cazzola *et al.*, “Grafting of the peppermint essential oil to a chemically treated Ti6Al4V

alloy to counteract the bacterial adhesion," *Surf. Coatings Technol.*, vol. 378, no. October, 2019, doi: 10.1016/j.surfcoat.2019.125011.

[208] A. Nina Adden, Lara J. Gamble, David G. Castner, Andrea Hoffmann, Gerhard Gross and H. Menzela, "Phosphonic Acid Monolayers for Binding of Bioactive Molecules to Titanium Surfaces," vol. 22, no. 19, pp. 8197–8204, 2008, doi: 10.1021/la060754c.Phosphonic.

[209] B. V. Crist, "Demo Version (87 pages) PDF Handbooks of Monochromatic XPS Spectra Volume 1 - The Elements and Native Oxides (for Ag-Au)," *Elements*, vol. 1, no. March, 1999.

[210] G. Riccucci, M. Cazzola, S. Ferraris, V. A. Gobbo, M. Guaita, and S. Spriano, "Surface functionalization of Ti6Al4V with an extract of polyphenols from red grape pomace," *Mater. Des.*, vol. 206, p. 109776, 2021, doi: 10.1016/j.matdes.2021.109776.

[211] M. Miola, A. Cochis, A. Kumar, C. R. Arciola, L. Rimondini, and E. Verné, "Copper-doped bioactive glass as filler for PMMA-based bone cements: Morphological, mechanical, reactivity, and preliminary antibacterial characterization," *Materials (Basel).*, vol. 11, no. 6, 2018, doi: 10.3390/ma11060961.

[212] R. Sorrentino *et al.*, "Reduced bacterial adhesion on ceramics used for arthroplasty applications," *J. Eur. Ceram. Soc.*, vol. 38, no. 3, pp. 963–970, 2018, doi: 10.1016/j.jeurceramsoc.2017.10.008.

[213] W. Zhang *et al.*, "Periosteum and development of the tissue-engineered periosteum for guided bone regeneration," *J. Orthop. Transl.*, vol. 33, no. February, pp. 41–54, 2022, doi: 10.1016/j.jot.2022.01.002.

[214] F. Gamna and S. Spriano, "Vitamin e: A review of its application and methods of detection when combined with implant biomaterials," *Materials (Basel).*, vol. 14, no. 13, 2021, doi: 10.3390/ma14133691.

[215] W. W. Yao, H. M. Peng, and R. D. Webster, "Electrochemistry of α-tocopherol (Vitamin E) and α-tocopherol quinone films deposited on electrode surfaces in the presence and absence of lipid multilayers," *J. Phys. Chem. C*, vol. 113, no. 52, pp. 21805–21814, 2009, doi: 10.1021/jp9079124.

[216] C. M. Sabliov, C. Fronczek, C. E. Astete, M. Khachaturyan, L. Khachatryan, and C. Leonardi, "Effects of Temperature and UV Light on Degradation of α-Tocopherol in Free and Dissolved Form," *JAOCS, J. Am. Oil Chem. Soc.*, vol. 86, no. 9, pp. 895–902, 2009, doi: 10.1007/s11746-009-1411-6.

[217] F. D. S. Vargas, D. G. Soares, A. P. D. Ribeiro, J. Hebling, and C. A. De Souza Costa, "Protective effect of alpha-tocopherol isomer from vitamin e against the H2O2 induced toxicity on dental pulp cells," *Biomed Res. Int.*, vol. 2014, 2014, doi: 10.1155/2014/895049.

[218] S. Browne and A. Pandit, "Biomaterial-mediated modification of the local inflammatory environment," *Front. Bioeng. Biotechnol.*, vol. 3, no. MAY, pp. 1–14, 2015, doi: 10.3389/fbioe.2015.00067.

[219] C. A. Loynes *et al.*, "PGE2 production at sites of tissue injury promotes an anti-inflammatory neutrophil phenotype and determines the outcome of inflammation resolution

in vivo," *Sci. Adv.*, vol. 4, no. 9, 2018, doi: 10.1126/sciadv.aar8320.

[220] C. Hetz, "The unfolded protein response: Controlling cell fate decisions under ER stress and beyond," *Nat. Rev. Mol. Cell Biol.*, vol. 13, no. 2, pp. 89–102, 2012, doi: 10.1038/nrm3270.

[221] G. S. Hotamisligil, "Endoplasmic Reticulum Stress and the Inflammatory Basis of Metabolic Disease," *Cell*, vol. 140, no. 6, pp. 900–917, 2010, doi: 10.1016/j.cell.2010.02.034.

[222] P. Wipt and K. M. George, "基因的改变NIH Public Access," *Bone*, vol. 23, no. 1, pp. 1–7, 2008, doi: 10.1038/nature07203.From.

[223] S. Z. Hasnain, R. Lourie, I. Das, A. C. H. Chen, and M. A. McGuckin, "The interplay between endoplasmic reticulum stress and inflammation," *Immunol. Cell Biol.*, vol. 90, no. 3, pp. 260–270, 2012, doi: 10.1038/icb.2011.112.

[224] M. Corazzari, M. Gagliardi, G. M. Fimia, and M. Piacentini, "Endoplasmic reticulum stress, unfolded protein response, and cancer cell fate," *Front. Oncol.*, vol. 7, no. APR, pp. 1–11, 2017, doi: 10.3389/fonc.2017.00078.

[225] A. Scalbert, I. T. Johnson, and M. Saltmarsh, "Polyphenols: antioxidants and beyond 1–3," vol. 81, no. February, pp. 215–217, 2018.

[226] M. Cazzola, I. Corazzari, E. Prenesti, E. Bertone, E. Vernè, and S. Ferraris, "Bioactive glass coupling with natural polyphenols: Surface modification, bioactivity and anti-oxidant ability," *Appl. Surf. Sci.*, vol. 367, pp. 237–248, 2016, doi: 10.1016/j.apsusc.2016.01.138.

[227] S. Rigacci, M. Jimenez, D. Rio, C. Velez-pardo, and A. Thapa, *Natural Compounds as Therapeutic Agents for Amyloidogenic Diseases*, no. September. 2015.

[228] M. Abbas, F. Saeed, F. M. Anjum, T. Tufail, M. S. Bashir, and A. Ishtiaq, "Natural polyphenols : An overview Natural polyphenols : An overview," *Int. J. Food Prop.*, vol. 20, no. 8, pp. 1689–1699, 2017, doi: 10.1080/10942912.2016.1220393.

[229] L. Zhang, Z. Han, and D. Granato, *Polyphenols in foods : Classification , methods of identification , and nutritional aspects in human health*, 1st ed. Elsevier Inc., 2021.

[230] M. Rentzsch, A. Wilkens, and P. Winterhalter, "Non-flavonoid Phenolic Compounds," 2009, doi: 10.1007/978-0-387-74118-5.

[231] W. V. and R. Nicholson, "FAMILIES OF PHENOLIC COMPOUNDS AND MEANS OF CLASSIFICATION," *Phenolic Compd. Biochem.*, pp. 1–34, 2006.

[232] B. Badhani, N. Sharma, and R. Kakkar, "Gallic acid: A versatile antioxidant with promising therapeutic and industrial applications," *RSC Adv.*, vol. 5, no. 35, pp. 27540–27557, 2015, doi: 10.1039/c5ra01911g.

[233] A. N. Panche, A. D. Diwan, and S. R. Chandra, "Flavonoids: An overview," *J. Nutr. Sci.*, vol. 5, 2016, doi: 10.1017/jns.2016.41.

[234] D. Chen and Q. P. Dou, "Tea polyphenols and their roles in cancer prevention and chemotherapy," *Int. J. Mol. Sci.*, vol. 9, no. 7, pp. 1196–1206, 2008, doi: 10.3390/ijms9071196.

[235] C. Musial, A. Kuban-Jankowska, and M. Gorska-Ponikowska, "Beneficial properties of green tea catechins," *Int. J. Mol. Sci.*, vol. 21, no. 5, 2020, doi: 10.3390/ijms21051744.

[236] Z. Yan, Y. Zhong, Y. Duan, Q. Chen, and F. Li, "Antioxidant mechanism of tea polyphenols and its impact on health benefits," *Anim. Nutr.*, vol. 6, no. 2, pp. 115–123, 2020, doi: 10.1016/j.aninu.2020.01.001.

[237] Z. Spáčil, L. Nováková, and P. Solich, "Comparison of positive and negative ion detection of tea catechins using tandem mass spectrometry and ultra high performance liquid chromatography," *Food Chem.*, vol. 123, no. 2, pp. 535–541, 2010, doi: 10.1016/j.foodchem.2010.04.048.

[238] M. Shkayeva, P. Gregory, M. Pickering, D. Hein, J. Hu, and A. Rodriguez, "Green Tea Product Epigallocatechin Gallate (EGCG) Content and Label Information: A Descriptive Analysis," *J. Nutr. Ther.*, vol. 4, no. 3, pp. 81–84, 2015, doi: 10.6000/1929-5634.2015.04.03.2.

[239] S. Losada-barreiro and C. Bravo-díaz, "European Journal of Medicinal Chemistry Free radicals and polyphenols : The redox chemistry of neurodegenerative diseases," *Eur. J. Med. Chem.*, vol. 133, pp. 379–402, 2017, doi: 10.1016/j.ejmech.2017.03.061.

[240] F. Di Meo, V. Lemaur, R. Lazzaroni, J. Duroux, Y. Olivier, and P. Trouillas, "Free Radical Scavenging by Natural Polyphenols : Atom versus Electron Transfer," vol. 2092, 2013.

[241] K. Durgo and A. Hu, *properties*. 2018.

[242] M. Kampa, P. Nifli, G. Notas, and E. Castanas, "Polyphenols and cancer cell growth," no. June, pp. 79–113, 2007, doi: 10.1007/112.

[243] S. Ramos, "Cancer chemoprevention and chemotherapy: Dietary polyphenols and signalling pathways," *Mol. Nutr. Food Res.*, vol. 52, no. 5, pp. 507–526, 2008, doi: 10.1002/mnfr.200700326.

[244] A. Mahbub, C. Maitre, S. Haywood-Small, G. McDougall, N. Cross, and N. Jordan-Mahy, "Differential Effects of Polyphenols on Proliferation and Apoptosis in Human Myeloid and Lymphoid Leukemia Cell Lines," *Anticancer. Agents Med. Chem.*, vol. 13, no. 10, pp. 1601–1613, 2013, doi: 10.2174/18715206113139990303.

[245] E. Scoditti *et al.*, "Mediterranean diet polyphenols reduce inflammatory angiogenesis through MMP-9 and COX-2 inhibition in human vascular endothelial cells: A potentially protective mechanism in atherosclerotic vascular disease and cancer," *Arch. Biochem. Biophys.*, vol. 527, no. 2, pp. 81–89, 2012, doi: 10.1016/j.abb.2012.05.003.

[246] H. Fujiki *et al.*, "Mechanistic findings of green tea as cancer preventive for humans," *Proc. Soc. Exp. Biol. Med.*, vol. 220, no. 4, pp. 225–228, 1999, doi: 10.1046/j.1525-1373.1999.d01-38.x.

[247] S. Harakeh, K. Abu-El-Ardat, M. Diab-Assaf, A. Niedzwiecki, M. El-Sabban, and M. Rath, "Epigallocatechin-3-gallate induces apoptosis and cell cycle arrest in HTLV-1-positive and -negative leukemia cells," *Med. Oncol.*, vol. 25, no. 1, pp. 30–39, 2008, doi: 10.1007/s12032-007-0036-6.

[248] S. Ahmed, N. Wang, M. Lalonde, V. M. Goldberg, and T. M. Haqqi, "Green Tea Polyphenol Epigallocatechin-3-gallate (EGCG) Differentially Inhibits Interleukin-1β-Induced Expression of Matrix Metalloproteinase-1 and -13 in Human Chondrocytes," *J. Pharmacol.*

Exp. Ther., vol. 308, no. 2, pp. 767–773, 2004, doi: 10.1124/jpet.103.059220.

[249] N. Khan, F. Afaq, M. Saleem, N. Ahmad, and H. Mukhtar, "Targeting multiple signaling pathways by green tea polyphenol (-)-epigallocatechin-3-gallate," *Cancer Res.*, vol. 66, no. 5, pp. 2500–2505, 2006, doi: 10.1158/0008-5472.CAN-05-3636.

[250] A. Niedzwiecki, M. W. Roomi, T. Kalinovsky, and M. Rath, "Anticancer efficacy of polyphenols and their combinations," *Nutrients*, vol. 8, no. 9, 2016, doi: 10.3390/nu8090552.

[251] H. Lin and R. Tsao, *Antimicrobials from plants - food preservation and shelf life extension*, Third Edit., vol. 4, no. October 2018. Elsevier, 2019.

[252] E. Coppo and A. Marchese, "Antibacterial Activity of Polyphenols Antibacterial Activity of Polyphenols," no. August 2014, 2016, doi: 10.2174/1389201015041408251211 42.

[253] M. Wu and A. C. Brown, "Applications of catechins in the treatment of bacterial infections," *Pathogens*, vol. 10, no. 5, 2021, doi: 10.3390/pathogens10050546.

[254] X. Xu, X. D. Zhou, and C. D. Wu, "The tea catechin epigallocatechin gallate suppresses cariogenic virulence factors of Streptococcus mutans," *Antimicrob. Agents Chemother.*, vol. 55, no. 3, pp. 1229–1236, 2011, doi: 10.1128/AAC.01016-10.

[255] K. Hara *et al.*, "The green tea polyphenol (-)-epigallocatechin gallate precipitates salivary proteins including alpha-amylase: Biochemical implications for oral health," *Eur. J. Oral Sci.*, vol. 120, no. 2, pp. 132–139, 2012, doi: 10.1111/j.1600-0722.2012.00947.x.

[256] Y. S. Cho, J. J. Oh, and K. H. Oh, "Synergistic anti-bacterial and proteomic effects of epigallocatechin gallate on clinical isolates of imipenem-resistant Klebsiella pneumoniae," *Phytomedicine*, vol. 18, no. 11, pp. 941–946, 2011, doi: 10.1016/j.phymed.2011.03.012.

[257] W. Reygaert and I. Jusufi, "Green tea as an effective antimicrobial for urinary tract infections caused by Escherichia coli," *Front. Microbiol.*, vol. 4, no. JUN, pp. 1–4, 2013, doi: 10.3389/fmicb.2013.00162.

[258] D. O. Serra, F. Mika, A. M. Richter, and R. Hengge, "The green tea polyphenol EGCG inhibits E. coli biofilm formation by impairing amyloid curli fibre assembly and downregulating the biofilm regulator CsgD via the σE-dependent sRNA RybB," *Mol. Microbiol.*, vol. 101, no. 1, pp. 136–151, 2016, doi: 10.1111/mmi.13379.

[259] L. E. E. Kang-Mu *et al.*, "Antipathogenic properties of green tea polyphenol epigallocatechin gallate at concentrations below the MIC against enterohemorrhagic escherichia coli O157:H7," *J. Food Prot.*, vol. 72, no. 2, pp. 325–331, 2009, doi: 10.4315/0362-028x-72.2.325.

[260] Y. Sugita-Konishi *et al.*, "Epigallocatechin gallate and gallocatechin gallate in green tea catechins inhibit extracellular release of Vero toxin from enterohemorrhagic Escherichia coli O157:H7," *Biochim. Biophys. Acta - Gen. Subj.*, vol. 1472, no. 1–2, pp. 42–50, 1999, doi: 10.1016/S0304-4165(99)00102-6.

[261] J. Jeon, J. H. Kim, C. K. Lee, C. H. Oh, and H. J. Song, "The antimicrobial activity of (-)-epigallocatehin-3-gallate and green tea extracts against Pseudomonas aeruginosa and Escherichia coli isolated from skin wounds," *Ann. Dermatol.*, vol. 26, no. 5, pp. 564–569,

2014, doi: 10.5021/ad.2014.26.5.564.

[262] N. Hosseini Jazani, S. Shahabi, A. Abdi Ali, and M. Zartoshti, “Antibacterial effects of water soluble green tea extracts on multi-antibiotic resistant isolates of Acinetobacter sp.,” *Pakistan J. Biol. Sci.*, vol. 10, no. 9, pp. 1477–1480, 2007, doi: 10.3923/pjbs.2007.1477.1480.

[263] Y. S. Cho, N. L. Schiller, and K. H. Oh, “Antibacterial effects of green tea polyphenols on clinical isolates of methicillin-resistant Staphylococcus aureus,” *Curr. Microbiol.*, vol. 57, no. 6, pp. 542–546, 2008, doi: 10.1007/s00284-008-9239-0.

[264] B. Huber, L. Eberl, W. Feucht, and J. Polster, “Influence of Polyphenols on Bacterial Biofilm Formation and Quorum-sensing,” *Zeitschrift fur Naturforsch. - Sect. C J. Biosci.*, vol. 58, no. 11–12, pp. 879–884, 2003, doi: 10.1515/znc-2003-11-1224.

[265] V. Domazetovic, G. Marcucci, T. Iantomasi, M. L. Brandi, and M. T. Vincenzini, “Oxidative stress in bone remodeling: Role of antioxidants,” *Clin. Cases Miner. Bone Metab.*, vol. 14, no. 2, pp. 209–216, 2017, doi: 10.11138/ccmbm/2017.14.2.209.

[266] D. Bellavia *et al.*, “Non-flavonoid polyphenols in osteoporosis: preclinical evidence,” *Trends Endocrinol. Metab.*, vol. 32, no. 7, pp. 515–529, 2021, doi: 10.1016/j.tem.2021.03.008.

[267] A. Trzeciakiewicz, V. Habauzit, and M. N. Horcajada, “When nutrition interacts with osteoblast function: Molecular mechanisms of polyphenols,” *Nutr. Res. Rev.*, vol. 22, no. 1, pp. 68–81, 2009, doi: 10.1017/S095442240926402X.

[268] H. T. Huang *et al.*, “Osteoprotective roles of green tea catechins,” *Antioxidants*, vol. 9, no. 11, pp. 1–25, 2020, doi: 10.3390/antiox9111136.

[269] C. H. Chen, M. L. Ho, J. K. Chang, S. H. Hung, and G. J. Wang, “Green tea catechin enhances osteogenesis in a bone marrow mesenchymal stem cell line,” *Osteoporos. Int.*, vol. 16, no. 12, pp. 2039–2045, 2005, doi: 10.1007/s00198-005-1995-0.

[270] J. Deng, H. Yang, E. Capanoglu, H. Cao, and J. Xiao, *Technological aspects and stability of polyphenols*. Elsevier Inc., 2018.

[271] H. Cao *et al.*, “Available technologies on improving the stability of polyphenols in food processing,” *Food Front.*, vol. 2, no. 2, pp. 109–139, 2021, doi: 10.1002/fft2.65.

[272] X. Zhou *et al.*, “Changes in browning degree and reducibility of polyphenols during autoxidation and enzymatic oxidation,” *Antioxidants*, vol. 10, no. 11, 2021, doi: 10.3390/antiox10111809.

[273] A. Shavandi, A. E. D. A. Bekhit, P. Saeedi, Z. Izadifar, A. A. Bekhit, and A. Khademhosseini, “Polyphenol uses in biomaterials engineering,” *Biomaterials*, vol. 167, pp. 91–106, 2018, doi: 10.1016/j.biomaterials.2018.03.018.

[274] L. Q. Xu, K. G. Neoh, and E. T. Kang, “Natural polyphenols as versatile platforms for material engineering and surface functionalization,” *Prog. Polym. Sci.*, vol. 87, pp. 165–196, 2018, doi: 10.1016/j.progpolymsci.2018.08.005.

[275] R. C. P. Scannavino, G. Riccucci, S. Ferraris, G. L. C. Duarte, P. T. De Oliveira, and S. Spriano, “Functionalization with Polyphenols of a Nano-Textured Ti Surface through a

High – Amino Acid Medium : A Chemical – Physical and Biological Characterization," 2022.

[276] S. Ferraris, M. Cazzola, G. Ubertalli, E. Prenesti, and S. Spriano, "Grafting of gallic acid to metallic surfaces," *Appl. Surf. Sci.*, vol. 511, no. October 2019, p. 145615, 2020, doi: 10.1016/j.apsusc.2020.145615.

[277] M. Cazzola *et al.*, "Green tea polyphenols coupled with a bioactive titanium alloy surface: In vitro characterization of osteoinductive behavior through a KUSA A1 cell study," *Int. J. Mol. Sci.*, vol. 19, no. 8, 2018, doi: 10.3390/ijms19082255.

[278] F. Weber *et al.*, "Can polyphenolic surface modifications prevent fungal colonization of titanium dental implants ?," *Colloids Surfaces B Biointerfaces*, vol. 219, no. July, p. 112813, 2022, doi: 10.1016/j.colsurfb.2022.112813.

[279] T. E. L. Douglas *et al.*, "Titanium surface functionalization with coatings of chitosan and polyphenol-rich plant extracts," *Mater. Lett.*, vol. 196, no. 24600, pp. 213–216, 2017, doi: 10.1016/j.matlet.2017.03.065.

[280] A. Mieszkowska *et al.*, "Phenolic-enriched collagen fibrillar coatings on titanium alloy to promote osteogenic differentiation and reduce inflammation," *Int. J. Mol. Sci.*, vol. 21, no. 17, pp. 1–15, 2020, doi: 10.3390/ijms21176406.

[281] H. Zhang *et al.*, "Ag-Incorporated Polydopamine/Tannic Acid Coating on Titanium With Enhanced Cytocompatible and Antibacterial Properties," *Front. Bioeng. Biotechnol.*, vol. 10, no. March, pp. 1–9, 2022, doi: 10.3389/fbioe.2022.877738.

[282] S. Lee *et al.*, "Surface engineering of titanium alloy using metal-polyphenol network coating with magnesium ions for improved osseointegration," *Biomater. Sci.*, vol. 8, no. 12, pp. 3404–3417, 2020, doi: 10.1039/d0bm00566e.

[283] N. Ikeda *et al.*, "Bioactivity and antibacterial activity of iodine-containing calcium titanate against implant-associated infection," *Biomater. Adv.*, vol. 138, no. May, p. 212952, 2022, doi: 10.1016/j.bioadv.2022.212952.

[284] S. Yamaguchi *et al.*, "Iodine-loaded calcium titanate for bone repair with sustainable antibacterial activity prepared by solution and heat treatment," *Nanomaterials*, vol. 11, no. 9, 2021, doi: 10.3390/nano11092199.

[285] T. Kokubo and H. Takadama, "How useful is SBF in predicting in vivo bone bioactivity?," *Biomaterials*, vol. 27, no. 15, pp. 2907–2915, 2006, doi: 10.1016/j.biomaterials.2006.01.017.

[286] P. Talamond, J. Verdeil, and G. Conéjéro, "Secondary Metabolite Localization by Autofluorescence in Living Plant Cells," pp. 5024–5037, 2015, doi: 10.3390/molecules20035024.

[287] S. Ferraris *et al.*, "Gallic acid grafting to a ferrimagnetic bioactive glass-ceramic," *J. Non. Cryst. Solids*, vol. 432, pp. 167–175, 2016, doi: 10.1016/j.jnoncrysol.2015.05.023.

[288] X. Zhang, S. Ferraris, E. Prenesti, and E. Verné, "Surface functionalization of bioactive glasses with natural molecules of biological significance, part I: Gallic acid as model molecule," *Appl. Surf. Sci.*, vol. 287, pp. 329–340, 2013, doi: 10.1016/j.apsusc.2013.09.151.

[289] H.-L. A. Satu Salo, “Antibacterial efficacy of plastic samples,” 2020.

[290] M. A. Bonifacio *et al.*, “From the sea to the bee: Gellan gum-honey-diatom composite to deliver resveratrol for cartilage regeneration under oxidative stress conditions,” *Carbohydr. Polym.*, vol. 245, no. February, p. 116410, 2020, doi: 10.1016/j.carbpol.2020.116410.

[291] N. Ikeda *et al.*, “Bioactivity and antibacterial activity of iodine-containing calcium titanate against implant-associated infection,” *Biomater. Adv.*, vol. 138, no. December 2021, p. 212952, 2022, doi: 10.1016/j.bioadv.2022.212952.

[292] W. C. Chou, R. C. C. Wang, C. Liu, C. Y. Yang, and T. M. Lee, “Surface modification of Direct-Current and radio-frequency oxygen plasma treatments enhance cell biocompatibility,” *Materials (Basel).*, vol. 10, no. 11, 2017, doi: 10.3390/ma10111223.

[293] G. Schmitz, “Inorganic reactions of iodine(+1) in acidic solutions,” *Int. J. Chem. Kinet.*, vol. 36, no. 9, pp. 480–493, 2004, doi: 10.1002/kin.20020.

[294] Y. Boulmokh, K. Belguidoum, F. Meddour, and H. Amira-Guebailia, “Investigation of antioxidant activity of epigallocatechin gallate and epicatechin as compared to resveratrol and ascorbic acid: experimental and theoretical insights,” *Struct. Chem.*, vol. 32, no. 5, pp. 1907–1923, 2021, doi: 10.1007/s11224-021-01763-5.

[295] S. Ferraris *et al.*, “The mechanical and chemical stability of the interfaces in bioactive materials: The substrate-bioactive surface layer and hydroxyapatite-bioactive surface layer interfaces,” *Mater. Sci. Eng. C*, vol. 116, no. April, p. 111238, 2020, doi: 10.1016/j.msec.2020.111238.

[296] B. Tang, H. Yuan, L. Cheng, X. Zhou, X. Huang, and J. Li, “Effects of gallic acid on the morphology and growth of hydroxyapatite crystals,” *Arch. Oral Biol.*, vol. 60, no. 1, pp. 167–173, 2015, doi: 10.1016/j.archoralbio.2014.09.011.

[297] B. Tang, H. Yuan, L. Cheng, X. Zhou, X. Huang, and J. Li, “Control of hydroxyapatite crystal growth by gallic acid,” *Dent. Mater. J.*, vol. 34, no. 1, pp. 108–113, 2015, doi: 10.4012/dmj.2014-175.

[298] L. R. Rivera *et al.*, “Antibacterial, pro-angiogenic and pro-osteointegrative zein-bioactive glass/copper based coatings for implantable stainless steel aimed at bone healing,” *Bioact. Mater.*, vol. 6, no. 5, pp. 1479–1490, 2021, doi: 10.1016/j.bioactmat.2020.11.001.

[299] W. Zuo, L. Yu, J. Lin, Y. Yang, and Q. Fei, “Properties improvement of titanium alloys scaffolds in bone tissue engineering: a literature review,” *Ann. Transl. Med.*, vol. 9, no. 15, pp. 1259–1259, 2021, doi: 10.21037/atm-20-8175.

[300] C. R. S. Prakoeswa *et al.*, “Resveratrol promotes secretion of wound healing related growth factors of mesenchymal stem cells originated from adult and fetal tissues,” *Artif. Cells, Nanomedicine Biotechnol.*, vol. 48, no. 1, pp. 1160–1167, 2020, doi: 10.1080/21691401.2020.1817057.

[301] S. Chen *et al.*, “Curcumin Modulates the Crosstalk Between Macrophages and Bone Mesenchymal Stem Cells to Ameliorate Osteogenesis,” *Front. Cell Dev. Biol.*, vol. 9, no. February, pp. 1–13, 2021, doi: 10.3389/fcell.2021.634650.

[302] C. Aceves, I. Mendieta, B. Anguiano, and E. Delgado-González, “Molecular iodine has

extrathyroidal effects as an antioxidant, differentiator, and immunomodulator," *Int. J. Mol. Sci.*, vol. 22, no. 3, pp. 1–15, 2021, doi: 10.3390/ijms22031228.

[303] A. Jekabsone *et al.*, "Investigation of antibacterial and antiinflammatory activities of proanthocyanidins from pelargonium sidoides dc root extract," *Nutrients*, vol. 11, no. 11, 2019, doi: 10.3390/nu11112829.

[304] N. Savickiene *et al.*, "Efficacy of proanthocyanidins from Pelargonium sidoides root extract in reducing P. gingivalis viability while preserving oral commensal S. salivarius," *Materials (Basel).*, vol. 11, no. 9, 2018, doi: 10.3390/ma11091499.

[305] M. Lallukka *et al.*, "Surface Functionalization of Ti6Al4V-ELI Alloy with Antimicrobial Peptide Nisin," *Nanomaterials*, vol. 12, no. 23, 2022, doi: 10.3390/nano12234332.

[306] L. Wang *et al.*, "Therapeutic peptides: current applications and future directions," *Signal Transduct. Target. Ther.*, vol. 7, no. 1, 2022, doi: 10.1038/s41392-022-00904-4.

[307] S. Frost, "3. Proteins," *Biocultural Creat.*, pp. 77–100, 2020, doi: 10.1515/9780822374350-005.

[308] J. Barberi, "Exploring proteins in Roughland : on the adsorption of proteins on biomaterials for osseointegration," 2022.

[309] C. Kamble, R. Chavan, and V. Kamble, "A review on amino acids," *Res. Rev. A J. Drug Des. Discov.*, vol. 8, no. 3, pp. 19–27, 2021.

[310] M. Akram *et al.*, "Amino acids: A review article," *J. Med. Plants Res.*, vol. 5, no. 17, pp. 3997–4000, 2011.

[311] M. Muttenthaler, G. F. King, D. J. Adams, and P. F. Alewood, "Trends in peptide drug discovery," *Nat. Rev. Drug Discov.*, vol. 20, no. 4, pp. 309–325, 2021, doi: 10.1038/s41573-020-00135-8.

[312] K. Rose, W. Zeng, P. O. Regamey, I. V. Chernushevich, K. G. Standing, and H. F. Gaertner, "Natural peptides as building blocks for the synthesis of large protein- like molecules with hydrazone and oxime linkages," *Bioconjug. Chem.*, vol. 7, no. 5, pp. 552–556, 1996, doi: 10.1021/bc960039m.

[313] J. L. Lau and M. K. Dunn, "Therapeutic peptides: Historical perspectives, current development trends, and future directions," *Bioorganic Med. Chem.*, vol. 26, no. 10, pp. 2700–2707, 2018, doi: 10.1016/j.bmc.2017.06.052.

[314] M. Erdem Büyükkiraz and Z. Kesmen, "Antimicrobial peptides (AMPs): A promising class of antimicrobial compounds," *J. Appl. Microbiol.*, vol. 132, no. 3, pp. 1573–1596, 2022, doi: 10.1111/jam.15314.

[315] J. Yeo and F. Shahidi, "Bioactive peptides in health and disease: an overview," *Biol. Act. Pept.*, pp. 1–26, 2021, doi: 10.1016/b978-0-12-821389-6.00007-8.

[316] Q. Y. Zhang *et al.*, "Antimicrobial peptides: mechanism of action, activity and clinical potential," *Mil. Med. Res.*, vol. 8, no. 1, pp. 1–25, 2021, doi: 10.1186/s40779-021-00343-2.

[317] M. Mahlapuu, J. Håkansson, L. Ringstad, and C. Björn, "Antimicrobial peptides: An emerging category of therapeutic agents," *Front. Cell. Infect. Microbiol.*, vol. 6, no. DEC, pp. 1–12, 2016, doi: 10.3389/fcimb.2016.00194.

[318] B. Bechinger and S. U. Gorr, “Antimicrobial Peptides: Mechanisms of Action and Resistance,” *J. Dent. Res.*, vol. 96, no. 3, pp. 254–260, 2017, doi: 10.1177/0022034516679973.

[319] T. Matthyssen, W. Li, J. A. Holden, J. C. Lenzo, S. Hadjigol, and N. M. O’Brien-Simpson, “The Potential of Modified and Multimeric Antimicrobial Peptide Materials as Superbug Killers,” *Front. Chem.*, vol. 9, no. January, pp. 1–23, 2022, doi: 10.3389/fchem.2021.795433.

[320] Y. Luo and Y. Song, “Mechanism of antimicrobial peptides: Antimicrobial, anti-inflammatory and antibiofilm activities,” *Int. J. Mol. Sci.*, vol. 22, no. 21, 2021, doi: 10.3390/ijms222111401.

[321] S. Nasseri and M. Sharifi, “Therapeutic Potential of Antimicrobial Peptides for Wound Healing,” *Int. J. Pept. Res. Ther.*, vol. 28, no. 1, pp. 1–15, 2022, doi: 10.1007/s10989-021-10350-5.

[322] M. Pasupuleti, A. Schmidtchen, and M. Malmsten, “Antimicrobial peptides: Key components of the innate immune system,” *Crit. Rev. Biotechnol.*, vol. 32, no. 2, pp. 143–171, 2012, doi: 10.3109/07388551.2011.594423.

[323] A. B. B. Austin P. Veith, Kayla Henderson, Adrianne Spencer, Andrew D. Sligar, “Therapeutic Strategies for Enhancing Angiogenesis in Wound Healing,” *Physiol. Behav.*, vol. 176, no. 10, pp. 139–148, 2019, doi: 10.1016/j.addr.2018.09.010.Therapeutic.

[324] J. J. Guzmán-Rodríguez, A. Ochoa-Zarzosa, R. López-Gómez, and J. E. López-Meza, “Plant antimicrobial peptides as potential anticancer agents,” *Biomed Res. Int.*, vol. 2015, no. 1, 2015, doi: 10.1155/2015/735087.

[325] D. Jung Kim *et al.*, “Efficacy of the designer antimicrobial peptide SHAP1 in wound healing and wound infection,” *Amino Acids*, vol. 46, no. 10, pp. 2333–2343, 2014, doi: 10.1007/s00726-014-1780-5.

[326] S. Khelissa, N. E. Chihib, and A. Gharsallaoui, “Conditions of nisin production by Lactococcus lactis subsp. lactis and its main uses as a food preservative,” *Arch. Microbiol.*, vol. 203, no. 2, pp. 465–480, 2021, doi: 10.1007/s00203-020-02054-z.

[327] J. Wu *et al.*, “Nisin: From a structural and meat preservation perspective,” *Food Microbiol.*, vol. 111, no. December 2022, p. 104207, 2023, doi: 10.1016/j.fm.2022.104207.

[328] A. A. T. Barbosa, M. R. de Melo, C. M. R. da Silva, S. Jain, and S. S. Dolabella, “Nisin resistance in Gram-positive bacteria and approaches to circumvent resistance for successful therapeutic use,” *Crit. Rev. Microbiol.*, vol. 47, no. 3, pp. 376–385, 2021, doi: 10.1080/1040841X.2021.1893264.

[329] H. Zhou, J. Fang, Y. Tian, and X. Y. Lu, “Mechanisms of nisin resistance in Gram-positive bacteria,” *Ann. Microbiol.*, vol. 64, no. 2, pp. 413–420, 2014, doi: 10.1007/s13213-013-0679-9.

[330] B. Li, J. P. J. Yu, J. S. Brunzelle, G. N. Moll, W. a Van Der Donk, and S. K. Nair, “in Nisin Biosynthesis,” *Analysis*, vol. 23808, no. March, pp. 1464–1467, 2006.

[331] P. Santativongchai and P. Tulayakul, “Enhancement of the Antibiofilm Activity of Nisin

against Listeria monocytogenes Using Food Plant Extracts," pp. 1–10, 2023.

[332] A. A. Sani *et al.*, "Inhibitory activities of propolis, nisin, melittin and essential oil compounds on Paenibacillus alvei and Bacillus subtilis," *J. Venom. Anim. Toxins Incl. Trop. Dis.*, vol. 28, no. May, pp. 1–13, 2022, doi: 10.1590/1678-9199-JVATITD-2022-0025.

[333] R. Weishaupt *et al.*, "Enhanced Antimicrobial Activity and Structural Transitions of a Nanofibrillated Cellulose-Nisin Biocomposite Suspension," *ACS Appl. Mater. Interfaces*, vol. 10, no. 23, pp. 20170–20181, 2018, doi: 10.1021/acsami.8b04470.

[334] Z. Tan, J. Luo, F. Liu, Q. Zhang, and S. Jia, "Effects of pH, temperature, storage time, and protective agents on Nisin antibacterial stability," *Lect. Notes Electr. Eng.*, vol. 333, pp. 305–312, 2015, doi: 10.1007/978-3-662-46318-5_33.

[335] J. Zhou *et al.*, "An injectable, natural peptide hydrogel with potent antimicrobial activity and excellent wound healing-promoting effects," *Nano Today*, vol. 49, p. 101801, 2023, doi: 10.1016/j.nantod.2023.101801.

[336] M. Ali *et al.*, "Physical and Functional Characterization of PLGA Nanoparticles Containing the Antimicrobial Peptide SAAP-148," *Int. J. Mol. Sci.*, vol. 24, no. 3, 2023, doi: 10.3390/ijms24032867.

[337] V. Patrulea, G. Borchard, and O. Jordan, "An update on antimicrobial peptides (Amps) and their delivery strategies for wound infections," *Pharmaceutics*, vol. 12, no. 9, pp. 1–39, 2020, doi: 10.3390/pharmaceutics12090840.

[338] M. Barbosa, F. Costa, C. Monteiro, F. Duarte, M. C. L. Martins, and P. Gomes, "Antimicrobial coatings prepared from Dhvar-5-click-grafted chitosan powders," *Acta Biomater.*, vol. 84, pp. 242–256, 2019, doi: 10.1016/j.actbio.2018.12.001.

[339] Y. Imura, M. Nishida, and K. Matsuzaki, "Action mechanism of PEGylated magainin 2 analogue peptide," *Biochim. Biophys. Acta - Biomembr.*, vol. 1768, no. 10, pp. 2578–2585, 2007, doi: 10.1016/j.bbamem.2007.06.013.

[340] B. Skerlavaj and G. Boix-Lemonche, "The Potential of Surface-Immobilized Antimicrobial Peptides for the Enhancement of Orthopaedic Medical Devices: A Review," *Antibiotics*, vol. 12, no. 2, p. 211, 2023, doi: 10.3390/antibiotics12020211.

[341] M. G. Drexelius and I. Neundorf, "Application of antimicrobial peptides on biomedical implants: Three ways to pursue peptide coatings," *Int. J. Mol. Sci.*, vol. 22, no. 24, 2021, doi: 10.3390/ijms222413212.

[342] F. M. T. A. Costa, S. R. Maia, P. A. C. Gomes, and M. C. L. Martins, "Dhvar5 antimicrobial peptide (AMP) chemoselective covalent immobilization results on higher antiadherence effect than simple physical adsorption," *Biomaterials*, vol. 52, no. 1, pp. 531–538, 2015, doi: 10.1016/j.biomaterials.2015.02.049.

[343] L. Zhou *et al.*, "Biofunctionalization of microgroove titanium surfaces with an antimicrobial peptide to enhance their bactericidal activity and cytocompatibility," *Colloids Surfaces B Biointerfaces*, vol. 128, pp. 552–560, 2015, doi: 10.1016/j.colsurfb.2015.03.008.

[344] M. Godoy-Gallardo *et al.*, "Antibacterial properties of hLf1-11 peptide onto titanium surfaces: A comparison study between silanization and surface initiated polymerization,"

Biomacromolecules, vol. 16, no. 2, pp. 483–496, 2015, doi: 10.1021/bm501528x.

[345] W. Lin *et al.*, "Multi-biofunctionalization of a titanium surface with a mixture of peptides to achieve excellent antimicrobial activity and biocompatibility," *J. Mater. Chem. B*, vol. 3, no. 1, pp. 30–33, 2015, doi: 10.1039/c4tb01318b.

[346] S. Makihira *et al.*, "Titanium immobilized with an antimicrobial peptide derived from histatin accelerates the differentiation of osteoblastic cell line, MC3T3-E1," *Int. J. Mol. Sci.*, vol. 11, no. 4, pp. 1458–1470, 2010, doi: 10.3390/ijms11041458.

[347] X. W. Tan *et al.*, "Dual functionalization of titanium with vascular endothelial growth factor and β-defensin analog for potential application in keratoprosthesis.," *J. Biomed. Mater. Res. B. Appl. Biomater.*, vol. 100, no. 8, pp. 2090–2100, 2012, doi: 10.1002/jbm.b.32774.

[348] B. Mishra and G. Wang, "Titanium surfaces immobilized with the major antimicrobial fragment FK-16 of human cathelicidin LL-37 are potent against multiple antibiotic-resistant bacteria," *Biofouling*, vol. 33, no. 7, pp. 544–555, 2017, doi: 10.1080/08927014.2017.1332186.

[349] B. Nie, H. Ao, J. Zhou, T. Tang, and B. Yue, "Biofunctionalization of titanium with bacitracin immobilizationshows potential for anti-bacteria, osteogenesis and reduction ofmacrophage inflammation," *Colloids Surfaces B Biointerfaces*, vol. 145, pp. 728–739, 2016, doi: 10.1016/j.colsurfb.2016.05.089.

[350] B. Nie, H. Ao, T. Long, J. Zhou, T. Tang, and B. Yue, "Immobilizing bacitracin on titanium for prophylaxis of infections and for improving osteoinductivity: An in vivo study," *Colloids Surfaces B Biointerfaces*, vol. 150, pp. 183–191, 2017, doi: 10.1016/j.colsurfb.2016.11.034.

[351] K. V. Holmberg, M. Abdolhosseini, Y. Li, X. Chen, S. U. Gorr, and C. Aparicio, "Bio-inspired stable antimicrobial peptide coatings for dental applications," *Acta Biomater.*, vol. 9, no. 9, pp. 8224–8231, 2013, doi: 10.1016/j.actbio.2013.06.017.

[352] P. Siwakul, L. Sirinnaphakorn, J. Suwanprateep, T. Hayakawa, and K. Pugdee, "Cellular responses of histatin-derived peptides immobilized titanium surface using a tresyl chloride-activated method," *Dent. Mater. J.*, vol. 40, no. 4, pp. 934–941, 2021, doi: 10.4012/dmj.2020-307.

[353] X. W. Tan *et al.*, "Effectiveness of antimicrobial peptide immobilization for preventing perioperative cornea implant-associated bacterial infection," *Antimicrob. Agents Chemother.*, vol. 58, no. 9, pp. 5229–5238, 2014, doi: 10.1128/AAC.02859-14.

[354] M. Hoyos-Nogués, F. Velasco, M. P. Ginebra, J. M. Manero, F. J. Gil, and C. Mas-Moruno, "Regenerating Bone via Multifunctional Coatings: The Blending of Cell Integration and Bacterial Inhibition Properties on the Surface of Biomaterials," *ACS Appl. Mater. Interfaces*, vol. 9, no. 26, pp. 21618–21630, 2017, doi: 10.1021/acsami.7b03127.

[355] M. Gabriel, K. Nazmi, E. C. Veerman, A. V. N. Amerongen, and A. Zentner, "Preparation of LL-37-grafted titanium surfaces with bactericidal activity," *Bioconjug. Chem.*, vol. 17, no. 2, pp. 548–550, 2006, doi: 10.1021/bc050091v.

[356] A. Andrea, N. Molchanova, and H. Jenssen, "Antibiofilm peptides and peptidomimetics with focus on surface immobilization," *Biomolecules*, vol. 8, no. 2, 2018, doi:

10.3390/biom8020027.

[357] M. Kazemzadeh-Narbat *et al.*, "Drug release and bone growth studies of antimicrobial peptide-loaded calcium phosphate coating on titanium," *J. Biomed. Mater. Res. - Part B Appl. Biomater.*, vol. 100 B, no. 5, pp. 1344–1352, 2012, doi: 10.1002/jbm.b.32701.

[358] M. Kazemzadeh-Narbat, J. Kindrachuk, K. Duan, H. Jenssen, R. E. W. Hancock, and R. Wang, "Antimicrobial peptides on calcium phosphate-coated titanium for the prevention of implant-associated infections," *Biomaterials*, vol. 31, no. 36, pp. 9519–9526, 2010, doi: 10.1016/j.biomaterials.2010.08.035.

[359] M. Yoshinari, T. Kato, K. Matsuzaka, T. Hayakawa, and K. Shiba, "Prevention of biofilm formation on titanium surfaces modified with conjugated molecules comprised of antimicrobial and titanium-binding peptides," *Biofouling*, vol. 26, no. 1, pp. 103–110, 2010, doi: 10.1080/08927010903216572.

[360] J. Chen *et al.*, "Antimicrobial Titanium Surface via Click-Immobilization of Peptide and Its in Vitro/Vivo Activity," *ACS Biomater. Sci. Eng.*, vol. 5, no. 2, pp. 1034–1044, 2019, doi: 10.1021/acsbiomaterials.8b01046.

[361] J. Hernandez-Montelongo *et al.*, "Electrostatic immobilization of antimicrobial peptides on polyethylenimine and their antibacterial effect against Staphylococcus epidermidis," *Colloids Surfaces B Biointerfaces*, vol. 164, pp. 370–378, 2018, doi: 10.1016/j.colsurfb.2018.02.002.

[362] R. Boöttger, R. Hoffmann, and D. Knappe, "Differential stability of therapeutic peptides with different proteolytic cleavage sites in blood, plasma and serum," *PLoS One*, vol. 12, no. 6, pp. 1–15, 2017, doi: 10.1371/journal.pone.0178943.

[363] J. S. Bond, "Proteases: History, discovery, and roles in health and disease," *J. Biol. Chem.*, vol. 294, no. 5, pp. 1643–1651, 2019, doi: 10.1074/jbc.TM118.004156.

[364] K. L. Zapadka, F. J. Becher, A. L. Gomes dos Santos, and S. E. Jackson, "Factors affecting the physical stability (aggregation) of peptide therapeutics," *Interface Focus*, vol. 7, no. 6, 2017, doi: 10.1098/rsfs.2017.0030.

[365] D. Psimadas, P. Georgoulias, V. Valotassiou, and G. Loudos, "Molecular Nanomedicine Towards Cancer :," *J. Pharm. Sci.*, vol. 101, no. 7, pp. 2271–2280, 2012, doi: 10.1002/jps.

[366] C. Adessi and C. Soto, "Converting a Peptide into a Drug: Strategies to Improve Stability and Bioavailability," *Curr. Med. Chem.*, vol. 9, no. 9, pp. 963–978, 2005, doi: 10.2174/0929867024606731.

[367] F. Pucci, R. Bourgeas, and M. Rooman, "Predicting protein thermal stability changes upon point mutations using statistical potentials: Introducing HoTMuSiC," *Sci. Rep.*, vol. 6, no. February, pp. 1–9, 2016, doi: 10.1038/srep23257.

[368] A. Saini and G. Verma, *Peptoids: tomorrow's therapeutics*. Elsevier Inc., 2017.

[369] J. Sun and R. N. Zuckermann, "Peptoid polymers: A highly designable bioinspired material," *ACS Nano*, vol. 7, no. 6, pp. 4715–4732, 2013, doi: 10.1021/nn4015714.

[370] M. T. Dohm, R. Kapoor, and A. E. Barron, "Peptoids: Bio-Inspired Polymers as Potential Pharmaceuticals," *Curr. Pharm. Des.*, vol. 17, no. 25, pp. 2732–2747, 2012, doi:

10.2174/138161211797416066.

[371] A. Sharma, A. Kumar, B. G. De La Torre, and F. Albericio, “Liquid-Phase Peptide Synthesis (LPPS): A Third Wave for the Preparation of Peptides,” *Chem. Rev.*, vol. 122, no. 16, pp. 13516–13546, 2022, doi: 10.1021/acs.chemrev.2c00132.

[372] A. M. Clapperton, J. Babi, and H. Tran, “A Field Guide to Optimizing Peptoid Synthesis,” *ACS Polym. Au*, vol. 2, no. 6, pp. 417–429, 2022, doi: 10.1021/acspolymersau.2c00036.

[373] S. Gottschalk *et al.*, “The antimicrobial lysine-peptoid hybrid LP5 inhibits DNA replication and induces the SOS response in Staphylococcus aureus,” *BMC Microbiol.*, vol. 13, no. 1, p. 1, 2013, doi: 10.1186/1471-2180-13-192.

[374] L. Xu *et al.*, “Antimicrobial activity and membrane-active mechanism of tryptophan zipper-like β-hairpin antimicrobial peptides,” *Amino Acids*, vol. 47, no. 11, pp. 2385–2397, 2015, doi: 10.1007/s00726-015-2029-7.

[375] B. Mojsoska, R. N. Zuckermann, and H. Jenssen, “Structure-activity relationship study of novel peptoids that mimic the structure of antimicrobial peptides,” *Antimicrob. Agents Chemother.*, vol. 59, no. 7, pp. 4112–4120, 2015, doi: 10.1128/AAC.00237-15.

[376] A. Lone, A. Arnous, P. R. Hansen, B. Mojsoska, and H. Jenssen, “Synthesis of Peptoids Containing Multiple Nhtrp and Ntrp Residues: A Comparative Study of Resin, Cleavage Conditions and Submonomer Protection,” *Front. Chem.*, vol. 8, no. April, pp. 1–12, 2020, doi: 10.3389/fchem.2020.00370.

[377] P. Saporito, B. Mojsoska, A. Løbner Olesen, and H. Jenssen, “ Antibacterial mechanisms of GN-2 derived peptides and peptoids against Escherichia coli ,” *Biopolymers*, vol. 110, no. 6, 2019, doi: 10.1002/bip.23275.

[378] J. J. Harrison, C. A. Stremick, R. J. Turner, N. D. Allan, M. E. Olson, and H. Ceri, “Microtiter susceptibility testing of microbes growing on peg lids : a miniaturized biofilm model for high-throughput screening,” *Nat. Protoc.*, 2010, doi: 10.1038/nprot.2010.71.

[379] C. Zvacek and F. Hagen, “An assessment of catalytic residue 3D- ensembles for the prediction of enzyme function FernUniversität in Hagen Prof . Dr . Jörg Keller An assessment of catalytic residue 3D-ensembles for the prediction of enzyme function Master ’ s thesis Submitted by :,” no. September 2014, 2016.

Appendix A

Article

Surface Functionalization of Ti6Al4V-ELI Alloy with Antimicrobial Peptide Nisin

Mari Lallukka, Francesca Gamna, Virginia Alessandra Gobbo, Mirko Prato, Ziba Najmi , Andrea Cochis, Lia Rimondini, Sara Ferraris and Silvia Spriano

Abstract: Implant-associated infections are a severe global concern, especially in the case of orthope- dic implants intended for long-term or permanent use. The traditional treatment through systemic antibiotic administration is often inefficient due to biofilm formation, and concerns regarding the development of highly resistant bacteria. Therefore, there is an unfulfilled need for antibiotic-free alternatives that could simultaneously support bone regeneration and prevent bacterial infection. This study aimed to perform, optimize, and characterize the surface functionalization of Ti6Al4V-ELI discs by an FDA-approved antimicrobial peptide, nisin, known to hold a broad antibacterial spectrum. Accordingly, nisin bioactivity was also evaluated by in vitro release tests both in physiological and

inflammatory pH conditions. Several methods, such as X-ray photoelectron spectroscopy (XPS), and Kelvin Probe atomic force microscopy confirmed the presence of a physisorbed nisin layer on the alloy surface. The functionalization performed at pH 6–7 was found to be especially effective due to the nisin configuration exposing its hydrophobic tail outwards, which is also responsible for its antimicrobial action. In addition, the first evidence of gradual nisin release both in physiological and inflammatory conditions was obtained: the static contact angle becomes half of the starting one after 7 days of soaking on the functionalized sample, while it becomes 0◦ on the control samples. Finally, the evaluation of the antibacterial performance toward the pathogen *Staphylococcus aureus* after 24 h of inoculation showed the ability of nisin adsorbed at pH 6 to prevent bacterial microfouling into biofilm-like aggregates in comparison with the uncoated specimens: viable bacterial colonies showed a reduction of about 40% with respect to the un-functionalized surface and the formation of (microcolonies (biofilm-like aggregates) is strongly affected.

1.Introduction

Metallic materials are one of the main categories of biomaterials employed for muscu- loskeletal applications. Especially, titanium-based alloys, such as Ti6Al4V typically used for medical implants, and its extra-low interstitial version Ti6Al4V-ELI with improved fracture toughness and corrosion resistance [1], are suitable for medical use. In general, titanium and its alloys are well tolerated by the human body. However, there are still challenges associated with infection, acute and chronic inflammation, osteolysis, implant loosening, and failure [2].

One of the main issues of modern orthopedics is to promote osteointegration and simultaneously prevent infection and biofilm formation. In addition, the increasing threat of antimicrobial resistance has shifted the research focus toward antibiotic-free alternatives [3].

Conventionally, antibiotics are administered systemically to the patient, but since the desired site is often covered by biofilm preventing antibiotic penetration, local delivery of an antibacterial agent or initial prevention of the bacterial adhesion would be more viable options [4]. In addition, local delivery of antibacterial agents could reduce the risk of toxic dosage and resistance building because a lower concentration of antimicrobials would be needed compared to systemic antibiotics [4].

To respond to the medical need for biocompatible and antibacterial orthopedic de- vices, several strategies to tailor metal implant surfaces are being studied. The surface modification strategy can either indirectly inhibit bacterial adhesion and biofilm formation (antiadhesive or anti-microfouling action) or directly kill adhered bacteria (bactericidal action) [5]. Currently investigated approaches include surface coatings, modification of surface chemistry and topography of the material, and the incorporation of antimicrobial agents into biomaterials [3]. Regarding the non-antibiotic antimicrobial agents, there are several options investigated, such as metal ions and oxides, polymers, enzymes, quorum sensing drugs, bacteriophages, or antimicrobial peptides [3,6–11].

Antimicrobial peptides (AMPs) are small, usually cationic peptides with a broad antimicrobial spectrum and immunomodulatory activity against bacteria, viruses, and fungi [12]. One of the most studied and used AMP is nisin, first identified in 1928 in fermented milk cultures. It is better known as a food preservative used in several products including dairy products. Nisin is FDA-approved and implemented worldwide in several food-related applications [13].

Regarding its structure, nisin ($C_{143}H_{230}N_{42}O_{37}S_7$) is a pentacyclic post-translationally modified peptide composed of 34 amino acids with a weight of 3354.12 Daltons [14]. It is a class I A lantibiotic bacteriocin produced by *Lactococcus lactis*. Lantibiotics refer to ribosoma- lly synthesized antimicrobial compounds of bacterial origin, which contain unusual amino acids, such as, in the case of nisin, didehydroalanine, didehydroaminobutyric acid, lanthio- nine, and β-methyl-lanthionine [14]. In addition, the structure of nisin is characterized by several internal disulphide bridges. There are several characterized forms of nisin, nisin A being the most active [15]. Nisin can be considered an amphiphilic molecule since it has both hydrophilic and hydrophobic residues in its structure [15].
The hydrophobic residues of nisin are identified to be responsible for its antimicrobial activity [16,17]. Concerning its stability, nisin is known to be highly stable in acidic pH, in which it can also withstand high temperatures [12]. The chemical structure of nisin is displayed in Figure 1A.

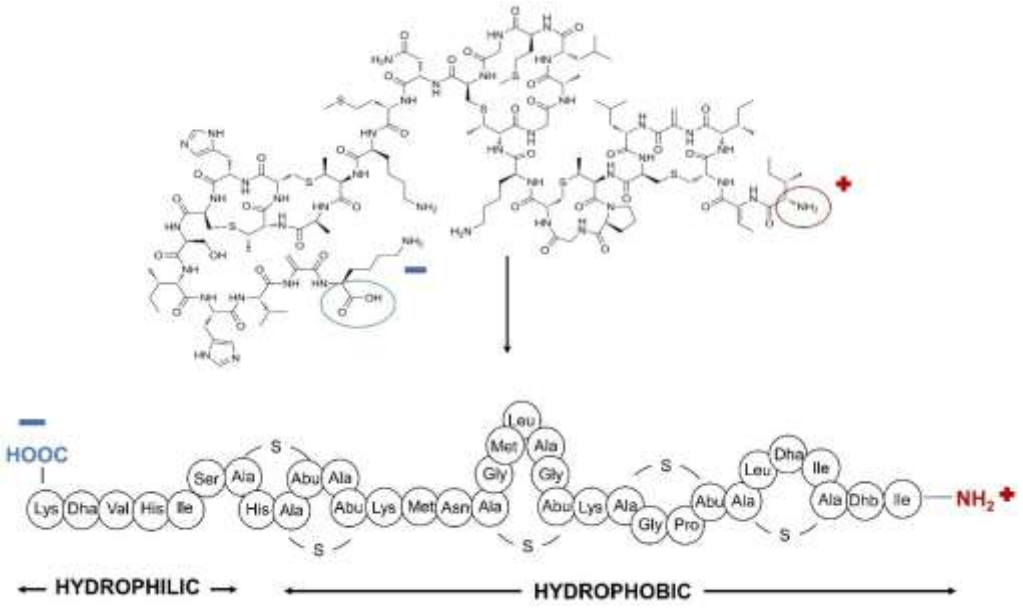

Figure 1A. Chemical and primary structures of the nisin polypeptide.

Nisin is known to exhibit antimicrobial activity mainly against Gram-positive bacte- ria. Gram-negative bacteria are problematic because nisin hardly penetrates their outer membrane barrier, and thus reaching its target lipid II in the inner membrane could be chal- lenging. However, nisin is effective also against Gram-negative bacteria when combined with chelating agents, such as ethylenediaminetetraacetic acid (EDTA), citrate monohy- drate, trisodium orthophosphate, or with heat treatments, or freezing [16]. The nisin mechanism of action is widely characterized and consists of several steps. Firstly, nisin binds to the anionic phospholipids (lipid II) on the cytoplasmic membrane of the bacteria, inhibiting their cell wall formation. Subsequently, the peptide forms an ion channel or a pore on the membrane, leading to a fatal efflux of intracellular products, such as adenosine triphosphate (ATP) and potassium [18].

Recently, in addition to its exploitation as a preservative in the food industry, the potential of nisin in biomedical applications has gained interest [4]. In the context of infections, the antimicrobial effects of nisin have been reported against mastitis [19], respira- tory [20], gastrointestinal [21,22], and skin infections [23]. Moreover, nisin has been found to exhibit selective cytotoxicity toward cancer cells and influence tumor growth [24–26]. In addition, besides antimicrobial properties, several studies suggest that nisin can also show immunomodulatory properties mainly by affecting cytokine production [27]. Some evidence of the effect of nisin on innate and adaptive immune cells also has been observed [28]. However, due to various discrepancies between the results and high variability in the experimental models, more studies are therefore required to verify the effect [15].

AMPs can be grafted on the surface with covalent bonds thanks to the amines, car- boxylic acids, thiols, and hydroxyls in their inherent structure [29]. Ideally, the peptide should stay stable and in its active form in the coating, without the impact of the envi- ronmental conditions on the contact surface that is exposed. Simultaneously, the peptide should be possible to be released from the surface so that it will provide antimicrobial performance [30]. Covalent bonding of nisin has been implemented to stainless steel sur- faces by previously applying a chitosan layer to increase the affinity, and the adsorbed peptides were found to decrease bacterial adhesion on the functionalized surface [31]. Immobilization and release of nisin nanoparticles have also been studied from the cracked and uncracked oxide films on stainless steel and titanium [30,32]. In addition to metal- lic materials, nisin has also been grafted onto glass substrates by using dopamine as a coupling agent [33].

In terms of incorporating AMPs as a coating to biomaterial surfaces, current challenges are related to the possible hydrolysis and denaturation of the coating due to pH and temperature, which could compromise their antimicrobial activity. It is also possible that the activity of AMP decreases because of its functional groups essential

for antimicrobial action covalently linking to the surface, rendering the peptide inactive [29].

This work aims to develop a biocompatible and antibacterial surface by nisin func- tionalization. To the extent of our knowledge, there is no work adsorbing nisin on the surface of Ti64ELI alloy. In this work, the surface functionalization process of the Ti64ELI titanium alloy with antimicrobial peptide nisin has been optimized, without the addition of any toxic linker, varying the process parameters such as the pH value of the nisin solution during the functionalization process. The surface functionalization is evidenced by several methods, followed by release tests both in physiological and inflammatory mimicking con- ditions assessing the expected mechanism of antibacterial action. Finally, the antibacterial

performance of the adsorbed nisin-coating has been assessed towards the *Staphylococcus aureus* (*S. aureus*) strain for 24 h showing promising anti-microfouling activity.

2.Materials and Methods

2.1. Sample Preparation

Ti6Al4V-ELI (Grade 23, Titanium Consulting and Trading S.r.l., Firenze, Italy) 10 mm diameter 2 mm thickness discs were employed for the experimental study. Discs were polished with SiC abrasive papers up to 4000 grit. The polished discs were then sonicated once for 5 min in acetone, and successively twice for 10 min in ultrapure (Milli-Q) water to remove contaminations eventually present on the sample surfaces. From now on, these samples will be named TI64ELI-MP (mechanically polished).

2.2. Functionalization of Sample Surfaces with Nisin

TI64ELI-MP samples were UV-C-irradiated (UV-C 40 W, 253.7 nm, Philips TUV T8) for one hour before functionalization to activate the surface. Antimicrobial peptide nisin (Nisin Ready Made Solution, 20,000–40,000 IU/mL in 0.02 N HCl, Sigma-Aldrich, Milan, Italy) was used for biological functionalization. A nisin concentration of 1 mg/mL in ultrapure water was used for the study in solutions with three different pH: pH 5, pH 6, and pH 7. The pH was adjusted by buffering the initial solution with 1 M NaOH and 1 M HCl, monitoring it with a pH meter (Edge pH, HANNA Instruments Italia S.r.l., Padova, Italy). An amount of 5 mL of the functionalization solution was used to treat each sample. Samples were left to functionalize for 24 h at room temperature in closed containers. After functionalization, samples were washed twice in ultrapure water and left to dry in the air. From now on, nisin-functionalized samples are referred to as TI64ELI-MP NISIN pH= 3/5/6/7. In addition, control samples (TI64ELI-MP CTRL pH = 5/6/7) were prepared by soaking the TI64ELI-MP samples in 5 mL of ultrapure water, previously pH-adjusted according to the respective pH values.

2.3. *Physical-Chemical Characterization*

2.3.1. Energy-Dispersive X-ray Spectroscopy (EDS)

EDS (JCM-6000 Plus Benchtop SEM, Jeol, equipped with EDS, Tokyo, Japan) was performed on both bare and nisin-functionalized samples to assess the changes in elemental composition using the accelerating voltage of 15 kV.

2.3.2. UV–Vis Spectroscopy and Reflectance

Reflectance measurement was performed for both bare and nisin-functionalized sam- ples by means of a UV–Vis spectrophotometer (UV-2600 Shimadzu, Kyoto, Japan, equipped with ISR-2600Plus integration sphere). The spectrum of 190–750 nm was evaluated in the measurements.

2.3.3. Surface Wettability

The surface wettability of the samples was evaluated utilizing static contact angle measurement by the sessile drop method (Krüss DSA 100, KRÜSS GmbH, Hamburg, Germany). Ultrapure water was used as a wetting fluid. A drop of water (5 μL) was deposited on the surface with a pipette and the contact angles were measured through the instrument software (DSA-100, Dropshape Analysis, KRÜSS GmbH, Hamburg, Germany).

2.3.4. Zeta Potential

The zeta potential measurements were performed using an electrokinetic analyzer (SurPASS 2, Anton Paar, Graz, Austria), equipped with an adjustable gap cell. The surface zeta potential was measured as a function of pH in a 0.001 M KCl electrolyte solution. Separate couples of TI64ELI discs were used for the two titrations to avoid artifacts due to possible surface reactions occurring during the measurements. First, acidic titration was performed by adding 0.05 M HCl. Secondly, basic titration was performed with 0.05 M NaOH. Four parallel measurements were carried out for each pH point measured.

In addition to solid sample zeta potential measurements, the zeta potential of 1 mg/mL nisin solution was measured using a dynamic light scattering (DLS) particle size and zeta potential analyzer (Nanosizer Nano Z, Malvern Instruments Ltd., Malvern, Worcestershire, UK). Concerning the functionalizing solution, the zeta

potential curve was obtained through the measurement of the electrophoretic mobility changing pH step by step from pH 2.5 to 9 by adding HCl 0.05 M or NaOH 0.05 M.

2.3.5. Kelvin Probe Force Microscopy (KPFM)

Nisin 1 mg/mL solution (pH 6) was added on top of the polished sample as a drop and left to functionalize overnight. The goal was to create an interface between bare and functionalized areas on the same sample surface. KPFM (Bruker Innova AFM, Billerica, MA, United States) in tapping mode was used to measure the surface potential of bare and nisin functionalized Ti64ELI, data were elaborated by the software Gwyddion (Gwyddion Version 2.62, Brno, Czech Republic).

2.3.6. X-ray Photoelectron Spectroscopy (XPS)

XPS (Kratos Axis UltraDLD, Kratos Analytical Co., Ltd., Manchester, UK) measure- ments were performed (survey spectra and high-resolution analyses of elemental regions) on the bare and nisin-functionalized samples to investigate the chemical composition of the outermost layer and, in addition, the presence of characteristic chemical groups for nisin. The hydrocarbon C 1s peak (284.80 eV) was used for the calibration of the binding energy scale.

2.3.7. Release Test

Release tests were performed following the procedure described in [34]. Shortly, tests were performed both in PBS (pH 7.4, Sigma Aldrich, Milan, Italy) and in hydrogen peroxide (50 mM H_2O_2, 30% *w/v*, PanReac Applichem, Monza, Italy; in PBS) with pH adjusted at 4.50 to mimic both physiological and inflammatory conditions, respectively. Each nisin- functionalized sample was soaked in a 5 mL solution for 7 days at 37 ˚C. The considered time points were 1 and 7 days. Afterward, the samples were washed once with ultrapure water and let to air dry. In addition, the contact angles of the samples were measured after soaking.

2.4. *Antibacterial Properties Evaluation*

2.4.1. Strain Growth Condition

Bacteria were purchased from the American Type Culture Collection (ATCC, Man- assas, VA, USA). Specimens' antibacterial properties were assayed towards the methi- cillin/oxacillin (MRSA) resistant *Staphylococcus aureus* strain (Gram-

positive, ATCC 43300). Bacteria were cultivated in trypticase soy agar plates (TSA, Sigma-Aldrich, Milan, Italy) and incubated at 37 °C until round single colonies were formed; then, 2–3 colonies were collected and spotted into 15 mL of Luria Bertani broth (LB, Sigma-Aldrich, Milan, Italy) and incubated overnight at 37 °C under agitation (120 rpm). The day after, a fresh broth culture was prepared before the experiments by diluting bacteria into a fresh medium to a final concentration of 1×10^3 bacteria/mL, corresponding to an optical density of 0.00001 at 600 nm wavelength using a spectrophotometer (Spark, from Tecan Trading AG, Mannedorf, Switzerland) [35].

2.4.2. Bacterial Metabolism, Number of Viable Colonies, and Morphology Evaluation

The International Standard ISO 22196 was applied to evaluate specimens' antibacterial properties [36]. Accordingly, the specimens (Ti64ELI-MP nisin pH6, Ti64ELI-MP nisin pH3, and Ti64ELI-MP, considered as control) were located into a 24-multiwell plate; then, 50 µL of the bacterial suspension was adjusted at a final concentration of 1×10^3 bacteria and it was directly dropped onto the specimens' surfaces. To confirm the nisin bioactivity at pH = 6, the samples prepared with the pH = 3 nisin stock solution from the manufacturer were also evaluated for their ability in preventing bacterial colonization.

The inoculated specimens were placed in an incubator at 37 °C for 24 h. Afterward, the colorimetric Alamar blue assay (AlamarBlue™, Life Technologies, Milan, Italy) was applied to test viable bacteria metabolic activity by spectrophotometry following the manufacturer's instructions. Briefly, the ready-to-use Alamar solution at concentration 0.0015% in PBS was added to each well containing the test specimen (1 mL per specimen), and the plate was incubated in the dark for 4 h at 37 °C allowing resazurin dye reduction into fluorescent resorufin upon entering living cells. Then, 100 µL were spotted into a black-bottom 96-well plate to minimize the background signal. The metabolic activity of bacteria was measured via spectrophotometer (λex = 570 nm and λem = 590 nm), and the results were presented as relative fluorescent units (RFU).

Then, to investigate the number of viable bacteria adhered to the samples' surface the colony forming unit (CFU) count was performed. Briefly, after washing 2 times with PBS to remove non-attached bacterial cells, the samples were submerged into 1 mL of PBS, sonicated, and vortexed for 5 min and 30 s, respectively (three times each). Next, an aliquot of 200 µL of the bacteria suspension was collected and transferred to a new 96 wells plate; here, 6 serials 1:10 dilutions were performed by mixing progressively 20 µL of the bacterial suspension with 180 µL of PBS. Then,

20 µL of each serial dilution were spotted into an LB agar plate and incubated for 24 h until round colonies were visually checked; the final number of CFU was calculated by using the following formula [37]:

CFU = [(number of colonies × dilution factor) (serial dilution)].

Finally, scanning electron microscopy (SEM, JSM-IT500, JEOL, Tokyo, Japan) imaging was used to investigate the bacterial microcolonies formed on the samples' surfaces; briefly, specimens were dehydrated by the alcohol scale (70–90–100% ethanol, 1 h each), swelled with hexamethyldisilazane, mounted onto stubs with conductive carbon tape and covered with a gold layer. Images were collected at different magnifications (2000× and 5000×) using secondary electrons. Additionally, the presence of single microcolonies or 3D biofilm- like aggregates on the samples' surfaces as well as their distribution were analyzed through 3D reconstructed images extracted from SEM images using the SMILE VIEW^{TM} map software (JEOL, Tokyo, Japan).

2.5. *Statistical Analysis of Data*

Experiments were performed in triplicate. Results were statistically analyzed using the SPSS software (v.20.0, IBM, New York, NY, USA). Groups were compared by the one-way ANOVA using Tukey's test as a post hoc analysis. Significant differences were established at $p < 0.05$.

3.Results and Discussion

3.1. Physical-Chemical Evaluation

First, this research is aimed at verifying the effectiveness of the surface functionaliza-tion of the Ti6Al4V-ELI alloy with nisin and comparing different functionalization processes at different pH values (pH = 5/6/7). The pH range of interest has been selected consideringthat strong acidic or basic solutions could corrode the titanium alloy. The presence of nisin on the functionalized surfaces was evaluated through EDS, XPS (survey quantitativeanalysis), UV–Vis reflectance, and KPFM.

The EDS analysis of the bare and nisin-functionalized samples (Figure 2A) evidences the presence of all the elements characteristic of the surface of the titanium alloy: Ti, Al, V,and O. A slight increase in nitrogen (N) is noticed comparing the bare and functionalized surfaces, suggesting the presence of the nisin polypeptide on the sample surface; this enhancement is much more significant for the sample functionalized at pH 6, where an increase in carbon (C) is also detectable. Considering the high penetration depth of EDS (higher than 1 micron) and the expected low thickness of the functionalized surface layer,the high standard deviation obtained by this analysis is not surprising. The surface chemical analysis was confirmed through XPS quantitative analysis, which is much more suitable for the chemical characterization of the outermost surface layer thanks to its nanoscale sampling depth, which makes it a more sensitive surface analysis technique [38].

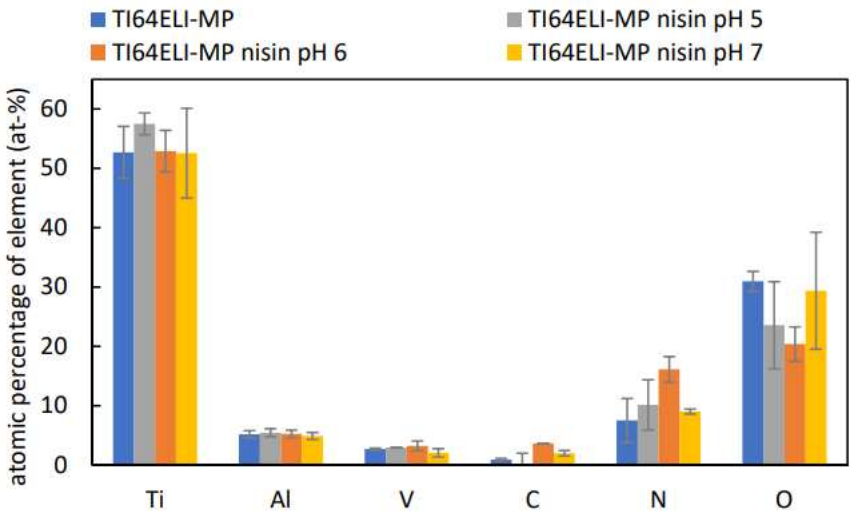

Figure 3A. EDS analysis of MP samples, both bare and functionalized surfaces with processes at different pH values (pH = 5/6/7).

The XPS quantitative analysis of the bare and functionalized surfaces, with processes at different pH values, is reported in Table 1.

Table 1A. XPS quantitative analysis of the bare MP sample and surfaces functionalized with processes at different pH values. Error for all the values is indicated at 0.1 at-%.

Elements (Atomic Percentage, at-%)	TI64ELI-MP	NISIN pH 5	NISIN pH 6	NISIN pH 7
C	35.9	64.3	60.2	56.2
O	43.3	24.4	25.3	28.4
N	0.5	4.7	4.5	4.2
Ti	11.1	4.3	5.4	6.0
Al	3.4	0.6	2.0	1.6
S	0.3	0.2	0.2	0.3
Others	5.5	1.4	2.6	3.2

The more detailed high-resolution spectra are discussed later in the article. A significant increment of C and N is observed after the functionalization at any pH, with respect to MP as a control. This is coherent with the expected formation of a polypeptide surface layer. Conversely, there is a decrease in Ti, O, and Al on nisin-functionalized surfaces, which is explainable because the titanium oxide layer and metal alloy are covered by the adsorbed nisin layer. S is detected in a too low amount compared to the amount on the MP control sample to be considered significant. No relevant

difference among the surfaces functionalized at the different pH is registered by this technique, apart from a slightly higher contribution from the adsorbed polypeptide (C and N) and lower from the elements of the titanium alloy in the case of the sample functionalized at pH 5–6.

The UV–Vis spectra of the bare and functionalized samples have been measured in reflectance (Figure 4A).

These data evidence an attenuation, after functionalization, of the surface reflectance along all the measured ranges of wavelength. This agrees with the presence of a surface adsorbed layer able to reduce the high reflectance of the metal surface. No significant difference among the surfaces functionalized at different pH values can be detected by this technique.

In addition, KPFM has been used for imaging the functionalized surface. A sample functionalized at pH 6 has been chosen for this experiment due to its highest amount of the adsorbed nisin evidenced by EDS and XPS measurements. An internal control surface is needed for this analysis. For this purpose, a sample functionalized only on the half surface and with a sharp border between the functionalized and un-functionalized area has been prepared. When comparing the bare (lighter area) and functionalized (darker) areas of this sample, a clear difference in the surface electrical potential is detected across the interface (Figure 5A). This is a further confirmation of the presence of the functionalized surface layer. No evident formation of nisin micrometric aggregates on the surface can be evidenced while the covering seems not homogeneous.

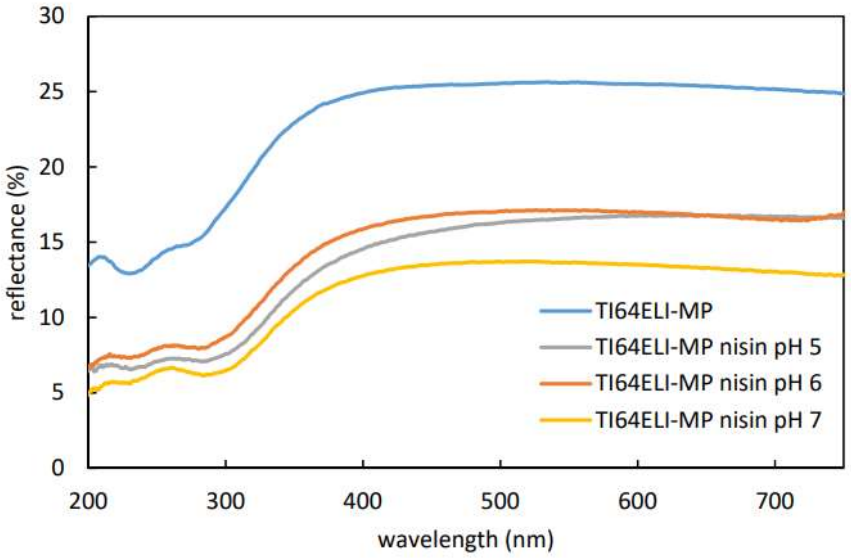

Figure 4A. UV–Vis reflectance spectra of the MP samples both bare and surfaces functionalized with processes at different pH values.

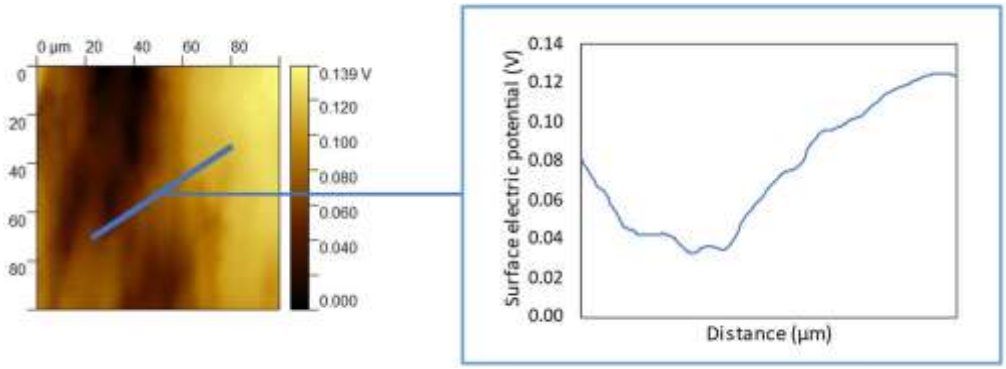

Figure 5A. KPFM surface potential as a function of the distance across the interface between a bare (light area) and nisin-functionalized (darker area) region (functionalization at pH 6).

In addition to evidencing the presence of the nisin layer on sample surfaces, further analyses have been performed to characterize the functionalized surfaces: contact angle measurement, zeta potential titration curves, and profile fitting of the XPS data (high-resolution spectra) have been acquired.

The modification in wettability due to the functionalization was verified by static contact angle measurements (Figure 6A).

It must be considered an eventual contribution due to a modification of the titanium oxide layer during the soaking in solutions at different pH, regardless of the presence of nisin. This effect has been considered by considering some control samples soaked, at any pH value, in analogous solutions without nisin (TI64MP-CTRL, blue bars in Figure 6A). As displayed in Figure 6A, the contact angle of the control samples decreases by increasing the pH of the solution. The opposite phenomenon is observed for the samples function- alized with nisin. At first, these data confirm the presence of nisin on the functionalized samples because of a different wettability than the bare and the control ones. Overall, all the functionalized samples are more hydrophilic than the bare substrate MP, with a maximum
difference for the sample functionalized at pH 5. In this case, the presence of nisin induces an increase in wettability even larger than the relative control. A conformation of the ad- sorbed nisin exposing the hydrophilic moieties outwards is then hypothesized.

Contrarily, the presence of nisin on the surface of the samples functionalized at pH 6 and 7 induces a lower wettability with respect to the control samples: a conformation of the adsorbed nisin exposing the hydrophobic moieties outwards can be supposed in these cases. Considering that the hydrophobic

tail is the active antibacterial functionality of nisin [39], it can be speculated that this process is much more effective for antimicrobial applications.

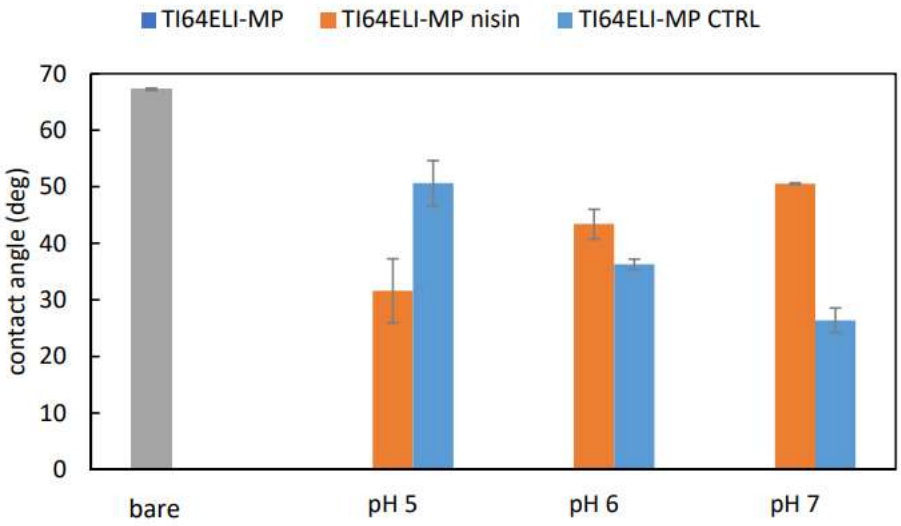

Figure 6A. The contact angles measured on the bare MP sample (grey), samples functionalized with processes at different pH values (orange), and control samples soaked in solutions at different pH without nisin (blue).

Through DLS, the hydrodynamic diameter and zeta potential of nisin in aqueous suspensions (1 mg/mL) at different pH were measured (Figure 7A).

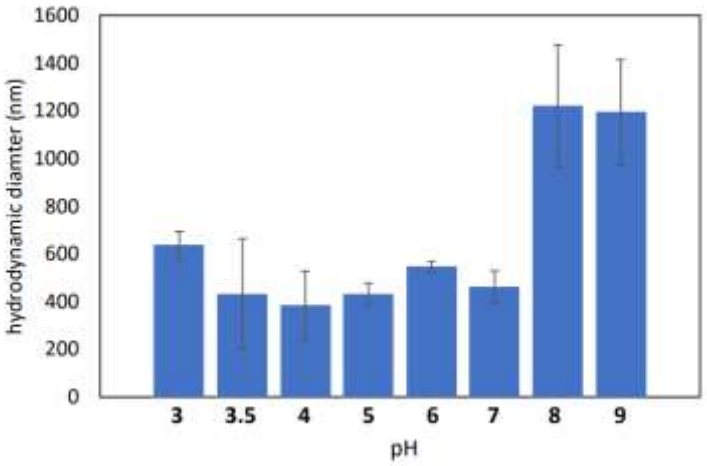

Figure 7A. The hydrodynamic diameter of nisin, measured by DLS analysis, in aqueous suspension as a function of pH.

The hydrodynamic diameter is about 400–600 nm at pH between 3 and 7, while itabruptly grows up to 1.2 microns above pH 8 evidencing that the colloidal suspension
becomes less soluble and unstable at alkaline pH values. According to these data, thefunctionalization process cannot be performed at pH equal to or higher than 8, if the formation of agglomerates must be avoided. This is also in agreement with the literature reporting the solubility of nisin to decrease with increasing pH value [40].

The zeta potential titration curves of the bare and nisin-functionalized samples areshown in Figure 8A, together with the zeta potential titration curve of the nisin solutionobtained by DLS.

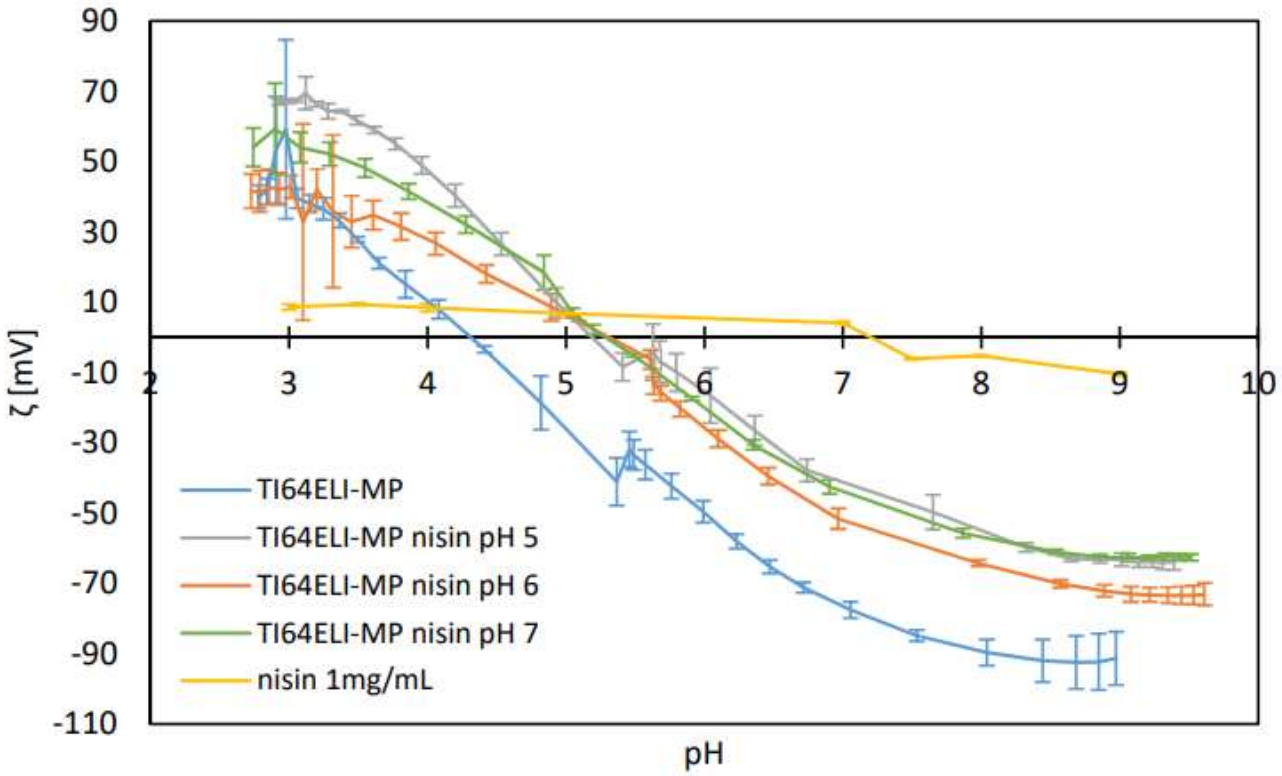

Figure 8A. Zeta potential titration curves of the bare MP sample, surfaces functionalized with processes at different pH values, and a solution of nisin.

Different information can be extracted from these curves: the isoelectric point (IEP),the chemical stability of the surface as a function of pH (related to the error bars of the zetapotential), and the expected difference of net charge between the biomolecule and titanium surface during the functionalization process.

The IEP of the bare MP sample is close to 4.5, which is expected for a surface without functional groups with a strong acid–basic behavior. The expected IEP value of nisin is approximately 8.5, based on the literature [40]. It has been experimentally detected here at pH 7.5, the difference with the literature data can be due to the low absolute value of the measured zeta potential and high sensitivity of IEP by changing the electrolytic solution. In agreement with the detected IEP, an increase in the hydrodynamic radius has also beenregistered above this value of pH, as previously reported.

The IEP of the nisin-functionalized samples can be seen to shift to more basic pH values than the MP sample, in the direction of the nisin IEP, indicating a successful and similar functionalization with nisin on all surfaces. The IEP of the functionalized samples is different from the nisin one, suggesting that there is not a covering coating on the surface,but a layer of adsorbed molecules that allow the exposition of the substrate to the solution. The error bars of all the functionalized surfaces are the lowest in the pH ranging from 7.5 down to 4.5, which is the region of pH expected to occur in physiological and inflammatory conditions, respectively. This means that the adsorbed nisin is expected to bechemically stable on the surface even if the surrounding chemical environment changes in
pH after implantation.

Lastly, it is crucial to highlight the difference in the sign of the net charge detectedon the MP sample and the one characterizing nisin solution at the pH values used for functionalization (pH 5, 6, 7). Physisorption with an electrostatic attraction between the negatively charged metal surface and the overall positively charged polypeptide can be expected during the functionalization processes.

Considering that nisin at pH 7 is close to its IEP (almost no net charge on the biomolecule at pH 7) and, on the other side, that the absolute value of the zeta potential of the bare TI64ELI-MP is the lowest at pH 5 (minimum surface charge of the substrate within the explored range of pH for functionalization), the highest electrostatic interaction between the substrate and the physisorbed biomolecule can be expected to occur at pH 6.

The high-resolution spectra of the C 1s, N 1s, O 1s, and S 2p region of the bare MP sample and surfaces functionalized with processes at different pH values are reported in Figure 9A.

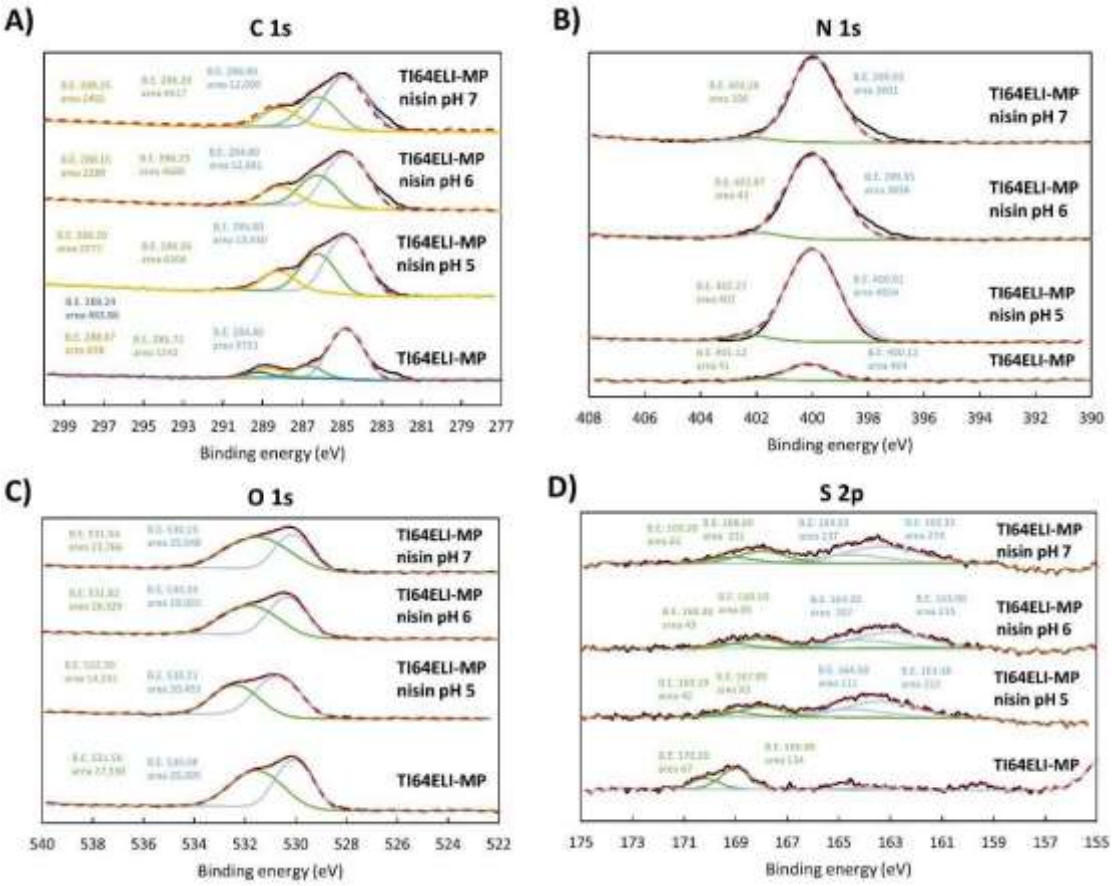

Figure 9A. High-resolution spectra of (**A**) C 1s, (**B**) N 1s, (**C**) O 1s, and (**D**) S 2p regions of the bare MP sample and surfaces functionalized with processes at different pH values. Black line (-): spectrum line, red dashed line (- - -): composite line.

Concerning the C peak (Figure 9A(A)), the peaks around 286 eV (C-O) and 285 eV (C-C)are higher on all the functionalized samples compared to the bare sample. An additional peak around 289 eV is evident on the bare sample, and it could relate to -COOH groups, while the one around 288 eV might be due to deprotonated ones.

The N peak (Figure 9A(B)) is significantly higher on the functionalized samples, as alreadynoticed, according to the presence of an adsorbed layer of the polypeptide. The peak coming
from the charged/protonated amino groups (NH_3^+) at 401.9 ± 0.2 eV is always very low with respect to the peak of the neutral aminic groups (NH_2) at 400.1 ± 0.2 eV, as evidenced by the profile fitting. This can be explained by hypothesizing a physisorption mechanism
for the functionalization, which would be coherent with the absence of any functional group with a net charge or high chemical reactivity on the substrate.

The presence of the adsorbed layer on the functionalized samples as a non-covering layer is confirmed by the profile fitting of the oxygen region (Figure 9A(C)). The peak dueto the Ti-O bond (~530 eV) of the titanium oxide layer is always observable. The peakat around 531.5 eV can be attributed to the OH -functional groups exposed by MP. This analysis consequently shows that the MP substrate is not completely lacking in functionalgroups.

Considering also the information obtained from the zeta potential titration curve,it can be concluded that the MP substrate has hydroxyl groups, but they do not have a strongly acidic or basic behavior and are not easily protonated or deprotonated in contact with liquid media. Consequently, they are not available for a chemisorption mechanism. A shift of this peak due to the presence of the peptide bond is observed in the functionalizedsamples. This is more evident in the case of the sample functionalized at pH 5, in agreement with the higher C and N amount detected on this sample in the survey chemical analysis.

Concerning the profile fitting of the S region (Figure 9A(D)), a contribution of the thioetherbridges -C-S-C- coming from the nisin backbone is observable on the functionalized samples. Regarding S high-resolution XPS data, each chemical state corresponds to a double ofpeaks, in the case of C-S-C (163 eV and 164 eV) [41]. The other detected S state, with the peak doublet approximately at 168 eV and 169 eV, could be due to the contribution of sulphonate groups ($C\text{-}SO_3\text{-}H$). However, as shown in the XPS survey scan (Table 1), no sound conclusion about the S contribution can be made due to the low detected amountsimilar to control samples without nisin.

Once characterized by the functionalized surfaces, two release tests have been per- formed to investigate the expected mechanism of action of the functionalized surface once in contact with a liquid environment chemically close to the physiological one. The samples functionalized at pH 6 have been used as an example, based on their expected high nisin content and the highest electrostatic difference between the substrate and the polypeptide, as discussed earlier. A control MP sample (without any functionalization layer) has been soaked in the same solution. The solution used for the first release test is PBS to mimic the physiological chemical environment. A second solution has been exploited to mimic an inflammatory chemical environment. It was obtained by adding hydrogen peroxide to PBS and reducing pH down to 4.5 [42]. The eventual change in the surfaces after the release tests has been monitored by the static contact angle measurements. The contact angle results of the release test are reported in Figure 10A.

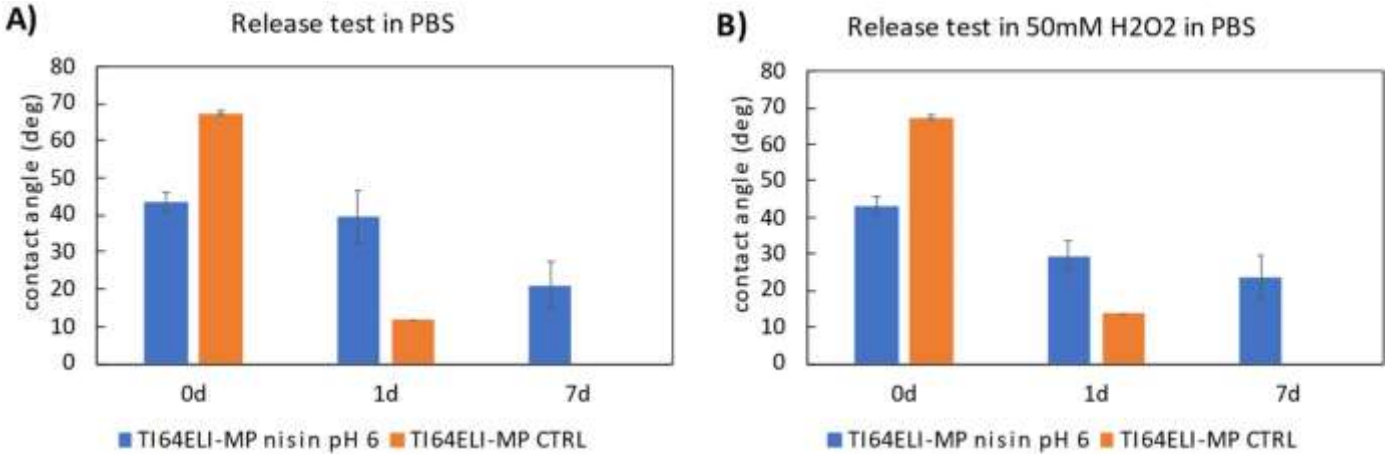

Figure 10A (**a**) The contact angles measured from non-soaked (0 d) and PBS-soaked (1 d, 7 d) samples. (**b**) The contact angles measured from non-soaked (0 d) and H_2O_2- soaked (1 d, 7 d) samples. Functionalization has been performed at pH 6.

A decrement in the contact angle is observed over the soaking time in both solutions. However, the contact angles of the functionalized and control samples are notably different, both after 1 and 7 days of soaking: this could mean that nisin is only partially released even after a week of soaking. According to these data, a double mechanism of action can be expected from the functionalized surface in a biological environment, through both release in the surrounding liquids (for a time longer than 1 day) and direct contact with cells and tissues (for a time shorter than 1 day). These data agree with the titration curves of the functionalized samples, where the surfaces show a stable zeta potential even changing the pH. Finally, a long-lasting effect can be expected by the functionalized surfaces, even longer than one week, which is not common concerning other functionalized surfaces [43].

To summarize, the presence of a physisorbed layer of nisin on the surface of func- tionalized samples was confirmed by several methods, such as EDS, XPS, and KPFM. In addition, the functionalization performed at pH 6 was found to favor the nisin configura- tion exposing its hydrophobic tail outwards, which is also known to be responsible for its antimicrobial action and to maximize the physisorption through electrostatic attraction. Fi-nally, as confirmed by the in vitro nisin release tests both in physiological and inflammatory conditions, evidence of gradual nisin release was obtained.

3.2. Physical-Chemical Evaluation

Finally, the antibacterial evaluation of the nisin-functionalized surfaces concerning Ti64ELI-MP (control specimen) was performed towards *Staphylococcus aureus* (*S. aureus*) which was selected as a reference strain due to its common involvement in bone infections.Moreover, specimens obtained by functionalization in the diluted stock solution of nisin at the original pH (pH = 3) were here exploited as a reference due to the known nisin sensibility to pH variation. Therefore, the Ti64ELI-MP nisin pH 6 was compared both to the bulk material and to the Ti64ELI-MP nisin pH 3 as well. The results of the colorimetric metabolic assay Alamar blue and SEM images are reported in Figure 11A (A,B), respectively,whereas Table 2 shows the viable bacterial colonies number (at serial dilution 10^5) from the CFU assay.

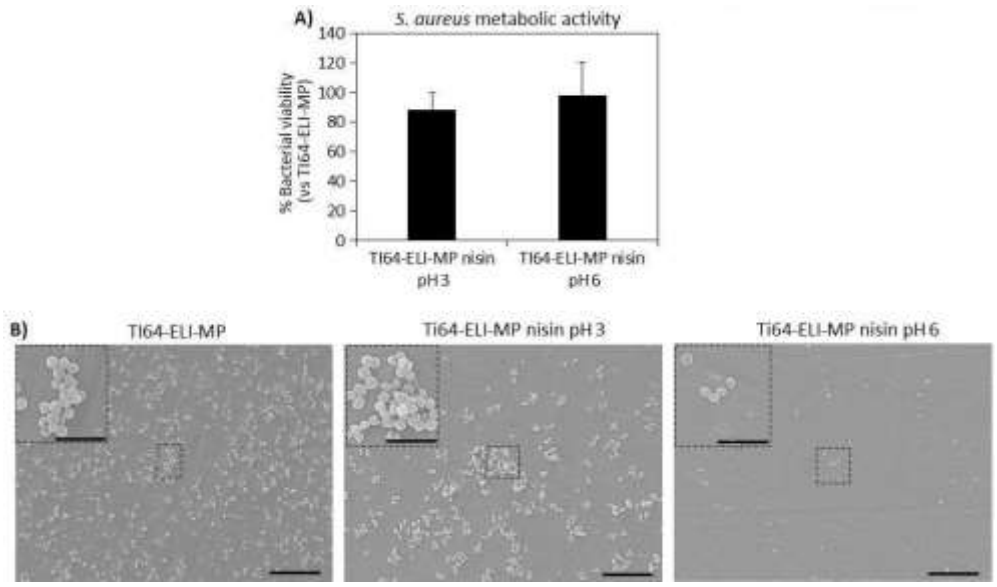

Figure 11A. Antibacterial activity evaluation of Ti64ELI-MP functionalized with nisin at pH 3 and pH 6 after 24 h; (**A**) metabolic activity of bacterial cells normalized towards bare substrate Ti64ELI-MP;
(**B**) SEM images at two magnifications: 2000× (scale bare = 10 µm) and 5000× (scale bar = 5 µm).

Table 2A. Viable bacterial colonies number (CFU count, means ±dev.st) after 24 h specimens' direct infection

Specimen	Viable Colonies Count (CFU, $\times 10^5$)
TI64ELI-MP	11 (±1)
TI64ELI-MP nisin pH 3	9 (±0.5)
TI64ELI-MP nisin pH 6	6.5 (±0.5)

In general, according to the metabolic activity assay, the samples functionalized with nisin at both pH 3 and pH 6 do not seem to show any statistically significant differences concerning bare Ti64ELI-MP substrates (Figure 11 A A, $p > 0.05$). However, viable bacterial colonies counting at serial dilution 10^5 (Table 2A) showed a reduction of about 40% and 28% in colonies number for Ti64ELI-MP nisin pH 6 in comparison to bare Ti64ELI-MP and Ti64ELI-MP nisin pH 3 samples' surfaces, respectively; this reduction is clearly noticed in SEM images collected from sample surfaces after 24 h of direct infection with bacteria (Figure 11A B). In fact, mostly single-round colonies were detected on the nisin-functionalized surfaces at pH 6 (Ti64ELI-MP nisin pH 6) whereas on the control (Ti64ELI-MP) and nisin-functionalized surfaces at pH 3 (Ti64ELI-MP nisin pH 3) the formation of many 3D micro-colonies (biofilm-like aggregates) was observed. Therefore, a promising anti-microfouling activity preventing the formation and maturation of microcolonies (biofilm-like aggregates) seems to be obtained by the functionalization with nisin, and the efficacy of the protocol at pH 6 is confirmed.

To investigate this activity in detail, 3D reconstructed images were prepared from SEM images at magnification 2000× and shown in Figure 12A. As reported in the cross- section of 3D reconstructed images of Ti64ELI-MP (Figure 12A C,D, extracted from SEM
image of Ti64ELI-MP shown in Figure 12A A) and Ti64ELI-MP nisin pH 3 (Figure 12A A G,H; extracted from SEM image of Ti64ELI-MP nisin pH 3 shown in Figure 12A E), almost all *S. aureus* formed 3D microcolonies aggregates on the samples' surfaces; in fact, Figure 11B,F show that the size of such microcolonies range between 4–5 µm for both Ti64ELI-MP and Ti64ELI-MP nisin pH 3 samples in comparison to the size of *S. aureus* of about 1–1.5 µm in- dicating that these 3D microcolonies are made up of about 3–4 layers of bacterial cells. The calculation of occupied surfaces with biofilm-like aggregates revealed 19.1% and 16.39% on the Ti64ELI-MP and Ti64ELI-MP nisin pH 3 were colonized by *S. aureus*, respectively (these data were extracted from the field of view of Figure 12A B,F as representatives of whole samples' surfaces). Surface analysis of 3D reconstructed images of Ti64ELI-MP nisin pH

6 (Figure 12A K,L; extracted from SEM image of Ti64ELI-MP nisin pH 6 shown in Figure 12A I) indicates that few bacterial colonies were able to form aggregates of more than 4 µm and most *S. aureus* remained as single cells (Figure 12A J,K,L); additionally, only 6.8% of the sample surface was occupied by bacterial microcolonies (these data were extracted from the field of view of Figure 12A J as a representative of whole samples' surfaces) in comparison to 19.1% for Ti64ELI-MP and 16.39% for Ti64ELI-MP nisin pH 3. From the results obtainedfrom the metabolic activity, viable bacterial colonies count (at serial dilution 10^5), SEM, and 3D reconstructed images analysis it can be concluded that Ti64ELI-MP functionalizedwith nisin at pH 6 have no bactericidal activity; however, it successfully prevented the bacterial aggregation into 3D biofilm-like aggregates thus reporting a promising antifouling activity. Similar results were found in another study where the synergistic antifouling properties of nisin and dopamine adsorbed to microstructured glasses with different sizes of grooves were reported against *Bacillus* sp. with respect to the control sample after 16 h [33]. Additionally, this similar effect was previously obtained by the authors intro-ducing a controlled nano-topography onto Ti alloys by electron beam technology thatprevented aggregates formation through a physical hindrance [44]; here, the nisin seems to play a similar role but via biochemical induction acting as an anti-aggregation sig- nal for adhered bacteria. Few comparable works can be found in the literature, but thepresence of nisin was previously shown by Blackman et al. [45] to reduce the surface con-tamination from bacterial aggregates in combination with a specific patterning as well as Kim et al. [46] demonstrated that the presence of nisin conferred outstanding fouling resistance to ultrafiltration PDMA membranes when infected.

One possible explanation for the observed ability of the nisin layer to prevent bacterial aggregates is the impact on biofilm maturation. In general, the formation of biofilm is known to consist of several steps including bacteria adhesion, irreversible attachment, biofilm maturation, bacteria dispersal, and bacterial migration. In addition, materials can behave as either anti-microfouling with bacteriostatic action, or as bactericides, acting with different mechanisms and on different stages of biofilm formation [47]. It can be speculated that the nisin-functionalized surface influences the maturation of the biofilm, therefore preventing the aggregation of bacteria. In the literature, nisin is also found to affect the composition and structure of the biofilm. Andre et al. evidenced the presence of nisin to result in a reduction of *S. aureus* biofilm polysaccharides and extracellular DNA, which can be associated with disrupted or decreased biofilm formation [48].

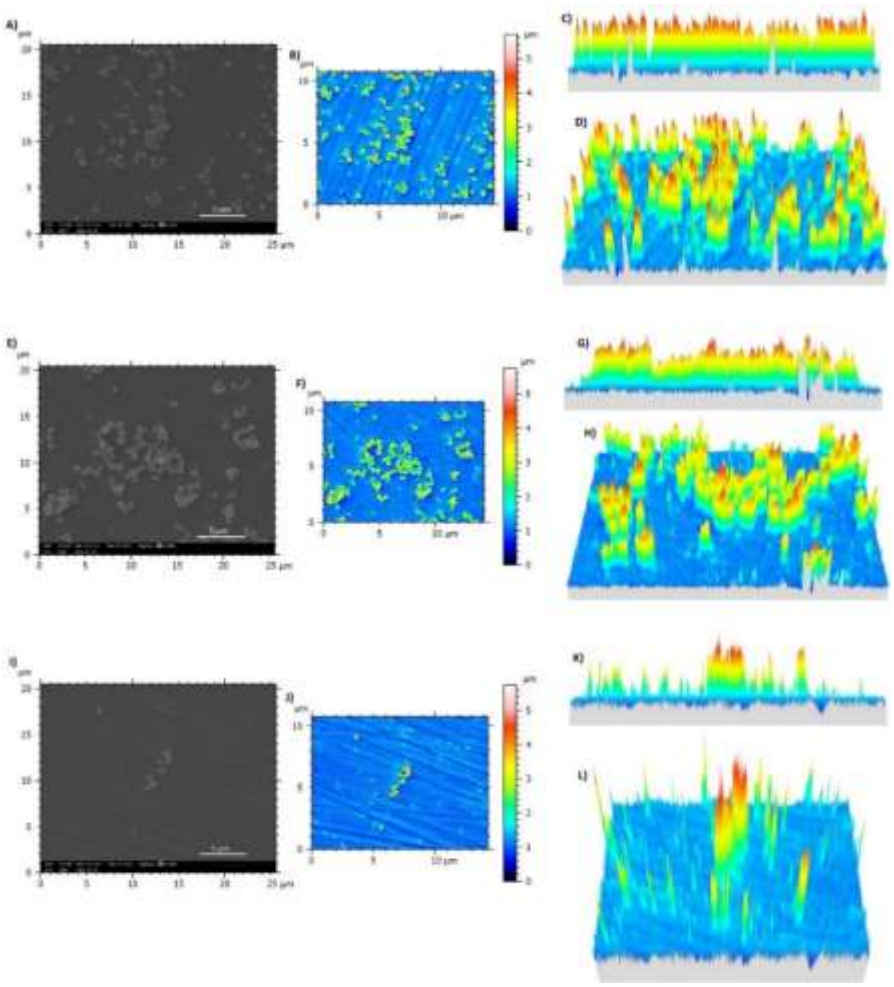

Figure 12A. Three-dimensional reconstructed images of bacterial microcolonies on samples' surfaces extracted from SEM images with SMILE VIEW^{TM} software. Ti64ELI-MP: (**A**) SEM image at magnifica- tion 2000× (scale bar= 5 µm); (**B**) reconstructed 3D image extracted from (**A**); (**C**) cross-section image of the bacterial microcolonies on the sample surface; (**D**) whole view of bacterial microcolonies from the selected section; Ti64ELI-MP nisin pH 3: (**E**) SEM image at magnification 2000× (scale bar= 5 µm);
(**F**) reconstructed 3D image extracted from (**E**); (**G**) cross-section of the bacterial microcolonies on the
sample surface; (**H**) whole view of bacterial microcolonies from the selected section; Ti64ELI-MP nisin pH 6: (**I**) SEM image at magnification 2000× (scale bar= 5 µm); (**J**) reconstructed 3D image extracted from (**I**); (**K**) cross-section of the bacterial microcolonies on the sample surface; (**L**) whole view of bacterial microcolonies from the selected section. Bars indicate the height of microcolonies (µm).

However, it seems evident that even though adsorbed nisin at pH 6 could prevent the formation of bacterial aggregates on the surface to some extent, the well-known antibacterial potential of nisin was not here fully maintained after surface functionalization. Similar results were found in another study where the antibacterial properties of nisin adsorbed to stainless steel against *Listeria monocytogenes* were similar with respect to control after 24 h [49]. The results obtained from the functionalization by using the nisin solutions at pH 3 and pH 6 seem to exclude the hypothesis that the low antibacterial activity is due to the molecule's sensitivity to pH variation: the functionalization at pH6 is revealed to be more effective in surface grafting and against microfouling and biofilm maturation. The contact-killing activity of nisin is mainly due to its binding with the bacterial membrane causing irreversible deadly pores [50]. So, further studies are still needed to improve the antibacterial efficacy of nisin, as well as other functionalization mechanisms, which could also be investigated to improve either the exposure of nisin's antibacterial groups or the release of the peptide to the solution.

Conclusions

The goal of this study was to characterize and optimize the surface functionalization of Ti6Al4V-ELI discs by the antimicrobial peptide nisin. The presence of nisin as a physisorbed layer on the surface was confirmed by different methods. It exposes the hydrophobic and anti-bacterial functionality toward the external environment when functionalization is performed at pH 6–7. In addition, the first evidence of gradual nisin release both in physiological and inflammatory conditions and as well as an anti-microfouling activity against bacteria, and the possible effect on biofilm maturation was preliminarily obtained.

References Appendix A

1. Eylon, D.; Fujishiro, S.; Postans, P.J.; Froes, F.H. High-temperature titanium alloys—A review. *JOM* **1984**, *36*, 55–62. [CrossRef]
2. Elias, C.N.; Lima, J.H.C.; Valiev, R.; Meyers, M. Biomedical applications of titanium and its alloys. *JOM* **2008**, *60*, 46–49. [CrossRef]
3. Sadowska, J.M.; Genoud, K.J.; Kelly, D.J.; O'Brien, F.J. Bone biomaterials for overcoming antimicrobial resistance: Advances in non-antibiotic antimicrobial approaches for regeneration of infected osseous tissue. *Mater. Today* **2021**, *46*, 136–154. [CrossRef]
4. Shin, J.M.; Gwak, J.W.; Kamarajan, P.; Fenno, J.C.; Rickard, A.H.; Kapila, Y.L. Biomedical applications of nisin. *J. Appl. Microbiol.* **2016**, *120*, 1449–1465. [CrossRef]
5. Yamaguchi, S.; Spriano, S.; Cazzola, M. 13—Fast and effective osseointegration of dental, spinal, and orthopedic implants through tailored chemistry of inorganic surfaces. In *Nanostructured Biomaterials for Regenerative Medicine*; Woodhead Publishing Series in Biomaterials; Guarino, V., Iafisco, M., Spriano, S., Eds.; Woodhead Publishing: Cambridge, UK, 2020; pp. 337–377.
6. Turner, R.J. Metal-based antimicrobial strategies. *Microb. Biotechnol.* **2017**, *10*, 1062–1065. [CrossRef]
7. Olmos, D.; González-Benito, J. Polymeric Materials with Antibacterial Activity: A Review. *Polymers* **2021**, *13*, 613. [CrossRef][PubMed]
8. Thallinger, B.; Prasetyo, E.N.; Nyanhongo, G.S.; Guebitz, G.M. Antimicrobial enzymes: An emerging strategy to fight microbes and microbial biofilms. *Biotechnol. J.* **2013**, *8*, 97–109. [CrossRef]
9. Jiang, Q.; Chen, J.; Yang, C.; Yin, Y.; Yao, K. Quorum Sensing: A Prospective Therapeutic Target for Bacterial Diseases. *BioMed Res. Int.* **2019**, *2019*, e2015978. [CrossRef]
10. Ling, H.; Lou, X.; Luo, Q.; He, Z.; Sun, M.; Sun, J. Recent advances in bacteriophage-based therapeutics: Insight into the post-antibiotic era. *Acta Pharm. Sin. B* **2022**. [CrossRef]
11. Boparai, J.K.; Sharma, P.K. Mini review on antimicrobial peptides, sources, mechanism and recent applications. *Protein Pept. Lett.* **2020**, *27*, 4–16. [CrossRef]
12. Sierra, J.M.; Fusté, E.; Rabanal, F.; Vinuesa, T.; Viñas, M. An overview of antimicrobial peptides and the latest advances in their development. *Expert Opin. Biol. Ther.* **2017**, *17*, 663–676. [CrossRef]
13. Gross, E.; Morell, J.L. The structure of nisin. *J. Am. Chem. Soc.* **1971**, *93*, 4634–4635. [CrossRef] [PubMed]

14. Małaczewska, J.; Kaczorek-Łukowska, E. Nisin—A lantibiotic with immunomodulatory properties: A review. *Peptides* **2020**, *137*, 170479. [CrossRef] [PubMed]
15. Khan, A.; Vu, K.D.; Riedl, B.; Lacroix, M. Optimization of the antimicrobial activity of nisin, Na-EDTA and pH against gram-negative and gram-positive bacteria. *LWT Food Sci. Technol.* **2015**, *61*, 124–129. [CrossRef]
16. Breukink, E.; de Kruijff, B. The lantibiotic nisin, a special case or not? *Biochim. Biophys. Acta BBA Biomembr.* **1999**, *1462*, 223–234. [CrossRef]
17. Zhou, H.; Fang, J.; Tian, Y.; Lu, X.Y. Mechanisms of nisin resistance in Gram-positive bacteria. *Ann. Microbiol.* **2014**, *64*, 413–420.[CrossRef]
18. Fernández, L.; Delgado, S.; Herrero, H.; Maldonado, A.; Rodríguez, J.M. The bacteriocin nisin, an effective agent for the treatment of staphylococcal mastitis during lactation. *J. Hum. Lact. Off. J. Int. Lact. Consult. Assoc.* **2008**, *24*, 311–316. [CrossRef]
19. De Kwaadsteniet, M.; Doeschate, K.T.; Dicks, L.M.T. Nisin F in the treatment of respiratory tract infections caused by *Staphylococcus aureus*. *Lett. Appl. Microbiol.* **2009**, *48*, 65–70. [CrossRef]
20. Millette, M.; Cornut, G.; Dupont, C.; Shareck, F.; Archambault, D.; Lacroix, M. Capacity of Human Nisin- and Pediocin-Producing Lactic Acid Bacteria To Reduce Intestinal Colonization by Vancomycin-Resistant Enterococci. *Appl. Environ. Microbiol.* **2008**, *74*, 1997–2003. [CrossRef] [PubMed]
21. Van Staden, D.A.; Brand, A.M.; Endo, A.; Dicks, L.M.T. Nisin F, intraperitoneally injected, may have a stabilizing effect on the bacterial population in the gastro-intestinal tract, as determined in a preliminary study with mice as model. *Lett. Appl. Microbiol.* **2011**, *53*, 198–201. [CrossRef]
22. Heunis, T.D.J.; Smith, C.; Dicks, L.M.T. Evaluation of a Nisin-Eluting Nanofiber Scaffold to Treat Staphylococcus aureus-Induced Skin Infections in Mice. *Antimicrob. Agents Chemother.* **2013**, *57*, 3928–3935. [CrossRef] [PubMed]
23. De Arauz, L.J.; Jozala, A.F.; Mazzola, P.G.; Vessoni Penna, T.C. Nisin biotechnological production and application: A review. *Trends Food Sci. Technol.* **2009**, *20*, 146–154. [CrossRef]
24. Joo, N.E.; Ritchie, K.; Kamarajan, P.; Miao, D.; Kapila, Y.L. Nisin, an apoptogenic bacteriocin and food preservative, attenuates HNSCC tumorigenesis via CHAC 1. *Cancer Med.* **2012**, *1*, 295–305. [CrossRef] [PubMed]
25. Preet, S.; Bharati, S.; Panjeta, A.; Tewari, R.; Rishi, P. Effect of nisin and

doxorubicin on DMBA-induced skin carcinogenesis—A possible adjunct therapy. *Tumour Biol.* **2015**, *36*, 8301–8308. [CrossRef] [PubMed]

26. Kamarajan, P.; Hayami, T.; Matte, B.; Liu, Y.; Danciu, T.; Ramamoorthy, A.; Worden, F.; Kapila, S.; Kapila, Y. Nisin ZP, a bacteriocin and food preservative, inhibits head and neck cancer tumorigenesis and prolongs survival. *PLoS ONE* **2015**, *10*, e0131008. [CrossRef]
27. Jia, Z.; He, M.; Wang, C.; Chen, A.; Zhang, X.; Xu, J.; Fu, H.; Liu, B. Nisin reduces uterine inflammation in rats by modulating concentrations of pro- and anti-inflammatory cytokines. *Am. J. Reprod. Immunol.* **2019**, *81*, e13096. [CrossRef]
28. Kindrachuk, J.; Jenssen, H.; Elliott, M.; Nijnik, A.; Magrangeas-Janot, L.; Pasupuleti, M.; Thorson, L.; Ma, S.; Easton, D.M.; Bains, M.; et al. Manipulation of innate immunity by a bacterial secreted peptide: Lantibiotic nisin Z is selectively immunomodu- latory. *Innate Immun.* **2012**, *19*, 315–327. [CrossRef]
29. Bastarrachea, L.J.; Denis-Rohr, A.; Goddard, J.M. Antimicrobial food equipment coatings: Applications and challenges. *Annu. Rev. Food Sci. Technol.* **2015**, *6*, 97–118. [CrossRef]
30. Espejo, H.M.; Bahr, D.F. Application of oxidized metallic surfaces as a medium to store biochemical agents with antimicrobial properties. *Surf. Coat. Technol.* **2019**, *372*, 312–318. [CrossRef]
31. Héquet, A.; Humblot, V.; Berjeaud, J.-M.; Pradier, C.-M. Optimized grafting of antimicrobial peptides on stainless steel surface and biofilm resistance tests. *Colloids Surf. B Biointerfaces* **2011**, *84*, 301–309. [CrossRef]
32. Espejo, H.M.; Díaz-Amaya, S.; Stanciu, L.A.; Bahr, D.F. Nisin infusion into surface cracks in oxide coatings to create an antibacterial metallic surface. *Mater. Sci. Eng. C* **2019**, *105*, 110034. [CrossRef] [PubMed]
33. Lou, T.; Bai, X.; He, X.; Yuan, C. Antifouling performance analysis of peptide-modified glass microstructural surfaces. *Appl. Surf. Sci.* **2021**, *541*, 148384. [CrossRef]
34. Riccucci, G.; Ferraris, S.; Reggio, C.; Bosso, A.; Örlygsson, G.; Ng, C.H.; Spriano, S. Polyphenols from Grape Pomace: Functional- ization of Chitosan-Coated Hydroxyapatite for Modulated Swelling and Release of Polyphenols. *Langmuir* **2021**, *37*, 14793–14804. [CrossRef] [PubMed]
35. Rivera, L.R.; Cochis, A.; Biser, S.; Canciani, E.; Ferraris, S.; Rimondini, L.; Boccaccini, A.R. Antibacterial, pro-angiogenic and pro-osteointegrative zein-bioactive glass/copper based coatings for implantable stainless steel aimed at bone healing. *Bioact. Mater.* **2021**, *6*, 1479–1490. [CrossRef] [PubMed]
36. Cochis, A.; Barberi, J.; Ferraris, S.; Miola, M.; Rimondini, L.; Vernè, E.; Yamaguchi, S.; Spriano, S. Competitive Surface Colonization of Antibacterial and

Bioactive Materials Doped with Strontium and/or Silver Ions. *Nanomaterials* **2020**, *10*, 120. [CrossRef] [PubMed]

37. Harrison, J.J.; Stremick, C.A.; Turner, R.J.; Allan, N.D.; Olson, M.; Ceri, H. Microtiter susceptibility testing of microbes growing on peg lids: A miniaturized biofilm model for high-throughput screening. *Nat. Protoc.* **2010**, *5*, 1236–1254. [CrossRef]
38. Aguilar, Z.P. Chapter 2—Types of Nanomaterials and Corresponding Methods of Synthesis. In *Nanomaterials for Medical Applications*; Elsevier: Amsterdam, The Netherlands, 2013; pp. 33–82.
39. Prince, A.; Sandhu, P.; Ror, P.; Dash, E.; Sharma, S.; Arakha, M.; Jha, S.; Akhter, Y.; Saleem, M. Lipid-II independent antimicrobial mechanism of nisin depends on its crowding and degree of oligomerization. *Sci. Rep.* **2016**, *6*, 37908. [CrossRef]
40. Rollema, H.S.; Kuipers, O.P.; Both, P.; de Vos, W.M.; Siezen, R.J. Improvement of solubility and stability of the antimicrobial peptide nisin by protein engineering. *Appl. Environ. Microbiol.* **1995**, *61*, 2873–2878. [CrossRef]
41. Powell, C. X-ray Photoelectron Spectroscopy Database XPS, Version 4.1, NIST Standard Reference Database 20. 1989. Available online: http://srdata.nist.gov/xps/ (accessed on 15 September 2022).
42. Brooks, E.K.; Brooks, R.P.; Ehrensberger, M.T. Effects of simulated inflammation on the corrosion of 316L stainless steel. *Mater. Sci. Eng. C Mater. Biol. Appl.* **2017**, *71*, 200–205. [CrossRef]
43. Chen, J.; Shi, X.; Zhu, Y.; Chen, Y.; Gao, M.; Gao, H.; Liu, L.; Wang, L.; Mao, C.; Wang, Y. On-demand storage and release of antimicrobial peptides using Pandora's box-like nanotubes gated with a bacterial infection-responsive polymer. *Theranostics* **2020**, *10*, 109–122. [CrossRef]
44. Ferraris, S.; Warchomicka, F.; Barberi, J.; Cochis, A.; Scalia, A.; Spriano, S. Contact Guidance Effect and Prevention of Microfouling on a Beta Titanium Alloy Surface Structured by Electron-Beam Technology. *Nanomaterials* **2021**, *11*, 1474. [CrossRef] [PubMed]
45. Blackman, L.D.; Fros, M.K.; Welch, N.G.; Gengenbach, T.R.; Qu, Y.; Pasic, P.; Gunatillake, P.A.; Thissen, H.; Cass, P.; Locock, K.E. Dual action antimicrobial surfaces: Alternating photopatterns maintain contact-killing properties with reduced biofilm formation. *Macromol. Mater. Eng.* **2020**, *305*, 2000371. [CrossRef]
46. Kim, J.J.; Kim, K.; Choi, Y.S.; Kang, H.; Kim, D.M.; Lee, J.C. Polysulfone based ultrafiltration membranes with dopamine and nisin moieties showing antifouling and antimicrobial properties. *Sep. Purif. Technol.* **2018**, *202*, 9–20. [CrossRef]
47. Li, W.; Thian, E.S.; Wang, M.; Wang, Z.; Ren, L. Surface Design for Antibacterial Materials: From Fundamentals to Advanced Strategies. *Adv. Sci.*

2021, *8*, 2100368. [CrossRef] [PubMed]

48. Andre, C.; de Jesus Pimentel-Filho, N.; de Almeida Costa, P.M.; Vanetti, M.C.D. Changes in the composition and architecture of staphylococcal biofilm by nisin. *Braz. J. Microbiol.* **2019**, *50*, 1083–1090. [CrossRef] [PubMed]
49. Hage, M.; Chihib, N.-E.; Abdallah, M.; Khelissa, S.; Crocco, B.; Akoum, H.; Bentiss, F.; Jama, C. Nisin-based coatings forthe prevention of biofilm formation: Surface characterization and antimicrobial assessments. *Surf. Interfaces* **2021**, *27*, 101564.[CrossRef]
50. Najmi, Z.; Kumar, A.; Scalia, A.C.; Cochis, A.; Obradovic, B.; Grassi, F.A.; Leigheb, M.; Lamghari, M.; Loinaz, I.; Gracia, R.; et al.Evaluation of Nisin and LL-37 Antimicrobial Peptides as Tool to Preserve Articular Cartilage Healing in a Septic Environment.*Front. Bioeng. Biotechnol.* **2020**, *8*, 561. [CrossRef]